SYNTHESIS, ASSEMBLY AND COLLOIDAL POLYMERIZATION OF POLYMER-COATED FERROMAGNETIC COBALT NANOPARTICLES

By

Pei Yuin Keng

A Dissertation Submitted to the Faculty of the

DEPARTMENT OF CHEMISTRY

In partial fulfillment of the requirements
For the Degree of

DOCTOR OF PHILOSOPHY

In the Graduate College

THE UNIVERSITY OF ARIZONA

2010

THE UNIVERSITY OF ARIZONA
GRADUATE COLLEGE

As members of the Dissertation Committee, we certify that we have read the dissertation

prepared by Pei Yuin Keng

entitled Synthesis, Assembly and Colloidal Polymerization of Ferromagnetic Cobalt Nanoparticles

and recommend that it be accepted as fulfilling the dissertation requirement for the

Degree of Doctor of Philosophy

_____ Date: 11/05/09
Dr. Jeffrey Pyun

_____ Date: 11/05/09
Dr. Dominic V. McGrath

_____ Date: 11/05/09
Dr. Eugene E. Mash

_____ Date: 11/05/09
Dr. Neal R. Armstrong

_____ Date: 11/05/09
Dr. Zhiping Zheng

Final approval and acceptance of this dissertation is contingent upon the candidate's submission of the final copies of the dissertation to the Graduate College.

I hereby certify that I have read this dissertation prepared under my direction and recommend that it be accepted as fulfilling the dissertation requirement.

_____ Date: 11/06/09
Dissertation Director: Dr. Jeffrey Pyun

STATEMENT BY AUTHOR

This dissertation has been submitted in partial fulfillment of requirements for an advanced degree at the University of Arizona and is deposited in the University Library to be made available to borrowers under rules of the Library.

SIGNED: Pei Yuin Keng

ACKNOWLEDGEMENTS

I would have never imagined myself writing this dissertation five years ago, and is greatly in-debt to those whom had helped me throughout the most challenging journey of my life.

First, I wish to express my deepest gratitude to my research advisor, Prof. Jeffrey Pyun for his guidance, training and patience. Jeff showed me how diligence and hard work can set apart those that are successful from the rest of the crowd. To Jeff, thank you for your commitment and mentorship throughout my scientific career.

I would like to thank my committee members, Dr. Eugene E. Mash, Dr. Dominic V. McGrath, Dr. Zhiping Zheng, and Dr. Armstrong for their advises and guidance. I wish to extend my gratitude especially to Dr. Armstrong and his group, for teaching me various aspects of electrochemistry, which has became a valuable research tool in my scientific career.

To my collaborators, Bryan Korth, Dr. Jason Benkoski (John Hopkins Institute), Dr. Inbo Shim (Kookmin University, Korea), Dr. Armstrong, Dr. Erin Ratcliff, Dr. Jeanne Pemberton, and Dr. Heemin Yoo whom all had add significant impact to my graduate research in various aspects ranging from synthesis, engineering, solid states characterization, spectroscopic and electrochemical analysis of novel nanomaterials presented in this dissertation.

I also want to thank the Pyun group members especially Boyun Kim, Dr. Heemin Yoo and Dr. Woo Jin Chung for their friendship, help and advices. To Bryan Korth, who provided initial guidance in the lab and continued to offer help and scientific discussions throughout my PhD. I am also truly fortunate to have known Diana Cedeno as a friend, whom I shared my frustrations and joys during our weekend bike rides. Thank you all, without you, I would not have finished these five challenging years of graduate school.

I would have never dreamed to pursue a graduate degree without Kai Fong. Kai gave me a lifetime opportunity to earn a college degree in the United States via a full tennis scholarship. Kai, whom I respect like a father, taught me many valuable lessons in life, gave me the confidence to do great things and reaching out to my best ability.

But none of these accomplishments is possible without my mother. I owe my PhD and life achievement to my mother, for all the love and sacrifices she had made for me. To my mom, thank you and I love you. To my loving husband, thank you for your patience and support in completing this journey with me.

DEDICATION

To my mom, husband and Kai

TABLE OF CONTENTS

TABLE OF CONTENTS - *Continued*

TABLE OF CONTENTS – *Continued*

TABLE OF CONTENTS - *Continued*

TABLE OF CONTENTS - *Continued*

LIST OF FIGURES

LIST OF FIGURES - *Continued*

LIST OF FIGURES - *Continued*

LIST OF FIGURES - *Continued*

LIST OF FIGURES - *Continued*

LIST OF FIGURES - *Continued*

LIST OF FIGURES – *Continued*

LIST OF FIGURES – *Continued*

LIST OF FIGURES - *Continued*

LIST OF FIGURES - *Continued*

LIST OF TABLES

LIST OF SCHEMES

LIST OF SCHEMES - *Continued*

ABSTRACT

This dissertation describes a novel methodology to prepare, functionalize, and assemble polymer-coated ferromagnetic cobalt nanoparticles (PS-CoNPs) and cobalt oxide nanowires. This research demonstrated the ability to use dipolar nanoparticles as 'colloidal monomers' to form electroactive 1-D mesostructures via self- and field-induced assembly. The central focus of this dissertation is in developing a novel methodology termed as 'Colloidal Polymerization', in the synthesis of well-defined cobalt oxide nanowires as nanostructured electrode materials for potential applications in energy storage and conversion.

Ferromagnetic nanoparticles are versatile building blocks due to their inherent spin dipole, which drive 1-D self-assembly of colloids. However, the preparation and utilization of ferromagnetic nanoparticles have not been extensively examined due to the synthetic challenges in preparing well-defined materials that can be easily handled. This dissertation has overcome these challenges through the hybridization of polymeric surfactants with an inorganic colloid to impart functionality, colloidal stability and improved processing characteristics. This modular synthetic approach was further simplified to prepare ferromagnetic nanoparticles in gram scale, which enabled further investigations to develop new chemistry and materials science with these materials. These polymer-coated magnetic nanoparticles self-assembled into extended linear chains due to strong dipolar attractions between colloids. Additionally, novel dipolar assemblies,

such as, flux-closure nanorings and lamellae type mesostructures were demonstrated by controlling the interparticle of attractive forces (dipolar versus van der Waals).

The research presented herein focused on utilizing polymer-coated ferromagnetic cobalt nanoparticles as ‘colloidal molecules’ to form interconnected 1-D mesostructures via ‘Colloidal Polymerization’. This process exploited the magnetic organization of dipolar colloids into 1-D mesostructures followed by a facile oxidation reaction to form interconnected electroactive cobalt oxide nanowires. This facile and template free approach enabled the large scale synthesis of semiconductor cobalt oxide nanowires, in which the electronic and electrochemical properties were confirmed for potential applications for energy storage and conversion. This work served as a platform in fabricating a wide range of semiconductor heterostructures, which allowed for structure-property investigation of new nanostructured electrodes.

CHAPTER 1

INTRODUCTION

1.1 Motivation in Utilizing Nanoparticles as Building Blocks

One-dimensional (1-D) organization of nanoparticles has generated tremendous interest due to their enhanced magnetic[1], optical[2] and electrical[3] properties, as a consequence of their mesoscopic ordering. New collective behavior in 1-D nanoparticle assemblies has been attributed to cooperative interactions between individual nanoparticles, which are not observed in isolated or random assemblies. Notably, 1-D alignment of Au and Ag nanoparticles induced a strong optical dichroism, which resulted in the modulation of the plasmonic absorption wavelengths. Furthermore, these materials have been manipulated into plasmonic waveguides to transport electromagnetic energy along 1-D arrays of gold nanoparticles.[2, 4] In the area of energy storage, 1-D assemblies of cobalt oxide nanoparticles templated onto engineered viruses showed significant improvement in the performance of Li-ion batteries.[5] The 1-D morphology of these nanostructured electrodes provided directional electron transport in electrochemical devices, thus improving the capacity and discharge kinetics of Li-ion batteries. Similar enhancement was observed in photovoltaic devices composed of vertically aligned ZnO nanowires. Photogenerated charges were directed along the nanowires, thus improving the overall charge collection in comparison to conventional nanoparticle films.[6]

Although 1-D organization of nanoparticles has been demonstrated to afford materials with enhanced properties, the development of facile strategies to form 1-D

assemblies of nanoparticles remains an important challenge. Template-assisted methods, specifically, using organic or inorganic templates, have provide a simple, straight-forward, and highly specific route toward the formation of 1-D nanostructures.[7, 8] Linear 'soft templates', such as, polyelectrolyte[9-11], DNA[3, 12], biomolecules[13-15], and block copolymers[16-19] have been exploited as platforms to generate 1-D nanomaterials. Additionally, hard-templates prepared by lithography have demonstrated precise 1-D assembly by confining nanoparticles on the surfaces of micropatterned wafers.[20, 21]

Recently, there has been a growing research interest in developing novel methods to organize nanoparticles into 1-D assemblies by exploiting the chemical and crystal lattice anisotropy of certain inorganic nanoparticles. Notably, CdTe nanoparticles self-assembled into 1-D chains due to inter-particle charge dipoles interactions arose from surface defects and crystal lattice anisotropy.[22] In this strategy, controlled displacement of steric stabilizers reduced the repulsive interactions and consequently increased the electric-dipole attractions between CdTe nanoparticles. This resulted in the spontaneous 1-D assembly of CdTe nanoparticles.

Recently, Stellaci et al. demonstrated an elegant strategy to selectively functionalize gold nanoparticles with reactive groups at two opposing defect points to form "divalent nanoparticles".[23] In this method, the phase separation of mixed ligands into alternated ring domains on the surfaces of the gold nanoparticles resulted in the formation of two opposing defect points.[24] Due to the instability of ligands at the defect points, carboxylic acid terminated ligands were selectively functionalized at the two poles of each nanoparticles via a controlled place-exchanged reaction. The carboxylic acid

functionalized divalent gold nanoparticles were subsequently polymerized with diamine molecules to form chains of gold nanoparticles that were covalently bound by amide bonds.[24-28]

Borrowing from the 'block copolymer' paradigm for phase segregation of amphiphilic ABA triblock copolymers at the molecular length scale, Kumacheva et al. translated these strategies to assemble amphiphilic gold nanorods in selective solvents.[29-31] In this system, the mesoscale ABA triblock copolymer consisted of a hydrophilic gold nanorod was selectively tethered with hydrophobic polystyrene ligands at both ends. By changing the solvent quality, selective aggregation of the constituent blocks could be achieved, which induced the self-assembly of the gold nanorods into chains, rings, bundles and nanospheres.

Various strategies in assembling isotropic nanoparticles into 1-D mesostructures on the micrometer scale will be emphasized in the following sections. In particular, magnetic assembly is a facile and robust strategy to overcome challenges in assembling isotropic nanoparticles due to their selective directionality embedded within the north-south dipolar cores. This magnetic core has been exploited to form 1-D mesostructures via self- or field-induced dipolar associations.

In this chapter, magnetic field-induced and self-assembly of (nano)particles into dipolar assemblies will be discussed in six main sections. First, a summary of magnetic materials will be provided. In the subsequent three sections (**1.3 – 1.5**), strategies to assemble magnetic colloids will be discussed over different size regimes: (i) micron-sized particles (D = 1 – 50 μm), (ii) ferromagnetic nanoparticles (D = 10 – 100 nm) and (iii)

superparamagnetic nanoparticles (D < 20 nm). In Section **1.6**, the concept of utilizing dipolar colloids as templates to form various 1-D nanostructures of metals, semiconductors and metal oxides will be emphasized based on the magnetic assembly strategies discussed in previous sections. Finally, a novel synthetic methodology referred to as 'Colloidal Polymerization' will be highlighted as a facile method to form functional 1-D mesostructures. Reviews on nanoparticles synthesis and assembly of magnetic nanoparticles into two-dimensional (2-D) and three-dimensional (3-D) arrays are reported elsewhere.[1, 7, 32-44]

1.2 Classification of Magnetic Materials

Magnetic substances iron, nickel, cobalt (Fe, Ni, Co) fall into a special class of transition metals that possess unpaired spin within a crystalline lattice, which gives rise to magnetic properties of bulk materials. Magnetic materials and their interactions with an applied field can be broadly categorized into four main classes[42, 44-46]:

(1) *diamagnetism:* Most non-metals are diamagnetic at room temperature and possess a negative magnetic susceptibility, $\kappa < 0$. Magnetic susceptibility, κ ($\kappa = M/H$), defines the effectiveness of an applied field (H) to induce magnetization (M) throughout a material. For diamagnetic substances, the interaction towards an applied field is weakly repulsive.

(2) *paramagnetism*: Most metals (except for Fe, Co and Ni) are paramagnetic at room temperature. In the presence of an applied field, magnetic interactions of paramagnetic particles are weakly attractive with magnetic susceptibilities, $\kappa > 0$ ($\sim 10^{-3 \text{ to } -5}$). Even under an applied field, only a small portion of the spins aligned in response to

an external magnetic field. As a consequence, induced magnetization in a paramagnet is much weaker than a ferromagnet and a superparamagnet.

(3) *ferromagnetism*: Fe, Co and Ni are classic examples of ferromagnets and exhibit spontaneous magnetization (in the absence of an applied field) below a critical temperature, defined as the Curie temperature (T_C). The Curie temperature for a bulk ferromagnetic metal such as Co and Fe is well above room temperature (T_C cobalt = 1131 ºC and T_C iron = 770 ºC).[44] Below T_C, all spins are coupled cooperatively to yield a large net magnetic moment. When the dimension of bulk ferromagnet is reduced to a critical size (depending on shape and composition), single domain ferromagnetic nanoparticles can be formed. The inherent magnetic dipoles embedded in certain ferromagnetic nanoparticles enable 1-D self assembly.

(4) *superparamagnetism*: As the dimensions of ferromagnetic nanoparticles are reduced below a critical size, these materials can no longer retain a dipole moment in the absence of a field due to the overall reduction of aligned spins. For superparamagnetic nanoparticles, thermal fluctuations perturb the magnetic interactions of neighboring spins, thus these nanomaterials do not exhibit spontaneous magnetization, in contrast to ferromagnetic nanoparticles. Similarly to ferromagnetic nanoparticles, the magnetic properties of superparamagnetic nanoparticles are strongly dependent on the temperature. At a critical temperature, defined as the *blocking temperature* (T_B), spontaneous magnetizations occur as all spins aligned to generate a large net dipole.

1.2.1 Ferrofluids

A special class of magnetic materials that are important in many areas of science and technology are ferrofluids.[47-49] Ferrofluids consist of a colloidal suspension of superparamagnetic nanoparticles (D ~ 5 - 15 nm) coated with passivating ligands to suppress agglomeration and promote dispersion in either aqueous or organic media.[47, 50-52] An important feature of ferrofluids is their ability to respond reversibly to the applied external fields. In the presence of an external field, magnetic nanoparticles were polarized within the ferrofluids, inducing structural changes to the dispersed colloids. Upon releasing the field, the ferrofluids return to isotropic dispersions and fluid-like behavior. Additionally, ferrofluids exhibit unusual shapes and interactions in an applied field, which are not observed in bulk iron because individual magnetic suspension in ferrofluids can respond microscopically with the field as shown in Figure 1.1.[47]

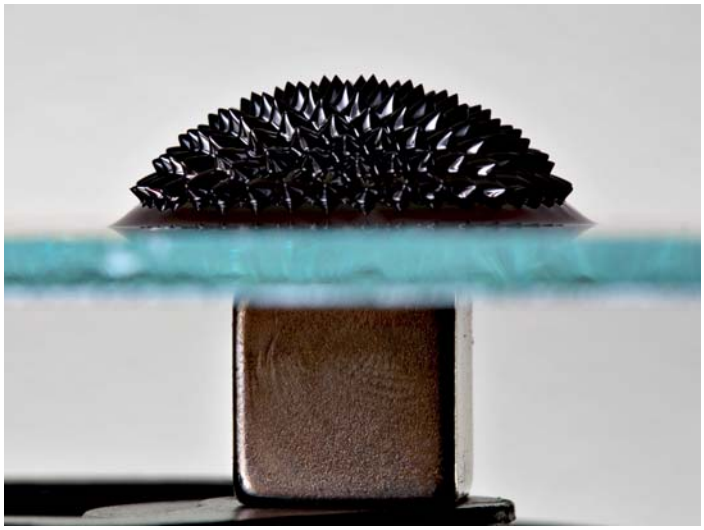

Figure 1.1: Optical image of the ferrofluids forming corrugated surfaces under a strong magnetic field. Reproduced with permission from ref. 47. Copyright 1982, Scientific American, Inc. [47]

1.3 1-D assemblies of Magnetic Particles with D ~ 1 - 50 micrometers

Micrometer sized magnetic colloids were widely studied in the 20th century due to the accessibility to uniformly sized emulsion beads.[53] The large particle size allowed the dynamics and collective processes of these magnetically assembled beads to be studied using optical microscopy (Figure 1.2). Additionally, the strength of particle-particle interactions could be tuned *in situ* with an external magnetic field.

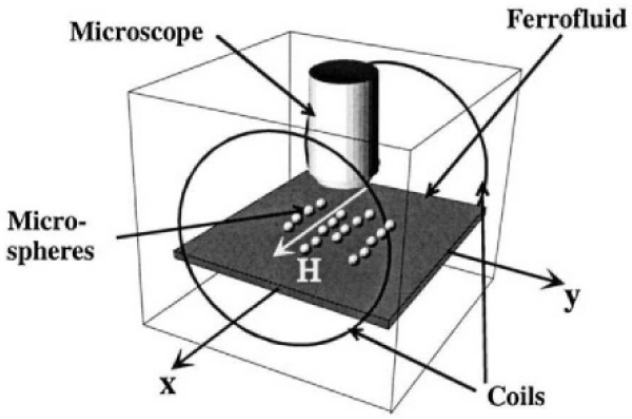

Figure 1.2: Schematic experimental setup for field induced chain formation of non-magnetic microspheres dispersed in thin layer of ferrofluid. Reproduced with permission from ref. 54. Copyright 2004, Kluwer Academic Publisher[54]

Skjeltorp et al. first demonstrated 1-D and 2-D assembly of blends composed of paramagnetic and non-magnetic beads based on the 'magnetic holes' effect.[54, 55] In this seminal work, diamagnetic polystyrene beads (D ~ 1 – 10 μm) were dispersed in colloidal suspensions of superparamagnetic nanoparticles (D ~ 6 - 10 nm) (ferrofluids). In the presence of an applied field, the surrounding ferrofluids aligned into fibrous structures in the direction of the applied field, while excluding the non-magnetic beads into their own domains. The depleted volumes occupied by the non-magnetic beads were termed as the

"magnetic holes." The assembly of magnetic holes was controlled by changing the orientation of the applied field as illustrated in Figure 1.3. In the presence of an external field parallel to the substrate, gap spanning chains of non-magnetic polystyrene beads were obtained (Figure 1.3 a, c). In a perpendicular magnetic field, the 2-D morphology of non-magnetic polystyrene beads was observed due to the repulsive interactions between the magnetic holes (Figure 1.3 b, d).[54] Additionally, paramagnetic latex beads self-assembled into flexible chains and loops at zero field conditions when dispersed in a magnetic fluid.[56] The latex beads experienced a greater polarization in magnetic fluids, which led to an increased of the effective magnetic moments of the beads, resulting in the formation of 1-D assemblies.

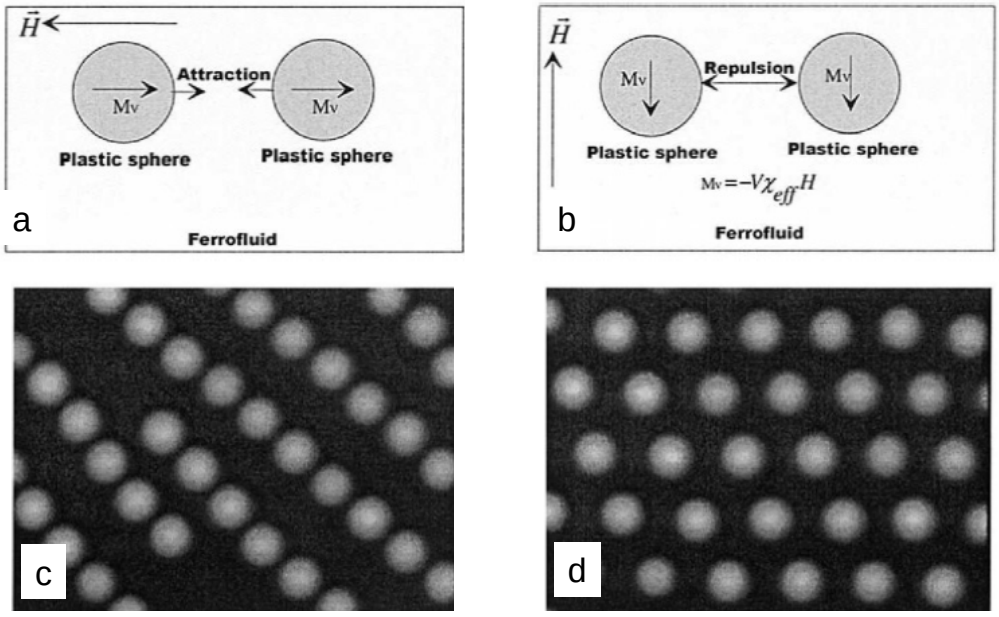

Figure 1.3: The principle of magnetic hole. (a) Two holes side by side repel each other. (b) Two holes with the centers collinear with the field lines will attract each other. (c) Structures of 10 μm spheres formed by magnetic field parallel to the substrate, and (d) perpendicular to the substrate. Reproduced with permission from ref. 54. Copyright 2004, Kluwer Academic Publisher.[54]

Based on a similar concept, Yellen et al. demonstrated 3-D crystallization and transport of non-magnetic beads on a patterned magnetic substrate via an external field.[57] More recently, Yellen and Rotello further expanded this methodology to prepare binary particle assemblies of colloidal superstructures with various symmetries.[58] In this work, micrometer-sized diamagnetic and paramagnetic beads were assembled into complex geometries such as 'Saturn rings' and flowers in magnetized ferrofluids (Figure 1.4). In this strategy, fundamental dipolar interactions of different magnetic particles in a magnetic field were applied to yield complex colloidal superstructures using simple building blocks.

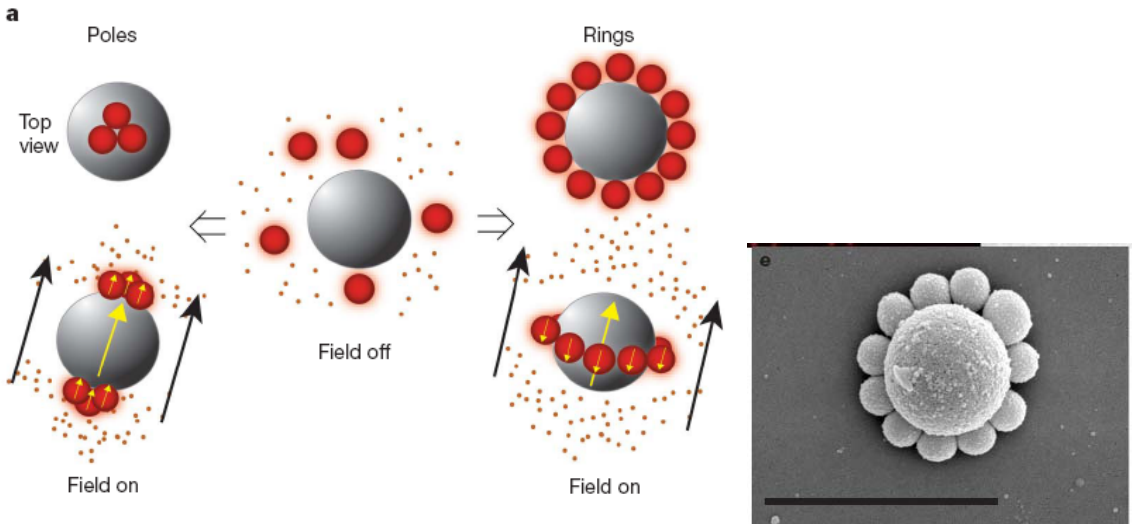

Figure 1.4: Illustration of magnetic assembly in colloidal particle mixtures. In an applied field (the black arrow denoted the field direction), equatorial and polar arrangement form when particle magnetizations are aligned antiparallel or parallel to the field direction, respectively. Inset showed SEM images of the 'Saturn-rings' assembly based on magnetostatic interaction between diamagnetic and paramagnetic particles within a magnetized ferrofluid. Reproduced with permission from ref. 58. Copyright 2009, Macmillan Publisher Limited.[58]

Magnetic fluids have also been demonstrated to be effective in aligning biological entities without destroying their physiological structure, based on the early work by

Skjeltorp in colloidal crystallization.[57] This technique, coupled with small angle neuron scattering (SANS) enabled the interrogation of molecular structure of tobacco mosaic virus (TMV) dispersions, which have been widely used as a model system for studying other protein-nucleic acid interaction and assembly.[59] At zero fields, TMV exhibited a scattering profile indicative of isotropic dispersion due to electrostatic repulsion interactions in aqueous media. Under modest applied magnetic fields (0.3 T), anisotropic scattering emerged suggesting that the viruses had aligned into nematic structures. Recently, Rotello et al. described a novel approach in ordering cellular structures dispersed in biocompatible ferrofluids.[58] In this method, iron oxide magnetic nanoparticles (D ~ 10 - 20 nm) induced effective magnetization in an extracellular matrix, enabling the organization of cells into linear assemblies. This approach enabled the organization of diamagnetic endothelial cells in a facile and inexpensive platform, which are being evaluated for potential applications in tissue engineering.

In the area of magnetorheological fluids, the rheological response is induced via the formation of gap spanning fibrous aggregates within a magnetic suspension.[60] This technology is widely used in applications such as clutches, brakes and hydraulic devices.[61-63] Recent theoretical work also suggested that controlled structures played important roles in rheological properties of the magnetic fluids.[64, 65] Seminal work by Gast et al. developed an effective method to probe the lowest energy structure of these paramagnetic colloids when pulsed with magnetic fields.[66] This work, for the first time, provided experimental insights into the equilibrium structure of magnetorheological fluids.[51]

In addition to symmetrical paramagnetic beads, magnetic assembly of Janus type particles had also been investigated. Janus particles have generated significant research interest due to their asymmetric surface properties as they can have unique advantages over symmetrical nanoparticles counterparts with uniform surface coating.[67] Janus particles with a magnetic compartment embedded in a spherical colloid have been fabricated and assembled into 1-D assemblies in the presence of an external field. In all cases, complicated zig-zag 1-D magnetic morphologies were formed due to the asymmetric nature of the particle. This morphology was directly influenced by the strong magnetic dipoles to form maximum dipolar attractions with neighboring magnetic cores.[29, 68-71] The preparation of asymmetric colloidal clusters was elegantly demonstrated by Pine and Bibette through proper control of the hydrophobicity of silica spheres, volume fraction of magnetic nanoparticles, and the rate of solvent evaporation.[72] The asymmetric colloidal cluster assembled into various isomeric forms of a polymer chain in an applied field to satisfy both steric and magnetic constraints. Additionally, chiral helical structures resembling double helix DNA were formed in this synthetic colloidal system by manipulating the colloid size, feed ratio, and electrostatic/magnetic interactions. These well-designed studies further expanded the library of colloidal assemblies, which could be a promising methodology in creating wide range of complex structures of colloidal mesopolymers, optical, and light-activated structures and serve as a model for enantiomeric separations (Figure 1.5).[72]

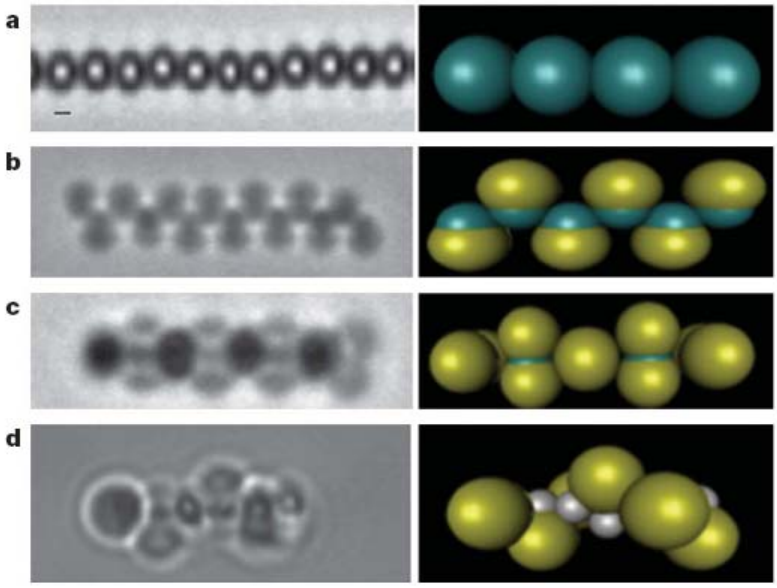

Figure 1.5: a-d, Optical microscope images and their corresponding schematic representations of the self-assembly of blocks into chains under an applied magnetic field. (a) Isotropic particles self-assemble into linear chains. (b) Self-assembly of caps by ordering alternatively up and down along the chain direction. (c) To satisfy both steric and magnetic constraints, symmetric dumbbell must rotate by 90º relative to their neighbors along the chain and field direction. (d) Asymmetric dumbbells self-assemble into helical structures, as a result of the steric hindrance induced by the size difference. Magnetic field, 10 mT; scale bars, 1 μm. Reproduced with permission from ref. 72 Copyright 2008, Nature Publishing Group.[72]

In the area of photonic crystals, Asher et al., first demonstrated a novel magnetically controllable photonic crystal through the self-assembly of colloidal spheres containing superparamagnetic iron oxide nanoparticles.[73, 74] In this system, the assembly of superparamagnetic spheres into crystalline colloidal arrays (CCA) resulted in the diffraction of visible light. Additionally, diffraction wavelengths can be controlled by altering the lattice constant of the colloidal arrays with an external magnetic field. Furthermore, the optical symmetry of these magnetic photonic crystals could be distorted with an applied field, which is crucial for the development of a full band gap photonic

crystal.[75] The same group later demonstrated the preparation and assembly of ferromagnetic cobalt ferrite encapsulated in latex beads, which were used to prepare magnetically controlled light modulators, optical switches, and mirrors.[76] Yin et al. further extended these studies by increasing the volume fraction of the Fe_3O_4 colloids, which led to an increased in magnetic moment and higher refractive indexes.[73] This system allowed for tunable diffraction wavelengths (~ 400 – 800 nm) with relatively high diffraction intensity, quick response time, and lower external field strength needed to induce diffraction changes. Xia and co-workers later developed synthetic methodologies in preparing new types of colloidal building blocks based on composites of magnetic core with a semiconductor shell. The Xia group illustrated the synthesis of monodispersed colloidal spheres of (Fe_3O_4-α-Se)-MSe (M = Zn^{2+}, Cd^{2+}, and Pb^{2+}) via continuous loading of iron oxide nanoparticles, followed by cation-exchange reactions. The presence of the superparamagnetic iron oxides core, allowed for all colloidal crystals to be aligned in chains morphology along the magnetic field lines.[75]

1.4 Assemblies of Ferromagnetic Nanoparticles with D ~ 20-100 nm

Scaling down from micrometer sized magnetic particles to nano-sized colloids, this section will focus on the 1-D assembly of ferromagnetic nanoparticles with particle size ranging from 15 to 100 nm. Ferromagnetic materials (Fe, Co, Ni) within this size regime have stimulated considerable research interest due to their potential as advanced materials, specifically in the area of high density recording media.[77, 78] Additionally, ordered long-range assemblies of monodispersed ferromagnetic nanoparticles have garnered increasing research interest due to their intriguing collective behaviors. In this

section, both experimental and theoretical aspects of dipolar assembly of ferromagnetic nanoparticles will be emphasized.

1.4.1 Theory of the assembly of ferromagnetic nanoparticles

Bulk ferromagnetic materials (Fe, Co, Ni) undergo spontaneous magnetization through the cooperative alignment of magnetic dipoles to minimize the overall magnetostatic energy.[79] However, bulk ferromagnets also have the tendency to break up into smaller magnetic domains to achieve the most favorable energy structure in zero field. This phenomenon led to the decrease in overall magnetization because magnetic spins are oriented in different directions within the ferromagnetic material. As predicted by Frenkel and Dorfman[80] and later quantitatively analyzed by Kittel[81], a true ferromagnet (single domain nanoparticle) could be realized by reducing the particle size down to the 20 nm regime, in which the formation of domain walls was not favorable due to the large exchange energy in aligning magnetic spins in an anti-parallel fashion.

As the dimensionality of the bulk material was reduced to the nanoscale, interesting properties were discovered to be important from both fundamental and applied perspectives.[82] Ferromagnetic nanoparticles exhibited interesting magnetic behaviors, such as, the ability to self-assemble into magnetic strings and networks under zero field conditions.[22, 83] Jacobs and Bean first considered the formation of chain like aggregates composed of individual magnetic particles in ferrofluids.[84] Later De Gennes and Pincus proposed the self-assembly of dipolar colloids into chains and flux-closure rings due to the strong dipolar coupling of single domain particles at zero field conditions.[85] Early theoretical predictions were later confirmed by Monte Carlo simulations pioneered by

Chantrell, confirming spontaneous formation of 1-D aggregates of single domain particles.[86-90] Since De Gennes and Pincus referred to dipolar chains as flexible polymeric macromolecules, fundamental concepts of polymer physics, such as, persistent chain length, chain length distribution, and chain to coil transition, were extended to colloidal assemblies.[91-94]

The formation of magnetic flux-closure rings under zero field condition (i.e.: absence of an external field) was first predicted by de Gennes.[85] Later, Clark and Patey calculated the formation of ring structures to be the lowest energy structure for a dipolar molecular cluster.[95] Lavender expanded this method in predicting the ring morphology as the most favorable magnetic assembly of dipolar colloids by considering both cohesive electrostatics and dipolar attractions.[96] The ring morphology is preferred due to the coupling of two unpaired spins within a linear chain resulted in zero net dipole moment and the attractive antiparallel dipolar interaction across the ring. Recent computational studies have indicated that a variety of possible self-assembled structures could form in a suspension of dipolar nanoparticles, depending on the interplay of the particle concentration, the strength of the dipolar attractions, and the strength of the isotropic attractive interactions.[83, 97-100] Notably, Douglas et al. generated a 2-D map of nanoparticle assemblies using a rule-based algorithm, which simulated the organization of colloids based on both van der Waals and dipolar attractions at varying dipolar strengths (0 k_BT to -100 k_BT).[101] Based on the 2-D map, formation of string-like and loop structures were predicted when dipolar attractions dominated over isotropic interactions (Figure 1.6: structures d1, d2, and d3). In the absence of dipolar forces, radially

symmetrical nanoparticle aggregates were expected due to the dominant isotropic van der Waals interactions (Figure 1.6: structure v1). In the case of competing attractive forces (dipolar and van der Waals), intermediate nanoparticle assemblies represented in Figure 1.6 as dv1, dv2, dv3 and dv4 with branched chains and networks were predicted from this rule-based simulation.

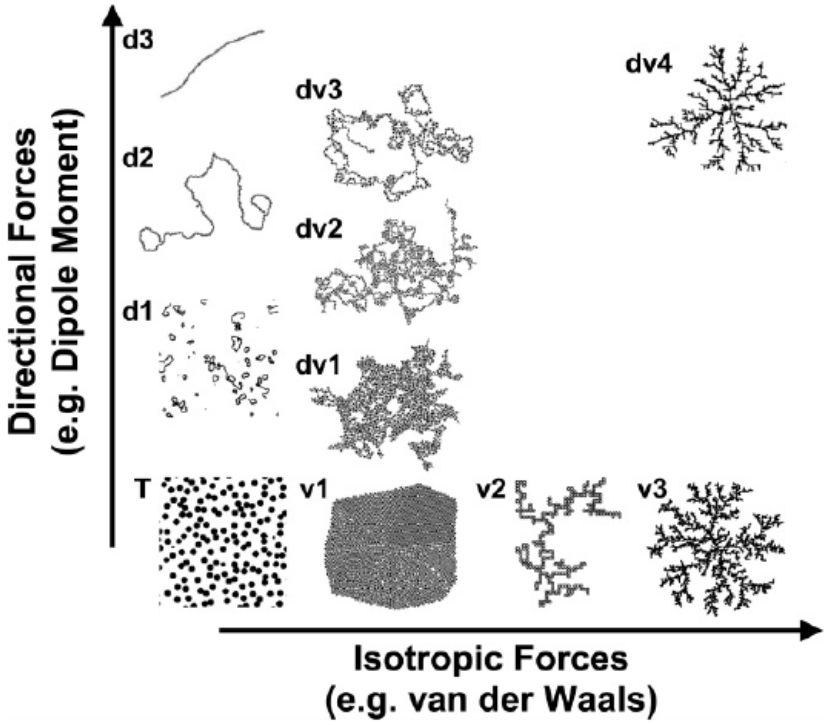

Figure 1.6: Morphological map for dipolar colloids with respect to the strength of van der Waals and dipolar interactions. Reproduced with permission from ref. 101. Copyright 2007, American Chemical Society.[101]

1.4.2 Synthesis and self-assembly of ferromagnetic nanoparticles into 1-D mesostructures

Dipolar assemblies of magnetic nanoparticles have been found in naturally occurring magnetotactic bacteria.[102] These biomineralized magnetite (Fe_3O_4), greigite

(Fe_3S_4), or pyrrhotite (Fe_7S_8) ferrimagnetic nanoparticles (D ~ 50 nm) are encapsulated within a membrane, in which the entire organelle is referred to as a magnetosome.[102, 103] Ferrimagnetic nanoparticles, similarly to ferromagnetic nanoparticles, possess a net dipole moment despite a non-equivalent antiparallel alignment of spins. In magnetotactic bacteria, the magnetosomes are aligned in either a single or double chain-like morphologies, as a consequence of the collective magnetic dipoles from individual colloids. The permanent magnetic dipoles, induced by the nanoparticle assembly, serve as a crucial tool for navigation along the Earth geomagnetic field lines.[103] The presence of the permanent magnetic dipoles was confirmed via magnetic measurements[104], magnetic force microscopy[105], and electron holography[106]. This 1-D self-organization of magnetic colloids, is an example of hierarchical nanoparticle assembly within a living organism.[107] Comprehensive reviews elucidating various aspects of magnetotactic bacteria with an emphasis on the characterization, biomineralization and isolation techniques of magnetotactic bacteria and ferromagnetic nanoparticles can be found elsewhere.[102, 103, 107-109] Although, ferrimagnetic nanoparticles could be mineralized from naturally occurring magnetotactic bacteria, the yield of bacteria is low and the dipolar colloids are difficult to purify from organic residues.[110] Furthermore, the biomineralization approach does not provide control in the particle size and shape. Therefore, there is a pressing need in developing a facile method to synthesize dipolar nanoparticles with controlled size and shape in appreciable quantities that are easily processable.

One of the earliest investigations on the synthesis and assembly of ferromagnetic cobalt nanoparticles was reported by Thomas at Chevron.[111-113] This seminal work was the first synthetic method reported for the preparation of single domain magnetic nanoparticles. In this work, functional copolymers composed of styrenic, methacrylate and 2-vinylpyrrolidone prepared via free radical polymerization, were used in the thermolysis of dicobalt octacarbonyl ($Co_2(CO)_8$) to yield polymer-coated cobalt nanoparticles. In this report, the as prepared cobalt nanoparticles self-assembled into a head-to-tail morphology when deposited on a supporting substrate under zero field conditions (Figure 1.7). Later, Hess and Parker conducted a comprehensive investigation using a wide range of polymer surfactants to determine the optimal conditions for the synthesis of ferromagnetic nanoparticles.[114] The concept of using functional polymeric surfactants to stabilize ferromagnetic Fe nanoparticles was later revisited by Smith et al. at Xerox using polybutadiene and poly(styrene-*random*-4-vinylpyridine) copolymer surfactants.[115, 116] In 2002, Stöver et al. elegantly demonstrated the synthesis of ferromagnetic polymer coated iron nanoparticles using a series of functional copolymers in the thermolysis of iron pentacarbonyl.[117] Using similar thermolysis reaction, Philipse et al. later reported the synthesis of polymer coated iron nanoparticles with tunable particle sizes in the range of 2 to 8 nm in diameter using polyisobutene as ligands. [118, 119]

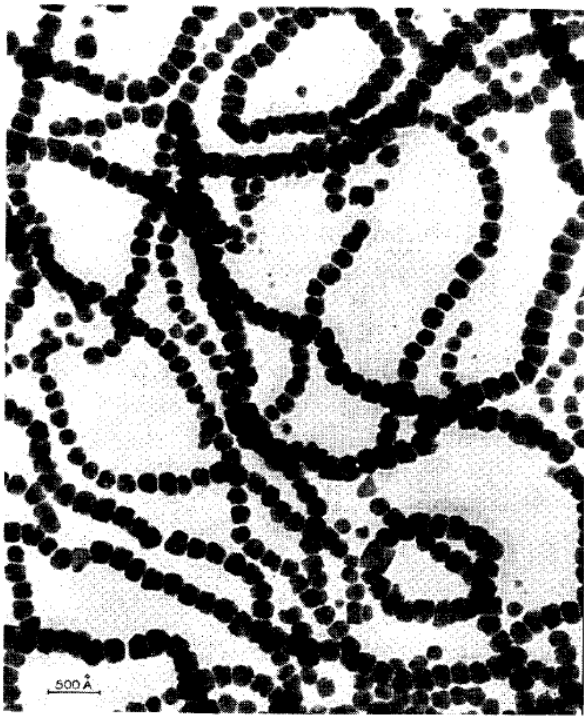

Figure 1.7: TEM image of ferromagnetic cobalt colloids prepared by the thermolysis of $Co_2(CO)_8$ using PVP terpolymer stabilizers. Reproduced with permission from ref. 111. Copyright 1966, American Institute of Physics.[111]

In previous methodologies, polymeric surfactants based on styrenic, methacrylate, 4-vinylpyridine and 2-vinylpyrrolidone used in the synthesis of magnetic nanoparticles were prepared via free radical polymerization, which were polydispersed and compositionally heterogeneous. Bronstein and Antonnieti were the first to report the utilization of well-defined block copolymer surfactants in the synthesis of core-shell polymer coated ferromagnetic nanoparticles.[120] In this method, amphiphilic block copolymers of poly(styrene-*block*-4-vinylpyridine) (PS-b-P4VP) of controlled molar mass and composition were exploited as micellar templates for the nucleation and growth of ferromagnetic nanoparticles. The PS-b-P4VP phase-separated into micelles with the outer corona of PS and the inner core of P4VP in a toluene dispersion containing dicobalt

octacarbonyl ($Co_2(CO)_8$) as the cobalt precursors. In this system, the thermolysis of $Co_2(CO)_8$ occurred both in and outside of the micellar templates at high loading of the cobalt precursors, which yielded both superparamagnetic and ferromagnetic nanoparticles with ill-defined size and morphology. Kramer et al. later revisited this strategy in using block copolymer surfactants of poly(styrene-*block*-2-vinylpyridine (PS-*b*-P2VP) as 'nanoreactors' to yield ferromagnetic cobalt nanoparticles that self-assembled into chains morphology.[121] Using PS-*b*-P2VP block copolymer films as templates, the Cohen group adopted a slightly different approach by first preparing a dispersion of $Co_2(CO)_8$ in the presence of excess 2-vinylpyridine.[122] In this modified method, the cobalt-pyridine organometallic clusters selectively sequestered into the poly(2-vinylpyridine) block during solvent casting. Upon thermal decomposition of the organometallic precursors within the PS-*b*-P2VP block copolymer film, the synthesis of ferromagnetic cobalt nanoparticles segregated within the PVP domains was demonstrated.

Despite numerous reports on the preparation of ferromagnetic nanoparticles since the 1960s, extensive investigations in this area have not been conducted due to the challenges in producing uniform sized nanoparticles that are easily isolated and readily handled. It was not until the late 1990s, when new synthetic techniques in preparing well-defined quantum dots were developed, which enabled the synthesis of nanoparticles with controlled size and shape.[33, 40, 123] In the case of dipolar magnetic nanoparticles, Alivisatos and Krishnan applied the facile hot injection method to synthesize uniform-sized magnetic cobalt nanoparticles using small molecule ligands (i.e.: oleic acid and trioctylphosphine oxides (TOPO)) (Figure 1.8).[124, 125] The synthesis of single domain

cobalt nanoparticles (Co diameter < 70 nm is single domain)[44] with tunable particle size (10 – 16 nm) were demonstrated by combining the small molecule surfactants in the thermolysis of dicobalt octacarbonyl ($Co_2(CO)_8$).[124, 126] In this elegant method, cobalt precursors were rapidly injected into a hot binary surfactants mixture (T = 185 ºC), which provided temporal separation of the nucleation and growth periods.[127] Additionally, the mixture of oleic acid and TOPO ligands enabled sufficient passivation of the cobalt nanoparticles, while promoting dynamic atom exchange with the metal species through Ostwald ripening. The combination of these factors enabled the synthesis of nearly monodisperse cobalt nanoparticles. 1-D and 2-D magnetic assemblies were realized using these well-defined building blocks due to their dipolar attractions, inter-particle interactions, and narrow size distributions.[128] Ferromagnetic cobalt nanoparticles (with diameter > 16 nm) that self-assembled in 1-D morphology were synthesized by varying the feed ratios between the cobalt precursors to the small molecule surfactants (Figure 1.7 (b)). In addition to the synthesis and assembly of well-defined spherical cobalt nanoparticles, Puntes and Alivisatos had also successfully prepared anisotropic cobalt nanodisks (dimensions = 4 x 35 nm) that self-assembled into linear arrays with co-facial stacking morphologies.[126, 129] In this system, the low aspect ratio nanodisks adopted an in-plane magnetization due to the dominant shape anisotropy, which was supported by both theoretical calculations and experimental studies of magnetic nanodisks prepared lithographically.[130, 131] The 1-D co-facial self-assemblies were explained by the favorable anti-parallel coupling of magnetic spins between neighboring nanodisks to minimize

magnetostatic energy of the system as well as the favorable van der Waals interactions between surfactant tails along the long axis of the nanodisks.

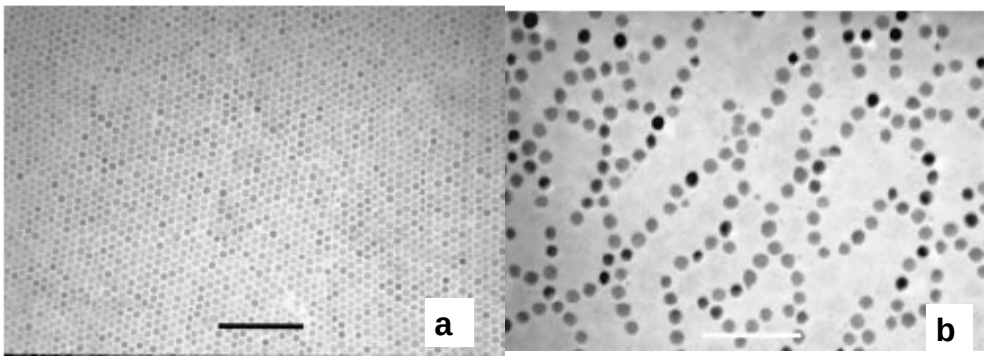

Figure 1.8: Self-assembly of small molecules capped cobalt nanoparticles prepared via hot injection method: (a) superparamagnetic CoNPs with D ~ 10 nm self-assembled into hexagonal 2-D arrays, and (b) ferromagnetic CoNPs with D ~ 16 nm self-assembled in nose-to-tail orientation. Reproduced with permission from ref. 124. Copyright 2001, AAAS. [124]

Further advancement in the development of ferromagnetic nanoparticle synthesis was explored by Keng et al. using well-defined polymeric ligands in the thermolysis of organometallic precursors. End functional polystyrenes bearing amine, phosphine oxide or carboxylic acid group were prepared via controlled radical polymerization, which enable facile controlled over polymer chain length, composition and functionality. This approach synergistically coupled the versatility of polymer surfactants and the hot injection method to yield uniform size polymer-coated ferromagnetic cobalt nanoparticles (D ~ 20 nm) that self-assembled into 1-D mesoscopic chains.[44, 132, 133] This system was attractive as the polymer shell imparted steric stabilization to the ferromagnetic core and enabled functionalization through the modification of the polymer corona. These polymer-coated ferromagnetic cobalt nanoparticles self-assembled into 1-D mesoscopic

chains due to their strong dipolar interactions, which was consistent with previous simulations of interacting dipolar colloids.[92, 94] In this work, rigid alignment of 1-D mesostructures composed of discrete nanoparticles were demonstrated upon application of an external field. Additionally, the study by Keng et al. demonstrated the formation of a novel dipolar morphology, which resembled lamellae-like folding of 1-D nanoparticle chains. This report provided the first experimental observation for the organization of strongly coupled dipolar colloids into dense arrays of lamellae-like morphologies, which was previously predicted by Weis et al.[97] In these Monte Carlo simulations, the formation of highly ordered 1-D mesostructures was due to the strong head-to-tail dipolar associations and weaker lateral associations between nanoparticle chains via anti-parallel alignment of unpaired spins (Figure 1.9))

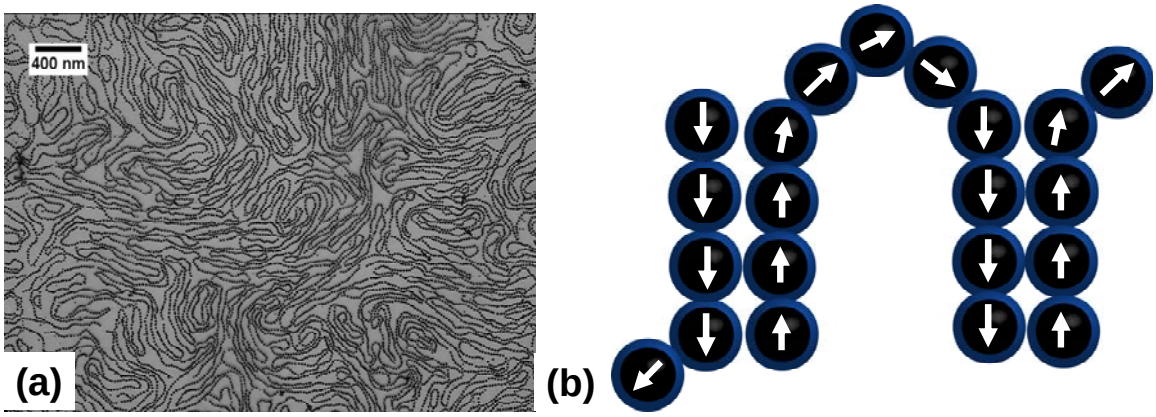

Figure 1.9: (a) TEM images of self-assembled PS-CoNPs (D ~ 21 nm) exhibiting local nematic liquid crystalline ordering in zero field. (b) Illustration of dipolar interactions in conjunction with lateral associations of nanoparticle chains via anti-parallel configurations of the magnetic moments as predicted by Monte Carlo simulations of Weis. Reproduced with permission from ref. 133. Copyright 2007, American Chemical Society.[133]

1.4.3 Self-assembly of ferromagnetic nanoparticles into flux-closure nanorings

The self-assembly (i.e.: zero field conditions) of ferromagnetic nanoparticles into flux-closure rings was first predicted by de Gennes and Pincus in the 1930's. Alivisatos[124] and Philipse[119] demonstrated the first experimental reports of the self-assembly of ferromagnetic nanoparticles into rings. In these reports, both chains and closed-loops morphologies were observed as competitive structures with high energy, high entropy (chains) and low energy, low entropy (closed-loops).[93] Wei et al. later showed that the assembly of dipolar colloids into bracelets can be controlled using sterically hindered resorcinarene surfactants.[134] Further investigation of the magnetic flux density via electron holography[108] confirmed that dipolar coupling between cobalt nanoparticles could be imaged, and the orientation within the nanoparticle rings exhibited well-defined reversible polarizations (clock-wise or counter-clock wise) (Figure 1.10 (d)).[106] These nanostructured magnetic bracelets (D ~ 100 nm) are attractive for potential application in ultradense information storage and as switches for non-volatile random-access memory (NVRAM).

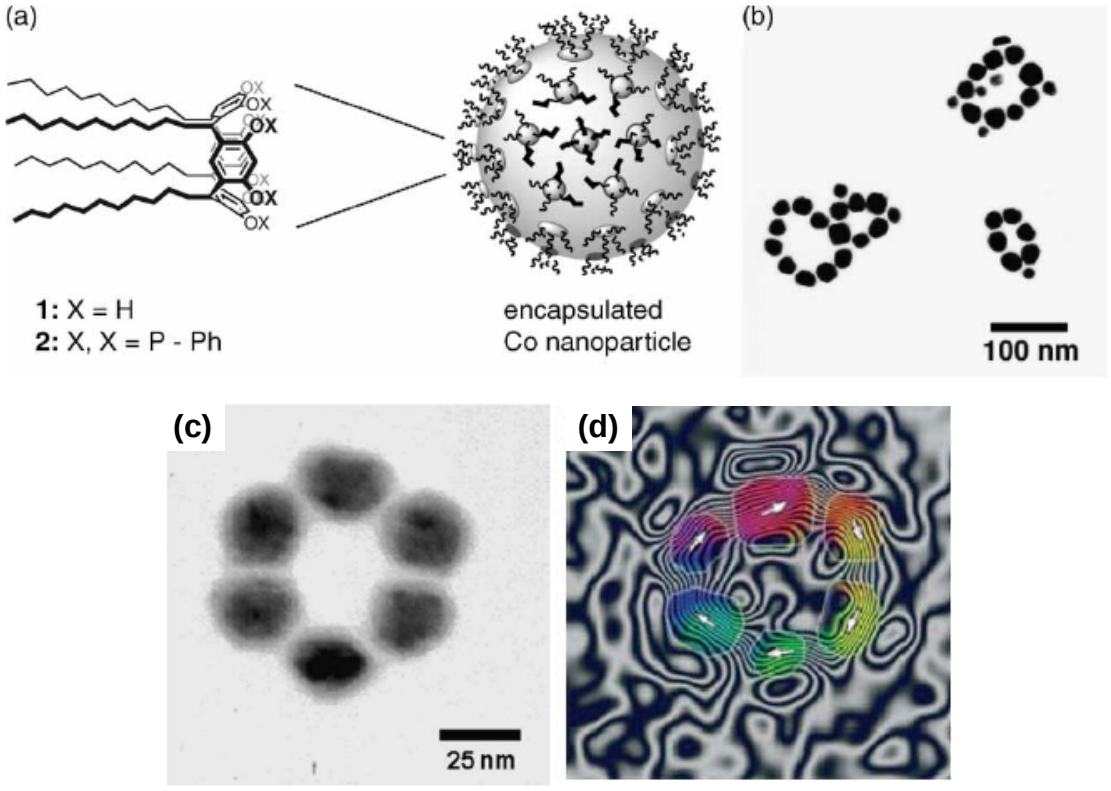

Figure 1.10: (a) Co nanoparticles stabilized with C-undecylcalix[4]resorcinarene were prepared by the thermolysis of $Co_2(CO)_8$. (b) TEM image of bracelet-like Co nanoparticles rings. (c) TEM image of the radially symmetric nanorings and (d) electron hologram of magnetic induction, with clockwise polarization indicated by the white arrows.[135] Reproduced with permission from ref. 135. Copyright 2002, American Chemical Society.[135]

Keng et al. reported the formation of magnetic bracelet assemblies by controlling the chain length and functionality of the polymeric ligands via controlled radical polymerization. In this system, bracelets were formed in high yield by increasing the polymer chain lengths from M_n = 4800 g/mole; M_w/M_n = 1.08 to M_n = 12000 g/mole; M_w/M_n = 1.10 used in the synthesis of ferromagnetic cobalt nanoparticles (Figure 1.11). The higher molecular weight polystyrene ligands resulted in increased separation between interacting colloids, thus weakening dipolar attractions of cobalt nanoparticles in

the system. This observation was supported by rule based simulations (Figure 1.6)[101], in which the formation of nanorings were observed with weakening of dipolar associations.[133]

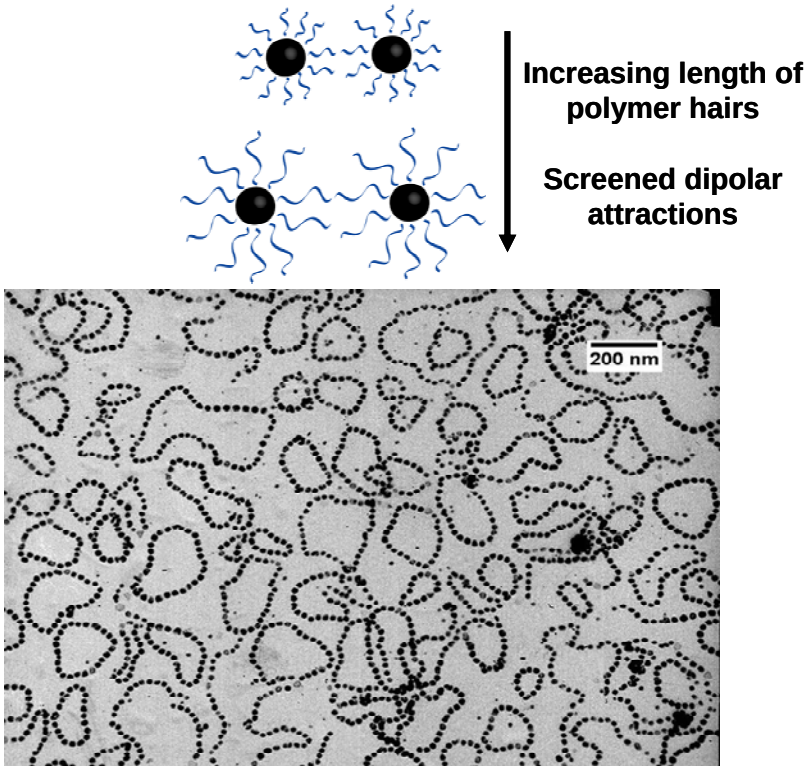

Figure 1.11: (Top) Illustration of the effect of increasing the length of the polymer hairs to the dipolar attractions. (Bottom) TEM image of bracelet-flux closure rings of PS-CoNPs cast from a chlorobenzene dispersion in zero field. Reproduced with permission from ref.133. Copyright 2007, American Chemical Society.[133]

Xiong et al. reported the synthesis of magnetite nanocubes (D = 50 nm) via the solvothermal oxidation approach in the presence of poly(vinylpyrrolidone). The magnetite nanocubes were found to preferentially assemble into flux-closure loops due to their strong magnetic dipoles. Additionally, the magnetic shape anisotropy arose from varying magnetization and orientation at different faces contributed to the overall magnetization. In a control experiment, 20 nm magnetite nanocubes were observed to

only self-assemble into chain structures, which indicated that only larger nanocubes possessing higher magnetization was necessary to overcome energetic barrier involved chain bending and an entropic cost of constraining unpaired end dipoles to the same region.[136] This hypothesis was further applied to Ni-Co magnetic alloy (D = 30 nm) that self-assembled into flux-closure nanorings.[137] When the magnetization of the Ni-Co nanoparticles was decreased by lowering the Ni content, only 1-D assembly was observed. The significance of this report was the stability of these magnetic bracelets. In an applied field, the ring morphology was maintained and aligned in the direction of the field (Figure 1.12). This behavior was reported for the first time, since in previous examples of flux-closure nanorings, the formation of linear assembly dominated upon application of an external field as the magnetic moment saturated along the direction of the field. This unique magnetic behavior suggested that these bracelets were permanently linked via metal-metal or metal-oxide bonding.

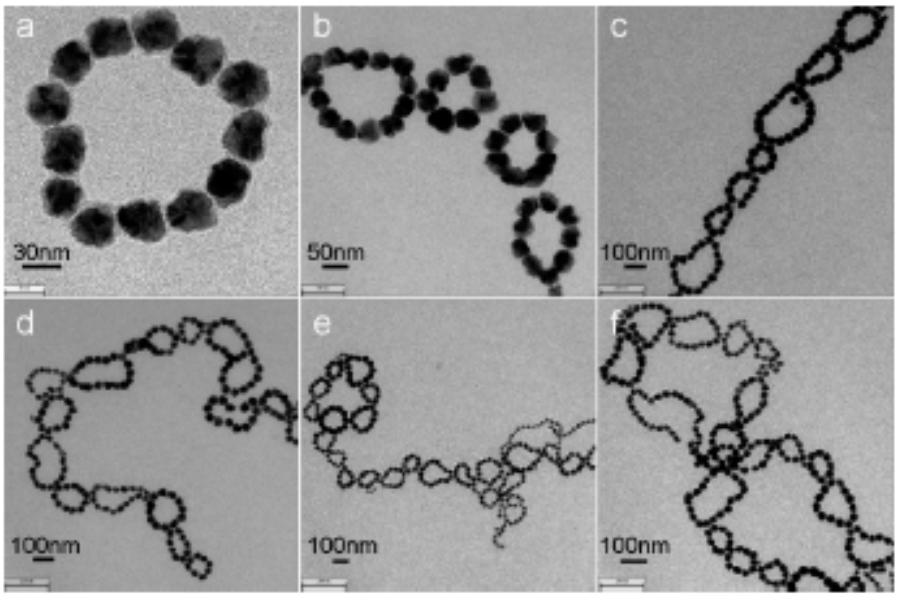

Figure 1.12: TEM images of NiCo nanorings with different assembled nanostructures. Reproduced with permission from ref. 137. Copyright 2008, American Chemical Society.[137]

1.4.4 In-situ characterization of dipolar assemblies

The self-assembly of dipolar nanoparticles into linear chains and flux-closure nanorings presented in previous sections were commonly studied using conventional transmission electron microscopy (TEM) technique due to the nanometer length scales. Although dipolar assembly of ferromagnetic colloids under zero field conditions have been investigated on supporting surfaces, in-situ experimental demonstrations of magnetic self-assembly were inhibited by the lack of a versatile imaging technique. The early work of Cebula et al. reported the utilization of small angle neuron scattering (SANS) technique to probe microstructures of cobalt particles dispersed in organic media.[138, 139] In the presence of an external magnetic field, strong anisotropic scattering were observed indicating the formation of chain-like structures. Although SANS has been proven to be effective in probing microstructures of dilute magnetic nanoparticles dispersions, this technique cannot readily distinguished structural differences between discrete linear chains and branched networks of nanoparticles.[140, 141] The ability to directly image defect structures from well-defined 1-D mesostructures is crucial in determining structure-property correlations for self-assembled nanomaterials.

The first *in situ* observation of dispersed magnetic nanoparticles in 1-D morphology was reported by Butter and Philipse via cryogenic-TEM.[90, 119] This technique involved a fast vitrification of nanoparticle dispersions, thus arresting the diffusion of magnetic colloids. As a result, direct visualization of the dispersed magnetic

colloids in solution can be achieved, confirming the early theoretical work by de Gennes and Pincus[85], as well as the Monte Carlo simulations reported by Chantrell.[86, 87] By systematically increasing the particle size and consequently the magnetization, the transition from discrete particles to randomly oriented linear aggregates or networks was elegantly demonstrated in this work.[119]

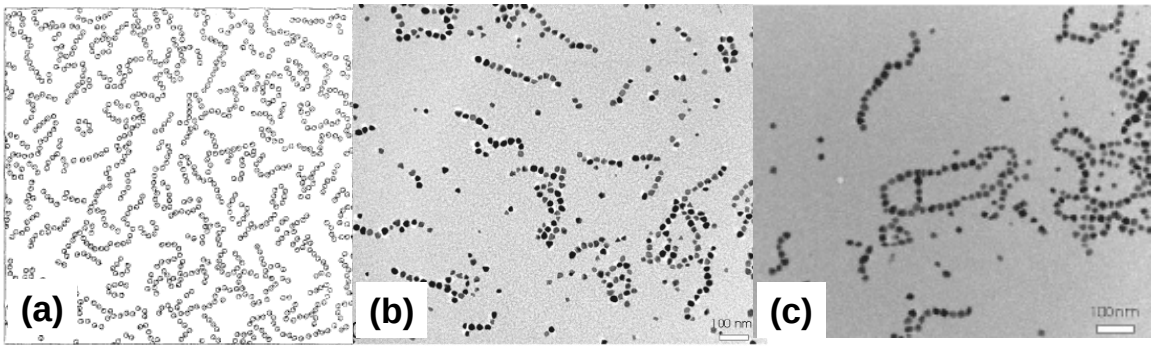

Figure 1.13: (a) A two-dimensional Monte Carlo simulation on 15 nm magnetic Co particles by Chantrell et al.[86] showing formation of dipolar and flux-closure rings in zero field. (b) and (c) A typical in situ cyro-TEM images (zero field) of vitrified magnetite dispersion (D ~ 21 nm) forming structures comparable to those of the simulation in (a). Reproduced with permission from ref. 90. Copyright 2004, American Chemical Society.[90]

An alternative method to observe *in situ* assembly of dipolar nanoparticles was developed by Benkoski et al.[101, 142, 143] In this method, known as Fossilized-Liquid-Assembly (FLA), magnetic nanoparticles were assembled at a crosslinkable oil-water interface under both field-induced and zero field conditions. Upon rapid photopolymerization, the segregated nanoparticles at the interface were permanently fixed, thus providing a 'snapshot' of the assembly process via atomic force microscopy (AFM) (Figure 1.14). This FLA technique provides an attractive alternative method to

cryogenic-TEM technique for direct visualization of dipolar assembly in dispersed organic media.

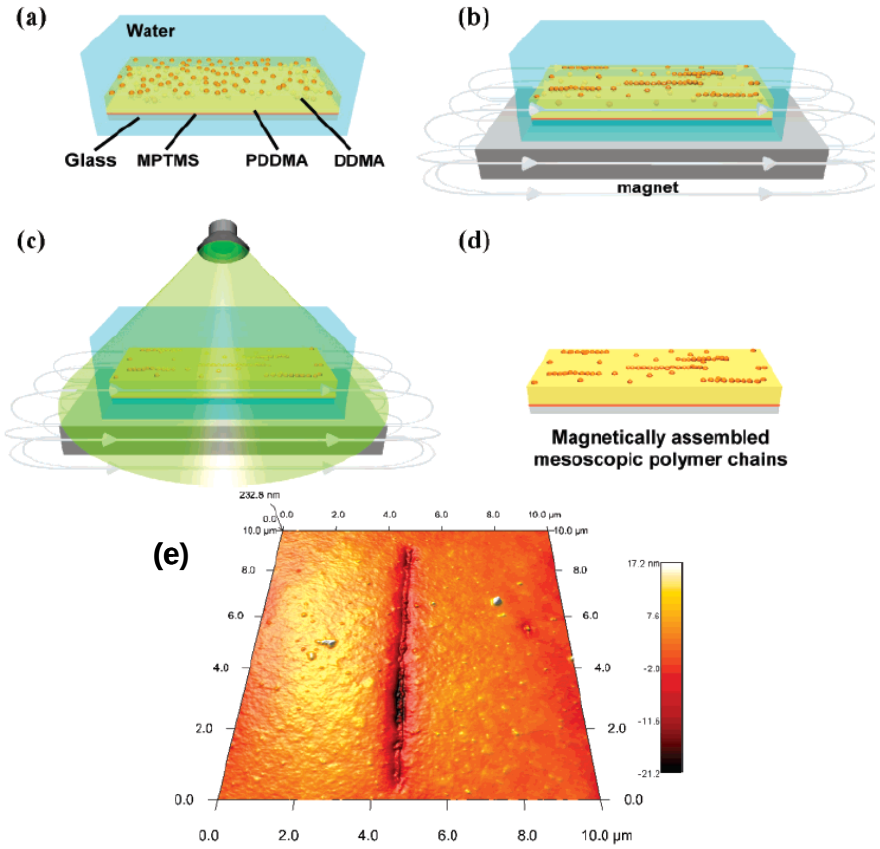

Figure 1.14: Schematic of Fossilized Liquid Assembly (FLA). (a) PS-CoNPs dispersed in a crosslinkable oil-water interface, (b) a permanent magnet with 8 mT field was applied, (c) Once PS-CoNPs segregated to the oil-water interface and aligned with the magnetic field, the sample is "fossilized" via UV photocrosslinking. (d) Sample was rinsed prior to AFM chacterization. (e) AFM height image of an aligned meso-polymer chain assembled under the influence of an 8 mT magnetic field from 24 nm PS-CoNPs. Reproduced with permission from ref. 144. Copyright 2007, American Chemical Society.[144]

1.5: 1-D Assemblies of Magnetic Nanoparticles with D < 20 nm

When the dimension of a single domain, ferromagnetic colloid (~ 20-100 nm) is decreased below a critical size (superparamagnetic sizes for Fe = 16 nm and Co = 7.6 nm

at 300 K)[145], the reduced number of aligned magnetic spins can no longer compete with thermal fluctuations (kT). Thus, superparamagnetic nanoparticles cannot self-assemble into dipolar morphologies, in an absence of a magnetic field, due to the lack of a net dipolar magnetization. The magnetic dipoles can be aligned to create a net magnetic moment by applying an external magnetic field. Upon removal of the field, superparamagnetic particles return to a random state with zero net moment. This behavior is found to be very similar to paramagnetic particles, except that the magnitude of magnetization in superparamagnetic nanoparticles is significantly higher; hence a relatively weak field is sufficient to reorient the magnetic spins. Another attractive feature of superparamagnetic nanoparticles is the small particle size ($D < 20$ nm), which makes these colloids suitable for a number of applications, ranging from magnetic fluid, MRI contrast agent, catalysis, bio-molecule tagging and separations.[41, 43, 146]

Investigation of magnetic fluids composed of single domain magnetite particles was pioneered by Elmore in the late 1930s.[147] The magnetization behavior of ferrofluids was determined experimentally by varying the applied magnetic fields (0-400 Gauss). The magnetic flux induced by the sample was detected using a sensitive galvanometer, in which magnetization curves for single domain ferrofluids were characterized. Later, Dave[148] and Hayes[149] reported the dynamics of ferrofluids at varying magnetic field strengths. Upon application of a static or an alternating field, colloidal suspensions aligned into aggregated needles that could be detected using optical microscopy. Upon removal of the applied field, the long needles began to break up into short chains and finally into an isotropic liquid.

Both parallel and perpendicular assemblies of superparamagnetic nanoparticles have been fabricated on supporting substrates by applying external magnetic fields during the assembly process. The formation of magnetic columns aligned parallel to the applied field has been achieved using magnetite nanoparticles (D = 8 – 12 nm) on GaAs substrate.[150] In the presence of strong magnetic fields (17 T), elongated clusters (length = 150 nm to 3500 nm with average width of 300 nm) of magnetite were formed along the direction of the applied field. The 1-D mesostructures exhibited significantly higher coercivity and remanence along their easy axis (parallel to the direction of the applied field) in comparison to the magnetizations measured in the perpendicular direction. Philipse and colleagues studied the dynamics of superparamagnetic nanoparticles assembly *in situ* via cryo-TEM. Based on this technique coupled with other simulations, gas-like structures of discrete superparamagnetic nanoparticles at zero field conditions were observed due to thermal fluctuations of the magnetic spins. In an applied field, the phase transition from discrete magnetite nanoparticles into a head-to-tail orientation with the nanoparticle easy axis aligned parallel to the applied field was observed via cryo-TEM. Additionally, the staggering of linear dipolar chains with neighboring chains to form columnar structures was observed in this study due to the strong dipole-dipole and coupling interactions to the magnetic field.[38, 90, 119, 151] Pileni et al. further investigated the influence of 1-D assembly on the collective magnetic properties of these assembled mesostructures.[1] Under the optimized conditions, discrete superparamagnetic cobalt nanoparticles were assembled into 2-D and 3-D columns parallel to the highly pyrolytic graphite (HOPG) substrate in an applied field.[1] The size and morphology of the columns

could be tuned by varying magnetic field strength. Magnetic properties of the assembled columns were found to increase both the dipolar coupling and remanence magnetization (M_r), in comparison to random assemblies of nanoparticles at zero field conditions. The enhancement in magnetic properties of the assembled columns was attributed to the structuring of nanocrystals into linear assemblies.[152]

Magnetic colloids have also been coupled with non-magnetic entities to improve their performance, reactivity, directional ordering and transport. In the field of electrochemical biosensors, Katz prepared conducting nanowires of Au-shell/$CoFe_2O_4$ by assembling the Au shell magnetic-core nanoparticles on an electrode surface in the presence of an external field. The core-shell nanowires showed enhancement in diffusional electrochemical processes in comparison to bare Au electrode due to the increased in surface area of the nanostructured electrode.[153]

In bulk samples, carbon nanotubes are randomly oriented, which results in lower electrical and thermal conductivities than expected.[154, 155] Various simulation studies have suggested that 1-D alignment of carbon nanotubes could improve the percolation pathways for direct electron transport in a macroscopic film, which remains a critical challenge for developing nanoelectronics.[155] To improve the electrical conductivities of carbon nanotubes, magnetic nanoparticles were utilized to align the random morphology of carbon nanotubes into a controlled, 1-D assembly. Specifically, magnetic nanoparticles were attached onto carbon nanotubes via electrostatic interactions, followed by magnetic alignment to yield discrete carbon nanotubes with 1-D ordering.[156] More recently, Muller et al. developed a versatile and template-free method called,

'magnetization-alignment-demagnetization' (MAD) process to assemble telluride nanorods into hierarchical 1-D mesostructures (Figure 1.15).[157] In the MAD process, the telluride nanorods were functionalized with superparamagnetic iron oxides via hydrophobic polymer interactions. Subsequently, the magnetic nanocylinders of telluride were assembled into ordered 1-D structures in an applied magnetic field. Finally, in the demagnetization step, iron oxide nanoparticles were etched away to yield 1-D assembly of telluride nanocylinders.

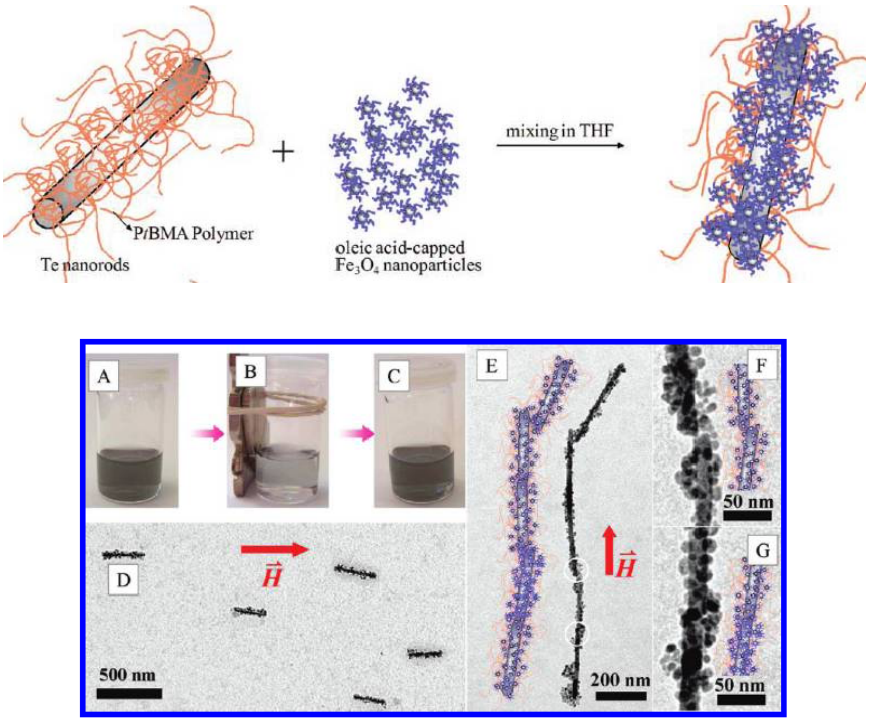

Figure 1.15: Illustration of the alignment of Te nanocylinders coated with superparamagnetic iron oxide nanoparticles (top), (a) – (c) Magnetoresponsive Te nanocylinder towards the external magnet; (d) TEM image of aligned magnetic nanocylinder when deposited onto a carbon-coated TEM grid in the presence of an magnetic field (0.3 T); (e) linear connection of aligned magnetic nanocylinders; (f) and (g) Enlarged views of the junctions of the magnetic nanocylinders indicated by the white circles panel E. Reproduced with permission from ref. 157. Copyright 2009, American Chemical Society.[157]

The use of 1-D magnetic assembly in biological applications was demonstrated using $CoFe_2O_4$-tagged microtubules. The functionalized microtubules could be easily placed and transported to a specific target via an external magnetic field, thus enhancing binding efficiency.[41, 158] Similarly, magnetic chains have been synthesized to bind and manipulate the placement of immuno-labeled cells via an external field.[159]

Previous magnetically-induced assembly approaches focused on the fabrication of 1-D nanostructures on surfaces. Walker et al. demonstrated the formation of centimeter-long, 1-D mesostructures of cobalt nanoparticles in solution via magnetic-field-induced (MFI) assembly.[160] Upon removal of the external field, the rigid chain relaxed into flexible polymers that formed closed loops to minimize magnetostatic energy of the unpaired dipoles. Further agitation resulted in the formation of 3-D globular structures and discrete nanoparticles. Later, Xiong et al. showed that magnetite nanochains prepared via MFI assembly could be isolated and redispersed. In this method, superparamagnetic magnetite nanoclusters (D ~ 120 nm) were assembled in the presence of an external field to afford 1-D nanochains that were stable against ultrasonic dispersion. Preservation of the chain-like morphology was attributed to the emergence of a collectively weak ferromagnetic behavior exhibited by the nanochains during MFI assembly (Figure 1.16).[161]

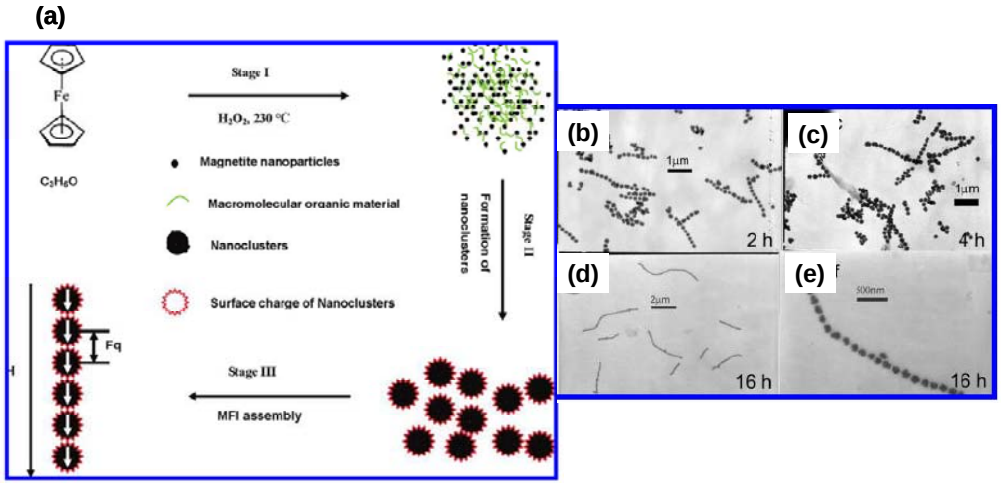

Figure 1.16: (a) Schematic illustration of the formation of 1D nanochain structures. TEM images of nanochains at different magnetization times: (b) 2 hr, (c) 4 hr, (d) and (e) 16 hr.[161] Reproduced with permission from ref. 161. Copyright 2009, American Chemical Society.

In addition to parallel alignment of magnetic nanoparticles on supporting substrates, perpendicular assemblies have also been demonstrated to form ordered columns spanning several micrometers in length. Pileni et al. first demonstrated the assembly of magnetic cobalt nanoparticles into dots, columns and labyrinth mesoscopic structures depending on the direction and strength of the applied magnetic field. In this work, highly oriented pyrolytic graphite (HOPG) substrate was immersed into a magnetic nanoparticle dispersion.[162] The solvent was evaporated in a controlled environment, which resulted in 1-D mesostructures that could be tuned by varying the strength of the applied field. At a low magnetic field (0.01 T), micrometer-sized dots assembled in hexagonal closed-packed arrays were obtained. At 0.27 T field strength, the magnetic dots transformed into columnar structures, while the formation of worm-like and labyrinth mesostructures were observed at high magnetic field strengths (0.78 T) (Figure 1.17).[162] One of the key parameters in influencing the formation of ordered mesoscopic

structures was the size distributions of the magnetic nanoparticle building blocks. Nanoparticles with large size distributions were found to induce coalescence of columns into a labyrinth-like morphology due to the presence of defect sites at the interfaces.[39, 163, 164] Based on similar strategy, columnar structures composed of cobalt nanoparticle building blocks were prepared on SiN_3 substrates by drop casting the nanoparticle dispersions in the presence of a perpendicular field.[165] Similarly to the work of Pileni et al., defective structures such as 'broken' and 'fallen' cylinders were present due to attractive capillary forces.[165]

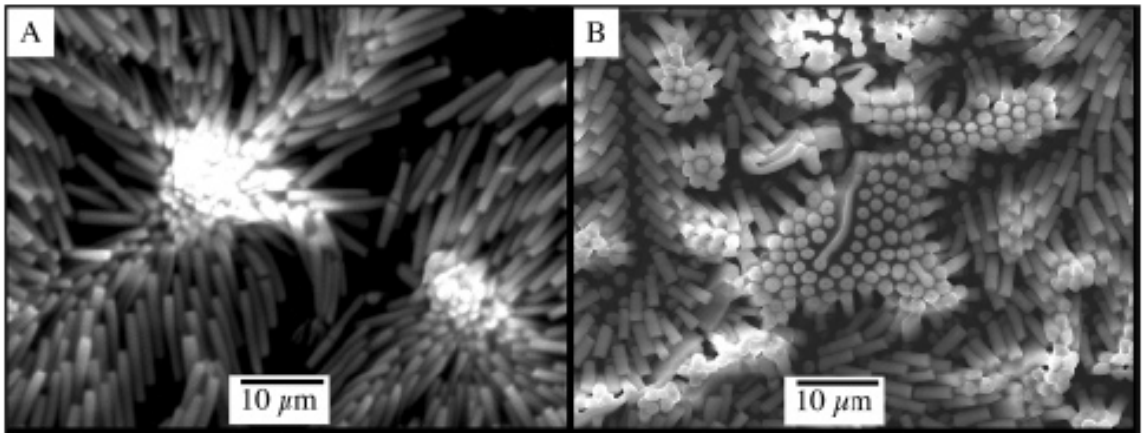

Figure 1.17: SEM patterns of columns formed with different magnetic field strengths: (a) 0.17 T, (b) 0.33 T on a HOPG substrate. Reproduced with permission from ref. 164. Copyright 2005, American Chemical Society.[164]

More recently, Cheon at al. successfully assembled cobalt nanoparticles into highly ordered and crystalline columnar structures between magnetic poles that were applied perpendicularly from the supporting substrate.[166] Under appropriate conditions, cobalt nanoparticles were magnetically assembled into highly crystalline face-centered-cubic (f.c.c) columns with controlled shape and size (Figure 1.18).[166] These supercrystal

Co nanorods exhibited unique and improved magnetic properties, which arose from the high crystallinity and anisotropy of these structures. Pileni et al. arrived at similar conclusions based on theoretical and experimental reports on the mesoscale alignment of magnetic nanoparticles.[1, 38, 167]

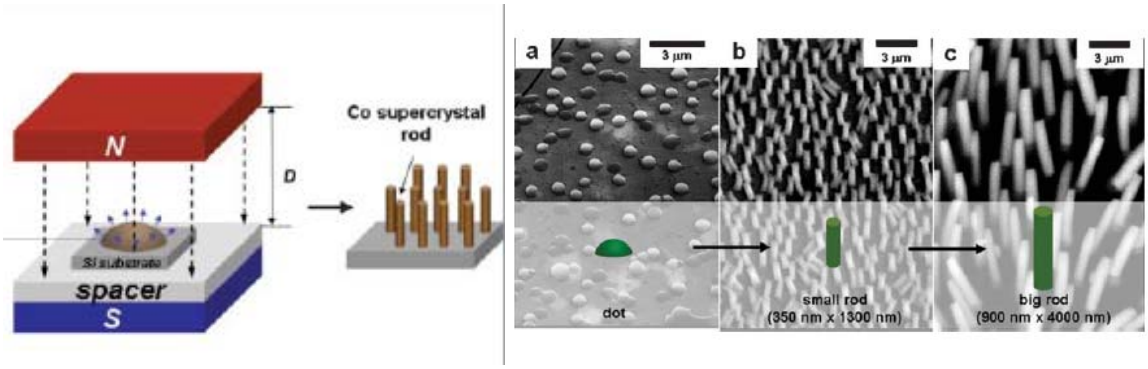

Figure 1.18: Schematic of Co supercrystal formation (left). (a) Supercrystal dots obtained in an absence of a magnetic field; (b) and (c) Supercrystal rods obtained by evaporation of 10 mM and 100 mM Co nanoparticle solutions, respectively. Reproduced with permission from ref. 166. Copyright 2004, Kluwer Academic Publisher [166]

1.6 Dipolar Assemblies and Chemical Crosslinking

There has been considerable research interest in manipulating colloids to mimic atoms and molecules as building blocks towards complex hierarchical structures at the colloidal length scale.[25, 168-170] This approach provides the opportunity to assemble and link nanoparticles in a controllable and predictable manner leading to novel 1-D functional materials. However, the development of robust synthetic routes to assemble nanoparticle building blocks into 1-D morphology remains unexplored.[171] This challenge can be overcome through the use of dipolar colloids with inherent north and south dipoles embedded within the inorganic core to direct 1-D assembly. This process can be considered to be analogous to step-growth polymerization, in which the magnetic

nanoparticle mimicks a difunctional A-B small molecule monomer. Akin to polymer chemistry, this approach is anticipated to produce a variety of new 1-D mesostructures through the selection of specific colloidal monomers. In this section, various "chemical reactions" that were employed to form interconnected 1-D mesostructures will be discussed based on the following strategies: (1.6.1) *polymer bridging*, (1.6.2) *crosslinking chemistry*, (1.6.3) *sol-gel processes*, (1.6.4) *carbonization*, (1.6.5) *galvanic exchange reaction* and (1.6.6) nanoscale *Kirkendall reaction.* Lastly, a novel strategy referred to as 'Colloidal Polymerization' will be highlighted as a facile method to form functional 1-D mesostructures.

1.6.1 Polymer bridging

The concept of forming magnetic filaments was first demonstrated by Philip and Bibette et al. in 1997 using polyacrylic acid (weak polyelectrolyte) in the presence of an external magnetic field to bridge magnetic colloids into 1-D mesostructures. By controlling the concentration of the polyacrylic acid surfactants and the magnetic field strength, one-particle-wide magnetic filaments could be obtained.[172] In this system, the bridging mechanism involved inter-particle dipolar attractions in the presence of an external magnetic field, which subsequently led to the interpenetration of the absorbed polyacrylic acid surfactants on the particles surfaces. Under a high concentration of polyacrylic polymers and prolonged incubation time, the formation of irreversible magnetic filaments was observed despite the removal of the external magnetic field. The dependence on the polymer concentration and incubation time for the formation of irreversible magnetic filaments was consistent with the polymer bridging mechanism.

In 2003, Bibette et al. expanded this synthetic methodology to obtain long and flexible magnetic filaments as mechanical sensors, which were able to adopt hairpin morphologies under certain applied field conditions. The rigidity and length of the filaments were controlled by the magnetic field strength and the incubation period, as illustrated in Figure 1.19. This method exhibited potential for broadening the tools of micromechanical measurements, where bending modes were emphasized.[173] Given the interesting magnetoresponsive properties exhibited by these magnetic filaments (i.e.: hair pin structures), the investigation of other physical parameters such as temperature, incubation time, field strength, polymer chain length and concentration were conducted. This study enabled greater control over polymer-colloid interactions, leading to well defined 1-D mesostructures (Figure 1.18).[174, 175] The concept of polymer bridging was further exploited by other groups in preparing fiber-like superstructures of hollow nickel microspheres. In this method, poly(2-vinylpyrrolidone) served as both the spherical template as well as the 'bridging' agent to form interconnected nickel microspheres in a dipolar orientation.[176]

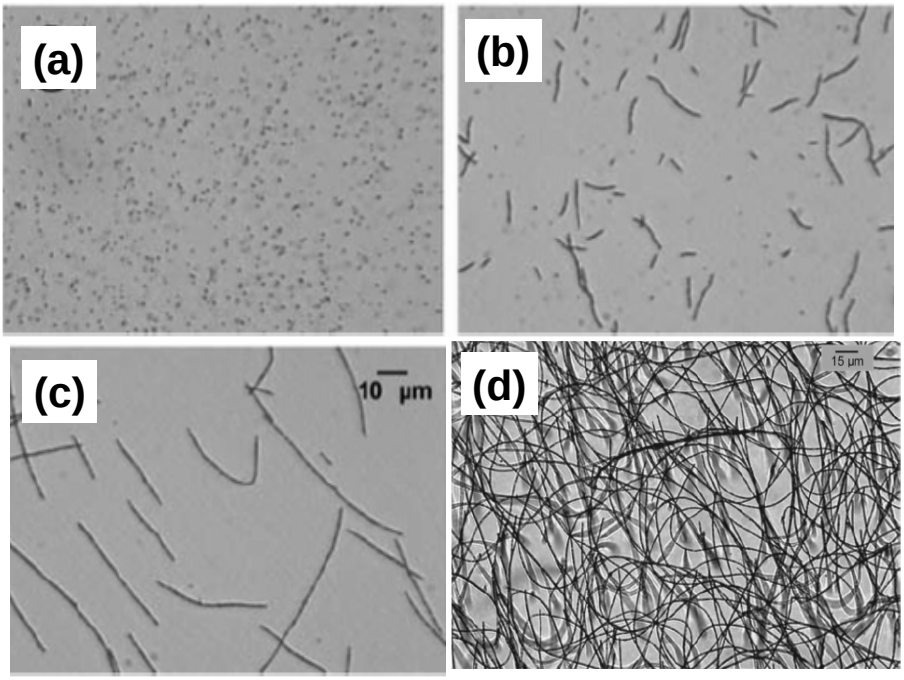

Figure 1.19: Optical images of the formation of magnetic filaments as a function of magnetic field intensity: (a) 5 mT, (b) 10 mT, (c) 15 mT and (d) 25 mT. Reproduced with permission from ref. 175. Copyright, 2005, American Chemical Society.[175]

Scaling down from sub-micrometer sized magnetic beads to nanometer sized superparamagnetic iron oxide nanoparticles (D = 10 – 12 nm), Minko et al. demonstrated the preparation of wire-like assembly by linking nano-sized superparamagnetic colloids using polyelectrolyte (poly(2-vinyl N-methylpyridinium iodide) under an applied field. In this work, the negatively charged Fe_3O_4 superparamagnetic nanoparticles were magnetically assembled in a dilute dispersion under an applied field. The pre-assembled nanoparticle chains were stabilized with the positively charged polyelectrolyte, yielding a robust magnetic nanowire.[177]

Based on a similar concept, Gu et al. demonstrated the assembly of cobalt nanoparticles into 1-D legume-like nanostructures by utilizing the combination of

magnetic field induced assembly and poly(2-vinylpyrrolidone) (PVP) as the bridging agent.[178] In this report, the 1-D assemblies of Co-PVP were preserved through the interpenetration of the absorbed PVP layers, despite the removal of the applied magnetic field. In separate reports, Gun'Ko showed that these aligned magnetic nanoparticles coated with either polyelectrolyte[179] or single stranded DNA[180], exhibited good biocompatibility with potential applications for *in vivo* MRI diagnostics. The aligned morphology revealed high relaxation times at a low field, which was attributed to the high local magnetic ordering of the superparamagnetic nanoparticles.

1.6.2 Chemical crosslinking

The seminal work of Gast et al. utilized a simple chemical crosslinking reaction to form permanent paramagnetic chains from micrometer sized beads.[181] These amine functionalized polystyrene beads (D ~ 1 μm) were assembled into chain-like structures by applying a perpendicular magnetic field in a flow cell (Figure 1.20). Due to the large particle sizes used in this system, the magnetic field induced assembly could be directly observed using optical microscopy. This versatile and convenient method allowed for particle concentration and the applied field strength to be tuned *in situ* to obtain well-defined 1-D assembly. Upon application of sufficient field strengths, dipolar interactions between paramagnetic beads exceeded thermal fluctuations, which forced particles to align into a head-to-tail morphology along the direction of the applied field. Then, the pre-assembled 1-D morphologies were locked by introducing a chemical crosslinker (gluteraldehyde), which resulted in the formation of permanent imine linkages along the magnetic chains. In an applied field, these magnetic chains rigidified and oriented along

the magnetic field lines. Upon removal of the field, these magnetic chains relaxed into flexible 1-D chains.

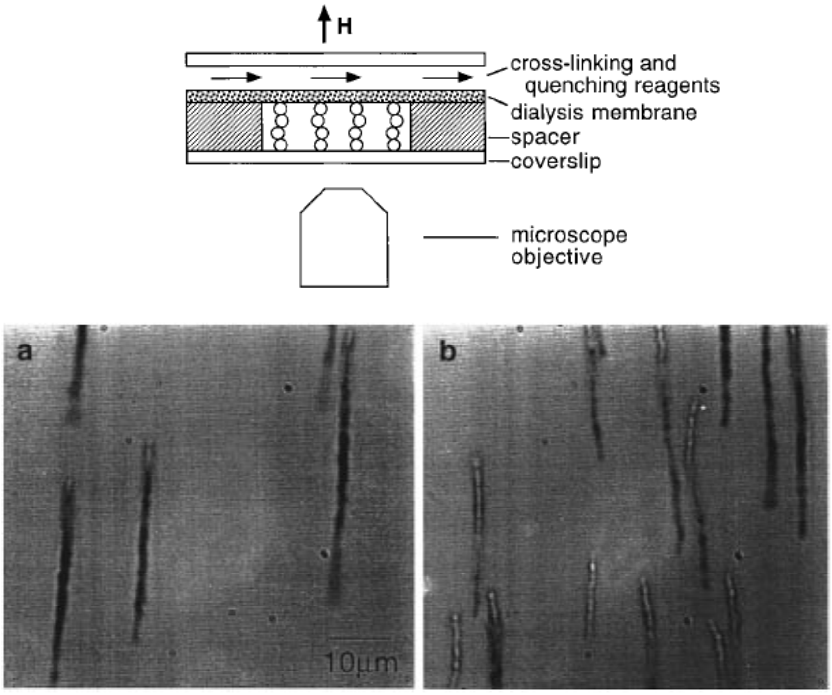

Figure 1.20: (Top) Schematic diagram of the flow cell showing monodisperse chain forming between a dialysis membrane and a glass cover slip. (b) Optical micrograph of chains oriented and rigid in field (b) chains showing flexibility when the field if off. Reproduced with permission from ref. 181. Copyright, 1998, American Chemical Society [181]

Furthermore, Gast et al. examined the mechanical properties of these covalently linked magnetic chains and aggregated magnetic columns via the optical trapping method. Briefly, in this technique, two laser beams are utilized independently in which, the first beam traps one end of the chain in a stationary position, while the second laser beam captures the other chain end to induce stretching and bending motions. In this investigation, tension was applied to the dipolar chains in the direction of the magnetic field for tensile strain ($\Delta L/L_0$) measurement. The tensile strain of a single magnetic chain

was found to increase with increasing field strengths. Additionally, to gain insight into the macroscopic properties of magnetorheological fluids, micromechanical properties of these dipolar chains were probed by inducing stress in the direction perpendicular to the applied field.[182, 183] This powerful and quantitative technique enabled the study of the mechanics of semi-flexible dipolar chains linked with poly(ethylene glycol) (PEG). Chain stiffness could be tuned by varying the length of the PEG crosslinker, which formed intriguing magnetoresponsive microstructures that can be exploited in microfluidic devices.[184] Later, Bibette et al. elegantly demonstrated the formation of a flexible artificial flagellum by linking magnetic colloids with complementary DNA. The magnetic filaments were subsequently coupled with a red blood cell to replicate the "swimming" motion in the presence of an oscillating magnetic field (Figure 1.21).[185] Recently, Biswal et al. further investigated the stability and interparticle spacing of these DNA-linked magnetic chains as a function of the magnetic field strength to control the assembly of these colloidal molecules into ordered mesostructures.[186]

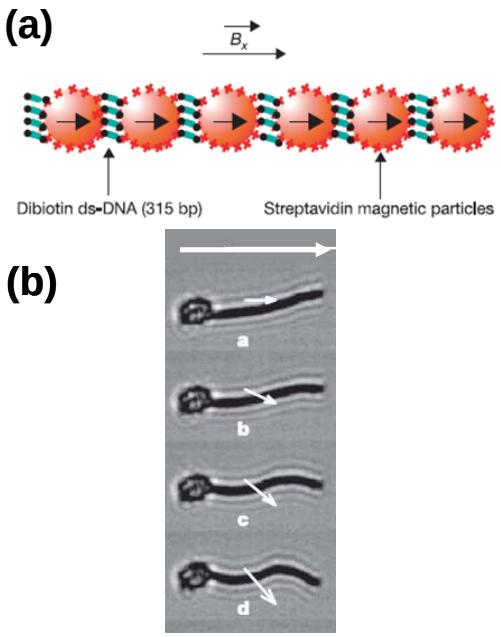

Figure 1.21: (a) Schematic representation of a flexible magnetic filament swimmer. The magnetic particles are coated with streptavidin (red cross symbols). Under an applied magnetic field B_x the particles form filaments. Double-stranded DNA with biotin at each end can bind the particles together via the specific biotion-streptavidin interaction. (b) Beating motion of the magnetic filament attached to a red blood cell.[185] Reproduced with permission from ref. 185. Copyright 2005, Nature Publishing Group.

Later, Hatton et al. demonstrated a similar magnetic assembly method using magnetic colloidal building blocks with D ~ 400 - 800 nm on a pre-patterned microchannel, which was previously reported by Hammond and Gast.[187] Hatton and his group improved the assembly process to a one-step method using polyelectrolyte coated magnetic beads that were absorbed onto the patterned spots, followed by covalent linking of the magnetically assembled beads via a simple amidation chemistry.[188]

The work by Gast and Hatton utilized sub-micrometer sized magnetic beads to fabricate magnetic filaments, which could be easily visualized under an optical microscope. As the particle size decreased to the nanometer regime, below the optical

diffraction limit, direct observation of these magnetic filaments was challenging and required cryogenic transmission electron microscopy technique under stringent conditions.[90] Despite these challenges, Benkoski et al. recently demonstrated the preparation of one-particle-wide magnetic filaments composed of 20 nm ferromagnetic nanoparticles. In this method, a custom built microscope stage was designed to observe the organization of nanoscopic building blocks into dense arrays of magnetic filaments anchored on a supporting substrate via magnetic attraction. These flexible microscopic filaments (1-15 μm) were oscillated with an alternating field, mimicking the actuation of cilium. Additionally, numerous control experiments were designed to confirm the formation of one-particle wide (D = 20 nm) magnetic filaments spanning micrometers in length.[189]

Similarly, Han et al. synthesized 20 nm ferromagnetic cobalt nanoparticles encapsulated with polymeric surfactants (poly(2-cinnamolyoxyethyl methacrylate)-block-poly(acrylic acid), PCEMA-*b*-PAA) (Scheme 1.1, Polymer I), functionalized with both passivating and crosslinking moieties.[161] The PAA segments selectively anchored onto the cobalt surfaces, while the PCEMA segments protruded into the solvent phase, allowing for further chemistry. Uniform sized ferromagnetic cobalt nanoparticles coated with PCEMA-*b*-PAA self-assembled into linear chains due to dipolar associations of the ferromagnetic core. The pre-assembled dipolar chains were crosslinked through the cinnamate functionality in the PCEMA segment via UV photolysis. In addition to TEM observations of the crosslinked polymer shells, the reaction was further verified by degrading the cobalt cores (Figure 1.22 (a)) with HCl. Hollow 1-D chains were observed

after the acid dissolution of the cobalt cores due to the preservation of the 1-D structures by the crosslinked polymer shells (Figure 1.22 (b)).

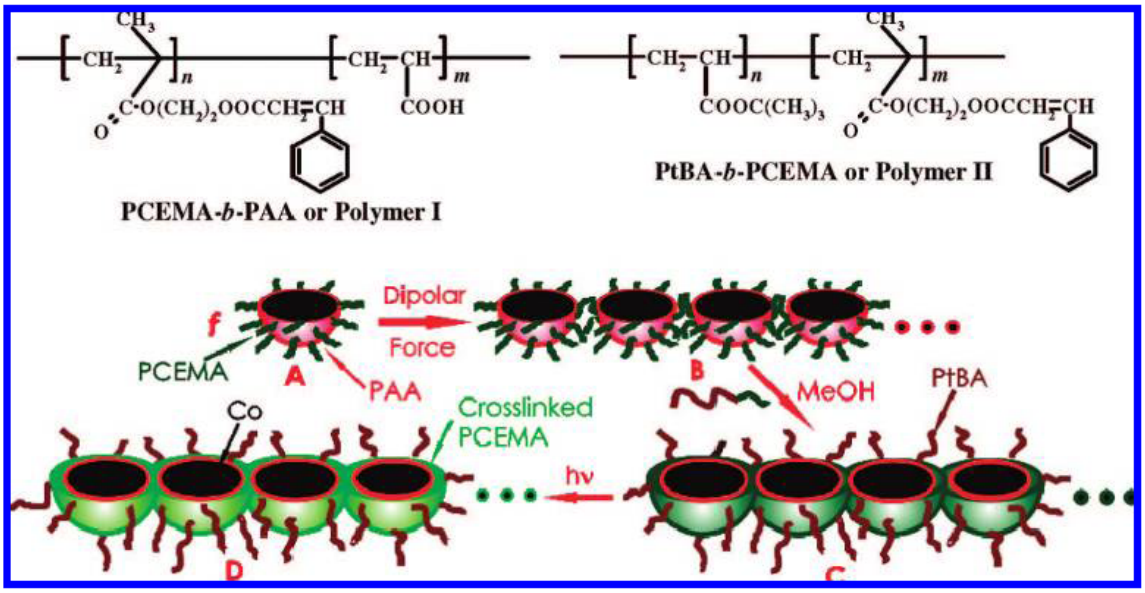

Scheme 1.1: Schematic representation for the formation of the permanently linked dipolar chains. PCEMA-b-PAA coated Co nanoparticles aggregated into linear chains due to magnetic dipole-dipole interaction. Subsequent photolysis with UV light crosslinked the PCEMA layer.[161] Reproduced with permission from ref. 161. Copyright 2009, American Chemical Society.

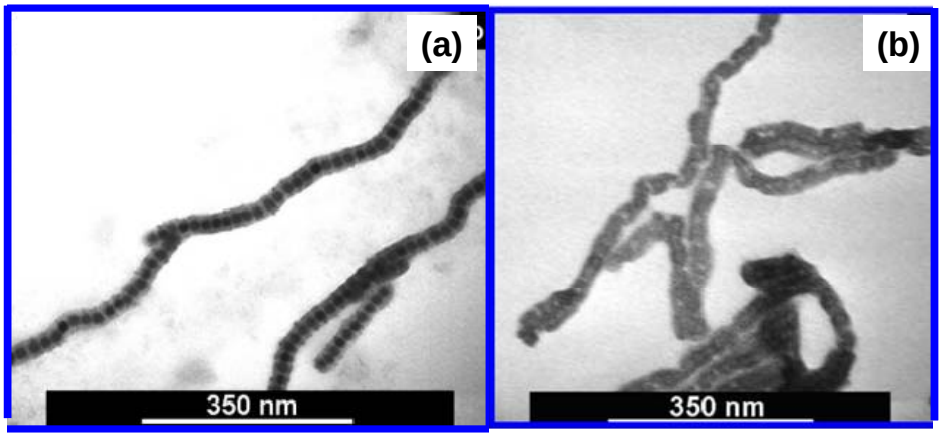

Figure 1.22: (a) TEM images of the polymer coated and crosslinked Co dipolar chains on carbon-coated copper grid. (b) TEM images of the residual polymer fibers (stained with RuO_4) with internal cavities after HCl dissolution of the Co core. Reproduced with permission from ref. 161. Copyright 2009, American Chemical Society.[161]

Stellacci and his group have successfully demonstrated an elegant strategy to assemble isotropic nanoparticles into anisotropic mesostructures. In this strategy, which was first demonstrated with gold nanoparticles, the phase separation of mixed ligands into alternated ring domains on nanoparticle surfaces resulted in the formation of two opposing defect points. These defect points allowed for selective functionalization of chemical handles at diametrically opposing poles.[25, 27, 28, 190] The chemical handles were subsequently reacted with a crosslinker molecule to form chains of nanoparticles. This concept was then extended to superparamagnetic iron oxide nanoparticles to create two defect points for further chemistry by decorating the nanoparticle surfaces with mixed ligands composed of nonanoic acid and 4-phenylbutyric acid (Figure 1.23).[191] The chaining reaction was performed by adding a diacid molecular linker into a two-phase polymerization reaction to yield 1-D assembly of iron oxide nanoparticles (Figure 1.23 (d)). The interparticle spacing could be tailored by adjusting the length of the molecular linker. Collective behavior of these 1-D chains of superparamagnetic iron oxides were studied via superconducting quantum interference device (SQUID). As expected, the 1-D chains of nanoparticles exhibited a higher blocking temperature (T_B) in comparison to isolated nanoparticles due to higher magnetic coupling along the dipolar chain.[170, 192-194] Rotello et al. demonstrated a different approach in controlling inter-particle spacing of superparamagnetic iron oxides by utilizing polyaminoamine dendrimers.[195] Based on this approach, the inter-particle spacing was systematically modulated by the dendrimer generation. As predicted, increased inter-particle spacing directly influenced the collective magnetic behavior of iron oxide nanoparticles, in which a decrease in blocking

temperature (T_B) was observed due to the weakening of magnetic coupling between particles.

In summary, chemical crosslinking reactions have been demonstrated as an efficient method to yield interconnected 1-D functional mesostructures via magnetic assemblies or selective ligand chemistry.

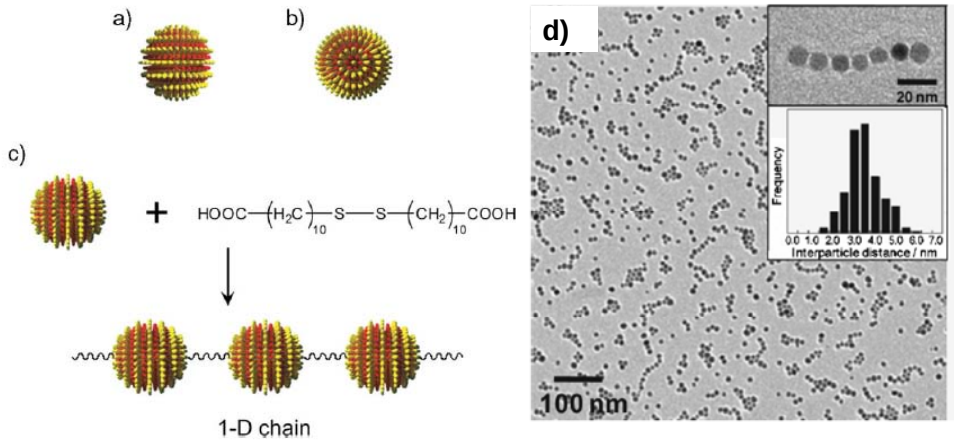

Figure 1.23: Schematic drawing of the (a) side view and (b) top view of the γ-Fe_2O_3 nanoparticles coated with mixed-ligand, nonanoic acid and 4-phenylbutyric acid. (c) The reaction of γ-Fe_2O_3 with molecular linker, 11-(10-carboxy-decyldisulfanyl)-undecanoic acid. (d) TEM image of the chains based on γ-Fe_2O_3 nanoparticles coated with mixed-ligand (nonanoic acid and 4-phenylbutyric acid, 1:1). Inset shows high magnification TEM image of the chain. Reproduced with permission from ref. 25. Copyright 2007, AAAS.[25]

1.6.3 Sol-gel processes

Philipse and colleagues demonstrated the fabrication of magnetic silica dispersions consisting of a single domain magnetite core encapsulated with silica shells.[196] Although the early work by Matijevic[197, 198] focused on protecting magnetic particles (hematite and iron) with silica shells, the main objective of this work was to develop a method to prepare core-shell particles that were stable in various media, and

were reversibly responsive to an external field.[196] Under appropriate conditions, magnetite-core silica-shell particles of varying shell thickness could be prepared by varying the amount of alkoxysilane precursors. During the sol-gel reaction, alkoxysilane precursors homogeneously nucleated onto the magnetite nanoparticles (D ~ 5 nm), yielding discrete core-shell nanoparticles with average diameter of 40 nm. When the exact reaction was performed in the presence of a static magnetic field, elongated shapes of magnetic silica nanostructures were formed. In the latter case, the strong external field oriented the dipoles in a head-to-tail morphology to achieve maximum interactions. The 1-D assembly was stable and persisted over a period of hours, allowing for the relatively slow condensation of tetraethoxysilanes to occur. Upon the hydrolysis and condensation reaction, dipolar assemblies were "cemented" into permanent 1-D nanostructures. Additionally, the effect of silica shell thickness to the dipolar attractions were determined both theoretically and experimentally. Experimentally, Philipse demonstrated that by increasing the silica shell thickness, the magnetic dipoles of the magnetite cores were completely screened by the non-magnetic layers. This observation could be explained theoretically by the increased of van der Waals interactions between two hard spheres with a diameter, σ. As the diameter of the core-shell increases, magnetic attraction decreases, following the simplified equation:

$$V_W(r) = -\sigma A/24(r - \sigma)$$

where A is the Hamaker constant, r is the distance between the two magnetic dipoles and σ is the diameter of the core-shell nanoparticles. Considering the interplay between

magnetic attractions and hard spheres repulsions, magnetite-silica core-shell nanoparticles with $r \sim \sigma$ behaved isotropically despite the presence of an external field.

Taking advantage of the advancement in nanoparticles synthesis since the late 1990s, Liz-Marzan and coworkers demonstrated an improved synthetic methodology towards the preparation of well-defined silica-coated cobalt nanoparticles via the sodium borohydride reduction method in the presence of citrate ions.[199] The size of the cobalt core and the silica shell thickness could be systematically tuned by varying the molar ratios of citrate ions, Co precursors, and the tetraethoxysilane. Based on this synthetic methodology, Salgueirino-Maceira and coworkers revisited the preparation of cobalt-core silica-shell 1-D nanostructures via a one-pot synthetic process.[200, 201] In the modified synthetic strategy, cobalt nanoparticles with D = 32 nm were first synthesized, followed by the addition of an ethanolic solution of the sol-gel precursor to yield 1-D cobalt nanoparticle chains that were encapsulated with a continuous silica shell. The chains formations were attributed to the dipole-dipole interactions between neighboring particles as the size of the cobalt core exceeded the critical diameter above which, the net dipole moment was larger than thermal fluctuations. As a result, spontaneous self-assembly of cobalt nanoparticles yielded chains resembling pearl necklaces and loops that were permanently locked with continuous silica shells. In the control experiment, the use of smaller size cobalt nanoparticles with D = 20 - 25 nm resulted in discrete cobalt-core silica-shell nanoparticles as the magnetic dipoles were randomized by thermal fluctuations. This work further exemplified the importance of dipolar assembly and suitable chemistries toward the formation of permanently locked 1-D mesostructures.

Later, Wang et al. demonstrated the polymerization of well defined ferromagnetic iron oxide (D ~ 80 nm) with a continuous silica shell.[202] Exploiting the spontaneous dipolar organization of ferromagnetic iron oxide in solution, the 1-D morphology was subsequently locked as the sol-gel reactions occurred on the surfaces of the pre-assembled nanoparticles chains. As a result, a permanently fixed 1-D magnetic nanostructure containing inclusions of iron oxide nanoparticle with a continuous silica shell was obtained. The length and morphology of the 1-D nanostructures could be controlled by the amplitude of sonication, while the thickness of the silica shell could be tuned by the amount of the sol-gel precursors used during the synthesis of the core-shell nanomaterials. This work described another example of combining magnetic assemblies and chemical reactions to yield well-defined 1-D nanostructures.

In 2005, Hatton et al. reported an elegant and versatile approach for the fabrication of well defined magnetoresponsive rods with tunable diameter, length and morphology (hollow versus solid) (Figure 1.24).[203] In the previous example, micrometer-sized latex beads coated with superparamagnetic nanoparticles were aligned and permanently linked via a simple amidation chemistry within a confined microchannel.[188] In this work, sol-gel chemistry was exploited to permanently link the pre-assembled magnetic beads with TiO_2 shells, yielding a new class of magnetoresponsive material. The advantages of utilizing sol-gel chemistry include, (1) tunable shell thickness, and thus the bonding strength of the titania coating along the magnetic chain, (2) the preparation of hollow nanochains by dissolving the polystyrene core, while the titania shell preserved the 1-D nanostructures, and (3) the semiconductor titania shell could

potentially be exploited as photocatalysts, in sensor technology, and as antimicrobial agents.

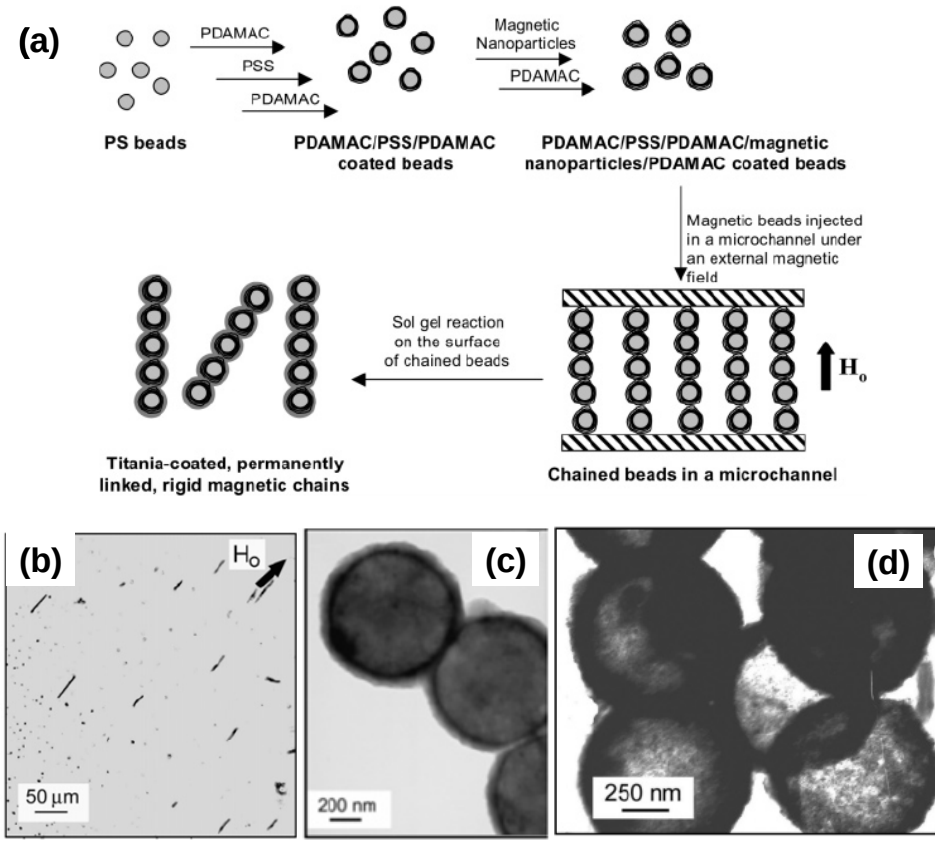

Figure 1.24: (a) Production of permanently linked rigid magnetic chains. Polystyrene beads coated with polyelectrolytes and magnetic nanoparticles using the layer-by-layer approach are aligned in a microchannel under an applied magnetic field and cemented together through hydrolysis of sol-gel precursors in the polyelectrolyte layer. (b) Optical micrograph shows the chains aligning with an external field. (c) Titania coated magnetite and (d) TEM images of hollow titania-linked magnetic chains prepared after calcination. Reproduced with permission from ref. 203. Copyright 2005, American Chemical Society.[203]

In previous examples, sol-gel polymerization was utilized to preserve the 1-D assembly of magnetic building blocks by coating a thin layer of silica shell onto the surfaces of the pre-assembled structures. Alternatively, sol-gel processes could also be

applied to form the matrix, which simultaneously froze the morphology of the magnetic assemblies. The work by Rolison et al. elegantly demonstrated this strategy by aligning iron particles in a sol-gel matrix. When the suspension of iron particles in the silica sol was placed on a NMR superconducting magnet, these magnetic nanoparticles instantly formed long needle-like structures that were permanently fixed upon gelation of the silica sol. The field-aligned iron particles within the silica matrix could be selectively removed to yield anisotropic silica with 3-dimensional macroporosity. Based on a similar concept described by Rolison et al., a permanently locked magnetic filament spanning micrometers in length was demonstrated by Collinson using biomolecules and magnetic particles as building blocks.[204] In this strategy, rod-shaped *Bacillus megaterium* (~ 2 x 10 μm) were covalently decorated with paramagnetic iron oxide particles via a standard carboimide coupling. When a solution containing both the 'magnetic-bacteria' and the sol gel precursor was placed on a glass substrate under an external magnetic field, long filaments oriented in the direction of the applied field were observed under optical microscopy. In contrast with the work by Rolison et al., the orientation of these magnetic filaments could be manipulated in both parallel and perpendicular directions. In all cases, the micrometer sized filaments oriented along the field lines at early times when the silica sol remained fluid-like. As the solution starts to gel, wire-like assemblies of magnetic bacteria were locked and fixed within the gelled matrix. Upon removal of the magnetic field, arrays of 1-D alignment were preserved within the silica gel. This method (the combination of magnetic assembly and sol-gel chemistry) has the potential to create interesting architectures and patterns for drug delivery or support for chemical sensors.

1.6.4 Carbonization

The 1-D assemblies of ferromagnetic colloids have been utilized as templates for the formation of continuous carbon nanostructures with metal nanoparticle inclusions.[144] In related studies, well-defined carbon nanostructures have been elegantly demonstrated via the pyrolysis of self-assembled block copolymers such as polyethylene oxide-*block*-polystyrene (PEO-*b*-PS)[205] and ABA triblock copolymers of acrylonitrile (AN) and n-butyl acrylate (nBA) (poly(AN-*b*-nBA-*b*-AN).[206] These carbon nanostructures were expected to have enhanced electrical properties for potential applications in nanoelectronics and electrochemical energy storage.[207] Pyun et al. reported a modular route towards 1-D carbonaceous nanomaterials using polyacrylonitrile (PAN) functionalized ferromagnetic nanoparticles as the soluble precursor building blocks. In this strategy, the PAN-coated ferromagnetic cobalt nanoparticles were pre-organized into 1-D mesostructures spanning micrometers in length on a supporting substrate. Subsequent pyrolysis reaction yielded continuous 1-D carbon nanoparticle chains with metallic nanoparticle inclusions (Figure 1.25). Raman spectroscopy confirmed that the carbonaceous shell composed both the graphitic and disordered phases. Manners et al. elegantly reported the synthesis of magnetic microspheres comprised of polyferrocenylsilane, which contained Fe atoms along the backbone of the polymers.[208] Upon pyrolysis, the polyferrocenylsilane microspheres transformed into α-Fe nanoclusters embedded within the silicon-carbide matrix, which organized into 1-D arrays in the presence of an external magnetic field. In another example, magnetite nanoparticles (D = 40 – 100 nm) oriented in 1-D morphology with an amorphous carbon

coating were reported based on the pyrolysis of ferrocene in the presence of dry ice and polyvinylpyrrolidone.[209]

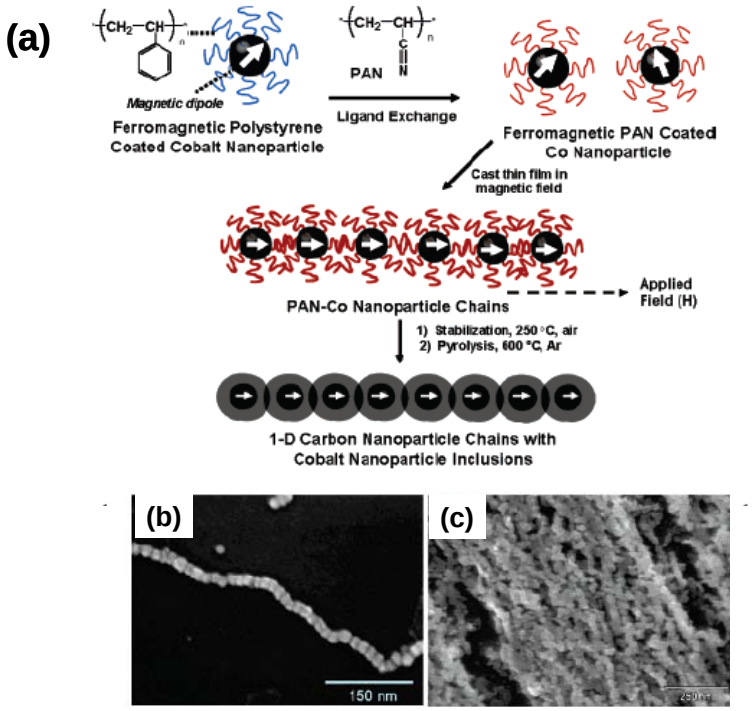

Figure 1.25: (a) Schematic representation of the synthesis of 1-D carbon nanostructures via functionalization of ferromagnetic colloids with PAN, magnetic assembly, and pyrolysis. (b) FESEM images of the 1-D carbon nanoparticle chain, and (c) FESEM of the carbonized thin film of magnetically aligned PAN-CoNPs chains. Reproduced with permission from ref. 144. Copyright 2007, American Chemical Society.[144]

1.6.5 Galvanic exchange

The fabrication of hollow nanomaterials has attracted considerable interest for a diverse range of applications in drug delivery, bioencapsulation[210, 211], catalysis[212], plasmonics[213, 214], and cell imaging[211, 215]. One of the facile approaches to prepare noble hollow metal nanostructures is based on the galvanic exchange reactions with suitable metallic nanoparticles. The fundamental basis for the galvanic exchange reaction is in

the large differences in the standard reduction potentials between two metal precursors. For example, the standard reduction potential for $PtCl_6^{2-}$/Pt redox pair is 0.735 V vs the standard hydrogen electrode (SHE), which is much higher than the Co^{2+}/Co redox pair (-0.277 V vs SHE).[216]

In this system, Pt^{4+} was spontaneously reduced to Pt^0, while oxidizing the Co^0 to Co ions. The reduction of Pt^{4+} was confined to the outer surfaces of the sacrificial templates (cobalt nanoparticles), therefore the cobalt nanoparticle precursors determined the resulting morphology of the Pt hollow nanostructures. Taking advantage of this facile galvanic exchange reactions in combination with magnetic assembly, various hollow nanospheres, nanotubes and nanowires with Au, Pt or Pd shells have been demonstrated using magnetic nanoparticles as sacrificial templates. Bai et al. elegantly demonstrated one of the first reports in utilizing magnetic cobalt nanoparticles (D ~ 24 nm) as sacrificial templates to prepare Pt hollow nanospheres.[217] As eluded previously, in the galvanic exchange reaction, cobalt nanoparticles were spontaneously oxidized, while reducing H_2PtCl_6 into a thin shell of Pt^0 surrounding the exterior of the cobalt nanoparticles. During the replacement reaction, the oxidized Co ions continuously diffused across the porous shell, yielding a hollow nanostructure coated with a thin Pt shell. Later, Schaak reported the formation of hollow nanospheres of PtCo alloy using superparamagnetic cobalt nanoparticles (D = 10 - 50 nm) as sacrificial templates. Here, the presence of excess reducing agent, $NaBH_4$, promoted the reduction of Co ions that were liberated during the Pt deposition. The co-reduction of both Co and Pt onto the outer surfaces of the sacrificial template resulted in a shell containing CoPt alloy.[218] This

synthetic methodology added to the growing toolbox of reactions in fabricating alloy nanomaterials such as CoPt and FePt with controlled morphology. Additionally, CoPt nanomaterials have attracted considerable research interest due to their potential use as electrocatalysts in energy conversion devices. In particular, the fabrication of Pt-based hollow nanomaterials is an attractive approach towards an economical and effective alternative catalyst to noble metals such as platinum. Several reports have shown an enhancement in catalytic activities of these hollow nanospheres with noble metal shells prepared via the galvanic exchange reactions.[218-220] This simple and facile methodology was extended to the preparation of hollow 1-D nanostructures with either Au, Pt or Pd shells. Based on similar principles, superparamagnetic cobalt nanoparticles were magnetically attracted and aligned on the electrode surfaces in the presence of an external field to form 1-D assemblies. Upon reaction with M^{x+} (M^{x+} denoted the metal salt precursors), the cobalt core spontaneously oxidized, while M^0 shells (M^0 denoted the metallic noble metal) were deposited onto the outer surfaces of the aligned cobalt nanoparticles chain. As the reaction proceeded, Co^0 were oxidized into Co^{2+} and diffused outward through the porous shell, leaving hollow inclusions along the 1-D nanostructures (Figure 1.26).[221] Furthermore, Dong et al. immobilized and directed 1-D assembly of hollow PtCo nanostructures on an electrode surface in the presence of an external magnetic field. The electrocatalytic activities of these 1-D PtCo nanomaterials towards oxygen reduction reactions were found to be tunable by tailoring the exposure time of the nanoparticle dispersion to the 'magnetized' electrode.[222]

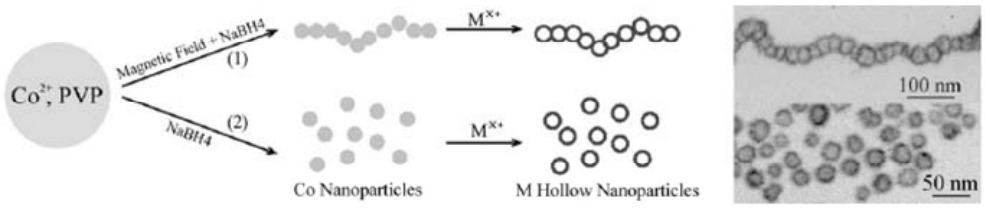

Figure 1.26: Schematic illustration of the magnetic-field-dependent preparation of noble-metal hollow nanostructures. Process (1) and (2) correspond to the presence and absence of the magnetic field, respectively. M^{x+} denotes Au^{3+}, Pt^{4+}, or Pd^{2+}.[221] Reproduced with permission from ref. 221. Copyright 2005, WILEY-VCH.

Based on similar principles, Hou et al. reported the preparation of necklace-like Au hollow chains with tunable optical properties.[221] In this one-pot synthesis, cobalt nanoparticles were first synthesized in the presence of an external field to induce the formation of 1-D chains. The chain-like morphology was subsequently locked together as noble metal precursors (Au^{3+}, Pt^{4+}, or Pd^{2+}) were reduced by the Co nanoparticles through the galvanic exchange reaction. The optical properties of the Au nanotubes could be tuned by varying the magnetic field strengths from 50 mT to 225 mT, which yielded Au nanotubes with varying chain lengths and morphologies. At the applied field strength of 50 mT, 125 mT and 225 mT, chain lengths of 200 nm, 2 micrometers and bundles of hollow Au nanostructures were prepared, respectively. The surface plasmon resonance peaks were also found to be red-shifted to 627, 690 and 800 nm for the short chains, long chains and bundles of Au nanotubes, respectively.

In a separate report, Zhang et al. demonstrated the synthesis of the continuous gold nanotubes via galvanic exchange reaction followed by an oxidation reaction to remove the residual cobalt metals. High resolution transmission electron microscopy (HRTEM) revealed that the entire Au nanotube was hollow and polycrystalline in nature.

This study indicated that the reduction of Au^{3+} salt only occurred on the exposed surface of the pre-formed Co nanoparticles chains and not within the interstitial spaces between the particles.[223] The application of an external magnetic field was determined to be essential in the formation of hollow nanotubes. As previously shown by Wan et al.,[224] only discrete Au hollow nanospheres were obtained when the galvanic reaction was performed in an absence of a field due to the thermal fluctuations of the magnetic spins in superparamagnetic cobalt nanoparticles.

1.6.6 Nanoscale Kirkendall reaction

The Kirkendall effect describes a non-uniform diffusion of two species across an interface, which resulted in the formation of voids. This phenomenon was first discovered by Smigelkas and Kirkendall[225] in 1947, and has recently garnered considerable research interest as a facile and efficient synthetic route towards various hollow nanostructures.[226] One of the first examples, described by Alivisatos et al., were the synthesis of CoO, $CoSe_2$, and Fe_3O_4 hollow nanostructures via the Kirkendall reaction by reacting the magnetic nanoparticles with either oxygen, sulfur or selenium at elevated temperatures.[227-229] In this reaction, cobalt or iron cations rapidly diffused to the interface and resulted in the supersaturation of vacancies within the nanoparticle, which then condensed into a hollow core. The size and morphology of the resulting hollow nanostructures were adopted from the magnetic nanoparticle precursors.

Xu et al. elegantly demonstrated the preparation of $CoSe_2$ nanowires by combining dipolar assembly of ferromagnetic cobalt nanoparticles and the facile nanoscale Kirkendall reaction.[230] In this strategy, ferromagnetic cobalt nanoparticles

with approximately 20 nm in diameter self-assembled (zero field conditions) into chains and necklaces in solution due to the strong inter-particle magnetic interactions. Upon the addition of selenium to the ferromagnetic cobalt nanoparticle dispersions, interconnected hollow $CoSe_2$ nanowires were formed. During the Kirkendall reaction, the Co ions rapidly diffused to the interface and reacted with selenium to form $CoSe_2$ shell around the exterior of the nanoparticle chains. The formation of $CoSe_2$ shell simultaneously locked the 1-D morphologies into interconnected $CoSe_2$ hollow nanowires (Figure 1.27). In a control experiment (process 2 in Figure 1.27), dipolar interactions of the 20 nm CoNPs were disrupted by an alternating magnetic field, which resulted in the formation of only discrete hollow $CoSe_2$ nanoparticles. In a separate control experiment, where superparamagnetic CoNPs (D = 6 nm) were used as the colloidal precursors in the reaction with selenium, only isolated hollow $CoSe_2$ nanoparticles were formed, emphasizing the importance of the ferromagnetic cores in the formation of 1-D mesostructures.

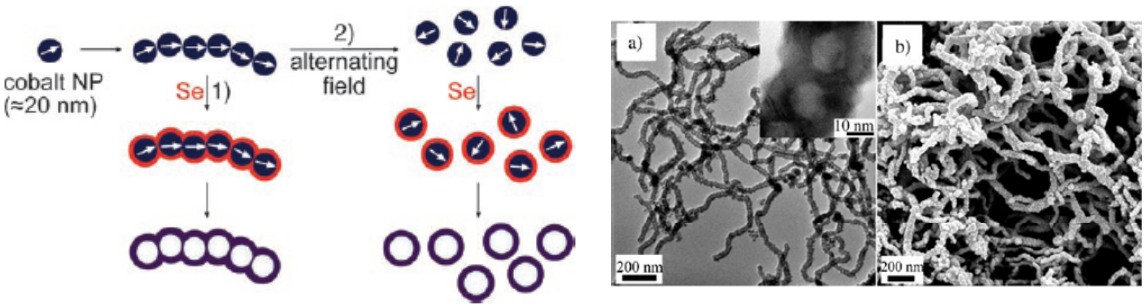

Figure 1.27: Formation of hollow $CoSe_2$ nanocrystals from cobalt nanoparticles in (1) absence and (2) presence of an alternating magnetic field. (a) TEM images of the (inset: HR-TEM), and (b) SEM images of the wires of hollow $CoSe_2$ nanocrystals. Reproduced with permission from ref. 230. Copyright 2006, WILEY-VCH [230]

1.7 Colloidal Polymerization

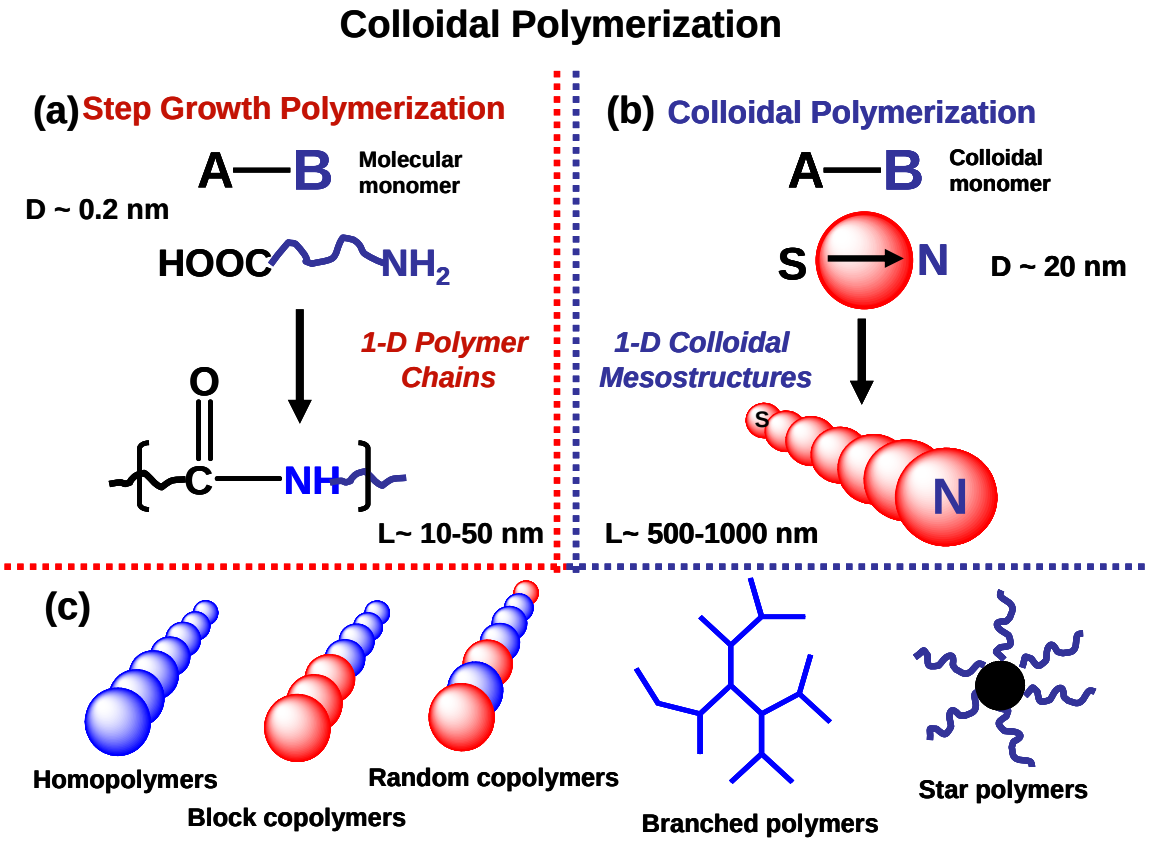

Figure 1.28: Illustration of the concept of *Colloidal Polymerization.* (a) Example of a step-growth polymerization using small molecule AB monomers. (b) *Colloidal Polymerization* using dipolar colloids as monomers to form 1-D interconnected mesostructures. (c) Examples of a wide range of colloidal mesopolymers that could be accessible via *Colloidal Polymerization*.

Colloidal Polymerization is a novel methodology described as the combination of dipolar nanoparticle assembly followed by a chemical reaction, converting the colloidal monomers into a fused 1-D nanomaterial. This concept is analogous to the small molecule polymerization, in which individual molecules are covalently attached to form extended polymeric chains that possessed distinctly different properties than the small molecule precursors (Figure 1.28 (a)). In *Colloidal Polymerization*, dipolar metallic

nanoparticles with inherent north-south dipoles were utilized as 'colloidal monomers' to organize into linear chains via selective head-to-tail magnetostatic interactions (Figure 1.28 (b)). Upon the 'polymerization' reaction, the reactive dipolar monomers were converted into thermodynamically stable 1-D mesopolymers that possessed distinctively different properties than the colloidal monomers. The Pyun group presented this novel methodology to fabricate well-defined cobalt oxide nanowires in gram quantities using ferromagnetic cobalt nanoparticles as colloidal monomers (Figure 1.29).[231] This demonstration further provided another example in developing a synthetic methodology to prepare novel 1-D functional mesostructures at larger length scales. Analogous to the step growth polymerization, colloidal mesoscopic polymers of different structure, composition and architecture were anticipated to be accessible via *Colloidal Polymerization* (Figure 1.28 (c)). Thus, this novel methodology provides a promising synthetic tool in controlling the nanoscale morphology of the nanostructured electrodes with potential applications in energy storage and conversion.

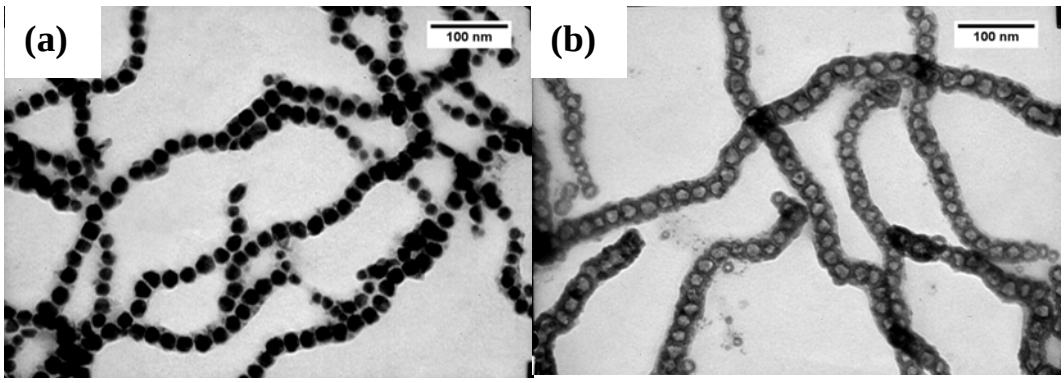

Figure 1.29: TEM images of (a) polystyrene coated cobalt nanoparticles with particle size, D = 20 ± 2.40 nm before oxidation and (b) polystyrene coated cobalt oxide nanowires after 1 week of oxidation, with particle diameter = 32 ± 3.5 nm. TEM samples were drop casted from 0.5 mg/mL toluene dispersion onto a carbon coated copper grid at

zero field. Reproduced with permission from ref. 231. Copyright 2009, American Chemical Society.

1.8 Goals of this research

In this research project, a novel methodology in preparing hybrid magnetic nanoparticles as 'chemical reagent' to form 1-D mesostructures was presented (Scheme 1.2). Large scale synthesis of uniform size polymer-coated ferromagnetic cobalt nanoparticles was developed to yield amenable quantities of nanoparticle 'reagents' for further chemistry. To impart desirable properties, functional copolymer surfactants were exchanged onto the pre-formed ferromagnetic nanoparticles. Ferromagnetic cobalt nanoparticles that were functionalized with crosslinkable polymer shells were utilized to form magnetoresponsive filaments spanning micrometers in length. Furthermore, the pre-organized cobalt nanoparticle chains were converted into cobalt oxide nanowires via a simple oxidation reaction. The electrochemical activity, electrical conductivity and the energy levels (valence and conduction bands) of these 1-D nanostructured electrodes were characterized in the present study. Finally, this synthetic platform also allows for the preparation of a wide range of 1-D heterostructured electrodes for potential applications in energy storage and conversion.

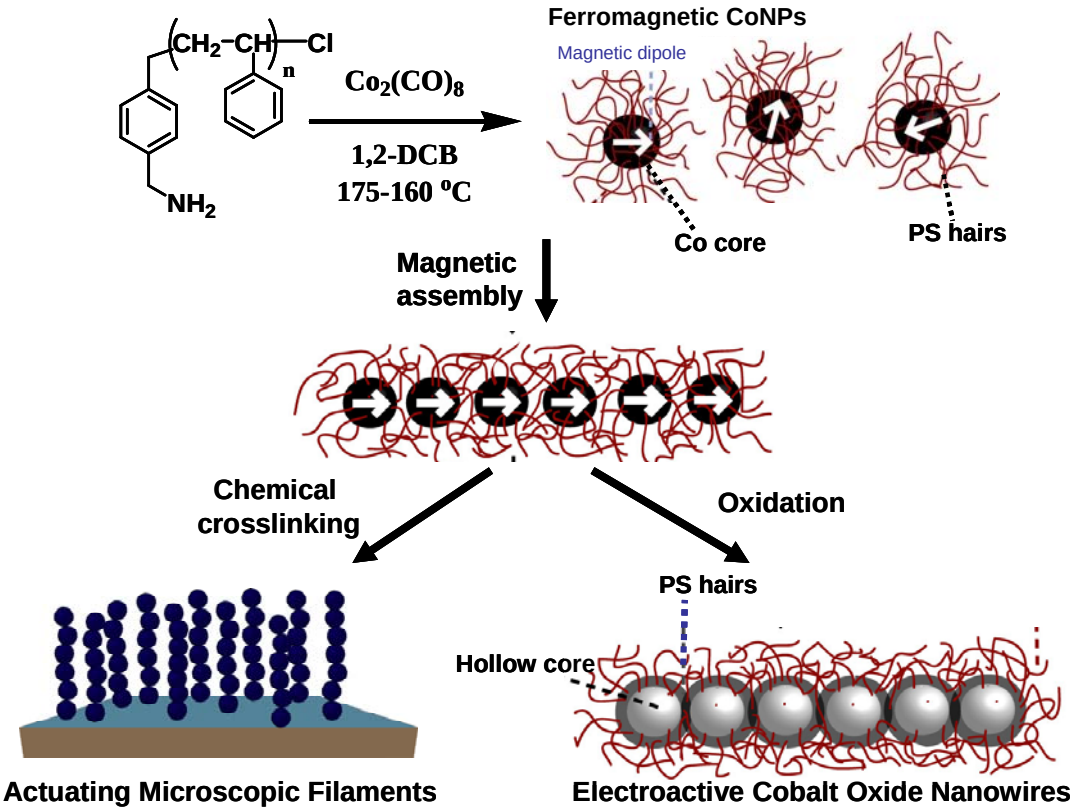

Scheme 1.2: Schematic diagram for the preparation of 1- D mesostructures of electroactive cobalt oxide nanowires and magnetoresponsive filaments using polymer coated ferromagnetic cobalt nanoparticles as 'colloidal monomers'.

1.9 References

1. Lalatonne, Y.; Motte, L.; Russier, V.; Ngo, A. T.; Bonville, P.; Pileni, M. P. *J. Phys. Chem. B* **2004,** *108*, (6), 1848-1854.

2. Maier, S.; Kik, P. G.; Atwater, H. A.; Meltzer, S.; Harel, E.; Koel, B. E.; Requicha, A. *Nature Mater.* **2003,** *2*, 229.

3. Braun, E.; Eichen, Y.; Sivan, U.; Ben-Yoseph, G. *Nature* **1998,** *391*, 775.

4. Fort, E.; Ricolleau, C.; Sau-Peuyo, J. *Nano Lett* **2003,** *3*, 65-67.

5. Nam, K. T.; Kim, D.-W.; Yoo, P. J.; Chiang, C.-Y.; Meethong, N.; Hammond, P. T.; Chiang, Y.-M.; Belcher, A. M. *Science* **2006,** *312*, (5775), 885-888.

6. Law, M.; Greene, L. E.; Johnson, J. C.; Saykally, R.; Yang, P. *Nat. Mater.* **2005,** *4*, (6), 455-459.

7. Sun, Y. G.; Mayers, B. T.; Xia, Y. *Adv. Mater.* **2003,** *15*, 641-646.

8. Kinge, S.; Crego-Calama, M.; Reinhoudt, D. N. *Chem. Phys. Chem.* **2008,** *9*, 20-42.

9. Minko, S.; A., K.; Gorodyska, G.; Stamm, M. *J. Am. Chem. Soc.* **2002,** *129*, 10912-10917.

10. Kiriy, A.; Minko, S.; Gorodyska, G.; Stamm, M. *Nano Lett* **2002,** *2*, 881-885.

11. Srivastava, S.; Kotov, N. A. *Soft Matter* **2009,** *5*, 1146-1156.

12. Warner, M. G.; Hutchison, J. E. *Nat. Mater.* **2003,** *2*, (4), 272-277.

13. Lee, J.; Govorov, A. O.; Kotov, N. A. *Angew. Chem. Int. Ed.* **2005,** *44*, (45), 7439-7442.

14. Dujardin, E.; Peet, C.; Stubbs, G.; Culver, J. N.; Mann, S. *Nano. Lett.* **2003,** *3*, 413-417.

15. Tang, Z.; Wang, Y.; Sun, K.; Kotov, N. A. *Adv. Mater.* **2005,** *17*, (3), 358-363.

16. Bockstaller, M. R.; Lapetnikov, Y.; Margel, S.; Thomas, E. L. *J. Am. Chem. Soc.* **2003,** *125*, 5276.

17. Bockstaller, M. R.; Mickiewics, R. A.; Thomas, E. L. *Adv. Mater.* **2005,** *17*, 1331-1349.

18. Wang, X.-S.; Guerin, G.; Wang, H.; Wang, Y.-S.; Manners, I.; Winnik, M. A. *Science* **2007,** *317*, 644-647.

19. Cui, H. G.; Chen, Z. Y.; Zhong, S.; Wooley, K. L.; Pochan, D. J. *Science* **2007,** *317*, 647-650.

20. Yin, Y.; Lu, Y.; Gates, B.; Xia, Y. N. **2001,** *123*, 8718-8729.

21. Yin, Y.; Xia, Y. *J. Am. Chem. Soc.* **2003,** *125*, (8), 2048-2049.

22. Safran, S. A. *Nature Mater.* **2003,** *2*, (2), 71-72.

23. DeVries, G. A.; Brunnbauer, M.; Hu, Y.; Jackson, A. M.; Long, B.; Neltner, B. T.; Uzun, O.; Wunsch, B. H.; Stellacci, F. *Science* **2007,** *315*, (5810), 358-361.

24. Jackson, A. M.; Myerson, J. W.; Stellacci, F. *Nat. Mater.* **2004,** *3*, (5), 330-336.

25. DeVries, G. A.; Brunnbauer, M.; Hu, Y.; Jackson, A. M.; Long, B.; Neltner, B. T.; Uzun, O.; Wunsch, B. H.; Stellacci, F. *Science* **2007,** *315*, (5810), 358-361.

26. Jackson, A. M.; Hu, Y.; Silva, P. J.; Stellacci, F. *J. Am. Chem. Soc.* **2006,** *128*, (34), 11135-11149.

27. DeVries, G. A.; Talley, C. E.; Carney, R. P.; Stellacci, F. *Adv. Mater.* **2008,** *20*, 4243-4247.

28. DeVries, G. A.; Centrone, A.; Stellacci, F. *Proc. SPIE* **2007,** *6788*, 676880Y.

29. Nie, Z.; Fava, D.; Kumacheva, E.; Zou, S.; Walker, G. C.; Rubinstein, M. *Nat. Mater.* **2007,** *6*, (8), 609-614.

30. Fava, D.; Nie, Z.-H.; Winnik, M. A.; Kumacheva, E. *Adv. Mater.* **2008,** *20*, 4318-4322.

31. Nie, Z.; Fava, D.; Rubinstein, M.; Kumacheva, E. *J. Am. Chem. Soc.* **2008,** *130*, (11), 3683-3689.

32. Pileni, M. P. *Acc. Chem. Res.* **2007,** *40*, (8), 685-693.

33. Murray, C. B.; Sun, S.; Gaschler, W.; Doyle, H.; Betley, T. A.; Kagan, C. R. *IBM J. Res. Dev.* **2001,** *45*, (1), 47-56.

34. Sobal, N. S.; Ebels, U.; Mhwald, H.; Giersig, M. *J. Phys. Chem. B* **2003,** *107*, 7351-7354.

35. Hyeon, T. *Chem. Commun.* **2003**, 927-934.

36. Murray, C. B.; Sun, S.; Doyle, H.; Betley, T. *MRS Bull.* **2001,** *26*, (12), 985-991.

37. Hilgendorff, M.; Tesche, B.; Giersig, M. *Aust. J. Chem.* **2001,** *54*, 497–501.

38. Lalatonne, Y.; Richardi, J.; Pileni, M. P. *Nat. Mater.* **2004,** *3*, (2), 121-125.

39. Germain, V.; Pileni, M. P. *Adv. Mater.* **2005,** *17*, 1424-1429.

40. Sun, S. *Adv. Mater.* **2006,** *18*, 393-403.

41. Latham, A. H.; Williams, M. E. *Acc. Chem. Res.* **2007,** *41*, 411-420.

42. Lu, A. H.; Salabas, E. L.; Schueth, F. *Angew. Chem. Int. Ed.* **2007,** *46*, (8), 1222-1244.

43. Jeong, U.; Teng, X.; Wang, Y.; Yang, H.; Xia, Y. *Adv. Mater.* **2007,** *19*, (1), 33-60.

44. Pyun, J. *Polym. Rev.* **2007,** *47*, 231-263.

45. Lin, X. M.; Jaeger, H. M.; Sorensen, C. M.; Klabunde, K. J. *J. Phys.Chem. B* **2001,** *105*, (17), 3353-3357.

46. Huber, D. L. *Small* **2005,** *1*, 482-501.

47. Rosensweig, R. E. *Sci. Am.* **1982,** *247-257*, 136.

48. Odenbach, S. *Proc. Appl. Math. Mech.* **2002,** *1*, 28-32.

49. Popplewell, J.; Rosensweig, R. E. *J. Appl. Phys. D* **1996,** *29*, (9), 2297-2203.

50. Elmore, W. C. *Phys. Rev.* **1938,** *54*, 309-310.

51. Liu, J.; Lawrence, E. M.; Wu, A.; Ivey, M. L.; Flores, G. A.; Javier, K.; Bibette, J.; Richard, J. *Phys. Rev. Lett.* **1995,** *74*, 2828-2831.

52. Massart, R. *IEEE Trans. Magn.* **1981,** *17*, 1247-1248.

53. Skjeltorp, A. T.; Ugelstad, J.; Ellingsen, T. *J. Colloid Interface Sci.* **1986,** *113*, (2), 577-82.

54. Skjeltorp, A. T.; Akselvoll, J.; de Lange Kristiansen, K.; Helgesen, G.; Toussaint, R.; Flekkoy, E. G.; Cernak, J., Self-assembly and dynamics of magnetic holes. In *Forces, growth and form in soft condensed matter: At the interface between physics and biology*, Belushkin, A. V., Ed. Kluwer Academic: Netherlands, 2004; pp 165-179.

55. Skjeltorp, A. T. *Phys. Rev. Lett.* **1983,** *51*, (25), 2306-9.

56. Skjeltorp, A. T. *J. Appl. Phys.* **1985,** *57*, (8, Pt. 2A), 3285-90.

57. Hayter, J. B.; Pynn, R.; Charles, S. W.; Skjeltorp, A. T.; Trewhella, J.; Stubbs, G.; Timmins, P. *Phys. Rev. Lett.* **1989,** *62*, 1667-1670.

58. Krebs, M. D.; Erb, R. M.; Yellen, B. B.; Samanta, B.; Bajaj, A.; Rotello, V. M.; Alsberg, E. *Nano Lett.* **2009,** *9*, 1812-1817.

59. Charles, S. W. *J. Magn. Magn. Mater.* **1990,** *85*, (1-3), 277-84.

60. Ginder, J. M. *MRS Bulletin* **1998,** *23*, (8), 26-29.

61. Winslow, W. M. *J. Appl. Phys.* **1949,** *20*, 1137-1141.

62. Bossis, G.; Lacis, S.; Meunier, A.; Volkova, O. *J. Magn. Magn. Mater.* **2002,** *252*, 224-228.

63. Jolly, M. *Mater. Res. Soc. Symp. Proc.* **2000,** *604*, 167-176.

64. Zubarev, A. Y.; Iskakova, L. Y. *Phys. Rev. E* **2000,** *61*, (5-B), 5415-5421.

65. Chantrell, R. W.; Bradbury, A.; Popplewell, J.; Charles, S. W. *J. Appl. Phys.* **1982,** *53*, 2742.

66. Promislow, J. H. E.; Gast, A. P. *Langmuir* **1996,** *12*, 4095-4102.

67. Lattuada, M.; Hatton, T. A. *J. Am. Chem. Soc.* **2007,** *129*, 12878-12889.

68. Isojima, T.; Suh, S. K.; Vander Sande, J. B.; Hatton, T. A. *Langmuir* **2009,** *25*, (14), 8292-8298.

69. Zhao, N.; Gao, M. *Adv. Mater.* **2009,** *21*, 184-187.

70. Dyab, A. K. F.; Ozmen, M.; Ersoz, M.; Paunov, V. N. *J. Mater. Chem.* **2009,** *19*, (21), 3475-3481.

71. Yuet, K. P.; Hwang, D. K.; Haghgooie, R.; Doyle, P. S. *Langmuir* **2010,** *26*, 4281-4287.

72. Zerrouki, D.; Baudry, J.; Pine, D.; Chaikin, P.; Bibette, J. *Nature* **2008,** *455*, (7211), 380-382.

73. Ge, J.-P.; Hu, Y.; Zhang, T.; Huynh, T.; Yin, Y. *Langmuir* **2008,** *24*, 3671-3680.

74. Xu, X.; Friedman, G.; Humfeld, K. D.; Majetich, S. A.; Asher, S. A. *Chem. Mater.* **2002,** *14*, 1249-1256.

75. Camargo, P. H. C.; Li, Z.-Y.; Xia, Y. *Soft Matter* **2007,** *3*, 1215-1222.

76. Xu, X.; Majetich, S. A.; Asher, S. A. *J. Am. Chem. Soc.* **2002,** *124*, (46), 13864-13868.

77. Jiles, D. C. *Acta Mater.* **2003,** *51*, (19), 5907-5939.

78. Ross, C. *Ann. Rev. Mater. Res.* **2001,** *31*, 203-235.

79. Majetich, S. A.; Jin, Y. *Science* **1999,** *284*, (5413), 470-473.

80. Frenkel, J.; Dorfman, J. *Nature* **1930,** *126*, (3173), 274.

81. Kittel, C. *Phys. Rev.* **1946,** *70*, 965-71.

82. Darling, S. B.; Bader, S. D. *J. Mater. Chem.* **2005,** *15*, (39), 4189-4195.

83. Tlusty, T.; Safran, S. A. *Science* **2000,** *290*, 1328-1331.

84. Jacobs, I. S.; Bean, C. P. *Phys Rev.* **1955,** *100*, 1060-1067.

85. de Gennes, P. G.; Pincus, P. A. *Phys.Kondens.Materie* **1970,** *11*, (3), 189-198.

86. Chantrell, R. W.; Bradbury, A.; Popplewell, J.; Charles, S. W. *J. Phys. D: Appl. Phys.* **1980,** *13*, (7), L119-L122.

87. Chantrell, R. W.; Bradbury, A.; Popplewell, J.; Charles, S. W. *J. Appl. Phys.* **1982,** *53*, (3, Pt. 2), 2742-4.

88. Weis, J. J.; Levesque, D. *Phys. Rev. Lett.* **1993,** *71*, (17), 2729-32.

89. Levesque, D.; Weis, J. J. *Phys. Rev. E.* **1994,** *49*, 5131-5140.

90. Klokkenburg, M.; Vonk, C.; Claesson, E. M.; Meeldijk, J. D.; Erne, B. H.; Philipse, A. P. *J. Am. Chem. Soc.* **2004,** *126*, (51), 16706-16707.

91. Morozov, K. I.; Shliomis, M. I. *Lecture Notes in Physics* **2002,** *594*, (Ferrofluids), 162-184.

92. Workum, K. V.; Douglas, J. F. *Phys. Rev. E.* **2005,** *71*, 031502.

93. Siracusano, S.; Stassi, A.; Baglio, V.; Arico, A. S.; Capitanio, F.; Tavares, A. C. *Electrochim. Acta* **2009,** *54*, 4844-4850.

94. Stambaugh, J.; Van Workum, K.; Douglas, J. F.; Losert, W. *Phys. Rev. E* **2005,** *72*, (3-1), 031301/1-031301/4.

95. Clarke, A. S.; Patey, G. N. *J. Chem. Phys.* **1994,** *100*, 2213-2219.

96. Lavender, H. B.; Iyer, A. K.; Singer, S. J. *J. Chem. Phys.* **1994,** *101*, (9), 7856-7867.

97. Weis, J. J. *J. Phys.: Condens. Matter* **2003,** *15*, S1471–S1495.

98. Wei, D.; Patey, G. N. *Phys. Rev. Lett.* **1992,** *68*, 2043-2045.

99. Stevens, M. J.; Grest, G. S. *Phys. Rev. Lett.* **1994,** *72*, (23), 3686-3689.

100. Stevens, M. J.; Grest, G. S. *Phys. Rev. E* **1995,** *51*, (6-A), 5976-5983.

101. Benkoski, J. J.; Jones, R. L.; Douglas, J. F.; Karim, A. *Langmuir* **2007,** *23*, 3530-3537.

102. Bazylinski, D. A.; Frankel, R. B. *Nat. Rev. Microbio.* **2004,** *2*, (3), 217-230.

103. Bazylinski, D. A.; Garratt-Reed, A. J.; Frankel, R. B. *Microsc. Res. Tech.* **1994,** *27*, (5), 389-401.

104. Penniga, I.; deWaard, H.; Moskowitz, B. M.; Bazylinski, D. A.; Frankel, R. B. *J. Magn. Magn. Mater.* **1995,** *149*, 279-286.

105. Proksh, R. B.; Schaffer, T. E.; Moskowitz, B. M.; Dahlberg, E. D.; Bazylinski, D. A.; Frankel, R. B. *Appl. Phys. Lett.* **1995,** *66*, 2582-2584.

106. Tripp, S. L.; Dunin-Borkowski, R. E.; Wei, A. *Angew. Chem. Int. Ed.* **2003,** *42*, (45), 5591-5593.

107. Klem, M. T.; Young, M.; Douglas, T. *Mater. Today* **2005,** *8*, (9), 28-37.

108. Midgley, P. A.; Dunin-Borkowski, R. *Nat. Mater.* **2009,** *8*, 271-280.

109. Kasama, T.; Posfai, M.; Chong, R. K. K.; Finlayson, A. P.; Buseck, P. R.; Frankel, R. B.; Dunin-Borkowski, R. *Am. Mineral.* **2006,** *91*, 1216-1229.

110. Philipse, A. P.; Maas, D. *Langmuir* **2002,** *18*, (9977-9984).

111. Thomas, J. R. *J. Appl. Phys.* **1966,** *37*, 2914-2915.

112. Harle, O. L.; Thomas, J. R. Dispersions of ferromagnetic cobalt particles. 3228882, 19620330., 1966.

113. Thomas, J. R. Dispersions of discrete particles of ferromagnetic metals. 3228881, 19630104., 1966.

114. Hess, P. H.; Parker, P. H., Jr. *J. Appl. Polym. Sci.* **1966,** *10*, (12), 1915-27.

115. Smith, T. W.; Wychick, D. *J. Phys. Chem.* **1980,** *84*, 1621-1629.

116. Griffiths, C. H.; O'Horo, M. P.; Smith, T. W. *J. Appl. Phys.* **1979,** *50*, 7108-7115.

117. Burke, N. A. D.; Stoever, H. D. H.; Dawson, F. P. *Chem. Mater.* **2002,** *14*, (11), 4752-4761.

118. Butter, K.; Philipse, A. P.; Vroege, G. J. *J. Magn. Magn. Mater.* **2002,** *252*, (1-3), 1-3.

119. Butter, K.; Bomans, P. H. H.; Frederick, P. M.; Vroege, J.; Philipse, A. P. *Nature Mater.* **2003,** *2*, 88.

120. Platonova, O. A.; Bronstein, L. M.; Solodovnikov, S. P.; Yanovskaya, I. M.; Obolonkova, E. S.; Valetsky, P. M.; Wenz, E.; Antonietti, M. *Colloid. Polym. Sci.* **1997,** *275*, (5), 426-431.

121. Diana, F. S.; Lee, S. H.; Petroff, P. M.; J., K. E. *Nano Letters* **2003,** *3*, 891-895.

122. Abes, J. I.; Cohen, R. E.; Ross, C. A. *Chem. Mater.* **2003,** *15*, 1125-1131.

123. Murray, C. B.; Norris, D. J.; Bawendi, M. G. *J. Am. Chem. Soc.* **1993,** *115*, 8706-8715.

124. Puntes, V. F.; Krishnan, K. M.; Alivisatos, A. P. *Science* **2001,** *291*, (5511), 2115-2117.

125. Puntes, V. F.; Gorostiza, P.; Aruguete, D. M.; Bastus, N. G.; Alivisatos, A. P. *Nature Mater.* **2004,** *3*, 263-268.

126. Puntes, V. F.; Zanchet, D.; Erdonmez, C. K.; Alivisatos, A. P. *J. Am. Chem. Soc.* **2002,** *124*, (43), 12874-12880.

127. Peng, X.-G.; Wickham, J.; Alivisatos, A. P. *J. Am. Chem. Soc.* **1998,** *120*, 5343-5344.

128. Puntes, V. F.; Bastus, N. G.; Pagonabarraga, I.; Iglesias, O.; Labarta, A.; Batlle, X. *Int. J. Nanotechnology* **2005,** *2*, 62-70.

129. Bao, Y.; Beerman, M.; Krishnan, K. M. *J. Magn. Magn. Mater.* **2003,** *266*, (3), L245-L249.

130. Chung, S. H.; McMichale, R. D.; Pierce, D. T.; Unguris, J. *Phys. Rev. B* **2010,** *81*, 024410-024417.

131. Ross, C. A.; Hwang, M.; Shima, M.; Cheng, J. Y.; Farhoud, M.; Savas, T. A.; Smith, H. I.; Schwarzacher, W. *Phys. Rev. B* **2002,** *65*, 144417-8.

132. Korth, B. D.; Keng, P.; Shim, I.; Bowles, S. E.; Tang, C.; Kowalewski, T.; Nebesny, K. W.; Pyun, J. *J. Am. Chem. Soc.* **2006,** *128*, (20), 6562-6563.

133. Keng, P. Y.; Kim, B. Y.; Shim, I.-B.; Sahoo, R.; Veneman, P. E.; Armstrong, N. R.; Yoo, H.; Pemberton, J. E.; Bull, M. M.; Griebel, J. J.; Ratcliff, E. L.; Nebesny, K. G.; Pyun, J. *ACS Nano* **2009,** *3*, 3143-3157.

134. Tripp, S. L.; Dunin-Borkowski, R. E.; Wei, A. *Angew. Chem. Int. Ed.* **2003,** *42*, 5591-5593.

135. Tripp, S. L.; Pusztay, S. V.; Ribbe, A. E.; Wei, A. *J. Am. Chem. Soc.* **2002,** *124*, (27), 7914-7915.

136. Chen, J.; Wiley, B.; McLellan, J.; Xiong, Y.; Li, Z.-Y.; Xia, Y. *Nano Lett.* **2005,** *5*, 2058-2062.

137. Hu, M.-J.; Lu, Y.; Zhang, S.; Guo, S.-R.; Lin, B.; Zhang, M.; Yu, S.-H. *J. Am. Chem. Soc.* **2008,** *130*, (11606-11607).

138. Cebula, D. J.; Charles, S. W.; Popplewell, J. *Colloid. Polym. Sci.* **1981,** *259*, 395.

139. Cebula, D. J.; Charles, S. W.; Popplewell, J. *J. Magn. Magn. Mater.* **1983,** *39*, 67.

140. Klokkenburg, M.; Erne, B. H.; Wiedenmann, A.; Petukhov, V.; Philipse, A. P. *Phys. Rev. E* **2007,** *75*, 051408.

141. Benkoski, J. J.; Bowles, S. E.; Jones, R. L.; Douglas, J. F.; Pyun, J.; Karim, A. *J. Polym. Sci., Part B: Polym. Phys.* **2008,** *46*, (20), 2267-2277.

142. Benkoski, J. J.; Bowles, S. E.; Korth, B., D.; Jones, R. A.; Douglas, J. F.; Karim, A.; Pyun, J. *J. Am. Chem. Soc.* **2007,** *129*, 6291-6297.

143. Benkoski, J. J.; Bowles, S. E.; Jones, R. A.; Douglas, J. F.; Pyun, J.; Karim, A. *J. Polym. Sci., Part B: Polym. Phys.* **2008,** *46*, 2267-2277.

144. Bowles, S. E.; Wu, W.; Kowalewski, T.; Schalnat, M.; Davis, R. J.; Pemberton, J. E.; Shim, I.; D., K. B.; Pyun, J. *J. Am. Chem. Soc.* **2007,** *129*, 8694-8695.

145. Sorensen, C. M., Magnetism. In *Nanoscale materials in chemistry*, Klabunde, K. J., Ed. John Wiley and Sons, Inc: 2001; pp 169-221.

146. Neuberger, T.; Schopf, B.; Hofmann, H.; Hofmann, M.; Von Rechenberg, B. *J. Magn. Magn. Mater.* **2005,** *293*, (1), 483-496.

147. Elmore, W. *Phys. Rev.* **1938,** *54*, 309.

148. Dave, M. J.; Mehta, R. V.; Shah, H. S.; Desai, J. N.; Naik, Y. G. *Indian J. Pure App. Phys.* **1968,** *6*, 364-366.

149. Hayes, C. F.; Hwang, S. R. *J. Coll. Inter. Sci.* **1977,** *60*, (3), 443-7.

150. Sahoo, Y.; Cheon, M.; Wang, S. X.; Luo, H.; Furlani, E. P.; Prasad, P. N. *J. Phys. Chem. B* **2004,** *108*, 3380-3383.

151. Klokkenburg, M.; Erne, B. H.; Meeldijk, J. D.; Wiedenmannm, A.; Petukhov, A. V.; Dullens, R. P. A.; Philipse, A. P. *Phys. Rev. Lett.* **2006,** *97*, 185702.

152. Pileni, M. P. *J. Phys. D: Appl. Phys.* **2008,** *41*, (134002), 1-9.

153. Jimenez, J.; Sheparovych, R.; Pita, M.; Garcia, A. N.; Dominguez, E.; Minko, S.; Katz, E. *J. Phys. Chem. C* **2008,** *112*, 7337-7344.

154. Hone, J.; Whitney, M.; Piskoti, C.; Zettl, A. *Phys. Rev. B* **1999,** *59*, R2514-R2516.

155. Du, F.; Fischer, J. E.; Winey, K. I. *Phys. Rev. B* **2005,** *72*, 121404-121404-4.

156. Correa-Duarte, M. A.; Grzelczak, M.; Salgueirino-Maceira, V.; Giersig, M.; Liz-Marzan, L. M.; Farle, M.; Sierazdki, K.; Diaz, R. *J. Phys. Chem. B.* **2005,** *109*, 19060-19063.

157. Yuan, J.; Gao, H.; Schacher, F.; Xu, Y.; Richter, R.; Tremel, W.; Muller, A. H. E. *ACS Nano* **2009,** *3*, 1441-1450.

158. Williams, M. E.; Hutchins, B. M.; Platt, M.; Hancock, W. O. *ECS Trans.* **2007,** *3*, 1-7.

159. Wilson, R. J.; Hu, W.; Wong, C. P. F.; Koh, A. L.; Gaster, R. S.; Earhart, C. M.; Fu, A.-H.; Heilshorn, S. C.; Sinclair, R.; Wang, S. X. *J. Magn. Magn. Mater.* **2009,** *321*, 1452-1458.

160. Cheng, G.; Romero, D.; Fraser, G. T.; Hight Walker, A. R. *Langmuir* **2005,** *21*, 12055-12059.

161. Wang, H.; Chen, Q.-W.; Sun, L.-X.; Qi, H.-P.; Yang, X.; Zhou, S.; Xiong, J. *Langmuir* **2009,** *25*, 7135-7139.

162. Legrand, J.; Ngo, A. T.; Petit, C.; Pileni, M. P. *Adv. Mater.* **2001,** *13*, (1), 58-62.

163. Germain, V.; Richard, J.; Ingert, D.; Pileni, M. P. *J. Phys. Chem. B.* **2005,** *109*, 5541-5547.

164. Germain, V.; Pileni, M. P. *J. Phys. Chem. B* **2005,** *109*, 5548-5553.

165. Chitu, L.; Chushkin, Y.; Luby, S.; Majkova, E.; Satka, A.; Ivan, J.; Smrcok, L.; Buchal, A.; Giersig, M.; Hilgendorff, M. *Mater. Sci. Eng. C* **2007,** *27*, 23-28.

166. Kim, Y.; Yoo, B. J.; Vittal, R.; Lee, Y.; Park, N.-G.; Kim, K.-J. *J. Power Sources* **2007,** *175*, 914-919.

167. Pileni, M. P. *Acc. Chem. Res.* **2007,** *40*, (8), 685-693.

168. Maye, M. M.; Nykypanchuk, D.; Cuisinier, M.; Lelie, D. v. d.; Gang, O. *Nature Mater.* **2009,** *8*, 388-391.

169. Shenhar, R.; Rotello, V. M. *Acc. Chem. Res.* **2003,** *36*, (7), 549-561.

170. Perepichka, D. F.; Rosei, F. *Angew. Chem. Int. Ed.* **2007,** *46*, 6006-6008.

171. Prabhu, V. M.; Hudson, S. D. *Nature Mater.* **2009,** *8*, 365-366.

172. Philip, J.; Mondain-Monval, O.; Calderon, F. L.; Bibette, J. *J. Phys. D: Appl. Phys.* **1997,** *30*, 2798-2803.

173. Goubault, C.; Jop, P.; Fermigier, M.; Baudry, J.; Bertrand, E.; Bibette, J. *Phys. Rev. Lett.* **2003,** *91*, (26, Pt. 1), 260802/1-260802/4.

174. Cohen-Tannoudji, L.; Bertrand, E.; Bressy, L.; Goubault, C.; Baudry, J.; Klein, J.; Joanny, J.-F.; Bibette, J. *Phys. Rev. Lett.* **2005,** *94*, (3), 038301/1-038301/4.

175. Goubault, C.; Leal-Calderon, F.; Viovy, J.-L.; Bibette, J. *Langmuir* **2005,** *21*, (9), 3725-3729.

176. Wang, N.; Cao, X.; Kong, D.; W., C.; Guo, L.; C., C. *J. Phys. Chem. C* **2008,** *112*, 6613-6619.

177. Sheparovych, R.; Sahoo, Y.; Motornov, M.; Wang, S. X.; Luo, H.; Prasad, P. N.; Sokolov, I.; Minko, S. *Chem. Mater.* **2006,** *18*, 591-593.

178. Xiong, Y.; Chen, Q.; Tao, N.; Ye, J.; Tang, Y.; Feng, J.; Gu, X. *Nanotechnology* **2007,** *18*, (34), 345301/1-345301/5.

179. Corr, S. A.; Byrne, S. J.; Tekoriute, R.; Meledandri, C. J.; Brougham, D. F.; Lynch, M.; Kerskens, C.; O'Dwyer, L.; Gun'ko, Y. K. *J. Am. Chem. Soc.* **2008,** *130*, (13), 4214-4215.

180. Byrne, S. J.; Corr, S. A.; Gun'ko, Y. K.; Kelly, J. M.; Brougham, D. F.; Ghosh, S. *Chem. Commun.* **2004**, (22), 2560-2561.

181. Furst, E. M.; Suzuki, C.; Fermigier, M.; Gast, A. P. *Langmuir* **1998,** *14*, (26), 7334-7336.

182. Furst, E. M.; P., G. A. *Phys. Rev. Lett.* **1999,** *82*, 4130-4133.

183. Furst, E. M.; Gast, A. P. *Phys. Rev. E: Stat. Phys., Plasmas, Fluids, Relat. Interdiscip. Top.* **2000,** *62*, (5-B), 6916-6925.

184. Biswal, S. L.; Gast, A. P. *Phys. Rev. E: Stat., Nonlinear, Soft Matter Phys.* **2003,** *68*, (2-1), 021402/1-021402/9.

185. Dreyfus, R.; Baudry, J.; Roper, M. L.; Fermigier, M.; Stone, H. A.; Bibette, J. *Nature* **2005,** *437*, 862.

186. Li, D.; Rogers, J.; Biswal, S. L. *Langmuir* **2009,** *25*, 8944-8950.

187. Lyles, B. F.; Terrot, M. S.; Hammond, P. T.; Gast, A. P. *Langmuir* **2004,** *20*, (8), 3028-3031.

188. Singh, H.; Laibinis, P. E.; Hatton, T. A. *Nano Lett.* **2005,** *5*, 2149-2154.

189. Benkoski, J. J.; Deacon, R. M.; Land, H. B.; Baird, L. M.; Breidenich, J. L.; Srivivasan, R.; Clatterbaugh, G. V.; Keng, P. Y.; Pyun, J. *Soft Matter* **2010,** 6, 602-609.

190. Centrone, A.; Hu, Y.; Jackson, A. M.; Zerbi, G.; Stellacci, F. *Small* **2007,** *3*, (5), 814-817.

191. Nakata, K.; Hu, Y.; Uzun, O.; Barkr, O.; Stellacci, F. *Adv. Mater.* **2008,** *20*, 4294-4299.

192. Redl, F. X.; Cho, K.-S.; Murray, C. B.; O'Brien, S. *Nature* **2003,** *423*, 968-971.

193. Manoharan, V. M.; Elsesser, M. T.; Pine, D. J. *Science* **2003,** *301*, 483-487.

194. Park, J.-I.; Kim, M. G.; Jun, Y.-W.; Lee, J. S.; Lee, W.-R.; Cheon, J. *J. Am. Chem. Soc.* **2004,** *126*, 9072-9078.

195. Frankamp, B. L.; Boal, A. K.; Tuominen, M.; Rotello, V. *J. Am. Chem. Soc.* **2005,** *127*, 9731-9735.

196. Philipse, A. P.; van Bruggen, M. P. B.; Pathmamanoharan, C. *Langmuir* **1994,** *10*, 92-99.

197. Ohmori, M.; Matijevic, E. *J. Coll. Inter. Sci.* **1992,** *150*, 594.

198. Ohmari, M.; Matijevic, E. *J. Coll. Inter. Sci.* **1993,** *160*, 288-292.

199. Kobayashi, K.; Horie, M.; Konno, M.; Rodriguez-Gonzalez, B.; Liz-Marzan, L. M. *J. Phys. Chem. B.* **2003,** *107*, 7420-7425.

200. Salgueirino-Maceira, V.; Correa-Duarte, M. A.; Hucht, A.; Farle, M. *J. Magn. Magn. Mater.* **2006,** *303*, (1), 163-166.

201. Salgueirino-Maceira, V.; Correa-Duarte, M. A. *J. Mater. Chem.* **2006,** *16*, 3593-3597.

202. Zhang, F.; Wang, C.-C. *J. Phys. Chem. C* **2008,** *112*, (39), 15151-15156.

203. Singh, H.; Laibinis, P. E.; Hatton, T. A. *Langmuir* **2005,** *21*, (24), 11500-11509.

204. Liu, S.; Wood, L. F.; Ohman, D. E.; Collinson, M. M. *Chem. Mater.* **2007,** *19*, 2752-2756.

205. Zhuang, J.; Wu, H.-M.; Yang, Y.-G.; Cao, C. *J. Am. Chem. Soc.* **2007,** *129*, 14166-14167.

206. Kowalewski, T.; Tsarevsky, N. V.; Matyjaszewski, K. *J. Am. Chem. Soc.* **2002,** *124*, 10632-10633.

207. Kulkarni, P.; McCullough, L. A.; Kowalewski, T.; Porter, L. M. *Synthetic Metals* **2009,** *159*, (3-4), 177-181.

208. Kulbaba, K.; Resendes, R.; Cheng, A.; Bartole, A.; Safa-Sefat, A.; Coombs, N.; Stover, H. D. H.; Greedan, J. E.; Ozin, G. A.; Manners, I. *Adv. Mater.* **2001,** *13*, 732-736.

209. Liu, Y.; Chen, Q. *Nanotechnology* **2008,** *19*, (47), 475603/1-475603/6.

210. Marinakos, S. M.; Novak, J. P.; Brousseau III, L. C.; House, B.; Edeki, E. M.; Feldhaus, J. C.; Feldheim, D. L. *J. Am. Chem. Soc.* **1999,** *121*, 8518-8522.

211. Skrabalak, S. E.; Chen, J.; Sun, Y.; Lu, X.; Au, L.; Cobley, C. M.; Xia, Y. *Acc. Chem. Res.* **2008,** *41*, (12), 1587-1595.

212. Kim, S.-W.; M., K.; Lee, W. Y.; Hyeon, T. *J. Am. Chem. Soc.* **2002,** *124*, 7642-7643.

213. Oldenburg, S. J.; Averitt, R. D.; Westcott, S. L.; Halas, N. J. *Chem. Phys. Lett.* **1998,** *288*, 243-247.

214. Chen, J.; Wiley, B. J.; J., M.; Xiong, Y.; Li, Z.-Y.; Xia, Y. N. *Nano. Lett.* **2005,** *5*, 2058-2062.

215. Chen, J.; Saeki, F.; Wiley, B. J.; Cang, H.; Cobb, M. J.; Li, Z.-Y.; Au, L.; Zhang, H.; Kimmey, M. B.; Li, X.; Xia, Y. N. *Nano Lett* **2005,** *5*, 473-477.

216. Bard, A. J.; Faulkner, L. R., *Electrochemical methods: Fundamentals and applications*. 2 ed.; John Wiley & Sons, Inc: 2001.

217. Liang, H.-P.; Zhang, H.-M.; Hu, J.-S.; Guo, Y.-G.; Wan, L.-J.; Bai, C.-L. *Angew. Chem., Int. Ed.* **2004,** *43*, 1540-1543.

218. Vasquez, Y.; Sra, A. K.; Schaak, R. E. *J. Am. Chem. Soc.* **2005,** *127*, 12504-12505.

219. Guo, S.; Fang, Y.; Dong, S.; Wang, E. *J. Phys. Chem. C.* **2007,** *111*, 17104-17109.

220. Guo, S.; Dong, S.; Wang, E. *J. Phys. Chem. C.* **2009,** *113*, 5485-5492.

221. Zeng, J.; Huang, J.; Lu, W.; Wang, X.; Wang, B.; Zhang, S.; Hou, J. *Adv. Mater.* **2007,** *19*, 2172-2176.

222. Zhai, J.; Huang, M.; Zhai, Y.; Dong, S. *J. Mater. Chem.* **2007,** *18*, 923-928.

223. Schwartzberg, A. M.; Olson, T. Y.; Talley, C. E.; Zhang, J. Z. *J. Phys. Chem. C* **2007,** *111*, (44), 16080-16082.

224. Liang, H.-P.; Wan, L.-J.; Bai, C.-L.; Jiang, L. *J. Phys. Chem. B* **2005,** *109*, 7795-7800.

225. Smigelskas, A. D.; Kirkendall, E. O. *Trans. AIME* **1947,** *171*, 130.

226. Fan, H. J.; Goseles, U.; Zacharias, M. *Small* **2007,** *3*, (10), 1660-1671.

227. Yin, Y.; Rioux, R. M.; Erdonmez, C. K.; Hughes, S.; Somorjai, G. A.; Alivisatos, A. P. *Science* **2004,** *304*, (5671), 711-714.

228. Yin, Y.; Erdonmez, C. K.; Cabot, A.; Hughes, S.; Alivisatos, A. P. *Adv. Funct. Mater.* **2006,** *16*, (11), 1389-1399.

229. Cabot, A.; Puntes, V. F.; Shevchenko, E.; Yin, Y.; Balcells, L.; Marcus, M. A.; Hughes, S.; Alivisatos, A. P. *J. Am. Chem. Soc.* **2007,** *129*, 10358-10360.

230. Gao, J.; Zhang, B.; Zhang, X.; Xu, B. *Angew. Chem. Int. Ed.* **2006,** *45*, 1220-1223.

231. Keng, P. Y.; Kim, B. Y.; Shim, I.; Sahoo, R.; Veneman, P. E.; Armstrong, N. R.; Yoo, H.-M.; Pemberton, J. E.; Bull, M. M.; Griebel, J. J.; Ratcliff, E. L.; W., N. K.; Pyun, J. *ACS Nano* **2009,** *3*, (10), 3143-3157.

CHAPTER 2

POLYMER-COATED FERROMAGNETIC COLLOIDS FROM WELL-DEFINED MACROMOLECULAR SURFACTANTS AND ASSEMBLY INTO NANOPARTICLE CHAINS*

2.1: Introduction

The functionalization and organization of magnetic nanoparticles into complex mesostructured assemblies has generated considerable interest as a novel approach to materials synthesis.[1-5] Ferromagnetic colloids are intriguing building blocks for self-or field-induced assembly into one-dimensional (1-D) nanostructures due to the dipolar associations between inorganic nanoparticles.[6-8] Our motivation in this area is to utilize the selective dipolar associations between ferromagnetic colloids as a novel approach for controlled nanoparticle assembly.

A number of groups have reported the incorporation of organic polymers to magnetic colloids using surface-initiated controlled polymerizations,[9, 10] in situ nanoparticle reactions, or block copolymer templates.[11-16] The preparation of polymer-coated ferromagnetic nano-particles is more challenging, as high-temperature annealing steps are often required to convert superparamagnetic colloids into ferromagnetic phases.[17] A few examples of polymer-coated ferro-magnetic nanoparticles of metallic cobalt (Co),[6, 11] or iron[18, 19] have been reported; however, methodologies to synthesize well-defined nanocomposite colloids of uniform size and tunable magnetic properties

have not been extensively developed.

The present study describes the synthesis and characterization of polymer-coated ferromagnetic nanoparticles that organize into extended one-dimensional assemblies when cast onto supporting surfaces. Controlled radical polymerization, specifically, nitroxide-mediated polymerizations,[20-22] enables the preparation of polymeric surfactants which were used as shells to coat ferromagnetic cobalt colloids and ensure uniformity of the particle size. By controlling the macromolecular structure and functionality, we demonstrate for the first time the use of well-defined end-functional polymers to prepare polystyrene-coated ferromagnetic cobalt colloids. The polymer shell imparts long-term colloidal stability to magnetic dispersions in solution, and in the solid state, forms a glassy coating that locks in the 1-D structure of assembled nanoparticle chains through interdigitation of polystyrene outer layers.

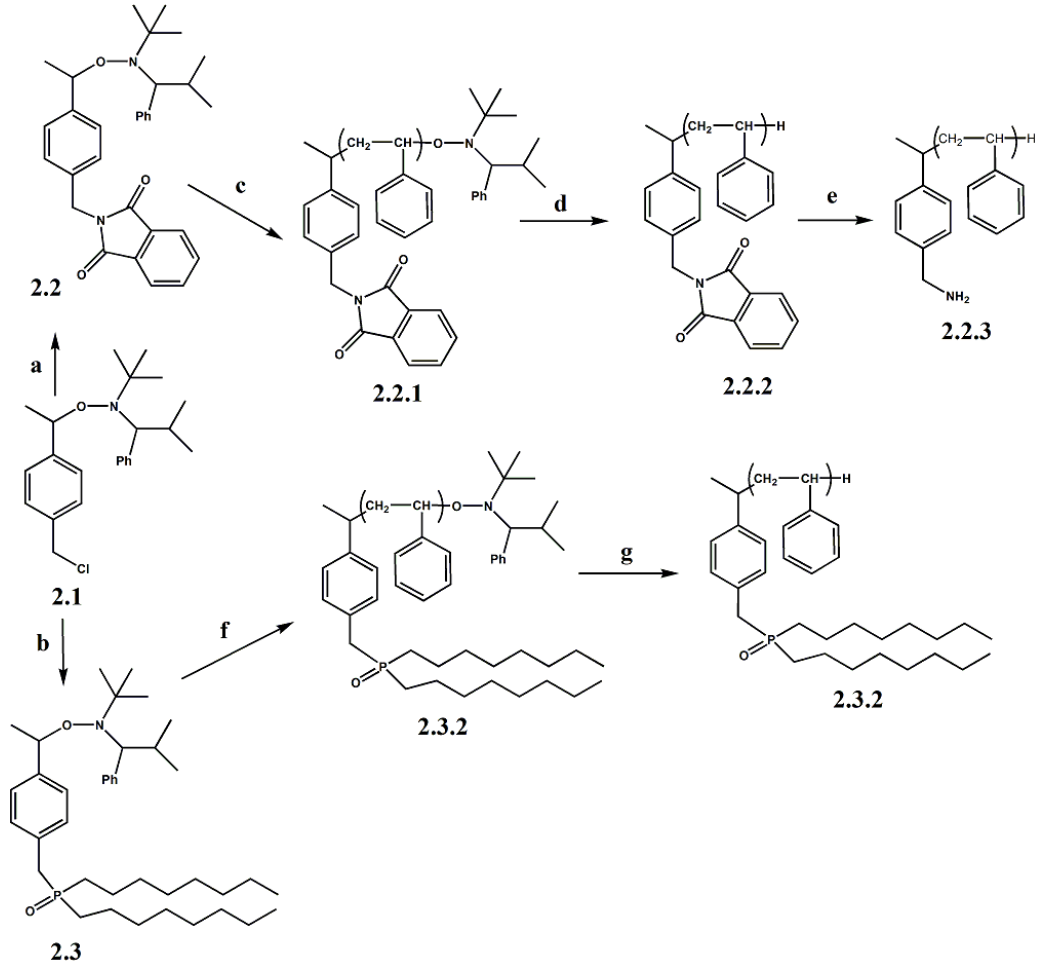

Scheme 2.1: Synthesis of amine end-terminal polystyrene (**2.2.3**) and trioctylphosphine oxide end-terminal (**2.3.2**) polystyrene surfactants via NMP of styrene using functional initiators **2.2** and **2.3**, respectively. Conditions: (a) potassium phthalimide, CH_3CN, 18-crown-6, 50ºC; (b) dioctylphosphine oxide, NaH, anhydrous THF, 50 ºC followed by dropwise addition of benzyl chloride in anhydrous THF, 50 ºC; (c) styrene, anisole, 125 ºC; (d) tributyltin hydride, xylene, 125 ºC; (e) NH_2NH_2, THF, MeOH, RT; (f) styrene, anisole, 125 ºC; (g) tributyltin hydride, xylene, 125 ºC.

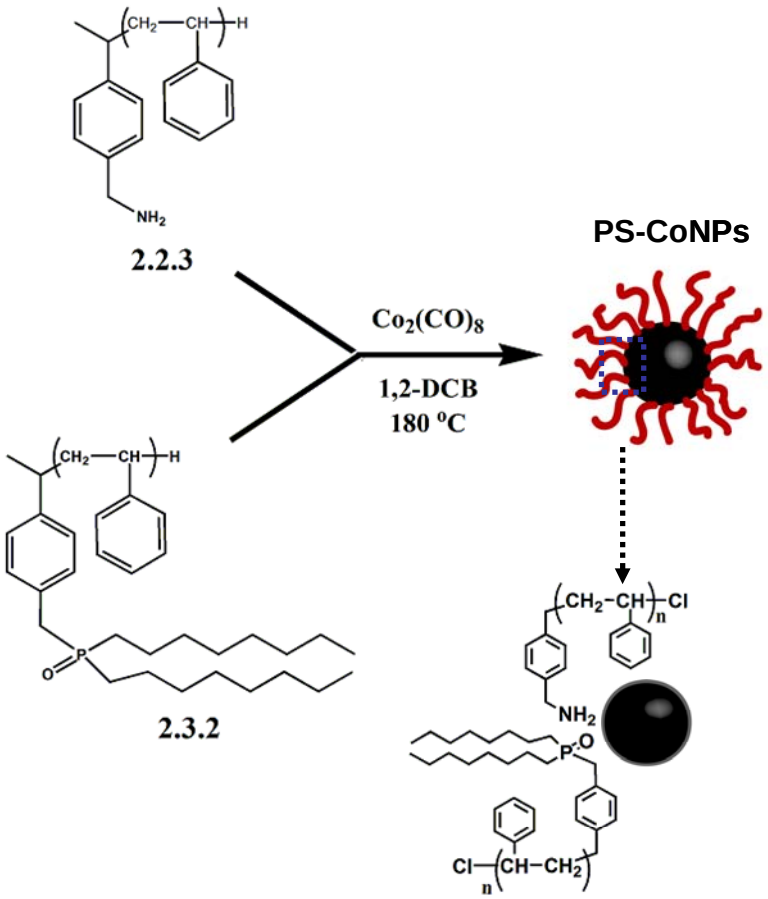

Scheme 2.2: Synthesis of ferromagnetic PS-CoNPs via thermolysis of $Co_2(CO)_8$ using polymeric surfactants **2.2.3** and **2.3.2**.

2.2: Results and discussion

Polystyrene (PS)-coated cobalt nanoparticles were synthesized by the thermolysis of dicobaltoctacarbonyl ($Co_2(CO)_8$) in the presence of end-functional polymeric surfactants in refluxing 1,2-dichlo-robenzene. Two different pS surfactants, **2.2.3** and **2.3.2** (Mn = 5000 g/mol; Mw/Mn =1.09), containing either a benzylamine or dioctylphosphine oxide[23] end group were synthesized to mimic the small molecule surfactant system developed by Alivisatos et al.,[24, 25] using aliphatic amines and

trioctylphosphine oxide (TOPO) (Scheme 2.1). The synthesis of amine functional pS was achieved by alkylation of benzyl chloride functional alkoxyamine **(**2,2,5-trimethyl-3-(1-(4'-chloromethyl)phenylethoxy)-4-phenyl-3-azahexane) (**2.1**) with potassium phthalimide, yielding alkoxyamine **2.2**, which was then used as an initiator in the polymerization of styrene. Phthalimide functional pS **2.2.1** was then reacted with tributyltin hydride to remove the thermally labile alkoxyamine end-group from polymer **2.2.2**. While the presence of the alkoxyamine end-group on pS surfactants was found to not affect the particle formation of ferromagnetic cobalt colloids, this step was performed to eliminate any concerns of alkoxyamine fragmentation during the thermolysis of $Co_2(CO)_8$. Deprotection of the phthalimide group using hydrazine afforded a well-defined amine end-functional polystyrene **2.2.3** ($M_{n\ SEC}$ = 4,950; M_w/M_n = 1.09). Phosphine oxide terminal polystyrene **2.3.2** (PS-DOPO, $M_{n\ SEC}$ = 5,100; M_w/M_n = 1.10) was synthesized using a similar strategy via the controlled polymerization of styrene using alkoxyamine **2.3** to afford **2.3.1**, followed by removal of the alkoxyamine chain end by treatment with tributyltin hydride yielding **2.3.2.**

A mixture of amine and phosphine oxide PS surfactants (4:1 wt ratio) was then used in the thermolysis of $Co_2(CO)_8$ to prepare polymer-coated cobalt nanoparticles, where the ligating end group passivated the colloidal surface (Scheme 2.2). The combination of both amine and phosphine oxide ligands was necessary to yield uniform ferromagnetic nanoparticles (Figure 2.1), which is in agreement with similar studies using small molecule surfactants.[17] Low-magnification TEM images of colloids cast onto surfaces reveal the formation of uniform colloids organizing into extended

nanoparticle chains spanning several microns in length (Figure 2.1 (a)). These chains are easily aligned by deposition of the colloidal dispersion in the presence of weak magnetic fields (100 mT) (Figure 2.1 (b)). TEM images of these 1-D chains at higher magnification clearly demonstrate the presence of individual cobalt nanoparticles ($D_{particle}$ =15 ± 1.5 nm) surrounded by a halo of pS (shell thickness) = 2.0 nm, Figure 2.1 c,d). The retention of the polymer coating on the cobalt colloid was confirmed using X-ray photoelectron spectroscopy, as evidenced by the characteristic signature of pS with peaks at 284 and 288 eV (Figure 2.9 (c)).[10]

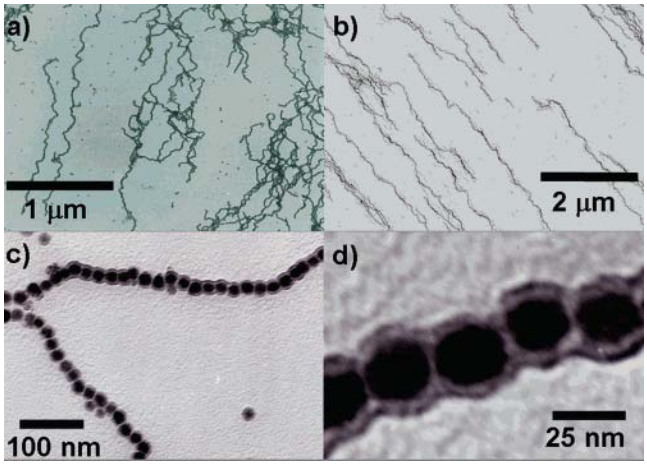

Figure 2.1: TEM images of ferromagnetic PS-CoNPs (a) self-assembled by deposition from toluene dispersions onto carbon-coated copper grids, (b) cast from toluene dispersion and aligned under a magnetic field (100 mT), (c) self-assembled single nanoparticle chains, and (d) high-magnification image visualizing cobalt colloidal core (dark center) and pS surfactant shell (light halo).

2.2.1 Effect of polymer molecular weight

Furthermore, ferromagnetic cobalt colloids were obtained for pS surfactant systems despite variation of the molar mass in the range of 2000-9000 g/mol. A systematic study varying the molecular weight of end-functional polymers was conducted

where different pS surfactants, ranging from M_n ~2000 to 9000 g/mol (Figure 2.2), were evaluated for the preparation of ferromagnetic cobalt nanoparticles. It was found that a mixed surfactant system possessing amine and phosphine oxide groups with a M_n = 5000 g/mol was optimal, resulting in well-defined ferromagnetic nanoparticles of uniform size and shape. In agreement with small molecule systems,[17] it was observed that the use of only one end-functional polymer resulted in poorer control of particle size and morphology, in comparison to the mixed ligand systems. It was observed that variation of polymer surfactant molar mass resulted in broad particle size distributions and decreased uniformity of prepared nanoparticles (Figures 2.3 and 2.4). When using a low molecular weight polymer surfactant system, M_n = 2000 g/mol, a particle size distribution of 15 nm ± 2.5 nm for cobalt cores was observed. In addition, the TEM image indicates a tendency of particles to aggregate together during the process of sample preparation and drying. Conversely, a higher molecular weight polystyrene system, M_n = 8500 g/mol, resulted in smaller, more isolated particles with decreased chaining. The TEM analysis indicated a particle size distribution of 13 nm ± 2.2 nm for cobalt cores. In each case, deviation from the 5,000 g/mol system resulted in broader particle size distributions.

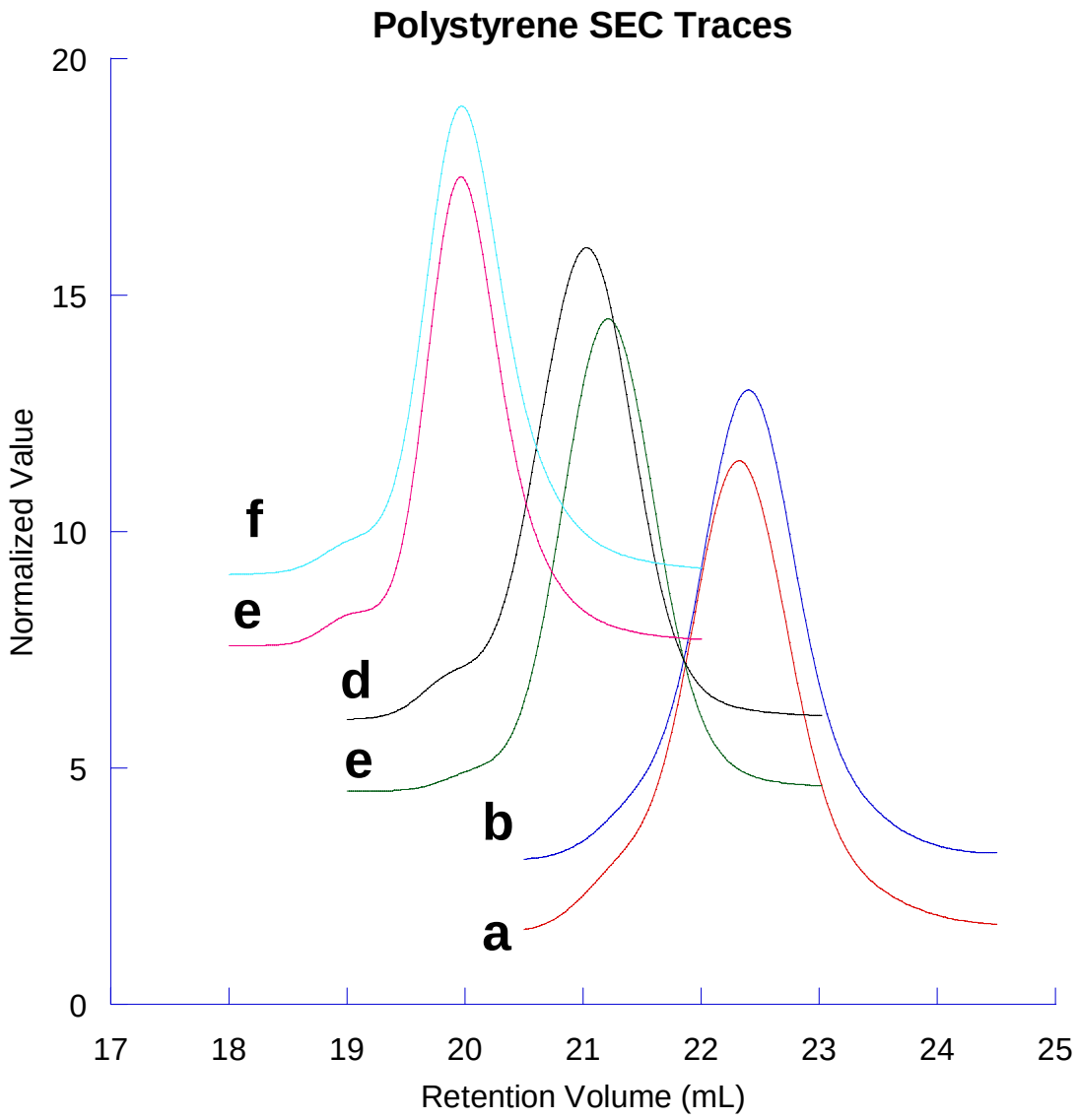

Figure 2.2: SEC traces of end functional polystyrenes used in molecular weight study. In ascending order, a) PS-Phthalimide, M_n= 2400 g/mol, pdi 1.11; b) PS-DOPO, M_n= 2400 g/mol, 1.09; c) PS-Phthalimide (**2.2.2)**, M_n= 4950 g/mol, pdi 1.09; d) PS-DOPO (**2.3.2**), M_n= 5100 g/mol , pdi 1.10; e) PS-Phthalimide, M_n= 8400 g/mol, pdi 1.08; f) PS-DOPO, M_n= 8300 g/mol, pdi 1.10.

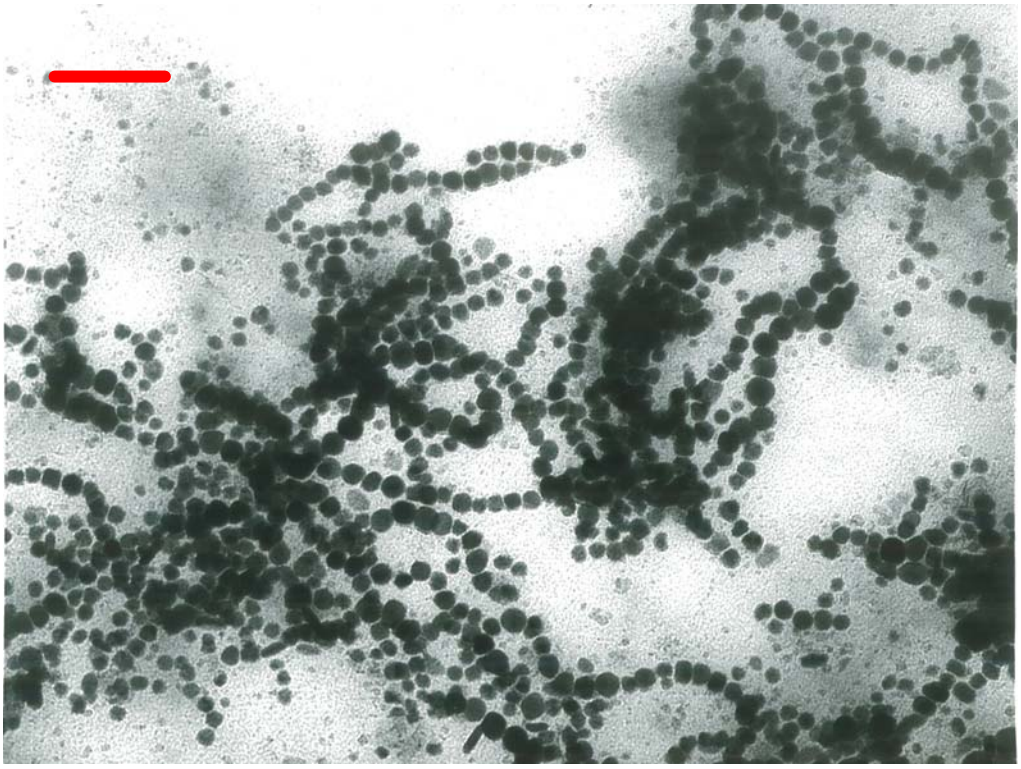

Figure 2.3: TEM image of polystyrene coated cobalt nanoparticles (15 nm ± 2.5 nm) prepared from 2k surfactant system. Bar = 100 nm

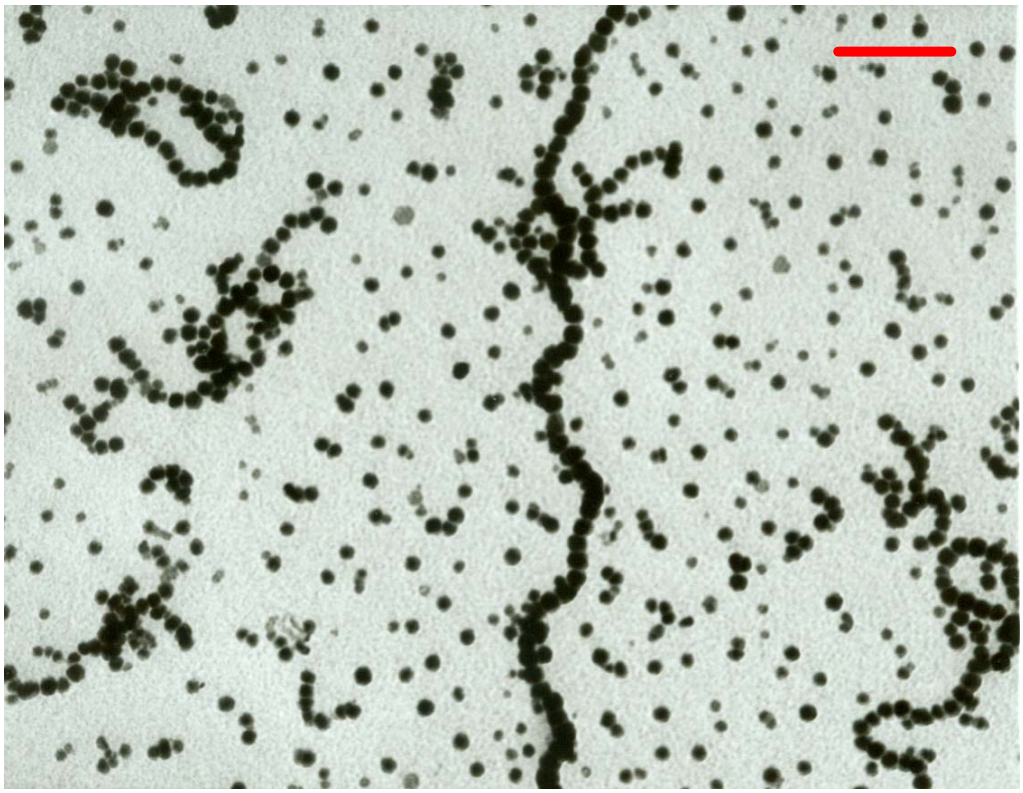

Figure 2.4: TEM image of polystyrene coated cobalt nanoparticles (13 nm ± 2.2 nm) prepared from 8.5k surfactant system. Bar =100 nm

Figure 2.5: TEM image of cobalt nanoparticles (19.7 ± 2.8 nm) prepared from oleic acid and TOPO. Bar= 100 nm

In addition to deviation in particle size, colloidal stability was also observed to be affected by molecular weight. Stable colloidal dispersions were obtained for nanoparticles prepared from polymer surfactants of 5,000 and 8,500 g/mol, where colloids remained dispersed in organic media (e.g., toluene, methylene chloride, THF) over a period of several months. Conversely, colloidal dispersions prepared from either polymer surfactants of 2000 g/mol, or small molecule surfactant (oleic acid, TOPO, Figure 2.5)[25] flocculated out of solution within a 24 hour period (Figure 2.6).

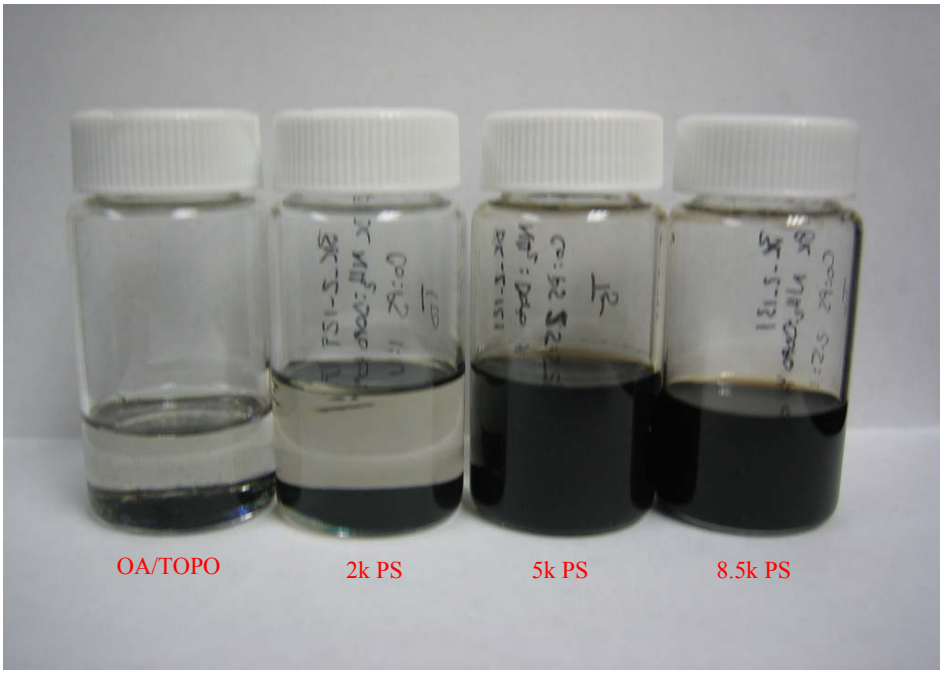

Figure 2.6: Digital image of prepared cobalt nanoparticles from various surfactant systems. In order from left to right, OA/TOPO, 2k PS, 5K PS, 8.5k PS

From these investigation, end-functional polymers possessing Mn = 5000 g/mol afforded the optimal combination of uniform particle size and long-term colloidal stability. This procedure was further optimized to yield gram-scale quantities of well-defined pS-coated cobalt nanoparticles presented in Chapter 3 of this dissertation.

2.2.2 Solid state characterization of PS-CoNPs

These polymer-coated cobalt nanoparticles (PS-CoNPs) were then characterized atomic force microscopy (AFM), and magnetic force microscopy (MFM) to determine the morphology of the polymer-coated magnetic colloids and nanoparticle chains.

Aligned chains of nanoparticles were also clearly evident in topographical AFM (Figure 2.7 a,c) and MFM (Figure 2.7 b) images. All particles in MFM images appeared brighter than the nearby substrate surface, and the observed contrast did not depend on

the direction of tip magnetization. Such behavior can be viewed as an indication that nanoparticle dipole moments were practically parallel to the surface.[10]

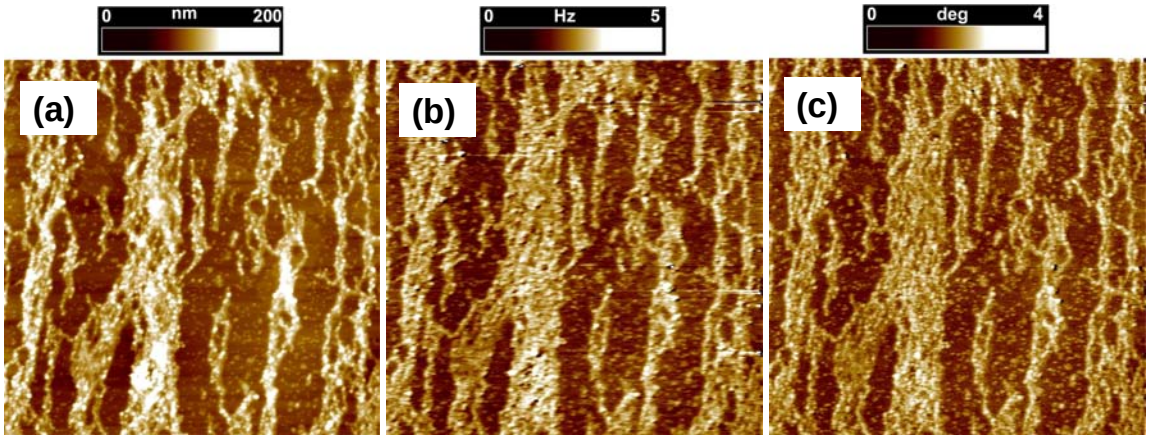

Figure 2.7: Topography and MFM images (size 10 × 10 μm^2) of pS-cobalt nanoparticles cast onto carbon-coated mica in the presence of external magnetic field. **(a)** AFM, height; **(b)** MFM, frequency; **(c)** AFM, phase.

The polymer coated nanoparticles crystalline phase was determined to be fcc-Co by XRD (Figure 2.8). The peaks determined experimentally correspond well with simulated XRD peaks for fcc cobalt nanoparticles previously reported.[25] The observation of fcc cobalt nanoparticles from this polymer surfactant system differs from the ε-phase cobalt nanoparticles typically seen from small molecule systems based aliphatic amines and TOPO.[5] However, the observation of the fcc phase is in agreement with previous reports of cobalt nanoparticle preparation from polymer surfactant systems.[6]

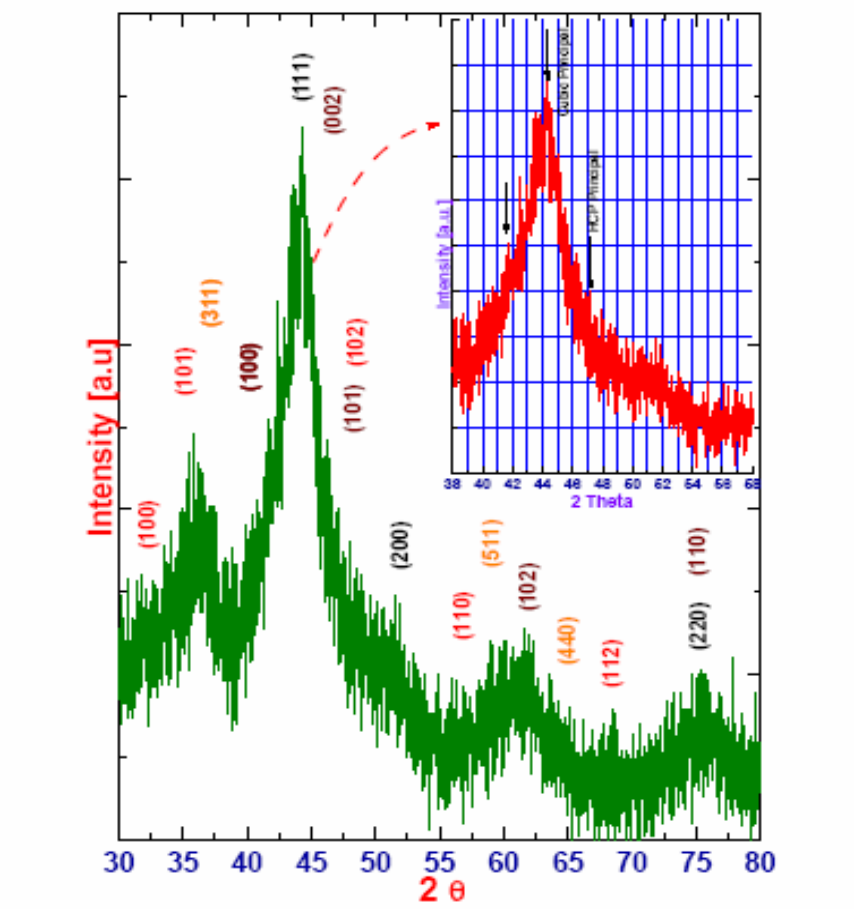

Figure 2.8: XRD spectra of polystyrene coated cobalt nanoparticles indicating fcc phase.

The presence of both polystyrene and metallic cobalt was confirmed using XPS on powders of nanocomposite materials (Figure 2.9). Samples were "demagnetized" before analysis by treatment in a magnetic field to randomize the orientation of nanoparticle dipoles. Peaks at 284 eV and 288 eV were assigned to C1s peaks present in polystyrene. XPS revealed the presence of oxygen (535 eV), cobalt (II) (780 eV) and cobalt (0) (776 eV) species, which confirmed the formation of metallic cobalt and cobalt oxide (CoO). Due to the limited penetration depth of XPS (~ few nanometers), the X-rays are able to more efficiently expel electrons from the pS and CoO shells, and to a

lesser degree from the cobalt metal core. Thus, the content of the CoO phase is inflated in the XPS spectrum, but nevertheless confirms the formation of a pS-cobalt nanocomposite material, in agreement with TEM, AFM and XRD data.

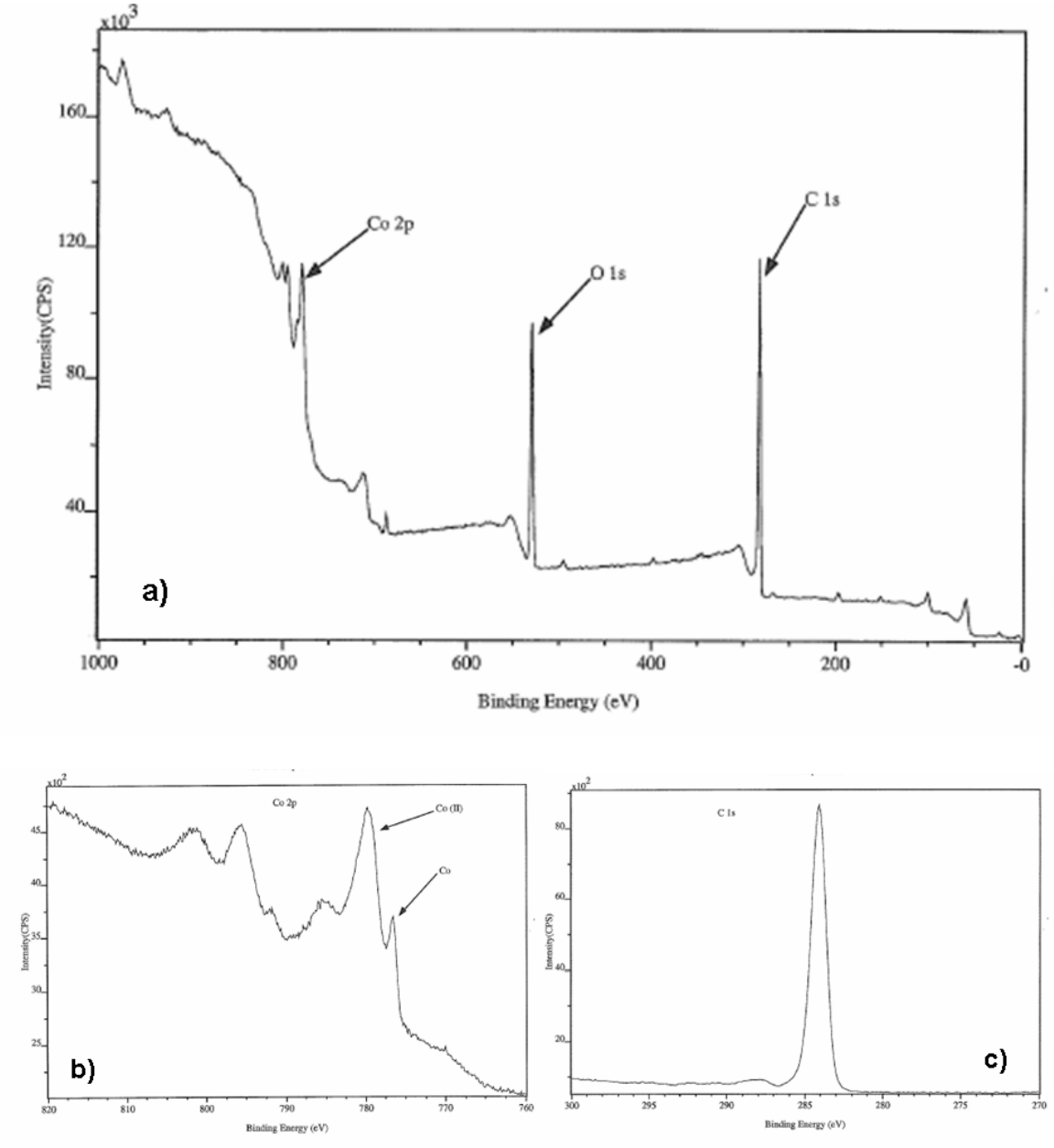

Figure 2.9: (a) XPS spectrum of pS-coated ferromagnetic cobalt colloids (b) expanded spectrum of cobalt peaks (c) expanded spectrum of carbon peaks

Vibrating sample magnetometry (VSM) confirmed that these hybrid materials were weakly ferromagnetic at room temperature (Ms = 38 emu/g, Hc = 100 Oe) and strongly ferromagnetic at 40 K (Ms = 38 emu/g; Hc = 2000 Oe). Significant enhancement of the magnetic coercivity (Hc = 340 Oe) was observed by aligning nanoparticle chains under a weak magnetic field at 300 K due to the coupling of magnetic dipole moments along the 1-D assembly (Figure 2.10).

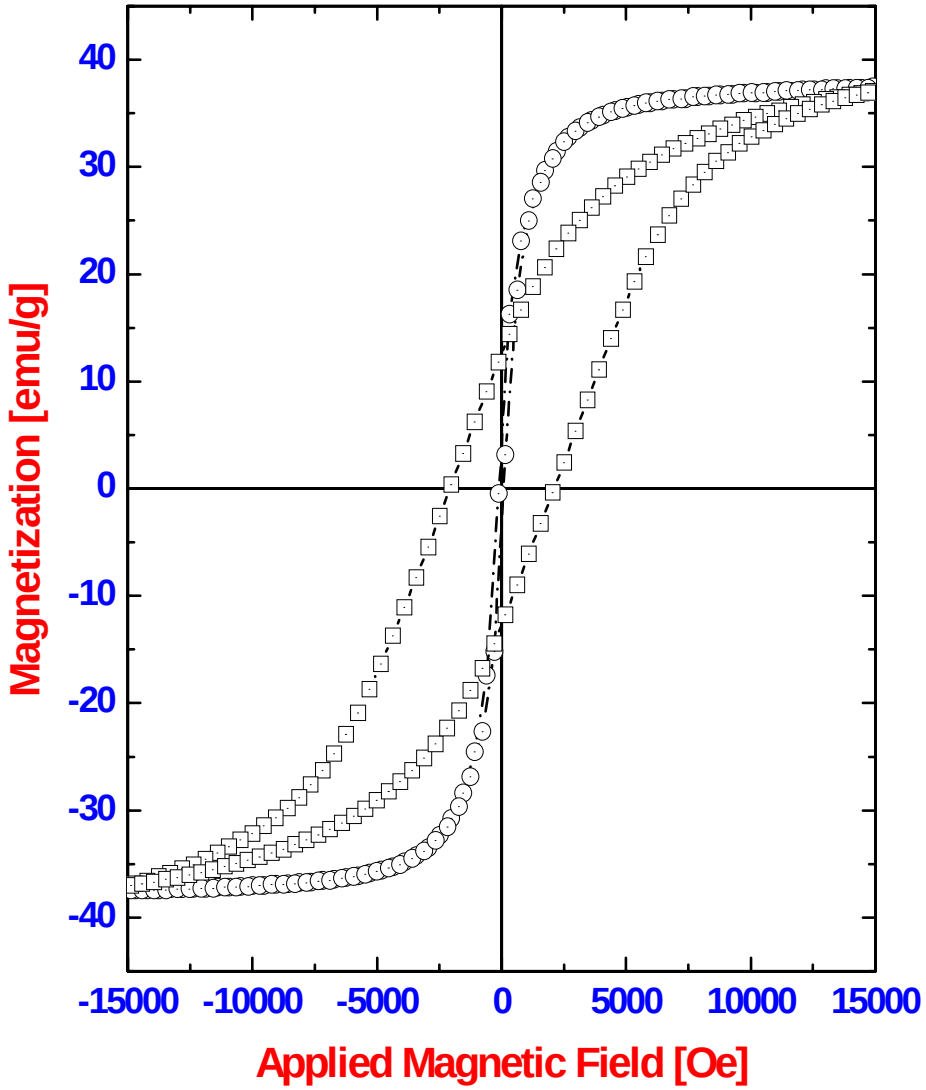

Figure 2.10: VSM spectra of polystyrene coated cobalt nanoparticle powder. □ - 40 K, ○ – 300 K.

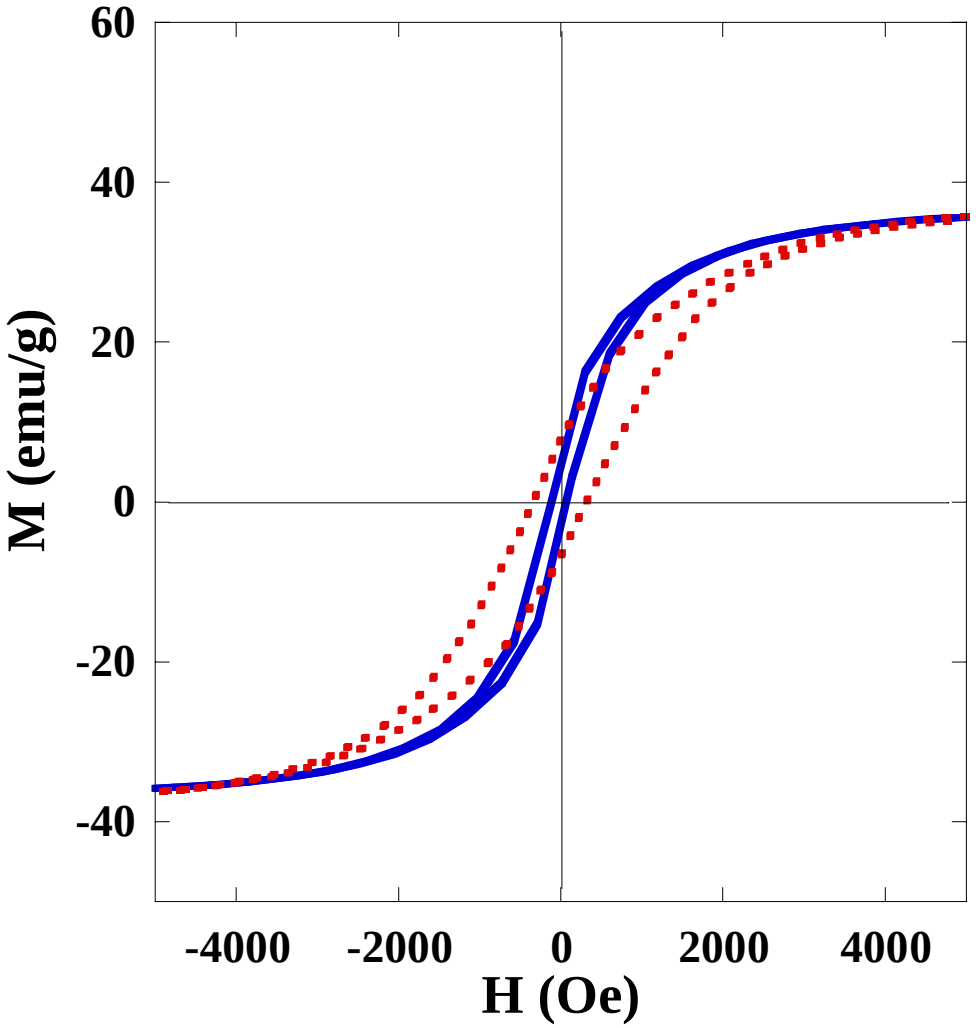

Figure 2.11: VSM spectra of polystyrene coated cobalt nanoparticle powder. Solid Line - 300 K, no alignment; Dotted Line – 300 K, aligned.

In order to investigate the collective magnetic behavior of the aligned cobalt nanoparticles, thin films of polystyrene coated cobalt nanoparticles were prepared in the presence of a weak magnetic field (0.1 T). The thin film was then subjected to VSM

measurement and the results indicated an increase in room temperature coercivity from 110 Oe to 340 Oe due to the magnetic alignment during the film casting process (Figure 2.11).

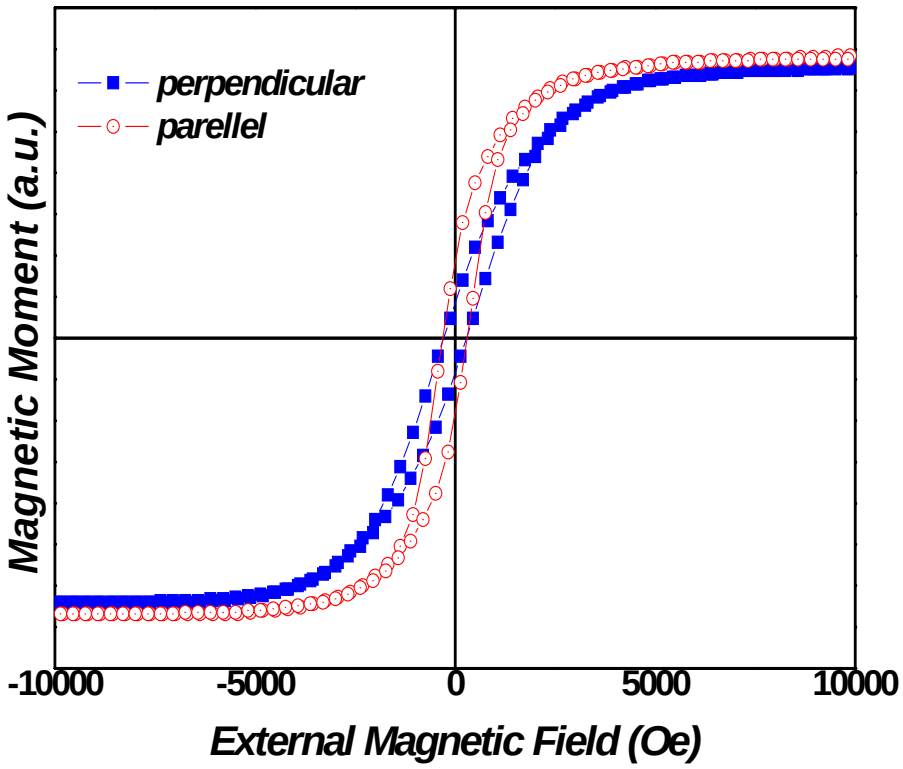

Figure 2.12: VSM spectra of polystyrene coated cobalt nanoparticle powder at 300K after alignment. Circles – parallel to alignment direction; Dotted Line-perpendicular to alignment direction.

Owing to the brittleness of polystyrene coated cobalt nanoparticles, films were cast onto polyethyleneteraphthalate (PET) substrates and VSM was performed from 40 K to 300 K temperature ranges (Figure 2.12). As seen in the M vs. H plots, measurements

parallel to the alignment axis generate standard hysteresis loops. Measurements perpendicular to the aligned film exhibit slightly different behavior, but possess comparable M_s and H_c values. When the applied magnetic field is parallel to the PET substrate, the remanence (M_r) to saturation magnetization (M_s) ratio; M_r/M_s is 0.27. The hysteresis loop is squarer than that obtained perpendicular direction. When the applied magnetic field is perpendicular to the PET substrate, the remanence to saturation magnetization ratio is 0.12. The hysteresis loop is smoother. This change is attributed to the magnetic shape anisotropy for polystyrene coated cobalt nanoparticles onto polyethyleneteraphthalate (PET) substrate. However, the differences of the magnetic hysteresis are weak, because these measurements were performed using thick films (~100 nm) of the nanoparticles. Therefore, the shape anisotropy behavior of polystyrene coated Co aligned chain is diminished because the total demagnetization factor of thick films is lower.

2.2.3 Binary nanoparticle assemblies

To illustrate the potential of 1-D nanoparticle chains for bottom-up binary nanoparticles assembly, ferromagnetic pS-cobalt colloids were blended with silica beads (D = 172 nm) and cast onto TEM grids. Binary assemblies of metallic, magnetic, and semiconductor nanoparticles have been elegantly demonstrated by Murray et al.[26] By controlling the particle size, ratio and deposition method, nanoparticles with different size and functionality self-assembled into binary superlattices yielding multifunctional nanocomposites.[27] Binary superlattices have gained significant research interest due to their potential in creating plethora of new materials with tunable properties and

placement of different components.[27, 28] For example, binary assembly of magnetic nanoparticles composed of FePt (hard phase) and Fe_3O_4 (soft phase) in hexagonal ordered arrays yielded nanocomposites with very high magnetic moment.[29]

In this study, a new binary assembly was demonstrated by exploiting the strong dipolar coupling between ferromagnetic cobalt nanoparticles and secondary forces (entropic, van der Waals, dipole-dipole and electrical charges)[27] of the silica particles to form binary assembly. Silica particles with a diameter of 172 nm ± 22 nm were prepared according to reported methods.[30] The as prepared silica particles based on the Stober method was stabilized via electrostatic interactions in aqueous media. In order to blend into organic solvents, without inducing irreversible flocculation, the silica colloids were functionalized with methacrylate or stearyl ligands based on reported literature.[31, 32]

When a dilute dispersion of binary nanoparticles were deposited at zero field condition, formation of micron-sized assemblies composed of isolated SiO_2 colloids dispersed in a matrix of pS-cobalt nanoparticle chains was imaged using TEM (Figure 2.13). Nanoparticle chains were observed to organize around larger silica inclusions. In a series of control experiments using both oleic acid/TOPO capped superparamagnetic and ferromagnetic cobalt nanoparticles, blends with SiO_2 colloids were performed identically, as for the PS-Co nanoparticles. In both cases, cobalt nanoparicles did not form 1-D assemblies and aggregated within the interstitial voids between SiO_2 particles (Figure 2.14). While the mechanism of this assembly process is yet to be determined, the result suggests the interstitial voids between SiO_2 colloids offer sufficient unoccupied volume for 1-D chains to organize and meander around the much larger SiO_2 inclusion

(Figure 2.13). This lack of mechanical integrity between small molecule surfactant capped cobalt nanoparticles indicates that for PS-Co assemblies, interdigitation of glassy polymers is able to hold together nanoparticle chains in these blending experiments.

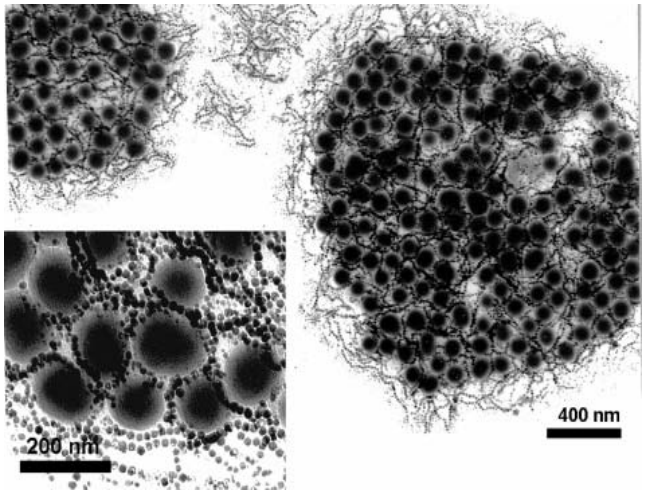

Figure 2.13: TEM image of binary assemblies composed of pS-coated cobalt nanoparticles and SiO_2 beads.

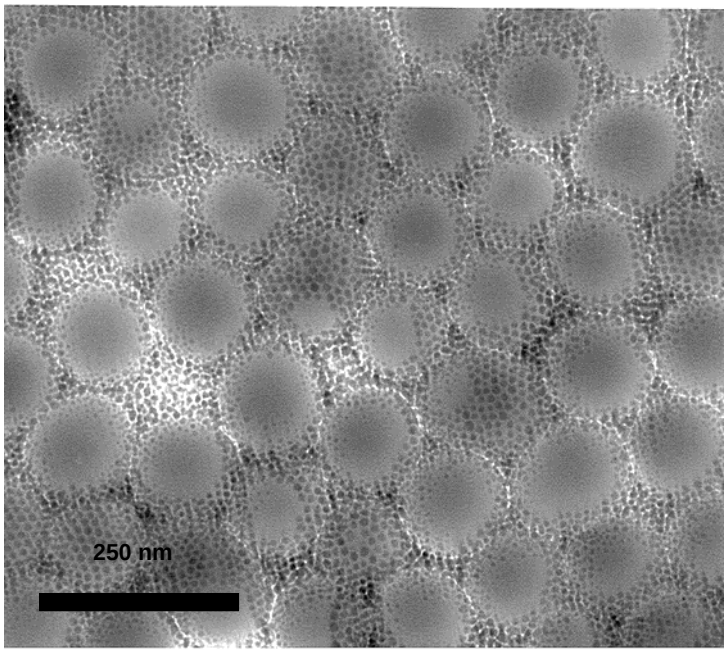

Figure 2.14. TEM image of oleic acid/TOPO capped cobalt nanoparticles (d = 12 nm) blended with methacrylate coated SiO_2 particles (172 nm ± 22nm) (4:1 wt ratio) in toluene (1-wt% solids) and cast onto carbon coated TEM grid

2.3: Conclusion

In conclusion, the synthesis of ferromagnetic cobalt nanoparticles using well-defined polymeric surfactants is described. By control of surfactant structure, ferromagnetic colloids possessing a polymeric shell were synthesized. These functional colloids are intriguing building blocks for bottom-up materials synthesis and novel mesoscopic assemblies. This first study established a synthetic methodology which enabled the preparation of well-defined magnetic nanoparticles as a 'chemical reagent' in the preparation of functional 1-D mesostructures.

2.4: Experimental

Materials: 1,2-Dichlorobenzene (DCB), toluene, anhydrous tetrahydrofuran, neutral alumina, 1,4,7,10,13,16-hexaoxacyclooctadecane (18-crown-6), acetonitrile (ACN), acetone, dichloromethane (DCM), hexanes (HEX), methanol (MeOH), anisole, hydrazine hydrate, tributyl tin hydride, magnesium sulfate, and potassium fluoride were purchased from Aldrich and used as received without further purification. Styrene was purchased from Aldrich and passed through a short column of neutral alumina to remove inhibitors prior to use in polymerizations. Dicobaltoctacarbonyl was purchased from Strem Chemicals and used as received. The synthesis of 2,2,5-trimethyl-3-(1-(4'-chloromethyl)phenylethoxy)-4-phenyl-3-azahexane (benzyl chloride initiator),[22] dioctyl phosphonite,[23, 33] and linear polymers of polystyrene[22] were prepared following reported methods. Flash chromatography was performed using silica gel from VWR (230-400 mesh) and TLC plates coated with silica gel (60 F_{254}) (Merck). Nuclear magnetic resonance (NMR) was performed using a Bruker DRX 500 MHz FT-NMR spectrometer, operating XWinNMR software (Bruker). Size exclusion chromatography (SEC) was performed in a tetrahydrofuran mobile phase with a Waters 1515 isocratic pump running three 5 μm PLgel columns (Polymer Labs, pore sizes 10^4, 10^3, 10^2Å) with a Waters 2414 differential refractometer and Waters 2487 dual wavelength UV-Vis spectrometer. Molar masses were calculated using the Empower software (Waters) calibrating against low polydispersity linear polystyrene standards. TEM images were obtained on a JEM100CX II transition electron microscope (JEOL) at an operating voltage of 60 kV, using in house prepared copper grids (Cu, hexagon, 270 mesh). Analysis of images was carried out using

ImagePro 4.1 software (MediaCybernetics). VSM measurements were obtained using a Waker HF 9H electromagnet with a Lakeshore 7300 controller and a Lakeshore 668 power supply. Magnetic measurements were carried out at room temperature (300 K) and low temperature (40 K), with a maximum applied field of 15 kOe, a ramp rate of 33 Oe/s and a time constant of 0.1. DSC data was obtained using a 2920 Modulated DSC (TA Instruments) running Thermal Solutions 1.4E (TA Instruments) software. DSC measurements were run in the range of -35° C to 200° C, at a ramp rate of 10° C per minute. TGA analysis was carried out using a TGA Q50 (TA Instruments) instrument and software from TA Instruments. TGA measurements were taken from 20° C to 900° C at a ramp rate of 20° C per minute. XRD measurements were performed using the X'pert x-ray diffractometer (PW1827) (Phillips) at room temperature with a CuKa radiation source at 40 kV and 30 mA. The scan angle was from 30 to 80 degrees with a scan size of 0.2 degrees and a scan time of 0.5 seconds per 0.2 degrees. XPS characterization was performed on a KRATOS 165 Ultra photoelectron spectrometer, using a monochromatic Al Kα radiation source. Magnetic force microscopy (MFM) studies were carried out with the aid of a Nanoscope III-M system (Digital Instruments, Santa Barbara, CA), equipped with a J-type "vertical engage" scanner. The MFM observations were performed at room temperature in air using silicon cantilevers with nominal spring constant of 1-5 N/m and nominal resonance frequency of 24-33 kHz (Co/Cr coated etched silicon probes). Topographic images were acquired with the cantilever oscillating at a frequency at which the oscillation amplitude was equal to 50% of amplitude on resonance. Typically, the ratio of cantilever operating amplitude *A* to

free amplitude A_o ranged from 0.7 to 0.8 with A_o = 2V (uncalibrated detector signal). Non-contact MFM images were acquired simultaneously with topography using interleaved lift mode, and frequency or phase shift detection. In the interleaved MFM scan, the cantilever was oscillated at its resonance frequency with the amplitude ranging from 7 to 14 V, and was scanned at the lift height of 150 nm above the previously recorded topographic profile. High lift heights and cantilever amplitudes employed here were shown by other authors to assure, respectively, good separation of magnetic effects from topography and improved signal-to-noise ratio.[34] All the images were acquired at a scan frequency of 1 Hz. Before imaging, the tips were magnetized with an external magnet and checked by imaging a standard magnetic recording tape. AFM/MFM samples were prepared by drop casting colloidal dispersions (1-wt% in toluene) onto carbon coated mica. Field aligned samples were prepared in a similar fashion between the poles of a horseshoe magnet (100 mT).

Preparation of 2,2,5-trimethyl-3-(1-(4'-phthalimidemethyl)phenylethoxy)-4-phenyl-3-azahexane (benzyl phthalimide initiator) (**2.2**). To a 25 mL round bottom flask equipped with a magnetic stir bar was added benzyl chloride initiator, **2.1** (2.00 g, 5.36 mmol), potassium phthalimide (1.41 g, 7.61 mmol), 18-crown-6 (0.20 g, 0.76 mmol), and acteonitrile (10 mL). The reaction was stirred at 50° C overnight under argon. The reaction was then filtered through a coarse glass frit, washed with acetone to remove any solids, and concentrated *in vacuo* to yield a yellow oil. The yellow oil was purified via flash chromatography with an initial hexanes/dichloromethane elution mixture of 4:1 with a gradual increase to a 1:1 mixture yielding a yellow oil (2.06 g, 79.4%) (R_f = 0.20,

1:1 Hexanes/Dichloromethane). ^{1}H NMR (500 MHz, $CDCl_3$, diastereomers) δ 7.83 (2H, dd, J = 5.4, 3.1 Hz, ArH), δ 7.69 (2H, dd, J = 5.4, 3.1 Hz, ArH), δ 7.412-7.3 (4H, m, ArH), δ 7.26-7.1 (5H, m, ArH), δ 4.9-4.75 (3H, m, CH+CH_2), δ 3.39, 3.28 (1H, d, J = 10.7 Hz, CH, diastereomers), δ 2.34-2.23 (1H, m, CH), δ 1.57, 1.495 (3H, d, J = 6.6 Hz, CH_3 diastereomers), δ 1.273, 0.88, 0.52, 0.16 (6H, d, J = 6.4 Hz, CH_3, diastereomers), δ 1.014, 0.765 (9H, s, CH_3, diastereomers); ^{13}C NMR (125 MHz, $CDCl_3$, diastereomers) δ 168.0, 145.3, 144.5, 142.3, 142.1, 135.3, 134.5, 133.9, 132.1, 130.9, 130.8, 128.3, 127.3, 127.1, 126.3, 126.1, 123.3, 83.0, 82.1, 72.1, 60.5, 53.4, 41.4, 32.0, 31.6, 28.4, 28.2, 24.7, 23.0, 22.1, 21.9, 21.1, 21.0. m/z found (Low Res, FAB): 485.07.

Preparation of 2,2,5-trimethyl-3-(1-(4'-dioctylphosphorylmethyl)phenylethoxy)-4-phenyl-3-azahexane (benzyl DOPO initiator) (**2.3**). To a 100 mL three neck round bottom flask equipped with a magnetic stir bar and condenser was added dioctylphosphine oxide (3.29 g, 12.03 mmol) and sodium hydride (0.33 g, 14.03 mmol) in anhydrous THF (30 mL). The reaction was heated under argon at 50° C for 30 minutes followed by the slow dropwise addition of benzyl chloride initiator **2.1** (3.00 g, 8.021 mmol) in anhydrous THF (20 mL) over a period of 30 minutes. The reaction was heated at 50° C overnight under argon. After cooling to room temperature, the reaction was quenched with H_2O (10 mL) and then concentrated *in vacuo* to give an oil. The oil was dissolved in dichloromethane, dried over $MgSO_4$, and re-concentrated *in vacuo*. The oil was purified via flash chromatography with an initial eluent of dichloromethane gradually increasing to a 10:1 mixture of dichloromethane/methanol yielding a slightly yellow oil (4.17 g, 84.9%) (R_f = 0.34, 10:1 Dichloromethane/Methanol). ^{1}H NMR (500

MHz, $CDCl_3$, diastereomers) δ 7.48-7.36 (2H, m, ArH), δ 7.28-7.12 (7H, m, ArH), δ 4.88 (1H, m, CH), δ 3.35, 3.28 (1H, d, J = 10.6 Hz, CH, diastereomers), δ 3.15, 3.09 (2H, d, J = 15 Hz, CH_2, diastereomers), δ 2.34-2.30 (1H, m, CH), δ 1.61-1.48 (12H, m, CH_3+CH_2), δ 1.42-1.19 (22H, m, CH_2), δ 1.04, 0.75 (9H, s, CH_3 diastereomers), δ 0.93-0.82 (6H, m, CH_2+CH_3) δ 0.54, 0.20 (3H, d, 6.6Hz, CH_3 diastereomers). ^{13}C NMR (125 MHz, $CDCl_3$, diastereomers) δ 144.3, 143.7, 142.3, 142.0, 131.5, 131.4, 130.9, 130.8, 129.0, 127.5, 127.3, 127.1, 126.7, 126.3, 126.1, 83.0, 82.5, 72.3, 72.0, 60.6, 60.3, 36.4, 36.3, 35.9, 35.8, 32.0, 31.8, 31.7, 31.2, 31.1, 29.0, 28.4, 28.2, 27.7, 27.4, 27.2, 26.9, 24.4, 23.2, 22.6, 22.2, 22.0, 21.6, 21.1, 21.0, 14.0. m/z found (Low Res, FAB): 612.2.

Preparation of benzyl phthalimide end functional polystyrene (**2.2.1**). To a 10 mL Schlenk flask equipped with stir bar was added **2.2** (0.23 g, 0.48 mmol), styrene (4.00 g, 38.4 mmol), and anisole (3.00 g). The reaction was bubbled with argon for 20 minutes followed by three freeze-pump-thaw cycles. The Schlenk flask was then submerged into an oil bath (125° C) for 12 hours. The reaction was diluted with dichloromethane (1 mL) and precipitated into stirring methanol (500 mL). The precipitation procedure was performed twice followed by drying *in vacuo*, to yield a white powder (3.00 g, M_n = 4950, M_w/M_n = 1.09, 89%). ^{1}H NMR (500 MHz, $CDCl_3$) δ 7.82 (b, ArH), δ 7.66 (b, ArH), δ 7.1-6.5 (bm, ArH), δ 4.77 (b, CH_2), δ 2.4-1.2 (bm, CH+CH_2), δ 1.05-0.7 (bm, CH_3), δ 0.6-0.4 (bm, CH_3).

Removal of alkoxyamine chain end functionality with tributyl tin hydride (**2.2.2**). To a 10 ml Schlenk flask equipped with stir bar was added **2.2.1** (M_n = 4,950 g/mol) (1.00 g, 0.208 mmol), xylene (2.00 g), and tributyl tin hydride (0.30 g, 1.042 mmol). The

reaction solution was bubbled with argon for 20 minutes and was followed by three freeze-pump-thaw cycles. The Schlenk flask was then submerged into an oil bath (125° C) for 12 hours. The reaction was precipitated into stirring methanol (600 ml) to yield a slightly yellow solid (0.78 g, 82% yield). Tin byproduct was removed by dissolving the polymer in dichloromethane and passing the solution through a short SiO_2/KF column (10% KF by weight) in a manner previously reported.[35] Residual tin byproduct indicated by NMR to be less than 5%. ^{1}H NMR (500 MHz, $CDCl_3$) δ 7.82 (b, ArH), δ 7.66 (b, ArH), δ 7.3-6.3 (bm, ArH), δ 4.77 (b, CH_2), δ 2.4-1.2 (bm, CH+CH_2), δ 1.0-0.9 (b, CH_3).

Reduction of phthalimide functionality with hydrazine hydrate to yield amine end-terminal polystyrene (**2.2.3**). To a screw cap scintillation vial equipped with a stir bar was added **2.2.2** (M_n = 4,950 g/mol) (1.50 g, 0.306 mmol) dissolved in THF (10mL). Methanol (0.63 g) was added dropwise followed by addition of hydrazine hydrate (0.200 g, 3.99 mmol). The reaction solution was stirred at room temperature for 24 hours, after which a white precipitate could be seen in the reaction media. The reaction mixture was concentrated and redissolved in tetrahydrofuran, followed by precipitation into stirring methanol (500ml). The precipitation sequence was carried out twice followed by drying *in vacuo* to yield benzyl amine end-functional polystyrene as a white powder (1.25 g, 86%). ^{1}H NMR (500 MHz, $CDCl_3$) δ 7.3-6.3 (bm, ArH), δ 3.85-3.75 (b, CH_2), δ 2.4-1.2 (bm, CH+CH_2), δ 1.05-0.9 (b, CH_3).

Preparation of benzyl DOPO end-functional polystyrene (**2.3.2**). To a 10 mL Schlenk flask equipped with stir bar was added **2.3** (0.23 g, 0.38 mmol), styrene (2.10 g, 20.19 mmol), and anisole (1.10 g). The reaction solution was bubbled with argon for 20

minutes and was followed by three freeze-pump-thaw cycles. The schlenk flask was then submerged into an oil bath (125° C) for 12 hours. The reaction was diluted with dichloromethane (1mL) and precipitated into stirring MeOH (500 mL). The precipitation was performed two times and was dried *in vacuo* to yield a white powder (1.7 g, 88%; M_n = 5,100; M_w/M_n = 1.10). ^{1}H NMR (500 MHz, $CDCl_3$, diastereomers) δ 7.3-6.3 (bm, ArH), δ 3.1-3.0 (b, CH_2), δ 2.4-1.2 (bm, CH+CH_2), δ 1.05-0.7 (bm, CH_3), δ 0.6-0.5 (bm, CH_3).

Removal of alkoxyamine chain end functionality with tributyl tin hydride (**2.3.2**). To a 10 ml Schlenk flask equipped with stir bar was added **2.3.1** (M_n = 5,300 g/mol) (1.0 g, 0.189 mmol), xylene (2.00 g), and tributyl tin hydride (0.274 g, 0.943 mmol). The reaction was then bubbled with argon for 20 minutes and was followed by three freeze-pump-thaw cycles applying a final argon backfill to provide positive atmosphere. The Schlenk flask was then submerged into an oil bath (125° C) for 12 hours. The reaction was precipitated into stirring MeOH (600 ml) to yield benzyl DOPO end functional polystyrene as slightly yellow solid (0.754 g, 75% yield). Tin byproducts were removed by dissolving polymer in dichloromethane and passing through a short SiO_2/KF column (10% KF by weight) in manner previously reported.[35] Residual tin byproducts were found to be less than 5% by NMR. ^{1}H NMR (500 MHz, $CDCl_3$) δ 7.3-6.3 (bm, ArH), δ 3.1-3.0 (b, CH_2), δ 2.44-1.3 (bm, CH+CH_2), δ 1.05-0.85 (bm, CH_3).

Preparation of polystyrene coated cobalt nanoparticles (**PS-CoNPs**). The synthesis of cobalt nanoparticles was adapted from the hot injection method pioneered by Bawendi and Murray in preparing uniform sized quantum dots.[17] In the hot injection method, an

organometallic precursor was rapidly injected into a hot coordinating solvent to achieve temporal discrete nucleation. Supersaturation of reagent concentration upon injection resulted in the burst of nuclei followed by the growth of precursor on existing nuclei. In the presence of suitable coordinating surfactants, homogeneous growth of nanoparticles was achieved.

To a three neck round bottom flask with a magnetic stir bar and condenser was added end-functional polystyrenes **2.2.3** (0.080 g, 0.017 mmol) and **2.3.2** (0.020 g, 4.1x 10^{-3} mmol) in dichlorobenzene (12 mL). The flask was flushed with argon for 10 minutes followed by submersion into an oil bath (180° C) for 10 minutes under argon. A solution of dicobaltoctacarbonyl (0.40 g, 1.17 mmol) in dichlorobenzene (4 mL) was injected into a refluxing, stirring solution over a period of 30 seconds. The evolution of a gas was observed. The reaction was heated for 15 minutes and was cooled to room temperature with continuous stirring under argon. The collected reaction mixture was then precipitated into stirring hexanes (500 mL). The precipitate was collected by sedimentation using a standard AlNiCo magnet followed by decanting of the hexanes phase. The resulting precipitate was then dried *in vacuo* to give a black powder (**PS-CoNPs**) (yield: 0.150 g) that was soluble in a wide range of non-polar solvents (e.g. toluene, THF, CH_2Cl_2) and was responsive to an external magnetic field.

Preparation of polystyrene coated cobalt nanoparticles for TEM imaging and analysis. Polystyrene coated cobalt colloids in powder form (5 mg) were dispersed in organic solvent (20 mL) from which a drop of solution was placed onto a carbon coated strip of mica and allowed to dry. Organic solvents, toluene and tetrahydrofuran, as well

as halogenated solvents, dichloromethane and chlorobenzene, were able to disperse the polystyrene coated cobalt nanoparticles to give colloidal dispersions that were stable over a period of several months prior to the submission of the manuscript. The carbon coating of the mica strip was lifted onto a droplet of nanopure water followed by lifting of the carbon layer onto a copper grid. The copper grid was allowed to dry prior to imaging. Images of the polystyrene coated cobalt nanoparticles indicated a cobalt core size of 15.0 nm ± 1.5 nm with a polymer shell of 2 nm (Figure 1d). It was observed in the TEM images that polymer coated nanoparticles self assembled into 1-D fiber like structures extending over microns in length, both in the absence and presence of an external magnetic field during drying.

***** Done in collaboration with Bryan Korth with focus on binary nanoparticles assemblies.

2.5: References

1. Klokkenburg, M.; Vonk, C.; Claesson, E. M.; Meeldijk, J. D.; Erne, B. H.; Philipse, A. P. *J. Am. Chem. Soc.* **2004,** *126*, (51), 16706-16707.

2. Goubault, C.; Leal-Calderon, F.; Viovy, J.-L.; Bibette, J. *Langmuir* **2005,** *21*, (9), 3725-3729.

3. Grzybowski, B. A.; Stone, H. A.; Whitesides, G. M. *Nature* **2000,** *405*, 1033-1036.

4. Germain, V.; Pileni, M.-P. *Adv. Mater.* **2005,** *17*, (11), 1424-1429.

5. Cheng, G.; Romero, D.; Fraser, G. T.; Walker, A. R. H. *Langmuir* **2005,** *21*, (26), 12055-12059.

6. Thomas, J. R. *J. Appl. Phys.* **1966,** *37*, (7), 2914-15.

7. Safran, S. A. *Nature Mater.* **2003,** *2*, (2), 71-72.

8. Bao, Y.; Beerman, M.; Krishnan, K. M. *J. Magn. Magn. Mater.* **2003,** *266*, (3), L245-L249.

9. Vestal, C. R.; Zhang, Z. J. *J. Am. Chem. Soc.* **2002,** *124*, (48), 14312-14313.

10. Marutani, E.; Yamamoto, S.; Ninjbadgar, T.; Tsujii, Y.; Fukuda, T.; Takano, M. *Polymer* **2004,** *45*, (7), 2231-2235.

11. Platonova, O. A.; Bronstein, L. M.; Solodovnikov, S. P.; Yanovskaya, I. M.; Obolonkova, E. S.; Valetsky, P. M.; Wenz, E.; Antonietti, M. *Colloid. Polym. Sci.* **1997,** *275*, (5), 426-431.

12. Rutnakornpituk, M.; Thompson, M. S.; Harris, L. A.; Farmer, K. E.; Esker, A. R.; Riffle, J. S.; Connolly, J.; St. Pierre, T. G. *Polymer* **2002,** *43*, (8), 2337-2348.

13. Sohn, B. H.; Cohen, R. E. *Chem. Mater.* **1997,** *9*, (1), 264-269.

14. Tadd, E. H.; Bradley, J.; Tannenbaum, R. *Langmuir* **2002,** *18*, (6), 2378-2384.

15. Wang, X.-S.; Arsenault, A.; Ozin, G. A.; Winnik, M. A.; Manners, I. *J. Am. Chem. Soc.* **2003,** *125*, (42), 12686-12687.

16. Garcia, C. B. W.; Zhang, Y.; Mahajan, S.; DiSalvo, F.; Wiesner, U. *J. Am. Chem. Soc.* **2003,** *125*, (44), 13310-13311.

17. Sun, S.; Murray, C. B. *J. Appl. Phys.* **1999,** *85*, (8, Part 2A), 4324-4330.

18. Griffiths, C. H.; O'Horo, M. P.; Smith, T. W. *J. Appl. Phys.* **1979,** *50*, 7108-7115.

19. Burke, N. A. D.; Stoever, H. D. H.; Dawson, F. P. *Chem. Mater.* **2002,** *14*, (11), 4752-4761.

20. Matyjaszewski, K.; Xia, J. *Chem. Rev.* **2001,** *101*, (9), 2921-2990.

21. Hawker, C. J.; Bosman, A. W.; Harth, E. *Chem. Rev.* **2001,** *101*, (12), 3661-3688.

22. Benoit, D.; Chaplinski, V.; Braslau, R.; Hawker, C. J. *J. Am. Chem. Soc.* **1999,** *121*, (16), 3904-3920.

23. Skaff, H.; Ilker, M. F.; Coughlin, E. B.; Emrick, T. *J. Am. Chem. Soc.* **2002,** *124*, (20), 5729-5733.

24. Puntes, V. F.; Krishnan, K. M.; Alivisatos, A. P. *Science* **2001,** *291*, (5511), 2115-2117.

25. Puntes, V. F.; Zanchet, D.; Erdonmez, C. K.; Alivisatos, A. P. *J. Am. Chem. Soc.* **2002,** *124*, (43), 12874-12880.

26. Redl, F. X.; Cho, K.-S.; Murray, C. B.; O'Brien, S. *Nature* **2003,** *423*, 968-971.

27. Shevchenko, E. V.; Talapin, D. V.; Rogach, A. L.; Weller, H. *Nanopart. Assem. Superstruct.* **2006**, 341-368.

28. Urban, J. J.; Talapin, D. V.; Shevchenko, E.; Kagan, C. R.; Murray, C. B. *Nature Mater.* **2007,** *6*, 115-121.

29. Zeng, H.; Li, J.; Liu, J. P.; Wang, Z. L.; Sun, S. *Nature* **2002,** *420*, 395.

30. Stober, W.; Fink, A. *J. Coll. Inter. Sci.* **1968,** *26*, 62-69.

31. Philipse, A. P.; Vrij, A. *J. Colloid Interface Sci.* **1989,** *128*, (1), 121-36.

32. Van Helden, A. K.; Jansen, J. W.; Vrij, A. *J. Coll. Inter. Sci.* **1981,** *2*, 354-368.

33. Latham, A. H.; Williams, M. E. *Acc. Chem. Res.* **2007,** *41*, 411-420.

34. Puntes, V. F.; Gorostiza, P.; Aruguete, D. M.; Bastus, N. G.; Alivisatos, A. P. *Nature Mater.* **2004,** *3*, (4), 263-268.

35. Harrowven, D. C.; Guy, I. L. *Chem. Comm.* **2004,** *17*, 1968-1969.

CHAPTER 3

SYNTHESIS AND SELF-ASSEMBLY OF POLYMER-COATED FERROMAGNETIC NANOPARTICLES

3.1: Introduction

In the present study, a simplified methodology in synthesizing polymer-coated ferromagnetic cobalt nanoparticles using well-defined macromolecules was developed expanding upon the previous investigation described in chapter 2. In the previous method, only 150 mg of cobalt nanoparticles were realized per reaction batch, inhibiting further utilization of these dipolar colloids. The 'bottle neck' of the polymer synthesis in the previous approach was the synthesis of the alkoxyamine initiators that involved multistep reactions, and the used of an expensive catalyst (Jacobsen's catalyst). This limitation prohibited the used of these dipolar colloids as building blocks for the investigation of magnetic assemblies, surface and core functionalization chemistries. In this chapter, a simplified methodology was developed to yield 1.3 g of well-defined polystyrene-coated cobalt nanoparticles. Additionally, novel dipolar assemblies were experimentally presented, which agreed with the 'rule-based' simulations performed by Jack Douglas.

The use of dipolar nanoparticles as building blocks to prepare organized hierarchical materials is an emerging area of great potential in materials chemistry. Ferromagnetic colloids are of interest for this application, as the inherent dipole moment of these materials enable one-dimensional (1-D) and two-dimensional (2-D) assembly

into novel mesostructures.[1-8] Numerous previous reports have demonstrated the formation of magnetic assemblies from both ferromagnetic and superparamagnetic nanoparticles (NPs) on supporting surfaces to form 1-D chains,[9-16] flux closure rings,[17-19] 2-D superlattices of closed packed nanocrystals[3, 20-26] and 3-D labyrinth-like suprastructures.[27-33] Additionally, organized assemblies of magnetic nanoparticle building blocks have also been directly observed in solution using cryogenic electron microscopy[34-37] and atomic force microscopy of assemblies at crosslinkable oil-water interfaces.[38, 39] One of the basic challenges of studying and utilizing these materials is obtaining appreciable quantities of ferromagnetic nanoparticles possessing uniform size and well-defined magnetic properties. Additionally, these ferromagnetic nanoparticles should also possess tunable surface chemistry and robust capping ligands that enable facile redispersion of isolated nanoparticle powders into common organic solvents after storage in air. Recent advances achieved in the solution synthesis of monodisperse magnetic NPs has enabled compositional control to enable preparation of metallic, metal oxide or bimetallic alloys using small molecule surfactants.[40, 41]

In addition to small molecule surfactants, the preparation of organic-inorganic magnetic nanocomposites that possess polymer shells and magnetic nanoparticle cores has also been conducted.[42, 43, 44] This approach is particularly attractive since the modular nature of polymeric materials enables the synthesis of a wide range of hybrid nanocomposites.[45-48] Pre-synthesized magnetic NPs (Fe, Co, Fe_2O_3, Fe_3O_4) have also been decorated with various functional macromolecules such as polyethylene glycol (PEG),[49-53] polyamidoamine (PAMAM) dendrimers,[54] and crosslinkable polymer

shells[55, 56] to impart water solubility, controlled interparticle spacing and colloidal stability, respectively. Alternatively, surface initiated polymerization has been employed to graft well-defined (co)polymers onto superparamagnetic nanoparticles enabling tunable film thickness, composition and mechanical properties.[57-67]

Polymer coated ferromagnetic nanoparticles (CoNPs) have been synthesized by the thermolysis of metal carbonyl precursors ($Co_2(CO)_8$, $Fe(CO)_5$) in the presence of functional polymeric surfactants such as random copolymers containing polar groups,[10, 68] and within block copolymer templates.[69-73] Stöver and coworkers have also demonstrated the preparation of polymer coated iron nanoparticles in multi-gram quantities.[44] However a simple preparation of uniform and well-defined polymer coated ferromagnetic cobalt nanoparticles in appreciable quantities has not been reported. Based on the pioneering work of Thomas,[10] and Alivisatos[74, 75] our group expanded upon these synthetic methodologies by preparing well defined end functional polystyrene surfactants bearing either amine, or phosphine oxide ligating moieties to mediate the growth of ferromagnetic polystyrene coated cobalt nanoparticles (PS-CoNPs).[76] This approach is attractive as the characteristics of polymers and small molecule surfactants are combined, enabling the preparation of uniform ferromagnetic colloids that assembled into 1-D mesoscopic chains. In our previous report, functional alkoxyamine initiators were synthesized by nitroxide mediated polymerization (NMP)[77, 78] to prepare end-functional polystyrene surfactants of precise molar mass and composition. However, this approach was not amenable to synthesize large quantities of PS-CoNPs due to the multi-step synthesis required for functional alkoxyamine initiators.

In the present study, a simplified synthesis of uniform ferromagnetic polystyrene coated cobalt nanoparticles (PS-CoNPs) from the thermolysis of dicobaltoctacarbonyl ($Co_2(CO)_8$) using end-functional polystyrene surfactants prepared using atom transfer radical polymerization (ATRP) is reported.[79] The use of ATRP to prepare polystyrene surfactants afforded a facile route to these materials using commercially available starting materials, or precursors that were readily prepared with a minimal number of synthetic steps. Furthermore, we report on our mechanistic investigation into the preparation of PS-CoNPs using various polymeric surfactants. During the course of this effort, a facile method to synthesize PS-CoNPs to nearly one-gram batches was developed which answered the need of sample production as previously discussed. The experimental observation of a novel dipolar assembled morphology using these ferromagnetic PS-CoNPs is also reported.

3.2: Results and Discussion

The general approach that was developed to synthesize polymer coated ferromagnetic nanoparticles utilized a dual-stage temperature thermolysis of $Co_2(CO)_8$ in the presence of end-functional polystyrene surfactants (Scheme 3.1). End-functionalized polystyrenes bearing amine, phosphine oxide or carboxylic acid ligands (PS-NH_2, PS-DOPO, PS-COOH, respectively) were prepared using initiators **3.1**, **3.2** (Scheme 3.1) and **3.3** (Scheme 3.2) for ATRP. Using this process, well-defined polystyrenes with precise molar mass and composition were prepared. In the current report, we investigated the effect of different polymeric surfactant combinations on the decomposition of $Co_2(CO)_8$ for the preparation of polystyrene coated ferromagnetic cobalt nanoparticles (PS-CoNPs).

These end-functional PS-NH_2, PS-DOPO, PS-COOH were polymeric analogues to commonly used small molecule surfactants of aliphatic/oleyl amines (AA), trioctylphosphine oxide (TOPO) and oleic acid (OA).[74, 75] It has previously been shown that these small molecule surfactants allowed for the preparation of a range of well-defined superparamagnetic and ferromagnetic CoNPs by combining these surfactants (e.g., TOPO/OA, AA/TOPO) in different feed ratios. This previous work served as a reference point in our own synthesis using polymeric surfactants PS-NH_2 (**3.1.2**), PS-DOPO (**3.2.1**), (Scheme 3.1) and PS-COOH (**3.3.1**) (Scheme 3.2). Molar masses (number average- M_n) in the regime of M_n = 5,000-10,000 g/mol were previously determined to be optimal to afford ferromagnetic PS-CoNPs.[76] In the course of this investigation, we have developed a simplified synthesis of PS-CoNPs that was amenable to 820 mg quantities per batch of relatively uniformly sized ferromagnetic nanoparticles with improved handling characteristics when isolated as powders.

3.2.1 Synthesis of end functionalized polystyrene surfactants.

In the preparation of PS-NH_2 (**3.1.2**) (M_n = 4,800 g/mol; M_w / M_n = 1.08), initiator **3.1** was synthesized by the statistical coupling reaction of α,α'-dichloro-p-xylene (DCX) with potassium phthalimide, ATRP of styrene, followed by deprotection using hydrazine hydrate to afford PS-NH_2 (**3.1.2**) (Scheme 3.1). The synthesis of PS-DOPO (**3.2.1**) utilized the preparation of 4-(methoxymethyl)benzyl chloride which was conducted via a statistical alkylation of DCX with $NaOCH_3$, followed by alkylation with dioctylphosphineoxide (DOPO) and deprotection with boron trichloride (BCl_3) to afford initiator **3.2**.[80 81, 82] Initial attempts to directly alkylate DXC with stoichiometric amounts

of DOPO resulted in unidentified byproducts that were most likely derived from the radical anionic species as discussed by Rachon *et al.*[83] ATRP of styrene using initiator **3.2** yielded PS-DOPO (**3.2.1**) (M_n = 4,500 g/mol; M_w / M_n = 1.15; Scheme 4.1). Initiator **3.3** was commercially available and was directly used in the solution ATRP of styrene to afford PS-COOH (**3.3.1**) (M_n = 9,500 g/mol; M_w/M_n = 1.11; Scheme 3.2). All ATRP reactions used a copper(I) halide (chloride or bromide) and bipyridine based ligands (4,4'-dinonyl-2,2'-bipyridine, or 2,2'-bipyridine) catalyst system in the presence of N,N-dimethylformamide (DMF-20 % volume fraction) as a cosolvent to dissolve the copper complex. The use of DMF as a cosolvent afforded homogeneous conditions for ATRP and enabled direct use of initiators **3.2** and **3.3** without the need for protecting group strategies.[84]

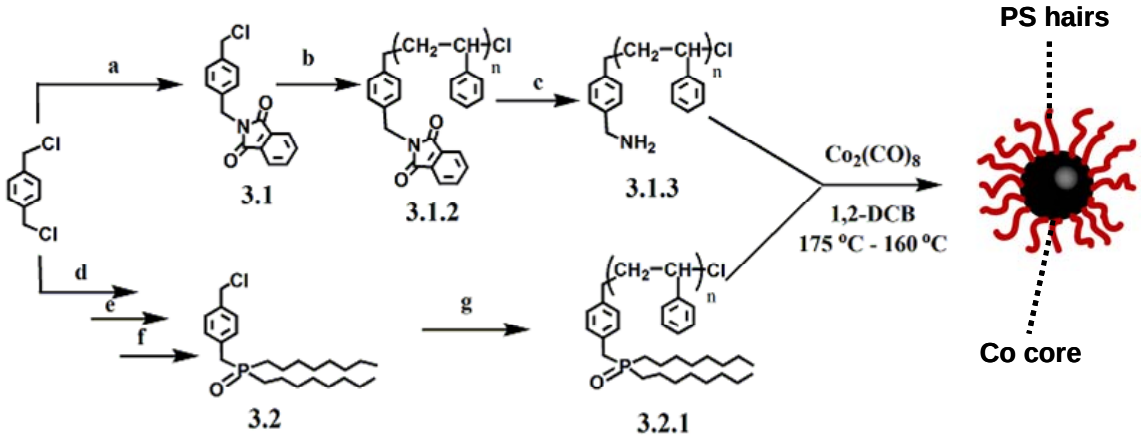

Scheme 3.1: Synthesis of ferromagnetic PS-CoNPs via thermolysis of $Co_2(CO)_8$ using a dual stage temperature process at 175 °C and 160 °C using PS-NH_2 (**3.1.2**) and PS-DOPO (**3.2.1**) surfactants. Synthesis of polymeric surfactants **3.1.2** and **3.2.1** was conducted via ATRP of styrene using functional initiators **3.1** and **3.2**, respectively. Conditions: (a) potassium phthalimide, CH_3CN, 80 ºC; (b) styrene, CuCl, 2,2'-bipyridine, DMF, 110 ºC; (c) NH_2NH_2, THF, MeOH, 25 ºC; (d) $NaOCH_3$, MeOH, THF, 25 ºC; (e) DOPO, NaH, THF, 65 ºC; (f) BCl_3, CH_2Cl_2, 0 ºC; (g) styrene, CuCl, 4,4'-dinonyl-2,2'-bipyridine, 110 ºC. (h) thermolysis of the $Co_2(CO)_8$ was performed at 175 ºC followed by growth at 160 ºC for 30 minutes.

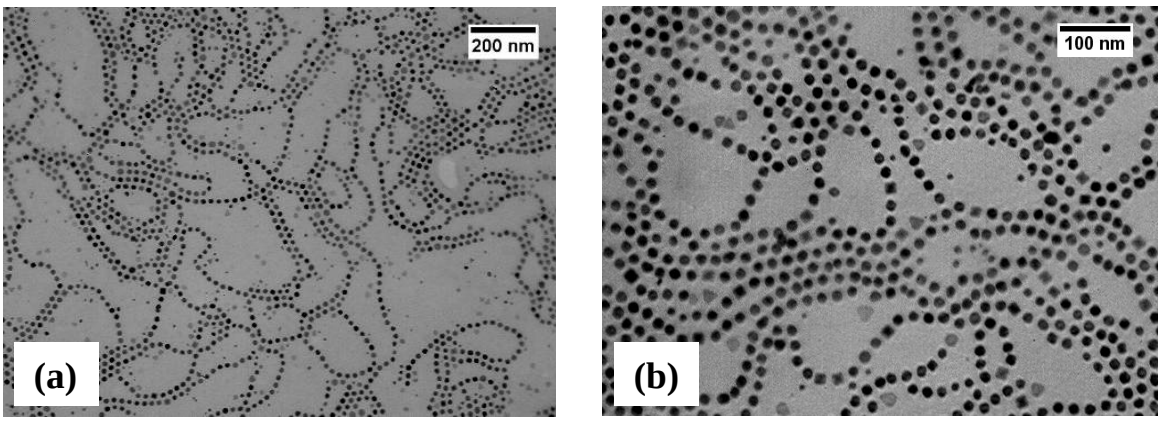

Figure 3.1: TEM micrographs of PS-CoNPs imaged at low (a) and high magnification (b) prepared using a mixture of PS-NH_2 (**3.1.2**) and PS-DOPO (**3.2.1**) in the thermolysis of $Co_2(CO)_8$ as shown in Scheme 1. The PS-CoNPs (as prepared; $D_{PS\text{-}CoNPs}$ = 17 nm ± 1.8 nm) were cast onto supported surfaces from a particle dispersion in toluene.

3.2.2 Preparation of PS-CoNPs

Following the preparation of end-functionalized polystyrene surfactants **3.1.2**, **3.2.1** and **3.3.1,** the synthesis of PS-CoNPs was investigated using a dual-stage temperature thermolysis of $Co_2(CO)_8$. Recently, Lin *et al.* demonstrated that uniformly sized superparamagnetic CoNPs (particle diameter (D) = 9.5 nm) could be prepared by using the small molecule surfactants OA/TOPO along with a dual-stage temperature (180 ºC and 130 ºC) treatment.[85] In our modified dual-stage particle synthesis, a room temperature solution of $Co_2(CO)_8$ was rapidly injected into a hot mixture of polymeric surfactants (T = 175 ºC) to induce a rapid homogeneous nucleation of nanoparticles and a subsequent drop in temperature to 160 ºC. Growth of the CoNP was maintained at 160 ºC for 30 min, yielding a viscous, stable ferrofluid. Initially, the dual-stage temperature treatment was evaluated using a mixture of PS-NH_2 (**3.2.2**) and PS-DOPO (**3.2.1**) prepared using ATRP as illustrated in Scheme 1. Transmission electron

microscopy (TEM) images (Fig. 3.1) of the resulting PS-CoNPs ($D_{PS\text{-}CoNPs}$ nm = 17 nm ± 1.8 nm) showed organization of dipolar colloids into extended nanoparticle chains when cast onto supporting surfaces from a toluene dispersion. An interesting additional phenomenon apparent in Figure 3.1 was the tendency of adjacent chains to form zippering configurations where the chains were in close contact and the particles in the adjacent chain were centered in the gap regions between the particles. Recent simulations have indicated that this behavior was expected when strong mutual isotropic attractive (Yukawa) interactions were present, in addition to the directional dipolar interactions arising from the magnetic interactions.[86] We will return to a discussion of these interactions below.

Additionally, stable, redispersable powders could be recovered after precipitation due to the presence of a hairy polystyrene corona coordinated onto the CoNP surfaces. PS-CoNPs obtained from the current procedure possessed comparable size and magnetic properties to materials prepared using our previously reported methodology where PS-NH_2 and PS-DOPO were synthesized using NMP.[76] This result confirmed that the size uniformity and magnetic properties of CoNPs synthesized from end-functional polystyrene surfactants were independent of the polymerization mechanism (i.e., ATRP versus NMP) used to prepare the polymeric surfactants, when using identical ligand chemistry and similar regimes of molar mass and polydispersity.

There is precedent for the feed ratios of metal precursor and surfactant to strongly affect particle size and magnetic properties.[9, 72, 74, 87] Similar trends using PS-NH_2/PS-DOPO surfactants were observed, where a 4:1 mass ratio of $Co_2(CO)_8$ to polymeric

surfactants was found to be optimal for the synthesis of ferromagnetic PS-CoNPs.[76] However, using the current synthetic conditions shown in Scheme 3.1, nearly uniform ferromagnetic PS-CoNPs were prepared ($D_{PS\text{-}CoNPs} \approx 17$ nm). This was found despite the variation in the feed of the metal precursors to the polymeric surfactants from 4:1 up to 1.5:1 mass ratios of $Co_2(CO)_8$ to PS-NH_2/PS-DOPO. PS-CoNPs prepared using this methodology contained a relative mass fraction of approximately 40 % of the organic polymer shell in comparison to the approximately 20 % relative mass indicated in our previous report[76], as determined by thermogravimetric analysis (TGA). While counter-intuitive, this series of experiments demonstrated that temperature conditions used in the thermolysis of $Co_2(CO)_8$ exhibited a stronger effect on particle size and magnetization than feed ratios of metal precursors to polymeric surfactants. Furthermore, the ability to add higher loadings of polymeric surfactant without compromising the growth of ferromagnetic CoNPs greatly improved the handling and storage characteristics of powders isolated by precipitation from stable ferrofluids. Isolated PS-CoNPs prepared from this process were easily dispersed in a wide range of non-polar organic solvents (e.g., toluene, chlorobenzene, tetrahydrofuran, dichloromethane) and were able to be stored in air without significant loss of magnetic properties over periods of weeks and months as confirmed from VSM and XRD. However, one significant limitation of this dual-stage temperature process was that only ferromagnetic CoNPs could be prepared, as the synthesis of superparamagnetic CoNPs could not be accessed by variation of metal precursor/surfactant feed ratios. Further mechanistic studies on the growth mechanism of CoNP under these conditions are under investigation.

The strategy to prepare ferromagnetic PS-CoNPs was further expanded to other combinations of polymeric surfactants (PS-NH_2 (**3.1.2**) and PS-COOH (**3.3.1**)), as inspired by work using AA and OA small molecule surfactant mixtures (Scheme 2.2).[74, 75, 88] This particular surfactant system was attractive, as carboxylic acid initiator **3.3** was commercially available and also able to be directly used in ATRP to prepare PS-COOH (**3.3.1**). Identical reaction conditions were employed in the preparation of ferromagnetic PS-CoNP using PS-NH_2 (**3.1.2**) and PS-COOH (**3.3.1**) as for PS-NH_2/PS-DOPO surfactants as previously discussed (Scheme 2.1). These TEM images showed that relatively well-defined PS-CoNPs ($D_{PS\text{-}CoNPs}$ = 21 nm ± 3.1 nm) were prepared using these conditions. While PS-CoNPs prepared using PS surfactants (**3.1.2**) and (**3.3.1**) were slightly larger than PS-CoNPs prepared from PS-NH_2/PS-DOPO surfactants, similar morphologies of nanoparticle chains were observed in TEM when cast from toluene dispersions onto carbon coated TEM grids (Figure 3.2).

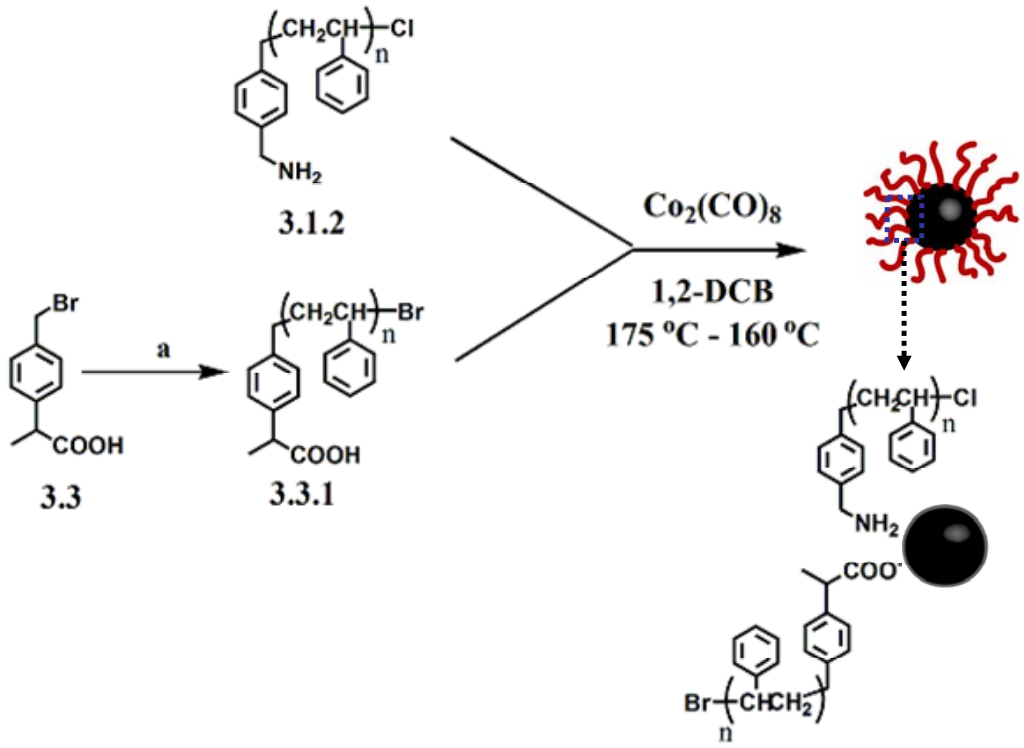

Scheme 3.2: Synthesis of ferromagnetic PS-CoNPs via thermolysis of $Co_2(CO)_8$ using a dual stage temperature process at 175 °C and 160 °C using PS-NH_2 (**3.1.2**) and PS-COOH (**3.3.1**) surfactants. Synthesis of PS-COOH (**3.3.1**) was conducting by the ATRP of styrene using functional initiator **3.3.** Conditions: (a) styrene, CuBr, 2,2'-bipyridine, DMF, 110 ºC; (b) thermolysis of the $Co_2(CO)_8$ was performed at 175 °C followed by growth at 160 °C for 30 minutes.

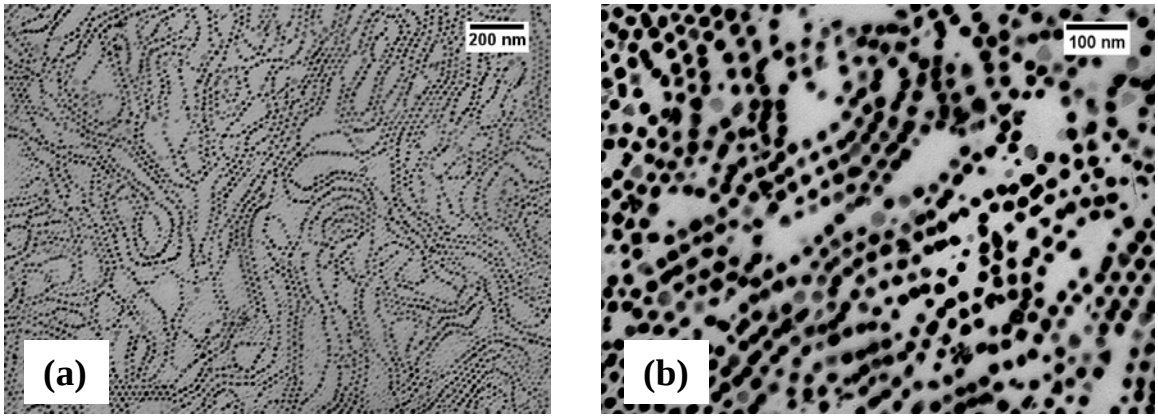

Figure 3.2: TEM images of self-assembled ferromagnetic PS-CoNPs ($D_{PS\text{-}CoNPs}$ = 21 nm ± 3.1 nm) at low (a) and high magnification (b) prepared from a mixture of PS-NH_2

(**3.1.2**) and PS-COOH (**3.3.1**) in the thermolysis of $Co_2(CO)_8$. The PS-CoNPs were cast onto supporting surfaces from a particle dispersion in toluene.

Control experiments were performed using a single surfactant of either PS-NH_2 (**3.1.2**) (Scheme 3) or PS-COOH (**3.3.1**) (Scheme 3.2) in the dual-stage temperature thermolysis of $Co_2(CO)_8$. Surprisingly, when the identical particle reactions were conducted using only PS-NH_2 (**3.1.2**) as a single surfactant system (Scheme 3.3), similar particle sizes and morphologies were produced as when surfactant combinations of PS-DOPO (**3.2.1**), or PS-COOH (**3.3.1**) were employed. TEM images (Fig. 3.3) of this sample showed relatively uniform particle size ferromagnetic PS-CoNPs ($D_{PS\text{-}CoNPs}$ = 21 nm ± 2.9 nm) and the formation of self-assembled nanoparticle chains. However, additional control experiments using only PS-COOH (**3.3.1**) (Scheme 3.4) under the same conditions resulted in large scale agglomeration and poorly-defined PS-CoNPs of varying sizes and morphologies (Figure 3.4).

Using this simplified synthetic procedure, we then prepared larger quantities of ferromagnetic PS-CoNPs. While numerous reports have shown the ability to prepare both superparamagnetic and ferromagnetic nanoparticles, the development of synthetic methods enabling access to larger quantities of ferromagnetic CoNPs that are able to isolated and redispersed into organic media remains an important challenge. This synthetic method using only PS-NH_2 (**3.1.2**) was particularly attractive for scaling up the preparation of ferromagnetic CoNPs as ATRP could be used to prepare multi-gram quantities of **PS-CoNPs** (see Experimental). By simply scaling up the quantities used in model small scale particle reactions, isolated yields of 240 mg, 400 mg, and 820 mg of

ferromagnetic PS-CoNPs were obtained. TEM confirmed that for all conditions, particle sizes were in the range of 17 nm to 21 nm with narrow size distributions (2 nm to 3 nm).

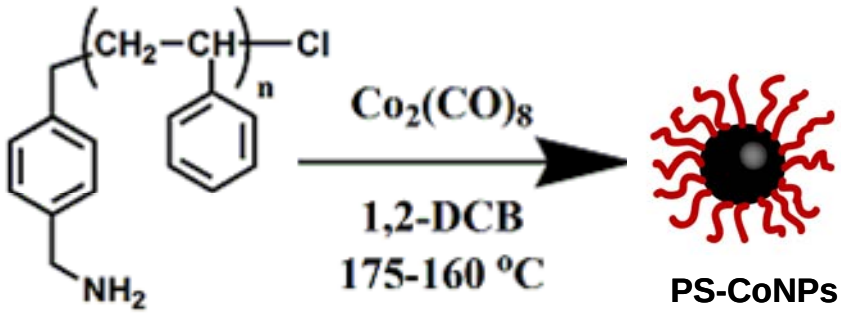

3.1.2

Scheme 3.3: Synthesis of PS-CoNPs using only PS-NH_2 (**3.1.2**) in the thermolysis of dicobalt octacarbonyl at 175 °C and 160 °C. The thermolysis of the $Co_2(CO)_8$ was performed at 175 ^oC followed by growth at 160 ^oC for 30 minutes.

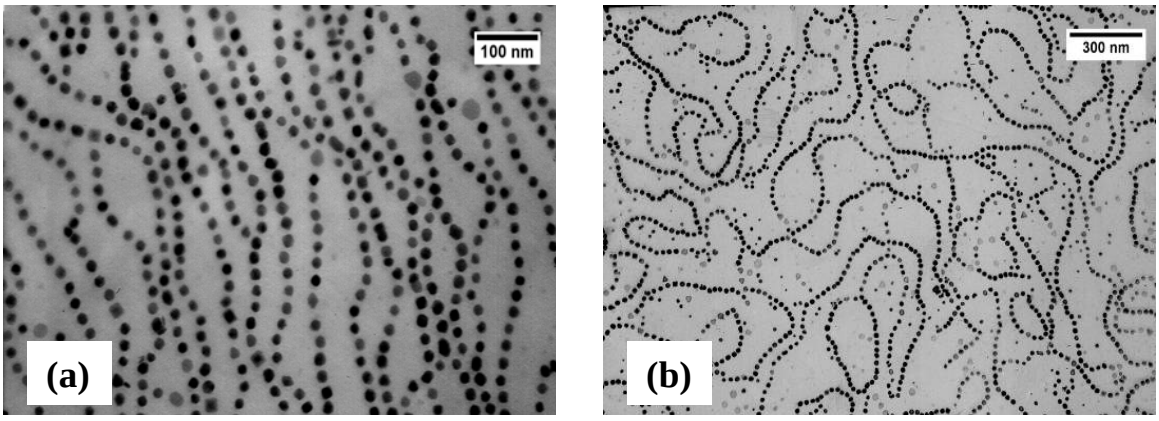

Figure 3.3: TEM images of PS-CoNPs prepared using only PS-NH_2 (**2.2**) in the thermolysis of $Co_2(CO)_8$ at high (a) and low (b) magnification, respectively. The PS-CoNPs (as prepared; $D_{PS\text{-}CoNPs}$ = 21 nm ± 2.9 nm) were cast onto supported surfaces from a particle dispersion in toluene.

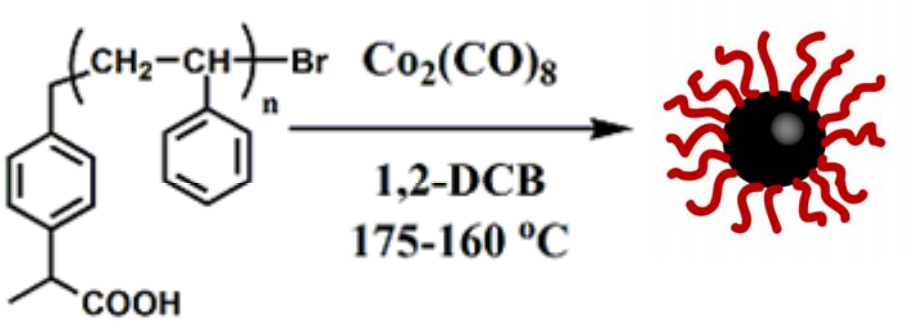

3.3.1

Scheme 3.4: Synthesis of PS-CoNPs using only PS-COOH (**3.3.1**) in the thermolysis of $Co_2(CO)_8$ at 175 °C and 160 °C. The thermolysis of the $Co_2(CO)_8$ was performed at 175 ^oC followed by growth at 160 ^oC for 30 minutes.

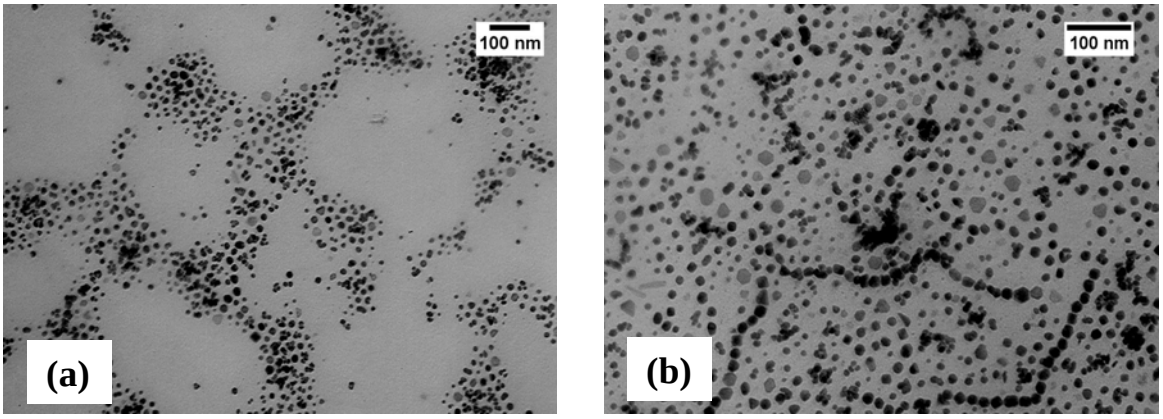

Figure 3.4: TEM images of self-assembled PS-CoNPs at low (a) and high magnification (b) prepared using the PS-COOH surfactant **3.3.1** shown in Scheme 3.4. The PS-CoNPs (as prepared; $D_{PS\text{-}CoNPs}$ = 16 nm ± 4.5 nm) were cast onto supported surfaces from a particle dispersion in toluene.

3.2.3 Solid States Characterization of PS-CoNPs

X-ray diffraction (XRD) was used to investigate the effect of different polymeric surfactants on the crystalline phases of metallic CoNPs prepared using the dual-stage

temperature thermolysis reaction at 175 ºC and 160 ºC. For all experiments conducted using mixtures of polystyrene surfactants, or only PS-NH_2 **(3.1.2)** as discussed in Schemes 3.1 - 3.3, the formation of primarily the epsilon (ε) Co crystalline phase was observed.[89, 90] This result was contrary to our previous report using PS-NH_2 and PS-DOPO surfactants prepared from NMP in the thermolysis of $Co_2(CO)_8$ at 180 ºC. The formation of ε-Co was likely a metastable condition that was favored as a consequence of using the 175 ºC and 160 ºC dual-stage thermolysis procedure to prepare ferromagnetic PS-CoNPs. XRD measurements on the PS-CoNPs prepared using PS-COOH (**3.3.1**) alone suggested that the majority of these particles adopt the ε-Co crystal phase. However, the XRD pattern appeared as a broad peak which indicated that the sample was amorphous and ill-defined. To determine if the polymerization mechanism used to prepare polymeric surfactants (i.e., ATRP versus NMP) affected the crystalline phase of CoNPs, an additional control experiment was conducted using PS-NH_2 and PS-DOPO surfactants prepared from NMP using a 175 ºC and 160 ºC dual-stage temperature process. ε-Co NPs ($D_{PS\text{-}CoNPS}$ = 16 nm ± 2.4 nm) were also prepared with these polymeric surfactants confirming that the method of polymerization used to prepare end-functional polystyrenes (i.e., ATRP versus NMP) did not affect size or the crystalline phase of PS-CoNPs formed under these conditions.

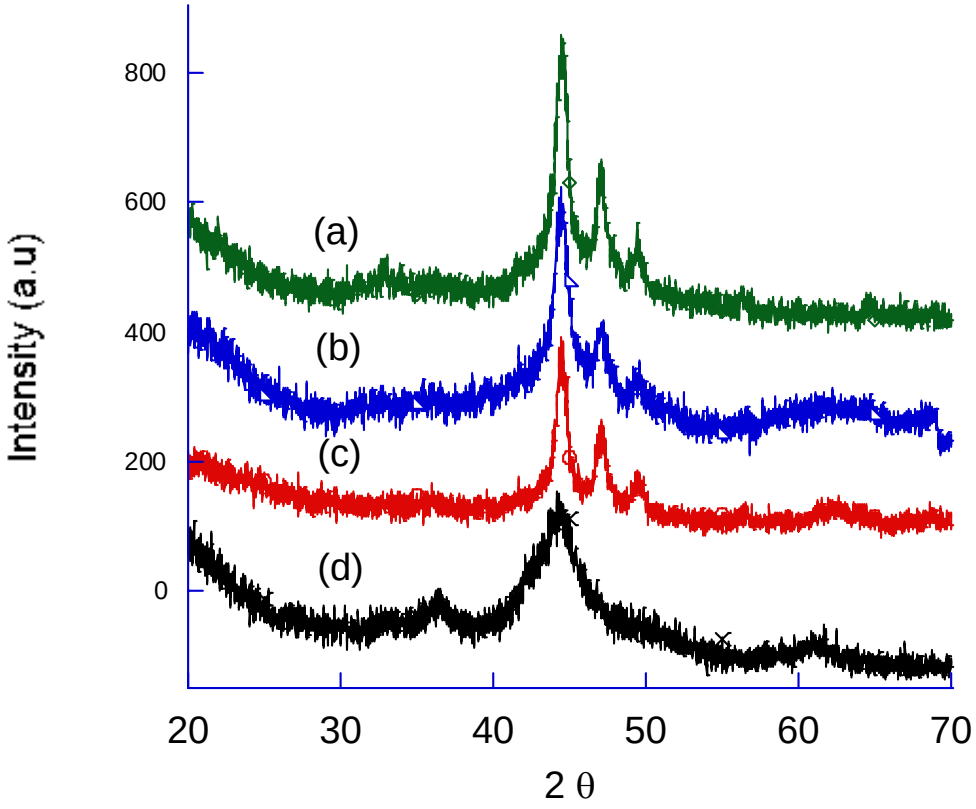

Figure 3.5: XRD patterns of PS-CoNPs prepared from (a) PS-NH_2 (**3.1.2**), (b) mixture of surfactants PS-NH_2 (**3.1.2**) and PS-COOH (**3.3.1**) and (c) mixture of PS-NH_2 (**3.1.2**) and PS-DOPO (**3.2.1**), (d) PS-COOH (**3.3.1**), where all polymeric surfactants were synthesized using ATRP.

Magnetic properties of the PS-CoNPs prepared from different surfactants systems as illustrated in Schemes 3.1 - 3.4 were measured using the vibrating sample magnetometry (VSM) at room temperature and -266 °C (77 K). Magnetic measurements confirmed that all of the prepared hybrid nanocomposites were weakly ferromagnetic at room temperature and strongly ferromagnetic at -266 °C (77 K). PS-CoNPs that were prepared using surfactants PS-NH_2 (**3.1.2**) and PS-DOPO (**3.2.1**) possessed comparable particle size (D = 17 nm), saturation magnetization (M_s = 44 emu/g) and magnetic coercivity (H_c = 10500 A/m) to materials prepared using our previously reported

methodology.[76] However a small increase in the coercivity of PS-CoNPs was observed when polymeric surfactants PS-NH_2 (**3.1.2**) and PS-COOH (**3.3.1**) were employed in the particle synthesis (M_s = 35.1 emu/g; H_c = 16100 A/m), presumably due to the slightly larger particle size (D = 21 nm).

VSM of PS-CoNPs prepared using only PS-NH_2 (**3.1.2**) is shown in Figure 3.6 (M_s = 34.2 emu/g; H_c = 20,700 A/m). Magnetization (M) vs. applied field strength (H) plots obtained for PS-CoNPs prepared using only PS-NH_2 (**3.1.2**) (Scheme 3.3) closely resembled magnetic behavior of PS-CoNPs prepared using a mixture of PS surfactants (Schemes 3.1 and 3.2) at both room temperature and at -266 °C (77 K). PS-CoNPs prepared using only PS-COOH (**3.3.1**) consisted of a mixture of ferromagnetic, antiferromagnetic and diamagnetic materials as suggested by the large increase of magnetic coercivity (H_c = 101,000 A/m) at - 266 °C (77 K). The presence of antiferromagnetic materials required higher magnetic fields to reorient spins in the opposite direction. The magnetic properties of PS-CoNPs prepared from PS-COOH (**3.3.1**) measured at low temperature were consistent with the poorly defined particle size (Figure 3.4) and low degree of crystallinity observed from XRD (Figure 3.5 (d)).

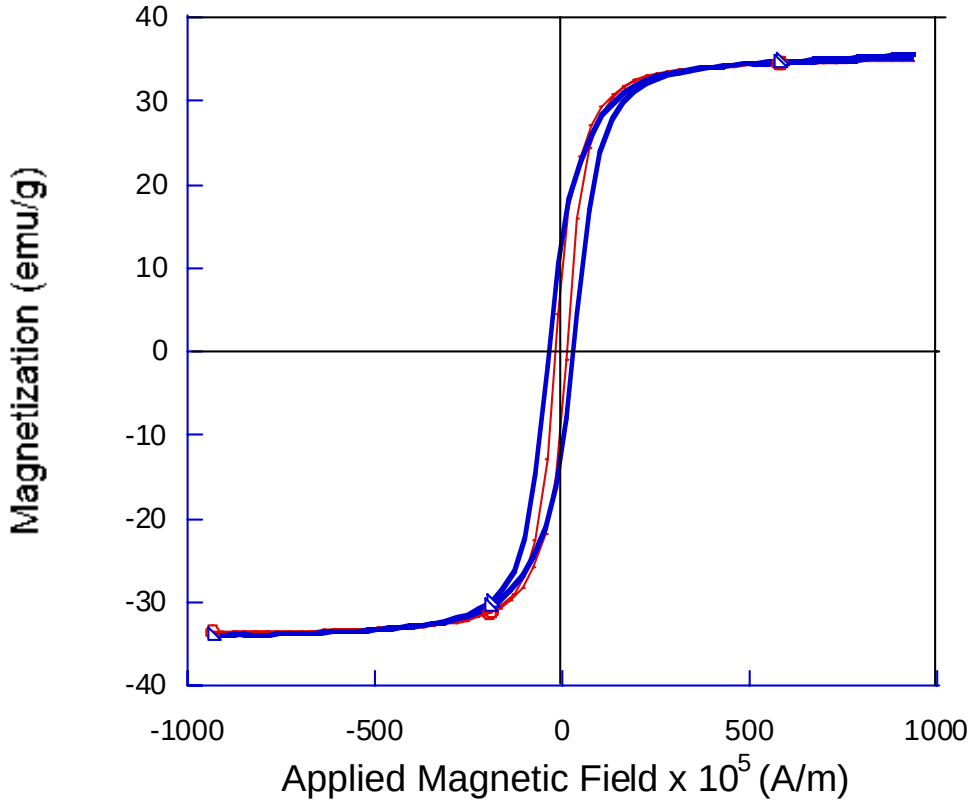

Figure 3.6: Magnetization versus applied magnetic field for ε-cobalt nanoparticles prepared from PS-NH_2 (**3.1.2**) with an average diameter of 21 nm. Thin red trace VSM measurement at room temperature, while the thick blue trace corresponds to T = - 266 °C (77 K).

3.2.4 Morphologies of Dipolar Assemblies of PS-CoNPs.

Numerous computational studies have indicated that a diversity of possible self-assembled structures should form in suspensions of dipolar nanoparticles, depending on an interplay between the particle concentration, the strength of the dipolar interaction, and the strength of the isotropic attractive interparticle interaction responsible for phase separation.[11, 13, 14, 39, 86, 91-95] The formation of anisotropic chain-like mesostructures has long been known to arise in particle systems where interactions were dominated by strong long-range dipole-dipole interactions that must exceed contributions from thermal

fluctuations. In this report, we observe the self-assembly of PS-CoNP chains, which was characteristic of this type of assembly when the nanoparticle dispersion were cast from solution onto supporting surfaces to form a variety of discrete dipolar assemblies. The PS-CoNPs used in these studies all possessed comparable particle size (D = 21 nm to 22 nm) and magnetic properties (M_s = 30 emu/g to 40 emu/g; H_c = 16,000 A/m to 24,000 A/m). These preliminary studies also provide evidence of the subtle interactions between these chain structures that have been observed previously only in simulation studies. For example, the relatively high concentrations of our nanoparticle dispersions allowed us to observe local nematic interactions that evidently caused the formation of appreciable domains where the dipolar chains shared a common orientation. It is our impression that these chain interactions make the chain structure more persistent (i.e., enhance chain stiffness), an effect that requires further quantification. We also see the formation of "zippered" chain configurations (See Figure 3.1 for (a) particularly good example) where the chains form side by side configurations even at low particle concentrations. The simulations of Weis[86] show that such structures were energetically favored when appreciable isotropic attractive interactions were present, (arising mainly from the grafting chains in the present experimental study) in addition to strong dipolar interactions. Our previous work on these PS-CoNP chains segregated to oil-water interfaces have indicated that the attractive interparticle interactions can be strong enough to induce chains to collapse into ball-like configurations on long timescales.[38] All of these general patterns of behavior have been predicted from Monte Carlo simulations[86, 96-98] of the self-assembly of dipolar particles with additional isotropic attractive

interactions. Future work to establish the interactions involved in these particle systems is underway to allow a more quantitative comparison with these simulations. From these previous simulation studies we infer that there are numerous experimental handles that can be used to control the morphology and we have indeed verified that the nanoparticle morphologies are highly dependent on nanoparticle concentration, the magnetic properties of the particles themselves, the external magnetic field strength and the choice of solvent when the nanoparticle solutions are cast onto carbon coated copper TEM grids.

Dipolar assembly of either self-assembled correlated domain structures (Fig. 3.7 (a)), randomly entangled chains (Figure 3.7 (b)), or nematic-like field-aligned mesostructures (Figure 3.7 (c,d)) can be easily obtained using a variety of organic solvents as the dispersing media and an external field. These types of assemblies have been observed in numerous reports both in simulations and imaging experiments. The formation of micron-sized 1-D mesostructures using ferromagnetic PS-CoNPs (D = 21 nm; PS shell corresponds to M_n = 4,800 g/mol) was confirmed when organic colloidal dispersions were cast onto carbon coated TEM grids. The formation of these types of morphologies, when cast from dilute particle dispersions, indicated that dipolar interactions dominated the assembly process in the organization of dipolar nanoparticles into mesoscopic chains.[11, 14, 95]

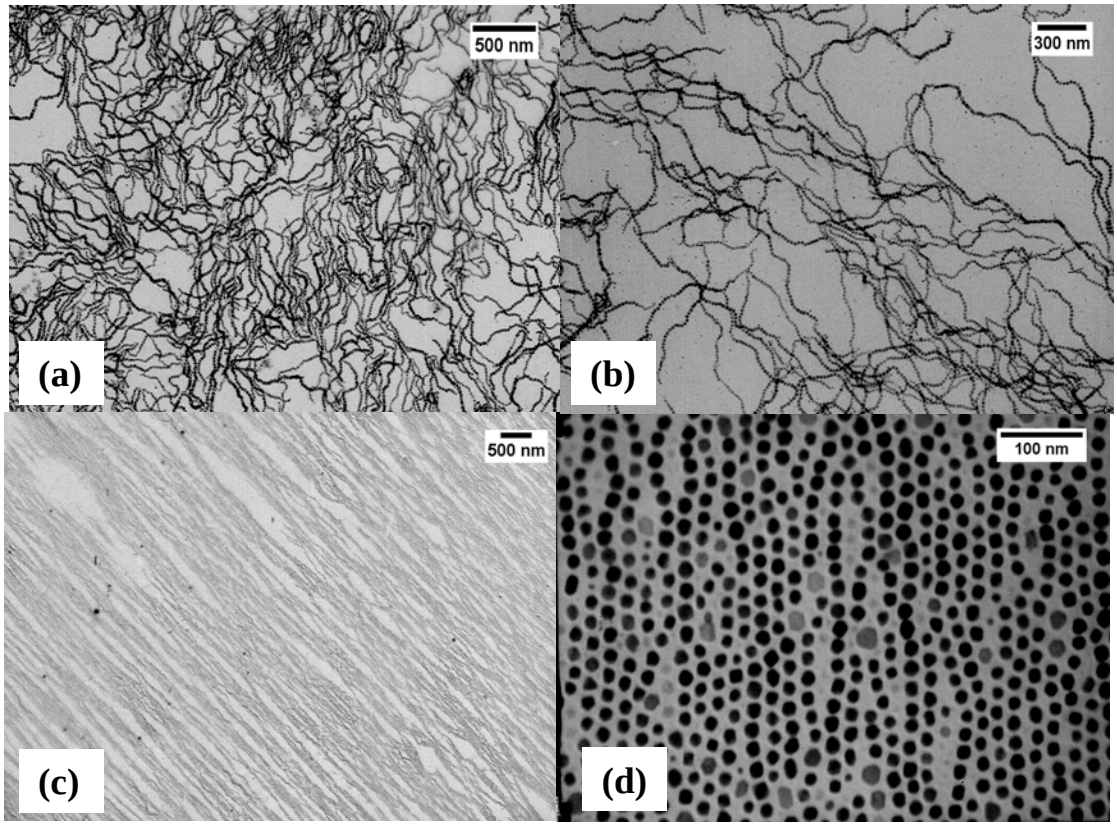

Figure 3.7: TEM images (a) and (b) of randomly entangled chains of PS-CoNP (D = 21 nm ± 3 nm) cast from a toluene dispersion (c = 0.5 mg/mL) in zero-field, (c) TEM image of aligned chains of PS-CoNPs (D = 21 nm ± 2.9 nm) cast from a dichlorobenzene dispersion (c = 0.5 mg/mL) in 100 mT, (d) high magnification TEM image of aligned PS-CoNP chains from Fig. 3.7c.

The formation of flux-closure rings or 'bracelet' dipolar assemblies has been experimentally reported for ferromagnetic CoNPs prepared using small molecule surfactants.[17-19, 74] While the formation of looped bracelets was entropically unfavorable, the assembly of dipoles into a closed circuit minimized both the magnetic moment and field outside of the ring-like structure. The formation of bracelet-like assemblies was observed using PS-CoNPs when colloidal dispersions were drop cast from a less-volatile organic solvent (chlorobenzene) and a slightly higher molecular weight (MW) PS surfactants (M_n = 12,000 g/mol; M_w / M_n = 1.10) for the preparation of PS-CoNPs.

Particle concentrations of 0.5 mg/mL were found to be optimal to afford bracelet assemblies, as higher and lower concentrations tended to afford linear chains. It is important to note that while the formation of bracelets was the preferred morphology for these PS-CoNPs, numerous defects structures were also typically observed in the form of short linear chains, or branched assemblies, an effect also established in simulations of strongly interacting dipolar fluids.[96] TEM images of the dipolar assemblies formed from PS-CoNPs with lower MW PS surfactants shown in Figure 3.7 (M_n = 4,800 g/mol for each system in Figure 3.7) exhibit a dramatically different morphologies than for bracelet-type structures formed from PS-CoNPs prepared using higher MW PS surfactants cast from chlorobenzene (Figure 3.8). These images confirm that the ferromagnetic nanoparticles form rings of varying size in the range of 10 to 100 colloids per colloidal assembly. The use of a less volatile solvent such as, chlorobenzene, led to a higher yield of these ring structures when the dispersion was cast onto carbon-coated copper TEM grids in the absence of an applied magnetic field. Deposition of PS-CoNPs from more volatile solvents, such as, tetrahydrofuran, or dichloromethane resulted in the formation of predominately short linear chains. This observed solvent dependence on ring formation is contrary to a recent report using poly(vinylpyrrolidone) coated magnetite nanoparticles.[19] The cause of these differences is currently under investigation and is complicated by the inherent differences in the nature of these materials. The presence of a higher MW PS-NH_2 surfactant (M_n = 12,000 g/mol) was also critical to ring self-assembly. The assembly of PS-CoNPs with a lower MW PS surfactant (M_n = 4,800 g/mol) cast from chlorobenzene under identical conditions did not lead to rings, as will be

discussed in later sections. Since the stiffness of the nanoparticle chains evidently increases with the strength of the dipolar interaction and the formation of dipolar chains of significant length increases with increasing chain stiffness, we can understand this trend with polymeric surfactant MW to arise from an increased separation of the dipolar particles and a corresponding weakening of the dipolar interactions with higher molar masses. Correspondingly, recent rule-based simulations of dipolar particle assembly have provided evidence for an enhanced tendency towards ring assembly upon lowering the strength of the dipolar particle interaction.[39]

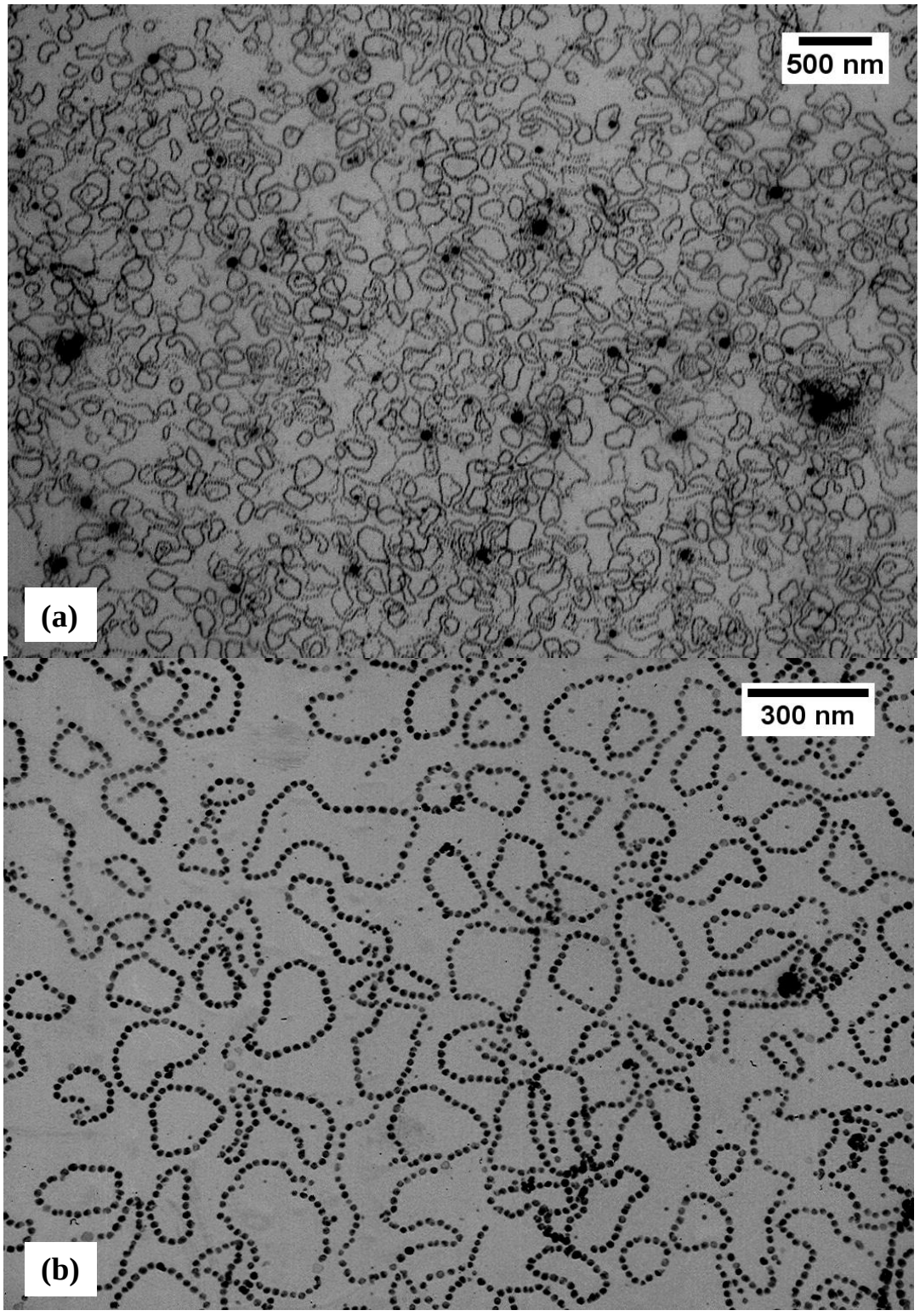
500 nm
(a)
300 nm
(b)

Figure 3.8: (a) TEM image of bracelet-flux closure rings of PS-CoNPs (D =21 nm ± 3.3 nm) cast from a chlorobenzene dispersion (c = 0.5 mg/mL) in zero-field, (b) high magnification TEM image of PS-CoNP assemblies from Fig. 8a which are consistent with Monte Carlo simulations of Douglas *et al.*[97]

A conspicuous aspect of the self-assembled rings in Figure 3.8 is that the rings are neither knotted, nor catenated. Unknotted rings or zippered rings are the lowest energy structure for dipolar particles with a strong dipolar interaction,[99] but recent calculations also indicate that if there are both directional dipolar and isotropic van der Waals interactions that are comparable in magnitude, then the low energy ring configurations involving non-trivial knot complexity may arise from the competing tendencies of the dipolar interaction to establish an open ring structure and the van der Waals interaction to drive the particle clusters into spherical droplet configurations.[100] Since we can tune the strength of the van der Waals interaction by varying the polymer surfactant molecular mass, we should be able to search for these knotted structures in the future.

As alluded to previously, the formation of a nematic-like ordering of ferromagnetic PS-CoNPs was only observed when colloids were prepared using lower MW PS surfactant (M_n = 4,800) and then cast from a chlorobenzene dispersion (Figure 3.9). Unlike the previously discussed bracelet morphology, under identical conditions and zero-field, the organization of nanoparticle chains exhibited local ordering of colloids into a "lamellae"-like folding of 1-D assemblies. This particular type of organization was observed for PS-CoNPs when casting from nonpolar and relatively nonvolatile solvents, such as, chlorobenzene and toluene, while more volatile solvents (THF, CH_2Cl_2) led to linear nanoparticle chains having an appearance similar to random walk chains. The formation of the folded lamellae nanoparticle chains was found to be prevalent in dilute

particle concentration regimes (0.5 mg/mL). Similar morphologies were found previously in the Monte Carlo simulations of Weis *et al*., where dense arrays of self-ordered 1-D mesostructures arise from both dipolar interactions forming chains, in conjunction with lateral associations of nanoparticle chains via anti-parallel configurations of the magnetic moments.[86] Although these structures are "expected", these dipolar nematic LC self-assembly patterns have not been observed experimentally in ferromagnetic nanoparticle dispersions. While the mechanism of this type local nematic ordering is still under investigation, it is anticipated that the presence of macromolecular PS surfactants enhanced short-range van der Waals associations which facilitated lateral nanoparticle association of anti-parallel dipole moments.

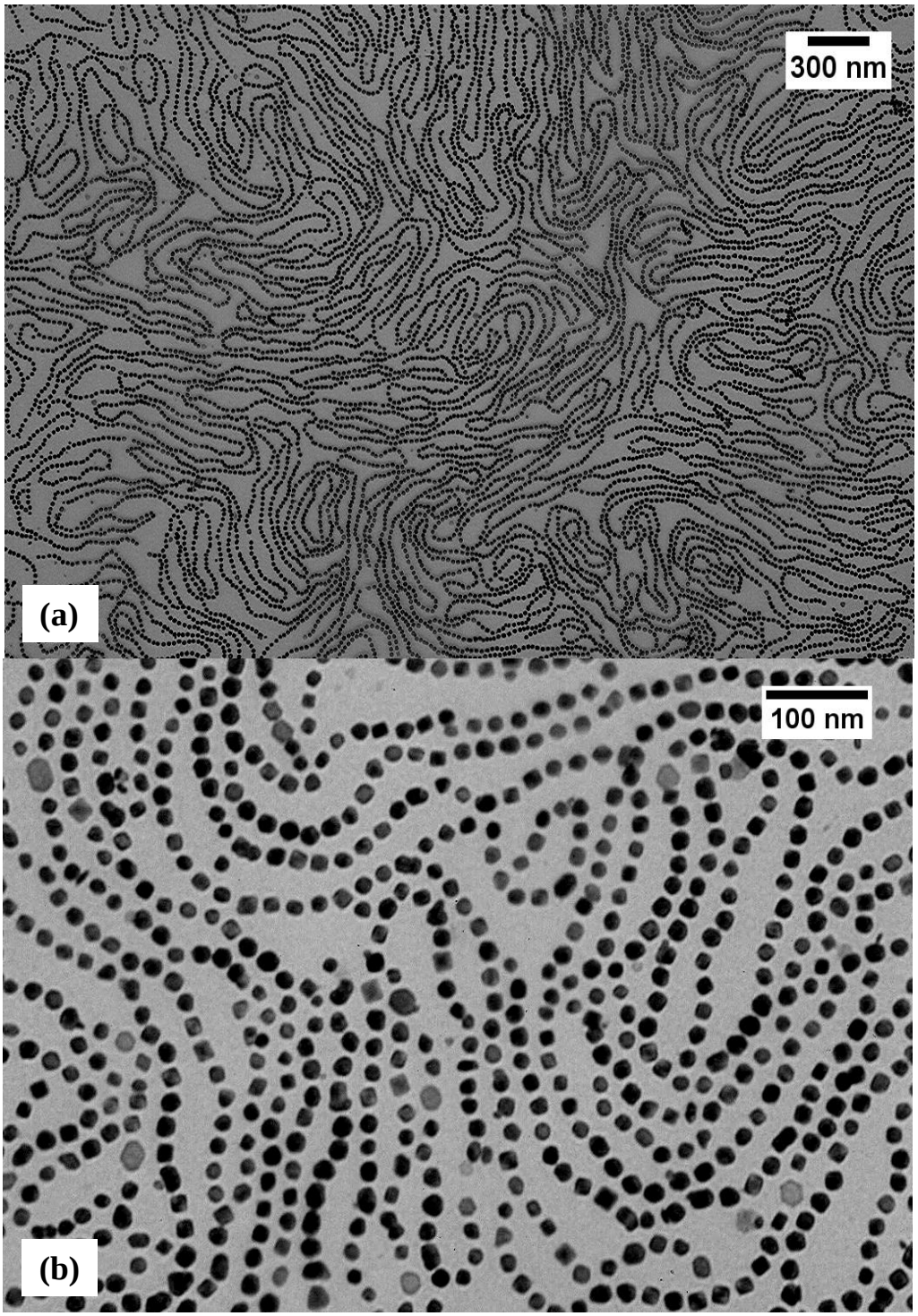

Figure 3.9: (a) TEM image of self-assembled PS-CoNPs (D = 21 nm ± 2.9 nm) exhibiting local nematic LC ordering cast from a chlorobenzene particle dispersion (c = 0.5 mg/mL) in zero-field, (b) high magnification TEM image of PS-CoNP assemblies

from Fig. 8a. These simulations resemble morphologies found in the Monte Carlo simulations of Weis.[86]

3.3: Conclusion

The preparation and characterization of ferromagnetic polystyrene coated cobalt nanoparticles is reported. The use of these synthetic routes using ATRP enabled the synthesis of multi-gram quantities of end-functional polystyrenic surfactants. The preparation of polymer coated ferromagnetic colloids was also improved by the utilization of a dual-stage temperature thermolysis protocol that enabled the synthesis of polystyrene coated ferromagnetic nanoparticles of cobalt on a nearly one-gram scale per reaction. Using these well-defined ferromagnetic nanoparticles, a novel magnetically assembled morphology was observed when cast onto supporting surfaces. The mesostructures formed from self-assembly of dipolar nanoparticles drop cast from solution onto substrates were found to be consistent with recent theoretical modeling and we look forward to fundamental studies of self-assembly based on these model particles. This study opened access to other surface functionalization and core conversion chemistries, which is presented in chapter 4 and chapter 5 of this dissertation, respectively.

3.4: Experimental

Materials: Anhydrous 1,2-dichlorobenzene (DCB), toluene, neutral alumina, 1,4,7,10,13,16-hexaoxacyclooctadecane (18-crown-6), acetonitrile (ACN), acetone, dichloromethane (DCM), hexanes (HEX), methanol (MeOH), N,N- dimethylformamide (DMF), hydrazine hydrate, magnesium sulfate, copper (I) chloride, 2,2'-dipyridyl (bipy),

4,4'-dinonyl-2,2'-dipyridyl (dNbipy), boron trichloride 1 M solution in dichloromethane, and sodium hydride (96 %), copper (I) chloride, 2,(4-bromomethyl)-phenyl propionic acid were purchased from Aldrich† and used as received without further purification. Copper (I) bromide was purified by stirring in glacial acetic acid overnight. Styrene was purchased from Aldrich and passed through a short column of neutral alumina to remove inhibitors prior to use in polymerizations. Deoxygenation of monomers, solvents and reaction mixtures was achieved by bubbling with argon gas for approximately 30 minutes prior to use in polymerizations. Dicobaltoctacarbonyl ($Co_2(CO)_8$) was purchased from Strem Chemicals and used as received. Thermolysis reactions were performed using an Omega temperature controller with a home-made K-type thermocouple and the PowerStat variable autotransformer at level 70/140. Flash chromatography was performed using silica gel from VWR (230-400 mesh) and TLC plates coated with silica gel (60 F254) (Merck). Nuclear magnetic resonance (NMR) was performed using a Bruker DRX 500 MHz FT-NMR and Bruker DRX 250 MHz FT-NMR spectrometer, operating XWinNMR software (Bruker). Size exclusion chromatography (SEC) was performed in a tetrahydrofuran mobile phase with a Waters 1515 isocratic pump running three 5 μm PLgel columns (Polymer Labs, pore sizes 10^4 Å, 10^3 Å, 10^2 Å) at a flow rate of 1 mL/min with a Waters 2414 differential refractometer and Waters 2487 dual wavelength UV-Vis spectrometer. Molar masses were calculated using the Empower software (Waters) calibrating against low polydispersity linear polystyrene standards. TEM images were obtained on a JEM100CX II transition electron microscope (JEOL) at an operating voltage of 60 kV, using in house prepared copper grids (Cu, hexagon, 300

mesh). Analysis of images was carried out using ImageJ software (Rasband, W.S., National Institute of Health, http://rsb.info.nih.gov/ij/, 1997-2007). Relative uncertainty of particle size determinations using ImageJ was found to be 1 % of diameter average (e.g., 20 nm $\pm$ 0.2 nm). VSM measurements were obtained using a Waker HF 9H electromagnet with a Lakeshore 7300 controller and a Lakeshore 668 power supply. Magnetic measurements were carried out at room temperature (27 °C, 300 K) and low temperature (-266 °C or 77 K), with a maximum S-2 applied field of 1190 kA/m, a ramp rate of 2630 $Am^{-1}s^{-1}$ and a time constant of 0.1. XRD measurements were performed using the X'pert x-ray diffractometer (PW1827) (Phillips) at room temperature with a CuKα radiation source at 40 kV and 30 mA.

Preparation of 4-(chloromethyl) benzyl phthalimide (3.1). To an oven dried three neck round bottom flask was added α, α'-dichloroxylene (6.59 g; 3.76 x 10^{-2} mol), potassium phthalimide (2.67 g; 1.44 x 10^{-2} mol), 18-crown-6 (0.240 g; 9.08 x 10^{-4} mol) and solids were then dissolved in acetonitrile (75 mL). The reaction mixture was refluxed overnight under argon, filtered through a coarse glass frit, washed with acetone and concentrated *in vacuo* to yield a white solid. The crude product was purified via flash chromatography eluting with a 1:1 hexane/DCM mixture with a gradual increase to DCM to yield a white crystalline solid (2.70 g; 67%; R_f = 0.2; 2:1 dichloromethane/ hexanes). ^{1}H NMR (500 MHz, $CDCl_3$, δ): 7.85 (dd, *J* = 5 Hz, 3 Hz, Ar H, 2H), 7.71 (dd, *J* = 5.5 Hz, 3 Hz, Ar H, 2H), 7.45-7.34 (m, Ar H, 4H), 4.84 (s, CH_2, 2H), 4.55 (s, CH_2, 2H). ^{13}C NMR (125 MHz, $CDCl_3$, δ): 167.79, 136.97, 136.49, 133.92, 131.94, 128.90, 128.81, 123.24, 45.73, 41.13. HRMS exact mass calculated for $[M + 1]^+$ $C_{16}H_{12}O_2ClN$ 287.0518, found: 285.0527.

Preparation of benzyl phthalimide end functionalized polystyrene (3.1.1). To a 25 mL Schlenk flask equipped with a stir bar was added **(3.1)** (0.500 g; 1.75 x 10^{-3} mol), Cu(I)Cl (0.173 g; 1.75 x 10^{-3} mol) and 2,2'-dipyridyl (0.546 g; 3.50 x 10^{-3} mol). The flask was fitted with a rubber septum, evacuated, back-filled with argon for three cycles and leaving the flask contents under argon. Deoxygenated DMF (2 mL) was added to the flask via syringe and stirred at room temperature until a red complex formed. Deoxygenated styrene (10.9 g; 12.0 mL; 1.05 x 10^{-1} mol) was added directly into the flask. The flask was placed in a thermostated oil bath held at 110 ºC for 16 h to reach a monomer conversion of 80%. The reaction mixture was diluted in 300 mL of dichloromethane and passed through an alumina plug to remove the copper catalyst. The polymer solution was concentrated and precipitated into stirring methanol (1000 mL) twice, followed by drying *in vacuo* to yield a white powder (7.71 g; 89% yield based on monomer conversion). ^{1}H NMR (250 MHz, $CDCl_3$, δ): 7.82 (b, Ar H, 2H), 7.67 (b, Ar H, 2H), 7.10-6.50 (bm, Ar H), 4.77 (bm, CH_2), 2.4-1.2 (bm, CH + CH_2). $M_{n\ SEC}$ = 4800 g/mole; M_w / M_n= 1.08.

Reduction of phthalimide functionality with hydrazine hydrate (PS-NH_2, 3.1.2). To a round bottom flask equipped with a stir bar was added **(3.1.1)** (7.71 g; 1.61 x 10^{-3} mol) and was dissolved in THF (50 mL). Methanol (5 mL) was added dropwise followed by the addition of hydrazine hydrate (0.640 g; 1.28 x 10^{-2} mol). The flask was fitted with a rubber septum and the reaction mixture was stirred at room temperature for 24 h, after which a white precipitate was observed. The reaction mixture was concentrated and redissolved in THF, followed by precipitation into stirring methanol (1000 mL). The

precipitation was repeated twice followed by drying *in vacuo* to yield the amine end functionalized polystyrene as a white powder (7.20 g; 93%). ^{1}H NMR (250 MHz, $CDCl_3$, δ): 7.10 to 6.50 (bm, Ar H), 3.85 to 3.75 (bm, CH_2), 2.40 to 1.20 (bm, CH+CH_2).

Preparation of carboxylic acid end functionalized polystyrene (PS-COOH, 3.3.1). To an oven dried 125 ml Schenk flask equipped with stir bar, was added Cu(I)Br (0.361 g, 2.52 x 10^{-3} mol), 2,(4-bromomethyl)phenyl propionic acid **(3.3)** (0.650 g, 2.50 x 10^{-3} mol), and 2,2-dipyridyl (0.786 g; 5.04 x 10^{-3} mol). The flask was fitted with a rubber septum, evacuated and back-filled with argon for three cycles. Deoxygenated DMF (7 mL) was added via syringe and stirred until a red complex formed. Deoxygenated styrene (34.5 g; 38.0 mL; 3.28 x 10^{-1} mol) was added via syringe to the reaction flask. The flask was placed in a thermostated oil bath held at 110 ºC for 16.5 h to reach a monomer conversion of 63%. The reaction mixture was diluted in 300 mL of dichloromethane and passed through a short alumina column to remove the copper catalyst. The polymer solution was concentrated and precipitated into stirring methanol twice followed by drying *in vacuo* to yield a white powder (17.9 g; 82% yield based on monomer conversion). ^{1}H NMR (250 MHz, $CDCl_3$, δ): 7.10 to 6.50 (bm, Ar H), 2.40 to 1.20 (bm, CH+CH_2). $M_{n\ SEC}$ = 9500 g/mole; M_w / M_n = 1.11.

Preparation of 1-(chloromethyl)-4-methoxymethyl benzene. To an oven dried three neck round bottom flask, was added α,α'-dichloroxylene (14.0 g; 8.00 x 10^{-2} mol) and solids were dissolved in THF (90 mL) under argon. Sodium methoxide (3.00 g; 5.55 x 10^{-2} mol) was dissolved in methanol (50 mL) and was slowly added via syringe. The reaction was stirred under argon overnight at room temperature. The reaction mixture

was filtered and quenched with HCl (0.1 M in DI water; 4 mL). The filtrate was extracted with deionized water twice and once with saturated brine. The combined organic layer was dried over magnesium sulfate, filtered and the solution was concentrated under reduced pressure to yield a yellow oil. The yellow oil was purified via flash chromatography with an initial 6:1 hexane/dichloromethane elution mixture with a gradual increase to 1:1 hexane/ dichloromethane to yield a yellow oil (4.60 g; 67% reaction yield). ^{1}H NMR (500 MHz, $CDCl_3$, δ): 7.38-7.31 (m, Ar H, 4H), 4.57 (s, CH_2Cl, 2H), 4.46 (s, CH_2O, 2H), 3.39 (s, OCH_3, 3H). ^{13}C NMR (125 MHz, CDCl3, δ): (138.34, 136.50, 128.61, 128.33, 127.59, 57.84, 45.74). MS (EI^+) m/z: 171.04 $[M+H]^+$.

Preparation of 4-(methoxymethyl)benzyl dioctylphosphine oxide. To an oven dried 100 mL three neck round bottom flask equipped with a magnetic stir bar and condenser was added dioctylphosphine oxide[81, 82] (1.30 g; 4.75 x 10^{-3} mol). Anhydrous THF (30 mL) was added to dissolve solids followed by the addition of NaH (0.200 g; 8.33 x 10^{-3} mol). The white suspension was heated at reflux temperature for 30 min under argon. A solution of 1-(chloromethyl) methoxymethylbenzene (0.540 g; 3.17 x 10^{-3} mol) in 3 mL of anhydrous THF was added dropwise via syringe. The reaction mixture was heated at reflux overnight under argon. Solvent was removed under reduced pressure to yield a yellow oil. The yellow oil was dissolved in dichloromethane and purified via flash chromatography (1: 0.3 dichloromethane/ diethyl ether mixture followed by 1: 0.1 dichloromethance / methanol) to yield a white crystalline solid (0.780 g; 52%). ^{1}H NMR (500 MHz, $CDCl_3$, δ): 7.39-7.22 (b, Ar H, 4H), 4.44 (s, CH_2Ph, 2H), 3.39 (s, CH_3O, 3H), 3.12 (d, J= 14 Hz, CH_2PO, 2H), 1.58 (m, CH_2, 8 H), δ 1.26 (m, CH_2, 20H), 0.88 (t, CH_3,

6H). ^{13}C NMR (125 MHz, CDCl3, δ): 136.77, 131.85, 129.43, 128.13, 74.30, 58.15, 36.04 (d, J = 59 Hz, CH_2PO), 31.77, 31.16, 31.05, 29.08, 27.36 (d, J = 32.63 Hz, CH_2PO), 22.61, 21.61, 14.08. HRMS exact mass calculated for $[M + 1]^+$ $C_{25}H_{45}O_2P$ 409.3235, found: 409.3247.

Preparation of 4-(chloromethyl)benzyl DOPO (3.2). Chloromethylation of 4-(methoxymethyl)benzyl dioctylphosphine oxide was performed according to a modified procedure reported elsewhere.[101, 102] To an oven dried three neck round bottom flask was added 4-(methoxymethyl)benzyl dioctylphosphine oxide (0.780 g; 1.91 x 10^{-3} mol) and solids were then dissolved in dichloromethane (8 mL). The solution mixture was cooled to 0 ^{o}C using an ice bath. Boron trichloride solution (4.00 mL, 4.00 x 10^{-3} mol) was added dropwise into the reaction mixture using syringe. The mixture was stirred at 0 ^{o}C for 2 h under argon. The reaction mixture was quenched with methanol followed by pouring the mixture into a stirred solution of 5 % NaOH (50 mL) cooled in ice. The layers were separated and the aqueous layer was then twice extracted with dichloromethane. The combined organic layer was washed with deionized water, dried over magnesium sulfate, filtered and the solvent was concentrated under reduced pressure to afford a yellow oil. The oil was purified via flash chromatography (1: 0.2 dichloromethane/ diethyl ether) to yield the product as a white crystalline solid (0.780 g; 52 % reaction yield). ^{1}H NMR (250 MHz, $CDCl_3$, δ) 7.33 (dd, J= 28 Hz, 8 Hz, 4H), 4.58 s, CH_2Cl, 2H), 3.12 (d, J= 14 Hz, CH_2PO, 2H), 1.58 (m, CH_2, 8H), 1.26 (m, CH_2, 20H), 0.88 (t, CH_3, 6H). ^{13}C NMR (125 MHz, $CDCl_3$, δ) 136.07, 132.81, 129.81, 129.01, 45.86, 36.08 (d, J = 58 Hz, CH_2PO) 31.78, 31.17, 31.06, 29.08, 27.55 (d, J = 65 Hz, CH_2PO),

22.62, 21.67, 14.08. HRMS exact mass calculated for $[M + 1]^+$ $C_{24}H_{43}ClOP$ 413.2740, while we found 413.2723.

Preparation of benzyl DOPO end functionalized polystyrene (PS-DOPO, 3.2.1). To a 10 mL Schlenk flask, was added with **3.2** (0.300 g; 7.28 x 10^{-4} mol), Cu(I)Cl (0.072 g; 7.27 x 10^{-4} mol), and dNbipy (0.600 g; 1.46 x 10^{-3} mol). The flask was fitted with a rubber septum, evacuated and back-filled with argon three times and left under argon. Deoxygenated styrene (4.50 g, 5.00 mL; 4.33 x 10^{-2} mol) was added via syringe to the flask, which was allowed to stir at room temperature until the catalyst was dissolved. The flask was placed into a thermostated oil bath held at 110 ºC for 4 h to reach a monomer conversion of 60%. After the heating was stopped, the reaction mixture was diluted in 200 mL of DCM and passed through a short alumina column. The polymer solution was concentrated and precipitated into methanol twice followed by drying *in vacuo* to yield DOPO end-functionalized polystyrene as a white powder (1.70 g; 63% yield based on monomer conversion). ^{1}H NMR (500 MHz, $CDCl_3$, δ) 7.15-6.43 (bm, ArH), 4.6 to 4.3 (bm, 1H, CHCl), 3.11 to 3.06 (bm, 2H, CH_2PO), 2.27 to 1.30 (bm, CH+ CH_2), 0.94 to 0.88 (b, CH_3). $M_{n\,SEC}$ = 4500 g/mole; M_w / M_n = 1.15.

Preparation of PS-CoNPs using end functionalized polystyrene surfactants, PS-NH_2 (3.1.2) and PS-DOPO (3.2.1). To an oven dried 100 mL three-neck round bottom flask equipped with a stir bar and condenser was added PS-NH_2 **(3.1.2)** (0.160 g; 3.33 x 10^{-2} mmol) and PS-DOPO **(3.2.1)** (0.040 g; 8.89 x 10^{-3} mmol). Polymers **3.1.2** and **3.2.1** were dissolved in anhydrous dichlorobenzene (20 mL) and heated to reflux under argon. A solution of dicobaltoctacarbonyl (0.300 g; 8.77 x 10^{-4} mol) dissolved in anhydrous

dichlorobenzene (4 mL) was rapidly injected into the hot mixture (175 ºC). Upon injection, the reaction temperature dropped to 160 ºC and the reaction mixture was maintained at 160 ºC for 30 min. The reaction mixture was then cooled to room temperature under argon. The as prepared ferrofluid (0.5 mL) was diluted in chlorobenzene (10 mL) for TEM imaging and analysis. A drop of this nanoparticle solution was cast onto a carbon coated copper grid and allowed to dry at room temperature. To isolate the polystyrene coated cobalt nanoparticle, the ferrofluids were precipitated into stirring hexanes (500 mL) to yield a black precipitate that was collected by sedimentation using a standard AlNiCo magnet and decanting of the hexanes phase. The resulting precipitate was dried *in vacuo* to yield a black powder (yield = 120 mg) that was soluble in a variety of organic solvents (e.g., toluene, THF, dichloromethane) and was responsive to an external magnetic field. Thermogravimetric analysis (TGA) revealed that an organic content of 43 % relative mass to the polymeric surfactant shell was present in the isolated product. The particle size of the PS-CoNPs (D =17 nm ± 1.8 nm) were determined by TEM. Magnetic properties of PS-CoNPs were measured using VSM at room temperature: M_s = 44 emu/g; H_c = 10500 A/m (131 Oe).

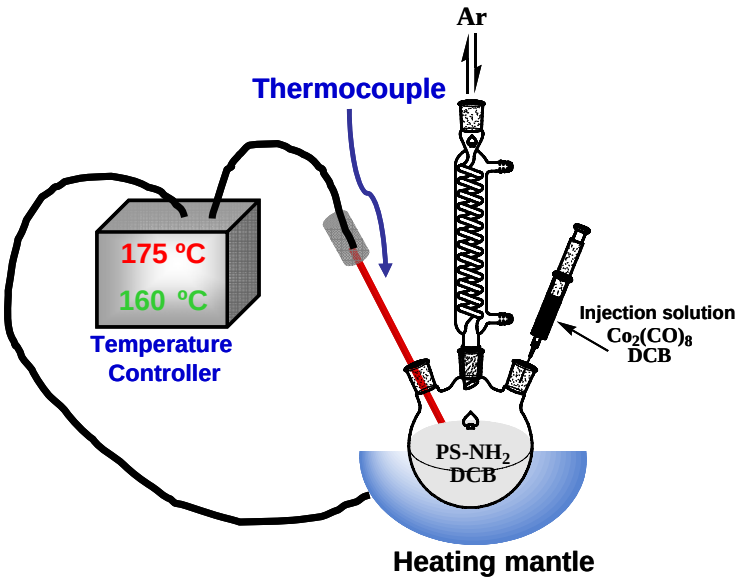

Figure 3.10: A general experimental setup for the dual-stage temperature thermolysis of $Co_2(CO)_8$ in the presence of polymeric surfactants.

Preparation of PS-CoNPs using end functionalized polystyrene surfactants, PS-NH_2 (3.1.2) and PS-COOH (3.3.1). To an oven dried 100 mL three-neck round bottom flask equipped with a stir bar and condenser was added PS-NH_2 **(3.1.2)** (0.160 g; 3.33 x 10^{-2} mmol) and PS-COOH (**3.3.1)** (0.040 g; 4.21 x 10^{-3} mmol). The polymers were dissolved in DCB (20 mL) and the solution was heated to 175 °C. Separately, $Co_2(CO)_8$ (0.300 g; 8.77 x 10^{-4} mol) was dissolved in DCB (4 mL) at room temperature in air, and was rapidly injected into the hot polymer solution. Identical heating protocols were followed as discussed previously. PS-CoNPs were purified by precipitation into hexanes (500 mL) yielding a black powder (yield = 240 mg). The particle size of the PS-CoNPs (D = 21 nm ± 3.1 nm) were determined by TEM. Magnetic properties of PS-CoNPs were measured using VSM at room temperature: M_s = 35.1 emu/g, H_c = 16100 A/m (202 Oe).

Preparation of PS-CoNPs using amine end functionalized polystyrene surfactants, PS-NH_2 (3.1.2). To an oven dried 100 mL three-neck round bottom flask equipped with a stir bar and condenser was added PS-NH_2 **(3.1.2)** (0.200 g; 4.17 x 10^{-2} mmol). Solids were dissolved in DCB (20 mL) and the solution was heated to 175 °C. Separately, $Co_2(CO)_8$ (0.300 g; 8.77 x 10^{-4} mol) was dissolved in DCB (4 mL) at room temperature in air, and was rapidly injected into the hot polymer solution. Identical heating protocols were followed as discussed previously. PS-CoNPs were purified by precipitation into hexanes (500 mL) yielding a black powder (yield = 240 mg). The particle size of the PS-CoNPs (D = 21 nm $\pm$ 2.9 nm) was determined using the TEM. Magnetic properties of PS-CoNPs were measured using VSM at room temperature: M_s = 34.0 emu/g, H_c = 20700 A/m (260 Oe).

Preparation of PS-CoNPs on 820 mg scale. To an oven dried 500 mL three-neck round bottom flask equipped with a stir bar and condenser was added PS-NH_2 **(3.1.2)** (0.800 g, 1.66 x 10^{-4} mol). Solids were dissolved in DCB (80 mL) and the solution was heated to 175 °C. Separately, $Co_2(CO)_8$ (1.20 g, 3.50 x 10^{-3} mol) was dissolved in DCB (16 mL) at room temperature in air, and was rapidly injected into the hot polymer solution. Identical heating protocols were followed as for the small scale model reaction discussed previously. PS-CoNPs were purified by precipitation into hexanes (1000 mL) yielding a black powder (yield: 820 mg). The particle size of the PS-CoNPs (D = 19 nm $\pm$ 3.3 nm) was determined using TEM. Magnetic properties of PS-CoNPs were measured using VSM at room temperature: M_s = 41.2 emu/g; H_c = 26300 A/m (330 Oe).

Deposition of PS-CoNPs dispersions onto carbon-coated TEM grid (300 mesh) exhibiting a variety of morphologies.

(1) Randomly entangled cobalt nanoparticle chains (Figure 3.7 (a and b)): PS-CoNPs (D = 21 nm ± 3 nm) were prepared using PS-NH_2 **(3.1.2)** (M_n= 4800 g/mole) in the thermolysis of $Co_2(CO)_8$. The as prepared ferrofluid (0.5 mL) was diluted in toluene (10 mL) to yield a PS-CoNPs dispersion (c = 0.5 mg/mL), a drop of which was deposited onto a carbon coated copper grid and dried in air.

(2) Nematic-like aligned chains (Figure 3.7 (c and d)): PS-CoNPs (D = 21 nm ± 2.9 nm) were prepared using PS-NH_2 **(3.1.2)** (M_n = 4800 g/mole) in the thermolysis of $Co_2(CO)_8$. The as prepared ferrofluid (0.5 mL) were diluted into dichlorobenzene (10.0 mL) to yield a PS-CoNPs dispersion (c = 0.5 mg/mL). A drop of this nanoparticle dispersion was deposited onto a carbon coated copper grid, and allowed to slowly evaporate in air under an applied magnetic field (100 mT).

(3) Flux-closure nanorings (Figure 3.7 (e and f)): PS-CoNPs (D = 21 nm ± 3.3 nm) were prepared using PS-NH_2 **(3.1.2)** (M_n = 12000 g/mole) in the thermolysis of $Co_2(CO)_8$. The as prepared ferrofluid 90.5 mL) was diluted in chlorobenzene (10 mL) to yield a PS-CoNPs dispersion (c = 0.5 mg/mL), a drop of which was deposited onto a carbon coated copper grid and dried in air.

(4) Folded lamellae nanoparticle chains (Figure 7 (g and h)): PS-CoNPs (D = 21 nm ± 2.9 nm) prepared from PS-NH_2 **(3.1.2)** (M_n = 4800 g/mole) in the thermolysis of $Co_2(CO)_8$. The as prepared ferrofluid (0.5 mL) was diluted in chlorobenzene (10 mL) to

yield a PS-CoNPs dispersion (c = 0.5 mg/mL), a drop of which was deposited onto a carbon coated grid and dried in air.

3.5: References

1. Furst, E. M.; Suzuki, C.; Fermigier, M.; Gast, A. P. *Langmuir* **1998,** *14*, (26), 7334-7336.

2. Furst, E. M.; Gast, A. P. *Phys. Rev. Lett.* **1999,** *82*, (20), 4130-4133.

3. Sun, S.; Murray, C. B.; Weller, D.; Folks, L.; Moser, A. *Science* **2000,** *287*, (5460), 1989-1992.

4. Cohen-Tannoudji, L.; Bertrand, E.; Bressy, L.; Goubault, C.; Baudry, J.; Klein, J.; Joanny, J.-F.; Bibette, J. *Phys. Rev. Lett.* **2005,** *94*, (3), 038301/1-038301/4.

5. Goubault, C.; Leal-Calderon, F.; Viovy, J.-L.; Bibette, J. *Langmuir* **2005,** *21*, (9), 3725-3729.

6. Singh, H.; Laibinis, P. E.; Hatton, T. A. *Nano Lett.* **2005,** *5*, 2149-2154.

7. Singh, H.; Laibinis, P. E.; Hatton, T. A. *Langmuir* **2005,** *21*, 11500-11509.

8. Singh, H.; Hatton, T. A. *J. Magn. Magn. Mater.* **2007,** *315*, 53-64.

9. Hess, P. H.; Parker, P. H., Jr. *J. Appl. Polym. Sci.* **1966,** *10*, (12), 1915-27.

10. Thomas, J. R. *J. Appl. Phys.* **1966,** *37*, 2914-2915.

11. de Gennes, P. G.; Pincus, P. A. *Phys.Kondens.Materie* **1970,** *11*, (3), 189-198.

12. Griffiths, C. H.; O'Horo, M. P.; Smith, T. W. *J. Appl. Phys.* **1979,** *50*, 7108-7115.

13. Chantrell, R. W.; Bradbury, A.; Popplewell, J.; Charles, S. W. *J. Phys. D: Appl. Phys.* **1980,** *13*, (7), L119-L122.

14. Chantrell, R. W.; Bradbury, A.; Popplewell, J.; Charles, S. W. *J. Appl. Phys.* **1982,** *53*, (3, Pt. 2), 2742-4.

15. Cheng, G.; Romero, D.; Fraser, G. T.; Hight Walker, A. R. *Langmuir* **2005,** *21*, 12055-12059.

16. Gao, J.; Zhang, B.; Zhang, X.; Xu, B. *Angew. Chem. Int. Ed.* **2006,** *45*, 1220-1223.

17. Tripp, S. L.; Puzstay, S. V.; Ribbe, A. E.; Wei, A. *J. Am. Chem. Soc.* **2002,** *124*, 7914-7915.

18. Tripp, S. L.; Dunin-Borkowski, R. E.; Wei, A. *Angew. Chem. Int. Ed.* **2003,** *42*, 5591-5593.

19. Xiong, Y.; Ye, J.; Gu, X.; Chen, Q. *J. Phys. Chem. B* **2007,** *111*, 6998-7003.

20. Chen, M.; Liu, J. P.; Sun, S. *J. Am. Chem. Soc.* **2004,** *126*, (27), 8394-8395.

21. Farrell, D.; Cheng, Y.; Ding, Y.; Yamamuro, S.; Sanchez-Hanke, C.; Kao, C.; Majetich, S. A. *J. Magn. Magn. Mater.* **2004,** *282*, 1-5.

22. Farrell, D.; Cheng, Y.; McCallum, R. W.; Sachan, M.; Majetich, S. A. *J. Phys. Chem. B* **2005,** *109*, 13409-13419.

23. Farrell, D.; Ding, Y.; Majetich, S. A.; Sanchez-Hanke, C.; Kao, C. *J. Appl. Phys.* **2004,** *95*, 6636-6638.

24. Goa, Y. H. B., Y.P.; Beerman, M.; Yasuhara, A.; Shindo, D.; Krishnan, K. *Appl. Phys. Lett.* **2004,** *84*, (17), 3361.

25. Puntes, V. F.; Gorostiza, P.; Aruguete, D. M.; Bastus, N. G.; Alivisatos, A. P. *Nature Mater.* **2004,** *3*, 263-268.

26. Sun, S.; Murray, C. B. *J. Appl. Phys.* **1999,** *85*, (8, Pt. 2A), 4325-4330.

27. Hilgendorff, M.; Tesche, B.; Giersig, M. *Aust. J. Chem.* **2001,** *54*, 497–501.

28. Pileni, M.-P. *Adv. Func. Mater.* **2001,** *11*, (5), 323-336.

29. Pileni, M. P. *J. Phys. Chem. B* **2001,** *105*, (17), 3358-3371.

30. Lalatonne, Y.; Motte, L.; Russier, V.; Ngo, A. T.; Bonville, P.; Pileni, M. P. *J. Phys. Chem. B* **2004,** *108*, (6), 1848-1854.

31. Lalatonne, Y.; Richardi, J.; Pileni, M. P. *Nature Mater.* **2004,** *3*, (2), 121-125.

32. Giersig, M.; Hilgendorff, M. *Eur. J. Inorg. Chem* **2005**, 3571-3583.

33. Pileni, M. P. *Acc. Chem. Res.* **2007,** *40*, (8), 685-693.

34. Shen, L.; Stachowiak, A.; Fateen, S.-E. K.; Hatton, T. A. *Langmuir* **2001,** *17*, 288-299.

35. Butter, K.; Philipse, A. P.; Vroege, G. J. *J. Magn. Magn. Mater.* **2002,** *252*, (1-3), 1-3.

36. Butter, K.; Bomans, P. H. H.; Frederik, P. M.; Vroege, G. J.; Philipse, A. P. *Nature Mater.* **2003,** *2*, (2), 88-91.

37. Klokkenburg, M.; Vonk, C.; Claesson, E.; Meeldijk.J.; Erne, B.; Philipse, A. *J. Am. Chem. Soc.* **2004,** *126*, 16706-16707.

38. Benkoski, J. J.; Bowles, S. E.; Korth, B. D.; Jones, R. L.; Douglas, J. F.; Karim, A.; Pyun, J. *J. Am. Chem. Soc.* **2007,** *129*, 6291-6297.

39. Benkoski, J. J.; Jones, R. L.; Douglas, J. F.; Karim, A. *Langmuir* **2007,** *23*, 3530-3537.

40. Hyeon, T. *Chem. Commun.* **2003**, 927-934.

41. Lu, A.-H.; Salabas, E. L.; Schuth, F. *Angew. Chem. Int. Ed.* **2007,** *46*, 1222-1224.

42. Leslie-Pelecky, D. L.; Rieke, R. D. *Chem. Mater.* **1996,** *8*, (8), 1770-1783.

43. Pyun, J. *Polym. Rev.* **2007,** *47*, 231-263.

44. Burke, N. A. D.; Stover, H. D. H.; Dawson, F. R. *Chem. Mater.* **2002,** *14*, 4752-4761.

45. Grubbs, R. B. *J. Polym. Sci., Part A: Polym. Chem.* **2005,** *43*, 4323-4336.

46. Balazs, A. C.; Emrick, T.; Russell, T. P. *Science* **2006,** *314*, 1107-1110.

47. Glogowski, E.; Tangirala, R.; Russell, T. P.; Emrick, T. *J. Polym. Sci., Part A: Polym. Chem.* **2006,** *44*, 5076-5086.

48. Grubbs, R. B. *Polym. Rev.* **2007,** *47*, 197-215.

49. Boal, A. K.; Frankamp, B. L.; Uzun, O.; Tuominen, M. T.; Rotello, V. M. *Chem. Mater.* **2004,** *16*, (17), 3252-3256.

50. Hong, R.; Fisher, N. O.; Emrick, T.; Rotello, V. M. *Chem. Mater* **2005,** *17*, 4617-4621.

51. Frankamp, B. L.; Fischer, N. O.; Hong, R.; Srivastava, S.; Rotello, V. M. *Chem Mater.* **2006,** *18*, (4), 956-959.

52. Lutz, J.-F.; Stiller, S.; Hoth, A.; Kaufner, L.; Pison, U.; Cartier, R. *Biomacromol.* **2006,** *7*, 3132-3138.

53. Xie, J.; Xu, C.; Xu, Z.; Hou, Y.; Young, K. L.; Wang, S. X.; Pourmond, N.; Sun, S. *Chem. Mater.* **2006,** *18*, (23), 5401-5403.

54. Frankamp, B. L.; Boal, A. K.; Tuominen, M. T.; Rotello, V. M. *J. Am. Chem. Soc.* **2005,** *127*, (27), 9731-9735.

55. Kim, B.-S.; Qiu, J.-M.; Wang, J.-P.; Taton, T. A. *Nano Lett.* **2005,** *5*, (10), 1987-1991

56. Kim, M. S.; Y.F., C.; Liu, Y. C.; Peng, X. G. *Adv. Mater.* **2005,** *17*, 1429-1432.

57. Vestal, C. R.; Zhang, Z. J. *J. Am. Chem. Soc.* **2002,** *124*, (48).

58. Matsuno, R.; Yamamoto, K.; Otsuka, H.; Takahara, A. *Chem. Mater.* **2003,** *15*, (1), 3-5.

59. Wang, Y.; Teng, X.; Wang, J.-S.; Yang, H. *Nano Letters* **2003,** *3*, 789-793.

60. Marutani, E.; Yamamoto, S.; Ninjbadgar, T.; Tsujii, Y.; Fukuda, T.; Takano, M. *Polymer* **2004,** *45*, (7), 2231-2235.

61. Matsuno, R.; Yamamoto, K.; Otsuka, H.; Takahara, A. *Macromol.* **2004,** *37*, (6), 2203-2209.

62. Ninjbadgar, T.; Yamamoto, S.; Fukuda, T. *Solid State Sci* **2004,** *6*, 879-885.

63. Gravano, S. M.; Dumas, R.; Liu, K.; Patten, T. E. *J. Polym. Sci., Part A: Polym. Sci.* **2005,** *43*, 3675-3688.

64. Gelbrich, T. F., M.; Schmidt, A. M. *Macromol.* **2006,** *39*, (9), 3469-3472.

65. Sun, Y.; Ding, X.; Zheng, Z.; Cheng, X.; Hu, X. P., Y. *Chem. Commun.* **2006,** *26*,

2765-2767.

66. Wakamatsu, H.; Yamamota, K.; Nakao, A.; Aoyagi, T. *J. Magn. Magn. Mater* **2006,** *302*, (2), 327-333.

67. Lattuada, M.; Hatton, T. A. *Langmuir* **2007,** *23*, 2158-2168.

68. Hess, P. H.; Parker, P. H. *J. Appl. Polym. Sci.* **1966,** *10*, 1915.

69. Platonova, O. A.; Bronstein, L. M.; Solodovnikov, S. P.; Yanovskaya, I. M.; Obolonkova, E. S.; Valetsky, P. M.; Wenz, E.; Antonietti, M. *Colloid Polym. Sci.* **1997,** *275*, 426-431.

70. Rutnakornpituk, M. T., M.S.; Harris, L.A.; Farmer K.E.; Esker, A.R.; Riffle, J.S.; Connolly, J.; Pierre, T.G. *Polymer* **2002,** *43*, 2337-2348.

71. Tadd, E.; Bradley, J.; Tannenbaum, R. *Langmuir* **2002,** *18*, 2378-2384.

72. Diana, F. S.; Lee, S.-H.; Petroff, P. M.; Kramer, E. J. *Nano Lett.* **2003,** *3*, (7), 891-895.

73. Liu, G. J.; Yan, X. H.; Curda, C.; Lal, J. *Chem. Mater.* **2005,** *17*, 4985-4991.

74. Puntes, V. F.; Krishnan, K. M.; Alivisatos, A. P. *Science* **2001,** *291*, (5511), 2115-2117.

75. Puntes, V. F.; Zanchet, D.; Erdonmez, C. K.; Alivisatos, A. P. *J. Am. Chem. Soc.* **2002,** *124*, (43), 12874-12880.

76. Korth, B. D.; Keng, P.; Shim, I.; Bowles, S. E.; Tang, C.; Kowalewski, T.; Nebesny, K. W.; Pyun, J. *J. Am. Chem. Soc.* **2006**, (128), 6562-6563.

77. Hawker, C. J.; Bosman, A. W.; Harth, E. *Chem. Rev.* **2001,** *101*, (12), 3661-3688.

78. Lacroix-Desmazes, P.; Lutz, J. F.; Chauvin, F.; Severac, R.; Boutevin, B. *Macromol.* **2001,** *34*, 8866-8871.

79. Matyjaszewski, K.; Xia, J. *Chem. Rev.* **2001,** *101*, 2921-2990.

80. Ing, H. R.; Manske, R. H. F. *J. Am. Chem. Soc.* **1926,** *48*, 2348-2351.

81. Williams, R. H.; Hamilton, L. A. *J. Am. Chem. Soc.* **1952,** *74*, 5418-5419.

82. Skaff, H.; Ilker, M. F.; Coughlin, E. B.; Emrick, T. *J. Am. Chem. Soc.* **2002,** *124*, (20), 5729-5733.

83. Witt, D.; Rachon, J. *Phosphorus, sulfur and silicon* **1994,** *91*, 153-164.

84. Pascual, S.; Coutin, B.; Tardi, M.; A., P.; J.-P, V. *Macromol.* **1999**, (32), 1432-1437.

85. Samia, A.; Hyzer, K.; Schlueter, J.; Qin, C.-J.; Jiang, S.; Bader, S.; Lin, X.-M. *J. Am. Chem. Soc.* **2005,** *127*, G126-4126.

86. Weis, J. J. *J. Phys.: Condens. Matter* **2003,** *15*, S1471–S1495.

87. Diehl, M. R.; Yu, J.-Y.; Heath, J. R.; Held, G. A.; Doyle, H.; Sun, S.; Murray, C. B. *J. Phys. Chem. B* **2001,** *105*, (33), 7913-7919.

88. Bao, Y.; Beerman, M.; Krishnan, K. M. *J. Magn. Magn. Mater.* **2003,** *266*, L245-L249.

89. Dinega, D. P.; Bawendi, M. G. *Angew. Chem. Int. Ed.* **1999,** *38*, (12), 1788-1791.

90. Sun, S.; Murray, C. B. *J. Appl. Phys.* **1999,** *85*, (8), 4325-4330.

91. Wei, D.; Patey, G. N. *Phys. Rev. Lett.* **1992,** *68*, 2043-2045.

92. Stevens, M. J.; Grest, G. S. *Phys. Rev. Lett.* **1994,** *72*, (23), 3686-3689.

93. Stevens, M. J.; Grest, G. S. *Phys. Rev. E* **1995,** *51*, (6-A), 5976-5983.

94. Stevens, M. J.; Grest, G. S. *Phys. Rev. E* **1995,** *51*, (6-A), 5962-75.

95. Tlusty, T.; Safran, S. A. *Science* **2000,** *290*, 1328-1331.

96. Stambaugh, J.; Van Workum, K.; Douglas, J. F.; Losert, W. *Phys. Rev. E* **2005,** *72*, (3-1), 031301/1-031301/4.

97. Van Workum, K.; Douglas, J. F. *Phys. Rev. E* **2005,** *71*, (3-1), 031502/1-031502/15.

98. Van Workum, K.; Douglas, J. F. *Phys. Rev. E* **2006,** *73*, (3-1), 031502/1-031502/17.

99. Lavender, H. B.; Iyer, A. K.; Singer, S. J. *J. Chem. Phys.* **1994,** *101*, (9), 7856-7867.

100. Miller, M. A.; Wales, D. J. *J. Phys. Chem. B* **2005,** *109*, 23109-23112.

101. Arshady, R.; Kenner, G. W.; Ledwith, A. *Makromol. Chem* **1976**, (177), 2911-2918.

102. Ryu, S. W.; Hirao, A. *Macromol.* **2000,** *33*, 4765-4771.

CHAPTER 4

DIPOLAR ASSEMBLY OF FERROMAGNETIC NANOPARTICLES INTO DENSE ARRAYS OF ACTUATING MICROSCOPIC FILAMENTS

4.1: Introduction

Taking inspiration from eukaryotic cilia, we investigate a method for growing dense arrays of actuating microscopic filaments using functional dipolar nanoparticles as "colloidal monomers". In collaboration with Jason Benkoski and his group at John Hopkins Institute, the bottom-up assembly of polymer coated cobalt nanoparticles, each segmented filament measures approximately 5 – 15 μm in length and 23.5 nm in diameter, which was commensurate with the width of single nanoparticles was achieved. A custom microscope stage actuates the filaments through orthogonal permanent and alternating magnetic fields. We implemented design of experiments (DOE) to efficiently screen the effects of cobalt nanoparticle concentration, crosslinker concentration, and surface chemistry. The results indicated that the formation of dense magnetic filaments could be explained by physical, non-covalent interactions (i.e. dipolar associations forces) rather than chemistry. The experiments also determined an optimal Co nanoparticle concentration of approximately 500 μg/ml for forming dense arrays near the ends of the permanent magnets, and a critical concentration of approximately 0.3 μg/ml, below which particle assembly into chains was not observed.

The miniaturization of robotics to centimeter length scales and below promises

unprecedented capabilities to sense, manipulate, and explore previously inaccessible environments.[1] Applications range from minimally invasive surgery[2, 3] to reconnaissance performed by flying robotic insects.[4] The capabilities of millirobots,[1, 5] microrobots,[6] or even nanorobots[7] are a function of power generation, locomotion, sensors, and control. For sensing and control, the requirements can nearly be met with commercially available equipment. In contrast, locomotion involves relatively bulky components with limited power efficiencies, and miniaturization to the micro-and nanoscale remains an important challenge.[1, 8] Consequently, miniaturized batteries and MEMS-based power generators still struggle to support autonomy for useful lengths of time or distance.[1]

As is frequently the case, an efficient solution to this problem can be found in nature. The cilium is among the smallest mechanical actuators found in living systems. Measuring 1 – 10 μm in length and 40 nm in diameter, cilium biomachinery employ a simple bending motion to generate locomotion or fluid flow. Operated in reverse, cilia can also detect local forces and acceleration. This simple yet elegant design is optimized according to the dueling needs of miniaturization and the fluid dynamics of the low Reynolds number environment.[9] We have taken inspiration from these design principles to fabricate microscopic mechanical actuators based on flexible magnetic filaments. Fabrication of "artificial cilia" has been achieved from the bottom-up assembly of 25 nm ferromagnetic cobalt nanoparticles, where each segmented filament measures approximately 1 – 10 μm in length and 25 nm in diameter. A custom microscope stage was built and utilized to visualize the actuation of filaments through orthogonally oriented permanent and alternating magnetic fields.

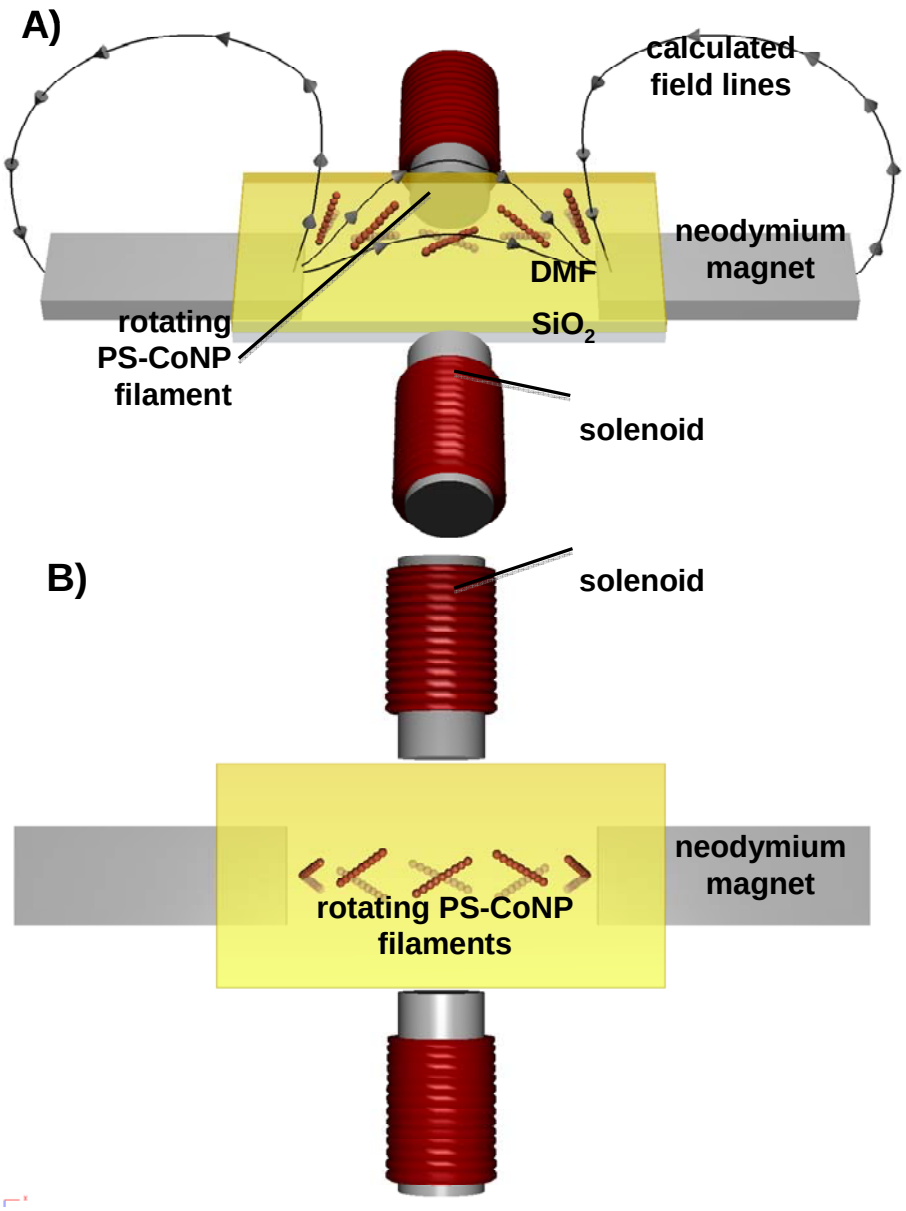

Scheme 4.1: Schematic of magnetic microscope stage. A) Setup for "*in situ*" experiments The magnetic field lines above the plane of the permanent magnets caused the Co filaments to have a different pitch depending upon the position on the Si wafer. The magnetic field lines for the pair of neodymium magnets, shown here calculated by the COMSOL multiphysics modeling application, were nearly vertical near the ends of the magnets and were horizontal when directly between. B) Top view of magnetic microscope stage, illustrating how the axis of rotation also depended on position. It

shifted from the center of the filament to the end of the filament as they approached the ends of the permanent magnets.

The synthesis and assembly of magnetic colloids has been extensively investigated as a bottom-up methodology to form self-organized mesostructures with one dimensional (1-D), 2-D and 3-D ordering. The seminal work of Gast *et al.* utilized micron-sized, magnetite-filled paramagnetic latex beads as colloidal building blocks to assemble and permanently link particles into microscopic magnetic chains while dispersed in aqueous media.[10, 11] The dipolar assembly of micron-sized paramagnetic beads in the presence of DNA has also been demonstrated by Bibette et al.[12] These filaments exhibited magneto-responsive mechanical behavior when exposed to oscillating external fields. Scaling of these systems below 1 μm was recently demonstrated by Hatton *et al.* using polyelectrolyte-coated latex beads in the 0.5 – 0.8 μm range.[13, 14] Superfine, *et al.* also outlined a procedure for producing high-aspect-ratio cantilevered micro- and nanorod arrays of a PDMS−ferrofluid composite material. The filament diameters ranged from 200 nm to 1 μm with aspect ratios as high as 125.[15] They demonstrated assembly of the beads into dispersed and surface tethered magnetic chains spanning 30-50 μm in length. In all of these earlier reports, the magnetic chains, or filaments, were large enough to be readily imaged using optical microscopy techniques as discrete 1-D assemblies that were dispersed in water.

The dipolar assembly of ferromagnetic nanoparticles (NPs) with sizes below 50 nm have more recently been explored to prepare responsive 1-D mesostructures. With the development of synthetic methods to prepare uniform, nanocrystalline magnetic

colloids, there has been significant interest to use these materials as "colloidal molecules" to form hierarchically ordered 1-D mesostructures.[16-18] We have recently developed the synthesis and characterization methods to form polystyrene-coated ferromagnetic cobalt nanoparticles (PS-CoNPs, diameter (D) = 20 nm) that have been observed to form micron sized mesoscopic 1-D assemblies when dispersed in crosslinkable organic solvents.[19, 20] In all of the nanoscopic systems, electron microscopy, or scanning probe microscopy (SPM) are required to confirm the formation of magnetic assemblies that were composed of individual NP repeat units. While direct visualization of micron-sized NP assemblies is easily conducted when cast onto surfaces using TEM, SEM, or SPM, *in situ* imaging of 1-D NP assembly in solution is considerably more challenging. We have recently confirmed the ability of *dispersed* PS-CoNPs to form micron sized "*mesoscopic polymers"* at an oil-water interface using the "Fossilized Liquid Assembly" technique.[20-23] However, direct *in situ* imaging of dispersed micron-sized dipolar assemblies from very small ferromagnetic NPs (D < 50 nm) has not been demonstrated.

Herein, we report perhaps the first example of optical visualization of ferromagnetic nanoparticles organizing into microscopic 1-D chains and actuating magnetic filaments while dispersed in DMF. Using a custom modified microscope, real-time imaging was captured of the hierarchical organization of 23.5 nm ferromagnetic PS-CoNPs into dense arrays of micron sized filaments on glass substrates. In constrast to previously published reports of magnetically driven artificial cilia,[15, 24, 25] these filaments are 10x narrower (23.5 nm), 3x greater in aspect ratio (400), and 100x greater in areal density (> 1 filament/μm^2). Even starker differences arise when compared to

optically driven artificial cilia,[26] which measure up to 1 mm in size. Perhaps most impressively, these arrays assemble in minutes without the need for templates or multiple fabrication steps.

A striking feature of this system is the ability to form dense filament arrays using only magnetic interactions on surfaces independent of substrate, or nanoparticle chemistry. The ability to grow and actuate these filaments using only magnetic interactions has several important consequences as a novel supramolecular system. We demonstrate with this magnetically assembled system that filament stiffness can be reversibly adjusted by control of applied field strength. Furthermore, the adhesion and actuation of assembled filaments to a variety of substrates was achieved by magnetic anchoring with static and oscillating external fields, respectively. It is worthwhile to note that conventional nanostructured assemblies typically require extensive chemical synthesis and a library of building blocks to achieve a comparable range of properties, all of which can be circumvented using magnetically assembled materials. With the ability to generate or detect forces at microscopic length scales, we envision applications in swarm robotics, distributed sensor systems, microfluidics, acoustic detection, and touch sensors.

4.2: Results and Discussion

4.2.1 Dipolar colloids

Ferromagnetic PS-CoNPs (D = 20 nm) were used as the colloidal precursor to form magnetic assemblies and filaments onto supporting glass substrates in the presence of external fields. However, these PS-CoNPs were found to be inherently dipolar and

have been extensively studied both in the solid state and solution to form mesoscopic polymer chains.[19, 20] The PS-CoNPs used in this study were imaged using both transmission and field emission scaning electron microscopies to confirm that single-NP chain-like structures were formed when cast onto surfaces (Figure 4.1). Reactive, aldehyde functional CoNPs were also synthesized with the expectation that chemical crosslinking would be necessary to form static 1D assemblies. However, we observed that dipolar associations between ferromagnetic CoNPs under the conditions used for assembly and imaging were sufficient to form 1-D NP chains, without the need for chemical crosslinking. Furthermore, both PS-CoNPs and aldehyde functional CoNPs exhibited similar behavior, despite subtle differences in NP surface chemistry.

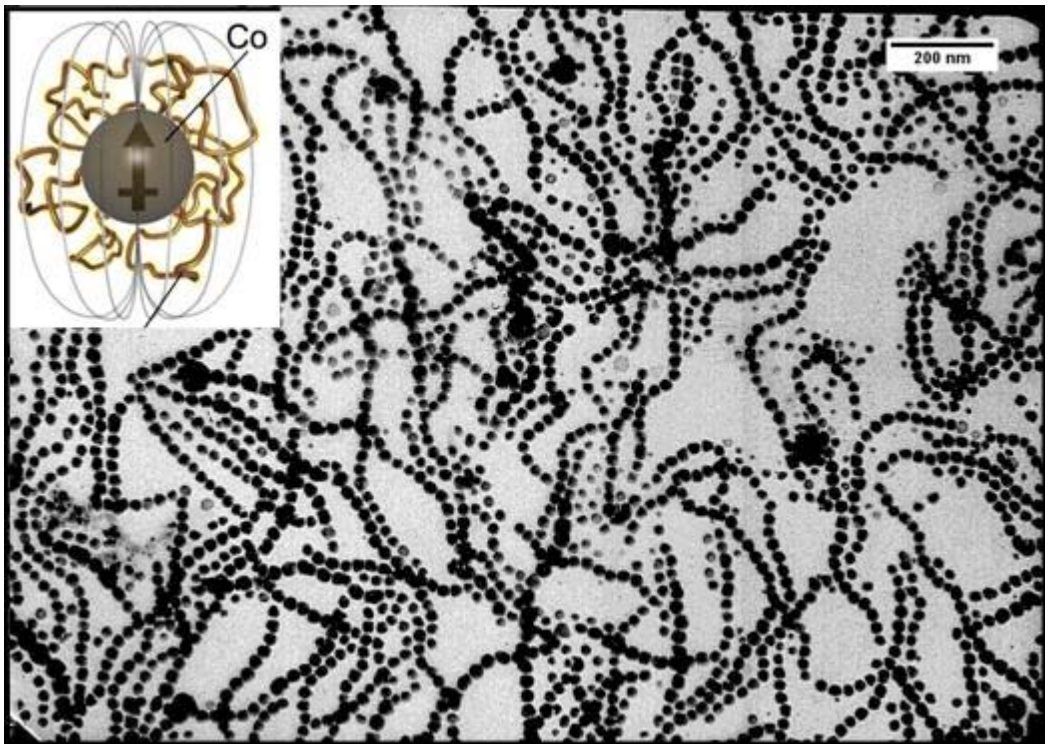

Figure 4.1: TEM image of Co nanoparticles coated with a shell of poly(Sty-r-BzAld).

The Co cores were monodisperse with an average diameter of 21 nm ± 2.5 nm. Including the 2.5 nm thick poly(Sty-r-BzAld) shell, the diameter averaged 23.5 ± 3.6 nm. The inset shows a schematic diagram of an individual ferromagnetic Co nanoparticle core with a poly(Sty-r-BzAld) shell.

4.2.2 Correlation of optical versus electron microscopy

The assembly process of dispersed ferromagnetic PS-CoNPs into mobile mesoscopic chains in DMF and as magnetically adsorbed filament arrays was investigated using optical imaging methods in the presence of external fields. Optical microscopy of dispersed PS-CoNPs in DMF was also conducted over a range of CoNP concentrations while confined between a glass slide and top coverslip under varying external magnetic fields. The assembly of DMF dispersions of PS-CoNPs into dense arrays of actuating magnetic filaments could be imaged *in situ* through the use of a custom-built magnetic stage where two permanent magnets induced vertical alignment of magnetic filaments perpendicular to the surface, while a complementary set of solenoids induced lateral rotation of assembled NP chains.

As shown in Figure 4.2, neighboring individual filaments were organized perpendicular to the underlying substrate while in DMF and did not cluster into dense bundled aggregates of filaments. Rather, the PS-CoNPs organize into evenly spaced arrays of discrete 1-D mesostructures. Compared to free standing columns formed in air, these filaments feature an unrivaled combination of aspect ratio and areal density. They measure 10 μm in length, 0.023 μm in diameter, and are spaced by less than 1 μm. Conventional etching techniques could not achieve these dimensions much less prevent the pillars from collapsing onto the surface or with each other. The formation of discrete non-aggregated filament brushes was attributed to the weak repulsive interactions

between magnetic dipoles of parallel spin orientations, which served to stabilize magnetic filaments from lateral bundling. Further preventing chain collapse were the decreased work of adhesion and PS steric repulsion achieved through solvent mediation of the filament interactions.

While under the influence of the magnetic field and in DMF, assembled filaments were predominately fixed on the surface in regions of magnetic flux lines that promoted vertical brush formation. The nature of this adhesion was primarily attributed to magnetic associations, but contributions from friction and short range van der Waals interactions are also likely promoting the surface tethering. Once in place, individual filaments in the vertically aligned brush array were magnetically actuated back and forth with an alternating magnetic field oriented perpendicular to the permanent magnets. Further evidence from the optical microscopy that the assembled, actuating filaments were indeed individual, non-bundled chains of PS-CoNPs was confirmed using *ex-situ* measurements discussed in a following section.

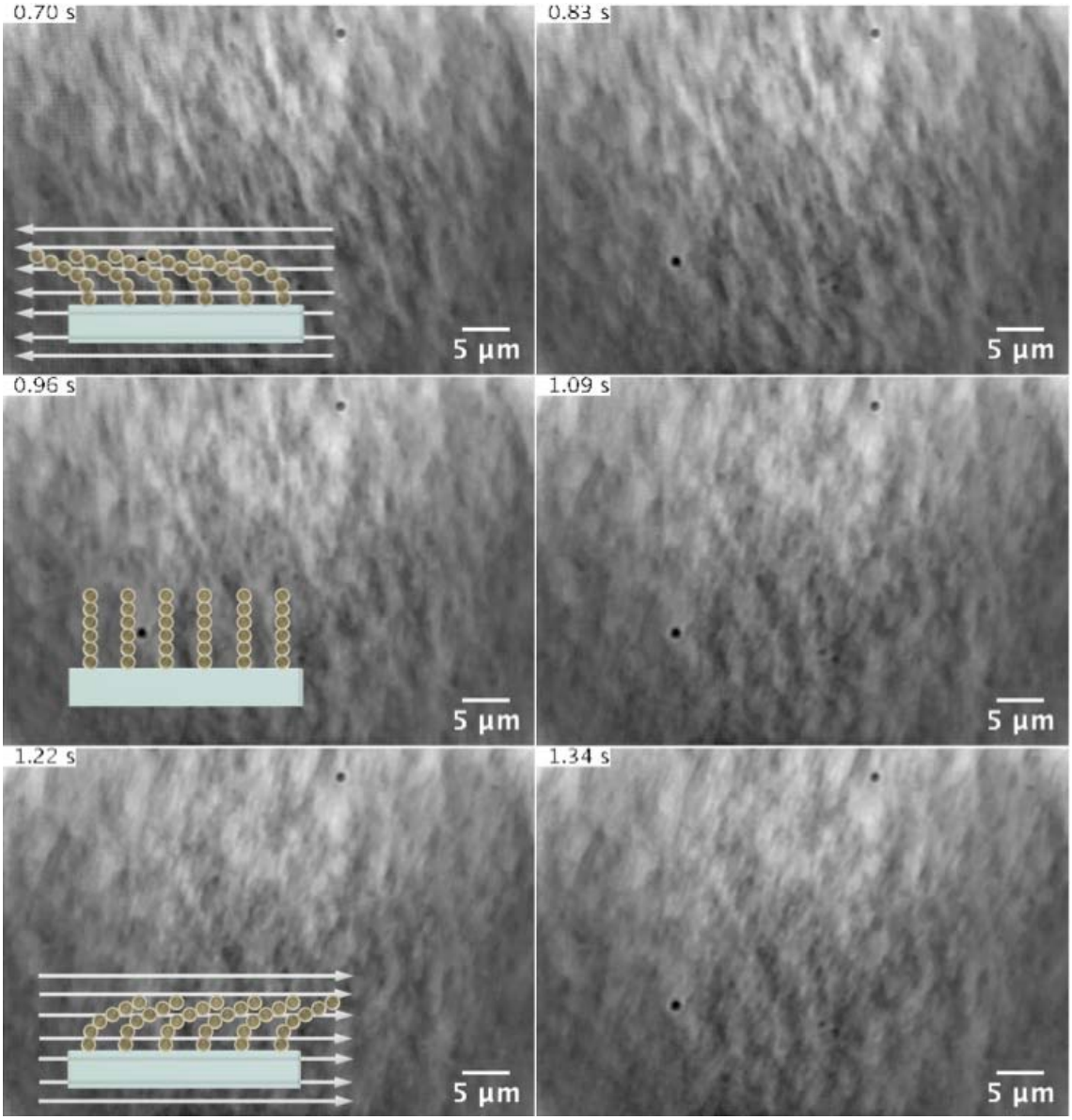

Figure 4.2: Time-lapsed optical image frames taken from a movie of a cilia-mimetic array taken at different times during oscillation. The sample was made from a 1000 µg/ml solution of Co nanoparticles in DMF. The filaments appear thicker than their actual diameter since it was necessary to under-focus in order to maximize contrast. The three insets on the left are diagrams illustrating the orientation of the filaments with respect to the substrate and the magnetic field applied by the pair of solenoids. For still images, it is generally only possible to discern the texture of the filament arrays, whereas movies improve the discernability of individual chains.

Dipolar assembly of dispersed PS-CoNPs into microscopic filaments proceeded through alignment with the external field, followed by accumulation of the filaments near

the ends of the neodymium magnets used as static poles. In this and previous studies,[19, 20] we observed that the PS-CoNPs self-organize into chains even in the absence of an external field (i.e., zero-field conditions). Figure 4.3 (a) illustrates prevalence of loops and branched chains under these conditions, which form in order to close the magnetic flux loops and therefore minimize the enthalpic penalty of free ends. These small 1-D assemblies are present prior to application of the external field. Rather than stimulating nucleation, the apparent role of the external field is to open the rings, align the chains with the external field, assist chain growth, and then draw them towards the ends of the permanent magnets, where the magnetic field gradient is steepest.

To illustrate these effects, SEM samples were deposited on the magnetic-optical stage and allowed to dry under the influence of its magnetic field (Figure 4.3 (b)). Note the presence of distinct nanoparticle chains, one nanoparticle in width, across the entire surface. This particular comparison was conducted to serve as an imaging reference to correlate morphologies observed in films visualized from SEM with those from optical microscopy of dispersed magnetic filaments (e.g., Figure 4.2). Because direct *in-situ* imaging of dispersed filaments and mesoscopic assemblies in DMF cannot be performed using SEM, it was important to qualitatively confirm that the magnetic filaments observed by optical microscopy were, in fact, discrete 1-D mesostructures that were one particle wide rather than thick, agglomerated assemblies.

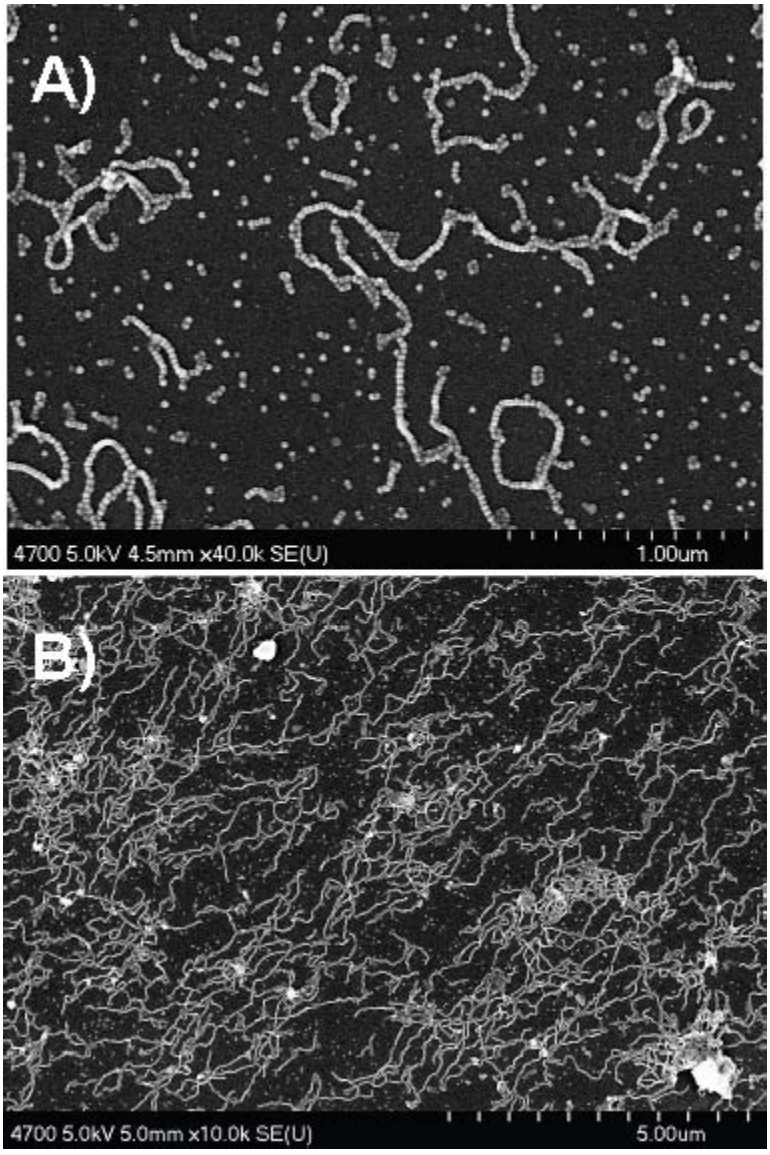

Figure 4.3: A) SEM micrograph of cobalt nanoparticle chains deposited under zero-field conditions from a 500 μg/ml Co nanoparticle solution in DMF. The micrograph demonstrates that a high concentration of chains is present before the solution is placed on the magnetic microscope stage. Note the prevalence of short chains, branches, and loops when an aligning field is not applied. B) SEM micrograph of the same solution the same solution dried atop the magnetic microscope stage. The areal density of chains decreased for decreasing Co nanoparticle concentrations, but discrete 1-D filaments were observed for all samples formed on the magnetic stage.

4.2.3 Orientation versus position

We observed an unexpected dependence of filament orientation on spatial positioning of PS-CoNPs with respect to the applied fields from the solenoids and permanent magnets on the optical stage. Neither the areal density of chains nor chain length varied measurably from sample to sample. Despite large changes in chemistry, the factorial design of experiments did not generate appreciable changes in dimension or morphology. The largest changes were noticed not from sample to sample, but rather from position to position with respect to the permanent magnets. This observation again points to the importance of the magnetic field in driving assembly. Even for large changes in PS-CoNP concentration, the length and areal density *in a given location* was unchanged. Generally, lower concentrations of PS-CoNPs resulted in longer times for the dense brushes to fill in, but the brushes themselves looked identical once fully formed.

As shown in Figure 4.4, the filaments assumed a more vertical orientation as they approached the ends of the permanent magnets. The characteristic "V" shape is an artifact caused by the vertically oriented filaments being longer than the depth of focus (Figure 4.4 a). Accordingly, magnetic filaments closer to the center of the stage (Figure 4.4 b, c) tended to align more parallel to surface, as observed by an apparent increase in filament length as visualized by optical microscopy. Finally, filaments completely parallel to the glass substrate were also observed near the center of the magnetic stage (Figure 4.4 d), directly tracking the flux lines from the pair of permanent magnets. These filaments appeared to range between 5 and 15 μm in length.

The magnetic field lines tended to converge at the ends of the neodymium magnets such that the magnetic field gradient was approximately 13 T/m. Many magnetic filaments therefore accelerated towards the two permanent magnets over time. They only came to rest when they either jammed against other filaments or were pinned by friction with the lower cover slip. By contrast, filaments in the center of the sample tended not to translate from their original position. The same behavior was observed regardless of surface treatment chemistry with ligating amines, hydrophobic alkyl chains, or un-modified polar glass surfaces.

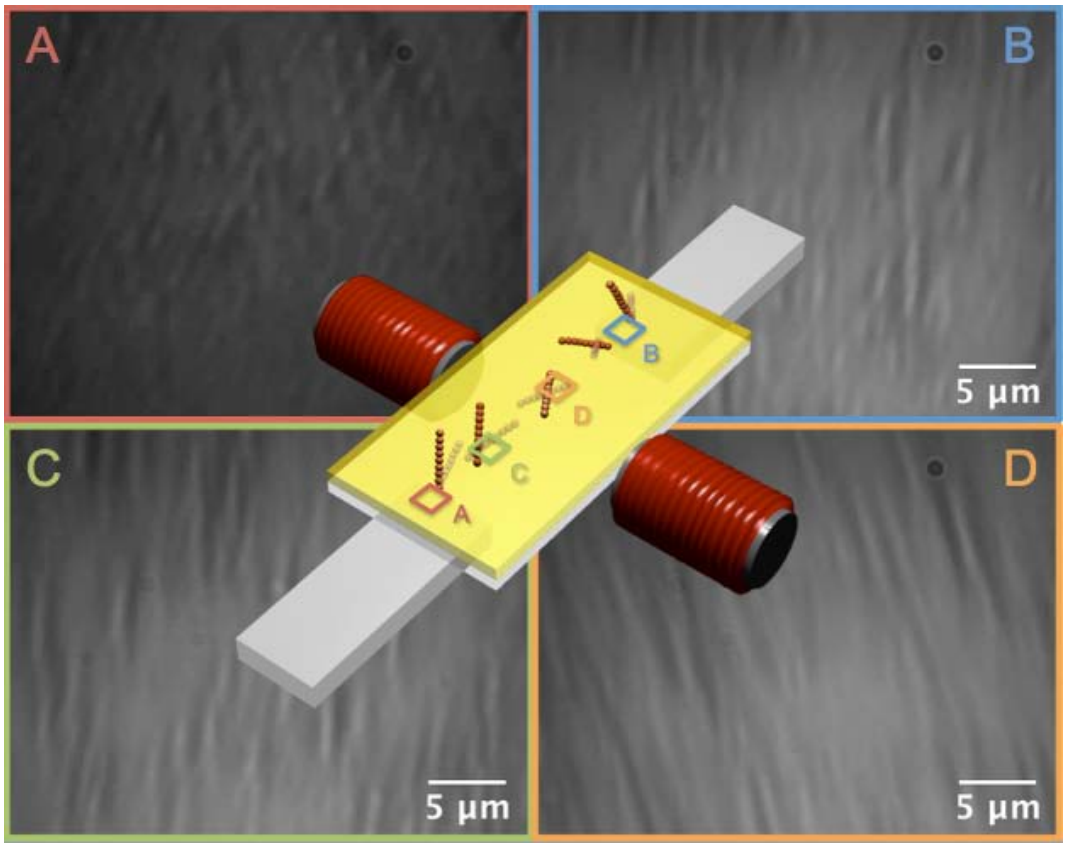

Figure 4.4: A series of optical micrographs illustrating how the incline of the filaments changes with respect to distance from the permanent magnet, accompanied by a graphical depiction of their position on the stage. A) The top-left image was taken directly above

the end of the magnet, B) the top-right image was taken about 2 mm away from the magnet, C) the bottom left image was taken approximately 4 mm from the magnet, and D) the bottom-right image was taken approximately 6 mm from the magnet, near the mid-point.

One of the most important fundamental questions to address in this study was the correlation of mesostructure and morphology of PS-CoNP magnetic filaments from both optical and electron microscopy. The targeted morphology for this study was densely aligned, non-aggregated single NP wide filaments organized perpendicular to supporting substrates, as shown in Figure 4.2. However, since PS-CoNPs diameters were significantly less than the optical diffraction limit, it was not possible to determine filament dimensions using optical microscopy directly. To circumvent this inherent problem, a series of magnetic filaments of varying aggregation number and thickness were prepared by organizing PS-CoNPs under varying concentration and applied field strength. These filaments dimensions were quantitied using SEM and were then correlated with morphologies observed under optical microscopy. The custom built magnetic stage was limited to a static 42 mT field perpendicular to the substrate and 0-75 mT fields parallel to the substrate. The limited space beneath the microscope objective necessitated the use of permanent magnets to allow *in situ* observation of magnetic assembly, but it precluded the ability to change the strength of the static field. To explore the effects of stronger applied fields, it was necessary perform *ex situ* experiments in which a DMF dispersion of PS-CoNPs was confined between a pair of glass slides and then sandwiched between a pair of large neodymium magnets. Measuring 100 x 50 x 12 mm, the magnets supplied a uniform 148 mT magnetic field perpendicular to the glass slides. A schematic of the experimental setup is shown in

Scheme 4.2.

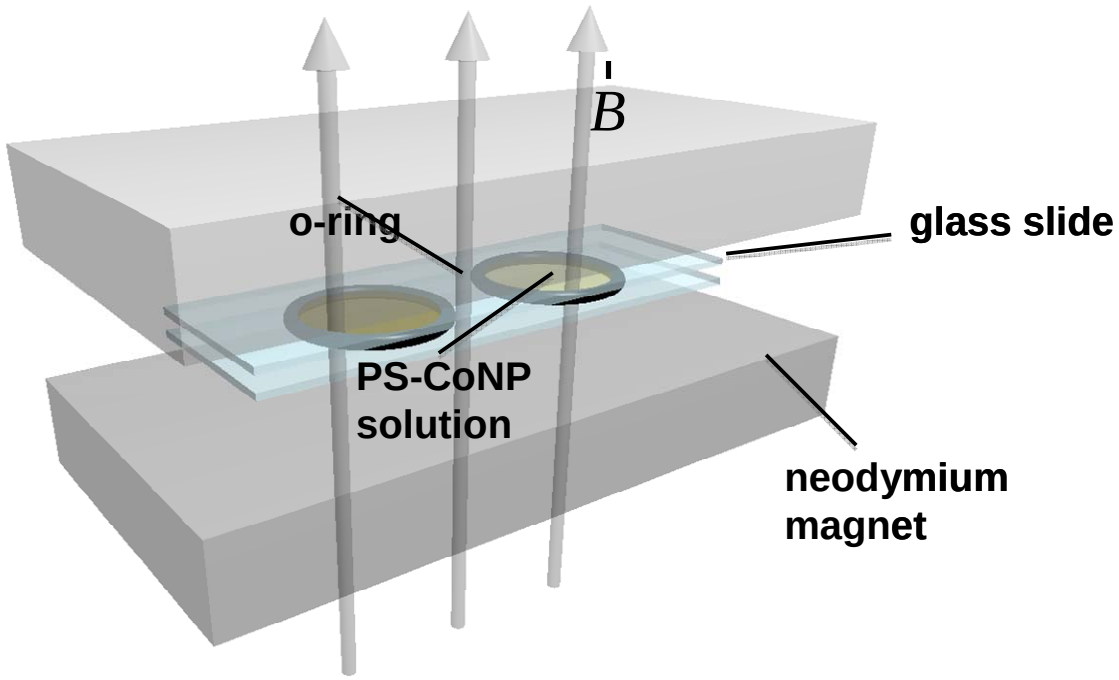

Scheme 4.2: Schematic of experimental setup for *ex situ* experiments drawn to scale. The PS-CoNP solutions were sandwiched between a pair of 75 x 25 x 1 mm glass slides and 20 x 1 mm viton o-rings. The assembly was clamped between a pair of 100 x 50 x 12 neodymium magnets that provided a transverse 148 mT field. Wooden spacers, not shown, were used to adjust the magnetic field strength by adjusting the distance between the permanent magnets.

Unlike the *in situ* experiments, the permanent field was not accompanied by an additional orthogonal alternating magnetic field. Control experiments had previously shown that the presence or absence of the alternating field did not measurably affect the morphology of the cilia-mimetic arrays. As seen in Figure 4.5 a-d, the stronger fields of the *ex situ* experiment resulted in thick, columnar aggregates that were deposited onto a supporting subtrate after removal of the magnetic field and DMF. Large filaments were easily discernable in optical microscopy images as collapsed fibers on the underlying glass substrate, with lengths up to 1 mm (the spacing of the glass slides) formed from

dipolar associations (Figure 4.5 c). The SEM imaging of two discrete assembled filaments organized using the same external field strength (148 mT) but at different concentrations (10, 100 μg/ml) formed fibular assemblies hundreds to thousands of nanometers wide. Correlation of these filament dimensions determined from SEM of solution deposited samples with optical images of DMF dispersed assemblies provided an important benchmark to qualitatively interpret the magnetic actuation experiment (Figure 4.1) to be composed of filaments a single PS-CoNP in width also show very clearly how the optical micrographs of thick bundles in Figure 4.5 a and 4.5 c are easy to distinguish from the discrete 1-D assemblies observed *in situ* in Figure 4.5 e. For comparison we have also included an SEM micrograph formed on the *in situ* magnetic microscope stage (Figure 4.5 f). Note that Figure 4.5 c and d were made at the same concentration as Figure 4.5 e and f. Generally speaking, an increase in PS-CoNP concentration at 148 mT (*ex situ* experiments) caused an increase in bundle thickness, whereas an increase in PS-CoNP concentration at 83 mT (*in situ* experiments) resulted in a greater number of discrete 1-D PS-CoNP chains on the magnetic stage. These sets of correlated SEM and optical images of different sized filaments from *ex-situ methods* suggested that the magnetically actuating filaments formed in *in-situ* experiments (Figure 4.2 and 4.4) and imaged via optical microscopy were likely single NP wide assemblies.

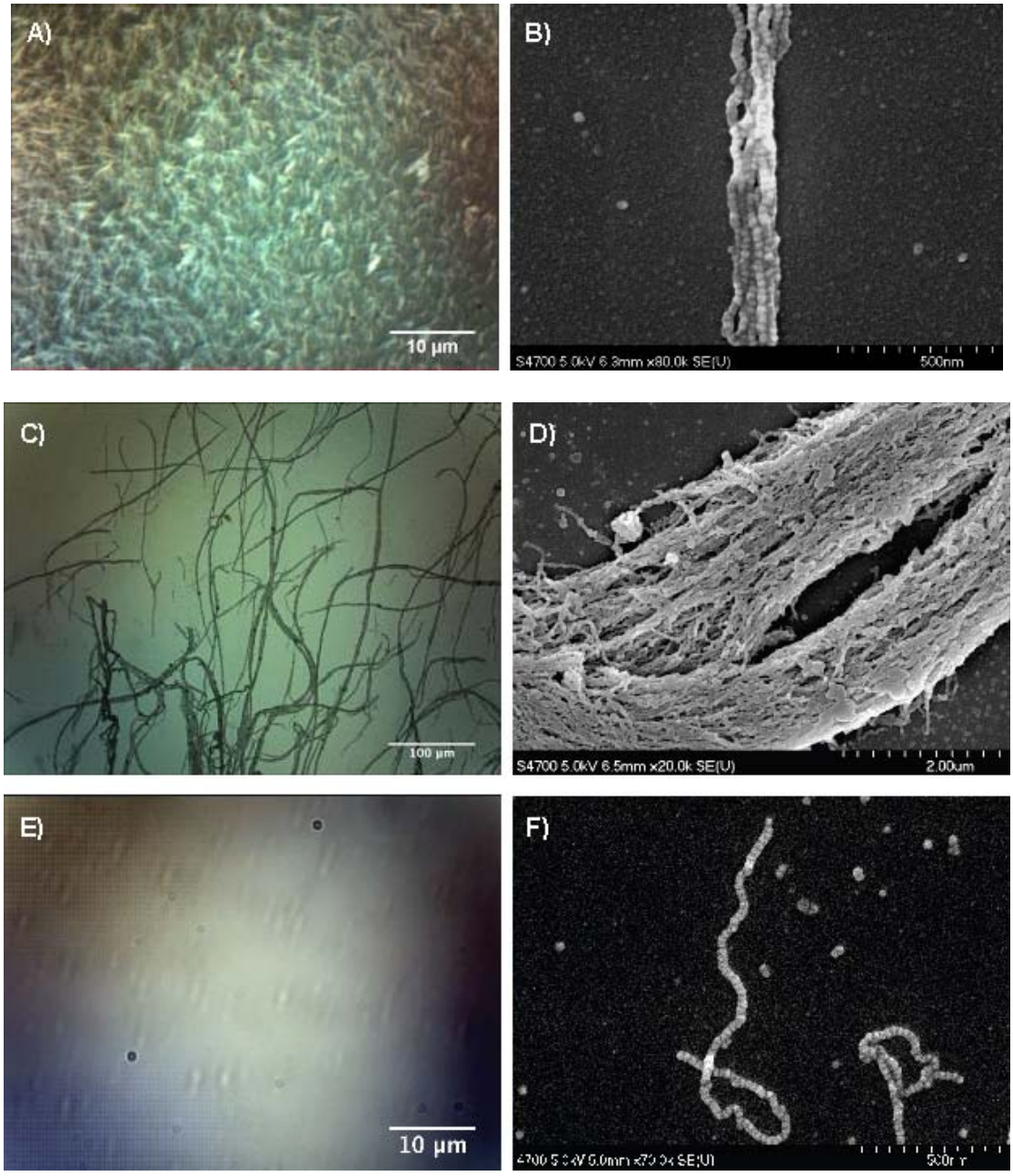

Figure 4.5: A) Large Co filaments formed on a glass slide from a 10 µg/ml Co nanoparticle suspension in the presence of a strong (148 mT) field perpendicular to the surface. B) A close-up SEM image of a pair of an isolated columnar aggregate formed under these conditions. C) Thicker columnar aggregates formed at a 100 µg/ml Co nanoparticle concentration with the same 148 mT field. D) SEM close-up of a pair of thick filaments from the same sample. E) The same 100 µg/ml PS-CoNP concentration except seen on the *in situ* magnetic microscope stage. F) The SEM image of the *in situ*

prepared sample verifies that the magnetic filaments seen in the optical micrographs are indeed one particle in width.

Columnar aggregates form at high field strength when the PS-CoNPs phase separate into a Co rich phase surrounded by a DMF-rich matrix.[27, 28] As described by Zubarev and Iskakova,[29] this phase transition begins with the formation of linear chainlike clusters which collapse into dense globules once they exceed a critical length. These globules then serve as nuclei for the growth of dense, Co-rich columns that span the gap between the pair of glass slides.

Experimentally, Klokkenburg, et al. also observed columnar aggregates of magnetite nanoparticles growing in strong magnetic fields.[32] Their quasi-2D system was inspected using cryo-transmission electron microscopy (cryo-TEM). Under zero-field conditions[30, 31] the magnetite nanoparticles formed discrete, 1D assemblies indistinguishable from those shown in Figure 4.3 a. Interestingly, the calculated pair interaction energies ranged from -4 to -9 k_BT depending on the diameter, very close to the value of -7 k_BT expected for the 23.5 nm PS-CoNPs in DMF.[33] However, efforts to visualize magnetic actuation of assemblied NP-chains dispersed in solution could not be conducted because of the use of cryo-TEM, which required vitrified samples that could not be addressed with external magnetic fields.

Whereas the formation of the dense columns constitutes a thermodynamic phase transition, the formation of linear chains of nanoparticles shares more in common thermodynamically with self-assembly processes such as micelle formation, growth of the tobacco mosaic virus, or the equilibrium polymerization of actin networks.[34 - 40] Even with the presence of chain-like assemblies above 0.3 μg/ml, the PS-CoNP dispersion is

still technically a single phase much like surfactant solutions above the critical micelle concentration. The significance of this distinction is that phase separation should be avoided if miniaturization and flexibility are desired.

The fact that physical, rather than chemical, interactions can tether and organize the magnetic filaments has profound implications on both the fabrication and use of these actuators. In practice, a patch of densely packed filaments can be created by simply backing a substrate with a patch of magnetic material and then dipping it into a solution of CoNPs. Another consequence of relying on magnetism is that the stiffness of the filaments and the adhesion force with the surface can be controlled independently. This control is possible without making changes to the material because stiffness of the filaments depends upon the magnitude of the field strength,[41-43] whereas the force holding the filaments to the surface depends on the steepness of the field gradient. The field strength and gradient can be controlled independently within limits. The final, and perhaps most interesting, consequence of relying on magnetism is that the adhesion of the filaments is self-healing. In contrast to covalent bonds, the magnetic attraction to the surface acts over a relatively large distance. If one were to pull a single filament from the surface, it would return to its original position having suffered no irreversible damage.

The arrays formed in this study are long lived, and remain in place even with temporary reorientation or removal of the applied field. The formation of dense arrays has also proven reproducible, with arrays similar to those shown in Figure 4.2 appearing in each experiment. Scaling up to larger areas may be possible if the local magnetic field conditions near the ends of the permanent magnets can be reproduced uniformly

over larger areas. Such experiments are currently in progress.

4.3: Conclusion

We successfully demonstrated the bottom-up fabrication of cilia-mimetic arrays of flexible magnetic filaments from cobalt nanoparticles and confirm the assembly of ferromagnetic colloids in solution using optical microscopy. We further demonstrated that these arrays can be actuated with an external magnetic field. By performing a multivariable DOE screening experiment, we determined that changes in chemistry—i.e. surface functionalization or crosslinker concentration—did not produce obvious changes in the filament structure or organization. Instead, the observed effects of the processing parameters can be explained almost entirely in terms of physical interactions. The biggest effects arose from changes from changes in position with respect to the permanent magnets. Near the ends of the magnets, the filaments were vertically aligned with a density of about 1 filament/μm^2. As one moved towards the center of the stage, the areal density decreased as did the inclination of the filaments with respect to the surface. Increasing the concentration of PS-CoNPs generally increased but not noticeably in length. The vast majority of these filaments were increased the number of chains and the rate at which the dense brush would form, but the length and areal density of chains were primarily a function of position and, therefore, magnetic field. The vast majority of these filaments were a single nanoparticle across. No chains were observed below a nanoparticle concentration of 0.3 μg/ml, and the propensity to form cilia-mimetic arrays did not appear to improve beyond 500 μg/ml. For strong magnetic fields (148 mT), the filaments increased in diameter with increasing nanoparticle concentration and increased

slightly in areal density. The lengths of the columnar filaments were constrained only by the distance between the pair of glass plates.

Although the spatially varying magnetic field in our magnetic test fixture complicated the interpretation of data, the wider range of field conditions across the samples proved useful for identifying the best conditions for forming cilia-like arrays. For the Co nanoparticles used in this study, we estimate that a magnetic field gradient no greater than 10 T/m normal to the surface is required for organizing the filaments into cilia-like arrays.

4.4: Experimental

Synthesis of Polystyrene Coated Ferromagnetic Colloids. PS-CoNPs were synthesized using amine terminated polystyrene (PS) surfactants in the thermolysis of dicobaltoctacarbonyl ($Co_2(CO)_8$) in refluxing 1,2-dichlorobenzene (DCB) yielding uniform ferromagnetic colloids (particle size = 18 nm $\pm$ 1.5 nm; mass magnetization, σ_s = 38 Am^2/kg, saturation magnetization, $M_s = 3.5 \times 10^5$ A/m; dipole moment, $m = 8.7 \times 10^{19}$ Am^2; coercivity, H_c = 8000 A/m at room temperature). Details of the preparation methodology can be found in reference 17 and 18.

Synthesis of 4-(vinylphenyloxy)benzaldehyde. 4-vinylbenzylchloride (5.00 g; 32.8 mmole), 4-hydroxybenzaldehyde (4.00 g; 32.8 mmole), K_2CO_3 (8.24 g; 59.6 mmole) and KI (0.272 g; 1.64 mmole) were suspended in acetone and then refluxed under argon overnight. After removing the inorganic salts, the solvents were evaporated. The crude yellow product was purified via flash chromatography starting from a 1:6 dichloromethane (DCM): hexanes elution and gradually increases to DCM elution to

obtain a white solid as pure product (3.89 g; 50 % yield) with a R_f value of 0.5 in DCM. ^{1}H NMR (250 MHz, $CDCl_3$, δ): 9.87 (s, 1H, CHO), 7.83 (d, J = 8.8 Hz, 2H. ArH), 7.41 (m, 4H, ArH), 7.06 (d, 2H, J = 8.8 Hz, ArH), 6.72 (dd, J = 11 Hz, 1H –CH=CH_2), 5.77 (d, J = 17.5 Hz, 1H –CH=CH_2), 5.27 (d, J = 11Hz, 1H, CH=CH_2), 5.12 (s, 2H, O-CH_2).

Ligand exchange of PS-CoNPs with poly(Sty-r-BzAld): 150 mg of PS-CoNPs were dispersed in 10 ml of toluene. In a separate vial, poly(styrene-r-styreneoxybenzaldehyde) (poly(Sty-r-BzAld); 0.65 g; 0.0429 mmole) was dissolved in 10 mL of toluene, added to the cobalt nanoparticle dispersion, and sonicated at 60 °C for 3 hours. The crude ligand exchange reaction was diluted to about 125 mL of toluene. To isolate the functional PS-CoNPs, a ball of steel wool was placed in the diluted dispersion on 2 pieces of Nd alloy magnets. The supernatant was decanted and the black residue collected in the steel wool was washed and transferred into a tared vial. Solvents were evaporated to obtain a black powder (69.1 mg). The dried powders (0.8 mg) were dispersed in 2 mL of toluene, sonicated until homogeneous and solvent-cast onto a carbon coated TEM grid in zero field (Figure 4.1). After ligand exchange, the particles plus the polymer shells had an average diameter of 22 ± 3.6 nm. Gel permeation chromatography (GPC) data for the polymer shells were obtained by first digesting the Co nanoparticle cores and then running the purified polymer through the GPC column (Figure 4.6).

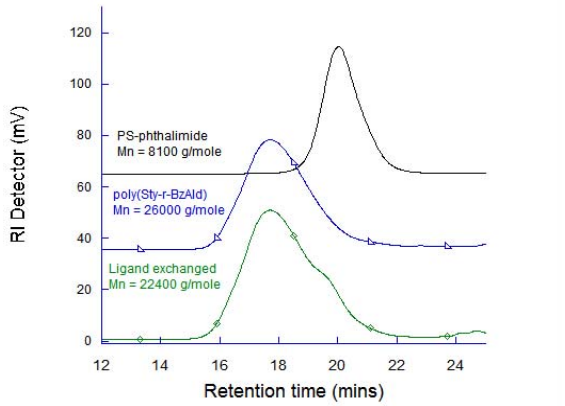

Figure 4.6: Spectroscopic characterizations of the isolated copolymers after HCl degradation of the cobalt core. (a) ^{1}H NMR showed the presence of the benzaldehyde moieties and (b) Overlay GPC of the copolymers isolated after the ligand exchanged reaction (green trace), which is commensurate with poly(Sty-r-BzAld) (blue trace).

Investigation of crosslinking reaction of poly(Styrene-r-Benzaldehyde) coated cobalt nanoparticles in organic media. The conversion of benzaldehyde to an imine were first investigated using monofunctional amine such as butylamine and amine end functional polystyrene. The reactions were performed in a variety of solvents (THF, toluene, chloroform and DMF) and temperatures (room temperatures, 50 °C, 70 °C and 90 °C), characterized via ^{1}H NMR and FTIR. FTIR was utilized to observe the formation of C=N stretching modes at 1653 cm^{-1} while the disappearance of the aldehyde C=O stretch at 1695 cm^{-1} in the crosslinking reactions.[44] This method is attractive because the formation of imine could be directly probed without the need for further purification, degradation and isolation procedures. From these studies, the crosslinking reactions were found to be highly depended on solvents and temperatures. In this case, the crosslinking reactions were only successful in DMF heated at 70 °C - 90 °C (Figure 4.7 and 4.8).

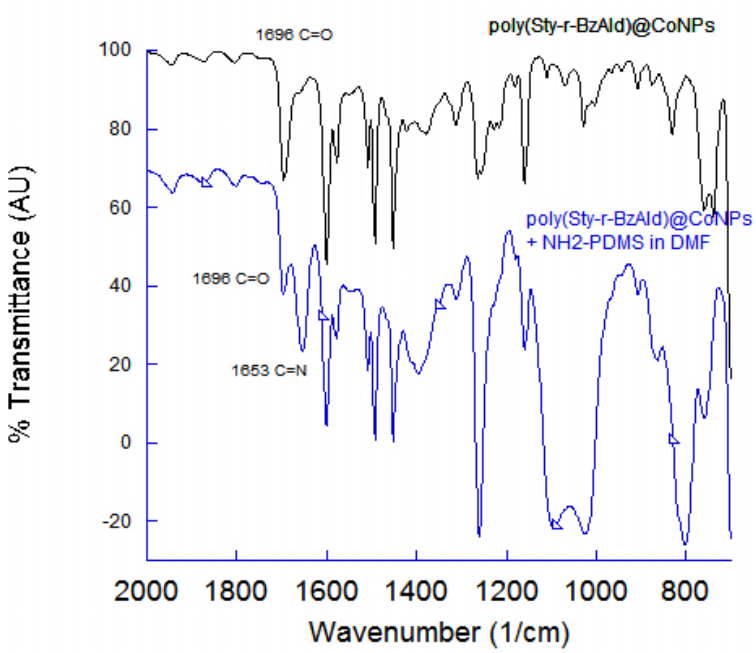

Figure 4.7: Overlay FTIR of poly(Sty-r-BzAld)@CoNPs (black trace) and crosslinked poly(Sty-r-BzAld)@CoNPs in the presence of a diamine crosslinker in DMF at 90 ºC. The crosslinking reaction between the aldehyde copolymers and the diamine resulted in the formation of an imine bond. Formation of the C=N asymmetric stretches at 1653 cm^{-1} confirmed the crosslinking reaction.

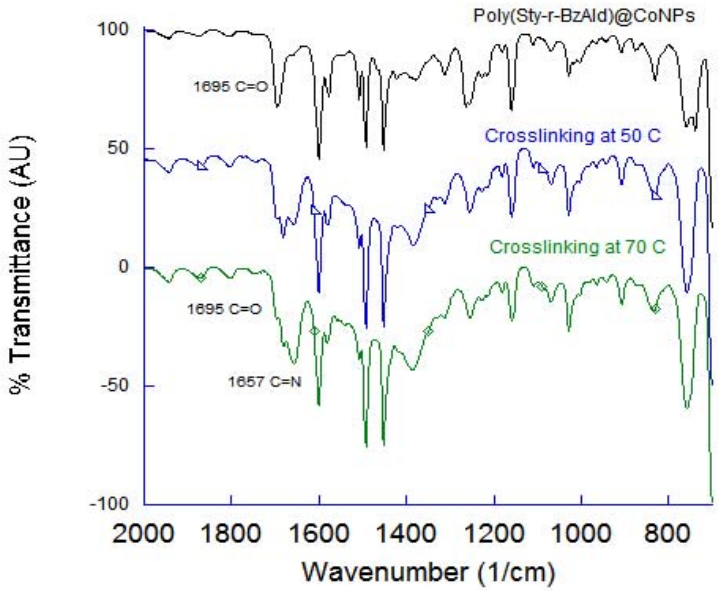

Figure 4.8: Overlay FTIR from the reactions of poly(Sty-r-BzAld)@CoNPs with a diamine crosslinker performed at 50 °C and 70 °C. The top black trace represents

poly(Sty-r-BzAld)@CoNPs, blue middle trace is the aldehyde functional CoNPs reacted with amine-PDMS in DMF at 50 °C and the green bottom trace is the reaction performed at 70 C. The vibrational mode at 1696 cm^{-1} is C=O stretching of the unreacted aldehyde, 1657 cm^{-1} is the C=N stretching mode, while the 1680 cm^{-1} is the C=O stretching due to the presence of residual DMF solvent.

In Situ Assembly. The directed-assembly of cobalt nanoparticles into flexible magnetic ilaments took place upon a custom-designed magnetic microscope stage. Two permanent magnets aligned the filaments parallel to the surface. A perpendicular pair of solenoids created a time varying magnetic field. In this design, the permanent magnets determine the primary direction of the assembled magnetic filaments whereas the solenoids drive the side-to-side rotation.

As shown in Scheme 4.1 the neodymium permanent magnets (Edmund Scientific, P/N 3082773) measure 10 x 4.5 x 1 mm. The static field across the 12 mm gap varies from 42 mT in the center to 120 mT at the face of the magnets. The two coils (Pontiac Coil, model L-11PL0112D-C) are each rated for 0.66 A at 12 V, 17 Ω, and 53.2 mH. At 12 V, they create a magnetic field that varies from 75 mT at the center of the 12 mm gap to 130 mT at the ends of the pole pieces. The alternating field was generated by an Instek GFG-8210 Function Generator, which was then driven by a custom-built, low frequency amplifier. The custom amplifier was designed and fabricated to provide a flat response from DC to ~10 kHz.

The magnetic filaments were assembled from a dimethylformamide (DMF) solution with cobalt nanoparticles ranging from 0.1 - 1000 μg/ml in concentration. Jeffamine XTJ-502 (H_2N-PEG-NH_2) was also added in concentrations ranging from 0 – 1000 μg/ml. The 2000 g/mol H_2N-PEG-NH_2 is a diamine-terminated polyethylene

glycol used to chemically crosslink the Co nanoparticles together. The diamine crosslinker reacted with the benzaldehyde moieties on the polymer shell to form imine bonds. The lower cover slip was chemically treated to one of the following three conditions: clean glass, epoxy functionalized, and fluorinated.[45] Since the solution spread to the edges of the 25 x 25 mm cover slip, the gap can be calculated to be approximately 64 μm. The nucleation and growth of the flexible magnetic filaments could then be observed *in situ* with an Olympus BX60M microscope under bright field conditions, in reflection mode, and using a pinhole diaphragm.

Due to the large parameter space, we implemented a multivariable design of experiments (DOE) technique. The screening design involved variation of cobalt nanoparticle concentration, crosslinker concentration, and surface treatment. The parameters for the various experiments are given in Table 4.1. The ensuing data was primarily qualitative rather than quantitative, but the factorial design allowed for more efficient screening of variables to determine those that had the greatest effect on the final structure. Also investigated was the possibility of cross-correlations among pairs of variables.

Ex-Situ Assembly. The custom-designed magnetic microscope stage had limited flexibility in terms of the possible magnetic field strengths, temperatures, and configurations. *Ex situ* observations were therefore performed to expand the parameter space. For these experiments, a DMF dispersion of PS-CoNPs was confined between a pair of glass slides and then sandwiched between a pair of large neodymium magnets, as shown in Scheme 4.2. Measuring 100 x 50 x 12 mm, the magnets applied a uniform

148 mT magnetic field perpendicular to the glass slides. After each experiment, the glass substrates were rinsed with DMF and dried, followed by imaging with either a Hitachi S4700 scanning electron microscope or an Olympus BX60M microscope.

Co Conc.	**H2N-PEG-NH2 Conc.**	**Surface Chemistry**
ug/ml	***ug/ml***	***e.g. clean glass***
5	50	Clean Glass
0.1	0	Clean Glass
100	1000	Clean Glass
5	50	Epoxy Treated
0.1	0	Epoxy Treated
100	0	Clean Glass
0.1	1000	Epoxy Treated
0.1	1000	Fluorinated
100	0	Epoxy Treated
0.1	0	Fluorinated
100	1000	Fluorinated
100	0	Fluorinated
100	1000	Epoxy Treated
0.1	1000	Clean Glass

Table 4.1: Experimental parameters for DOE screening experiments

4.5: References

1 Fearing, R. S. "Challenges for Effective Millirobots," *Int. Symp. on Micro-NanoMechatronics and Human Science*, Nagoya Japan: Nov. 5-8, **2006**.

2 Phee, L.; Accoto, D.; Menciassi, A.; Stefanini, C.; Carrozza, M. C.; Dario, P. *IEEE Trans. on Biomedical Engin.* **2002**, *49*, 613.

3 Hill, C.; Amodeo, A.; Joseph, J. V.; Patel, H. R. H. *Expert Rev. Anticancer Ther.* **2008**, *8*, 1891.

4 Wood, R. J.; Avadhanula, S.; Fearing, R. S. *IEEE Int. Conf. on Intelligent Robots and Systems*, Las Vegas, NV: Oct 28-30, **2003**.

5 Sahai, R.; Avadhanula, S.; Groff, R.; Steltz, E.; Wood, R.; Fearing, R. S. *Proc. 2006 IEEE Intl. Conf. on Robotics and Automation*, Orlando, FL: May, **2006**.

6 Abbott, J. J.; Nagy, Z.; Beyeler, F.; Nelson, B. J. *IEEE Robotics & Automation Magazine* **2007**, *14*, 92.

7 Dong, L.; Nelson, B. J. *IEEE Robotics & Automation Magazine* **2007**, *14*, 111.

8 Wood, R. J.; Steltz, E.; Fearing, R. S., *IEEE Int. Conf. on Robotics and Automation*,Barcelona: April, **2005**.

9 E. M. Purcell, "Life at low Reynolds number," *Am. J. Phys*. **1977**, *45*, 3.

10 Furst, E. M.; Suzuki, C.; Fermigier, M.; Gast, A. P. Langmuir **1998**, *14*, 7334.

11 Furst, E. M.; Gast, A. P. Phys. Rev. Lett. **1999**, *82*, 4130.

12 Dreyfus, R.; Baudry, J.; Roper, M. L.; Fermigier, M.; Stone, H. A.; Bibette, J. *Nature* **2005**, *437*, 862.

13 Singh, H.; Laibinis, P. E.; Hatton, T. A. *Nano Lett*. **2005**, *5*, 2149-2154.

14 Singh, H.; Laibinis, P. E.; Hatton, T. A. *Langmuir* **2005**, *21*, 11500-11509.

15 Evans, B. A.; Shields, A. R.; Lloyd, C. R.; Washburn, S.; Falvo, M. R.; Superfine, R. *Nano Lett*. **2007**, 7, 1428.

16 Zhou, Z. H.; Liu, G. J.; Han, D. H. *ACS Nano* **2009**, *3*, 165.

17 Keng, P. Y.; Shim, I.; Korth, B. D.; Douglas, J. F.; Pyun, J. *ACS Nano* **2007**, *1*, 279.

18 Korth, B. D.; Keng, P.; Shim, I.; Bowles, S.; Nebesny, K.; Tang, C.; Kowalewski, T.; Pyun, J. *J. Am. Chem. Soc*. **2006**, *128*, 6562.

19 Bowles, S. E.; Wu, W.; Kowalewski, T.; Schalnat, M. C.; Davis, R. J.; Pemberton, J. E.; Shim, I.; Korth, B. D.; Pyun, J. *J. Am. Chem. Soc.* **2007**, *129*, 8694.

20 Benkoski, J. J.; Bowles S. E.; Jones, R. L.; Douglas, J. F.; Pyun, J.; Karim, A. *J. Polym. Sci. Part B-Polym. Phys.* **2008**, *46*, 2267.

21 Benkoski, J. J.; Bowles S. E.; Korth, B. D.; Jones, R. L.; Douglas, J. F.; Karim, A.; Pyun, J. *J. Am. Chem. Soc*. **2007**, *129*, 6291-6297

22 Benkoski, J. J.; Jones, R. L.; Douglas, J. F.; Karim, A. *Langmuir* **2007**, *23*, 3530.

23 Benkoski, J. J.; Hu, H.; Karim, A. *Macromol. Rapid Commun.* **2006**, *27*, 1212.

24 den Toonder, J. M. J.; Bos, F. M.; Broer, D. J.; Filippini, L.; Gillies, M.; de Goede, J.; Mol, G. N.; Reime, M.; Talen, W.; Wilderbeek, J. T. A.; Khatavkar, V.; Anderson, P. D. *Lab Chip* **2008**, **8**, 533.

25 Tabata, O.; Kojima, H.; Kasatani, T.; Isono, Y.; Yoshida, R., Micro Electro Mechanical Systems, **2003**. MEMS-03 Kyoto. IEEE The Sixteenth Annual International Conference 2003, 12.

26 van Oosten, C. L.; Bastiaansen, C. W. M.; Broer, D. J. *Nature Materials* **2009**, *8,* 677.

27 Zubarev, A. Y.; Iskakova L. Y. *Physica A* **2006**, *367*, 55.

28 Buyevich, Y. A.; Ivanov, A. O. *Physica A* **1992**, *190*, 276.

29 Zubarev, A. Y.; Iskakova, L. Y. *Physica A* **2004**, *335*, 325.

30 Klokkenburg, M.; Erné, B. H.; Meeldijk, J. D.; Wiedenmann, A.; Petukhov, A. V.; Dullens, R. P. A.; Philipse, A. P. *Phys. Rev. Lett.* **2006**, *97*, 185702.

31 Klokkenburg, M.; Dullens, R. P. A.; Kegel, W. K.; Erné, B. H.; Philipse, A. P. *Phys. Rev. Lett.* **2006**, *96*, 037203.

32 Klokkenburg, M.; Erné, B. H. *J. Magnetism and Magnetic Matls.* **2006**, *306*, 85.

33 One can calculate the strength of the magnetic dipolar interaction energy (E_{mag}) for two PS-CoNPs in contact: $E_{mag} = -\mu^2 \left(2\pi\mu_r\mu_0 r^3\right)^{-1}$ where μ is the magnetic dipole moment, μ_0 is the permeability of free space, μ_r is the relative permeability of water, and r is the center-to-center distance between the two particles in contact. For 23.5 nm PS-CoNPs in a poor solvent such as water, this value is 10x greater than thermal energy at room temperature (1 k_BT). However, if the polystyrene shell swells by a factor of 2 in a good solvent such as DMF, the magnetic attraction drops to -7 k_BT.

34 van Workum, K.; Douglas, J. F. *Macromol. Symp.* **2005**, *227*, 1.

35 van Workum, K.; Douglas, J. F. *Phys. Rev. E* **2005**, *71*, 031502.

36 Stambaugh, J.; van Workum, K.; Douglas, J. F.; Losert, W. *Phys. Rev. E* **2005**, *72*, 031301.

37 Tavares, J. M.; Weis, J. J.; Telo da Gama, M. M. *Phys. Rev. E* **2002**, *65*, 061201.

38 Klug, A *Angew. Chem. Int. Ed.* **1983** *22*, 565.

39 Pollard, T. D.; Cooper, J. A. *Ann. Rev. Biochem.* **1986**, *55*, 987.

40 Disanza, A.; Steffen, A.; Hertzog, M. *Cell Mol. Life Sci.* **2005**, *62*, 955.

41 Cebers, A. *Curr. Opin. Coll. Int. Sc.*, **2005**, *10*, 167.

42 Cebers, A. *Magnitnaya Gidrodinamika*, **2005**, *41*, 63.

43 Belovs, M.; Cebers, A. *Phys.Rev.E*, **2009**, *79*, 051503 (Erratum, **2009**, *79*, 069906 (E)).

44 Silverstein, R. M.; Webster, F. X. Spectrometric Identification of Organic Compounds. John Wiley & Sons, Inc: **1998**.

45 Untreated glass slides were cleaned prior to use using a Harrick plasma cleaner. For the 5 min exposure, the chamber was pumped down to 500 millitorr with 10 W supplied to the RF coil. Epoxy-functionalized cover slips were prepared by immersing them in a 1 vol % solution of (3-glycidoxypropyl)trimethoxy silane in toluene. The cover slips were immersed overnight before rinsing with toluene and drying with nitrogen gas. Fluorinated cover slips were prepared by exposing them to a saturated vapor of (heptadecafluoro-1,1,2,2-tetrahydrodecyl)dimethylchlorosilane for three hours. Excess silane was removed by first rinsing with acetone followed by a gentle wash with soap and water.

CHAPTER 5

COLLOIDAL POLYMERIZATION OF POLYMER COATED FERROMAGNETIC NANOPARTICLES INTO COBALT OXIDE NANOWIRES

5.1: Introduction

The preparation of nanostructured conductive metal oxides is an important technological challenge toward the creation of improved materials for energy storage and (photo)electrochemical catalysis for water splitting.[1-4] Semiconductor metal oxides, such as, TiO_2, RuO_2, Fe_2O_3, and Co_3O_4, have been widely explored as electrode materials in a number of energy related applications in photovoltaics, (photo)electrolytic water splitting, batteries and supercapacitors.[5-8] Cobalt oxides, such as, cobalt cobaltite (Co_3O_4) have been widely investigated as electrode materials for lithium batteries, catalysts for water reduction and carbon monoxide oxidation, electrochromic materials and gas sensors.[9-16]

The preparation of nanostructured Co_3O_4 has been explored as a route to enhance the electrochemical and catalytic properties of these materials via both an increase in the electroactive surface of the electrode films and improved charge transport from nanoscale ordering.[11, 12, 14] Co_3O_4 thin films have been prepared by numerous routes, including electrodeposition and sputtering techniques.[17-25] Colloidal forms of Co_3O_4 have been synthesized using solvothermal/hydrothermal techniques to synthesize well-defined nanocrystals and hollow nanospheres.[26-40] Nanostructured mesoporous materials have also been prepared using sol-gel precipitation in the presence of either hard, or soft

templates.[41-43] One-dimensional (1-D) Co_3O_4 nanomaterials have also recently been prepared using a variety of different approaches, namely, sol-gel precipitation,[13, 15] oxidation of metallic cobalt (Co) foils,[44] hydrothermal processes,[45, 46] polyol reduction[47] and electrospinning.[48-50] Despite these numerous advances, the preparation of high aspect ratio 1-D Co_3O_4 nanowires, without the use of structure-directing templates, remains an important synthetic challenge in gram-scale quantities.

The use of nanoparticle precursors as chemical reagents has recently gained significant attention as a novel approach to prepare hierarchically complex materials. Recent examples of using nanoparticles as "colloidal molecules" have been reported for the preparation of novel colloidal crystals,[51] well-defined clusters,[52] supramolecular amphiphiles[53] and mesoscopic polymer chains.[54, 55] The assembly of nanoparticles into one-dimensional (1-D) nanomaterials has been achieved using a number of approaches, notably, selective ligand chemistry on Au, or iron oxide NPs[56-59] and chemical linking of dipolar colloids.[55, 60-75] An elegant demonstration of using nanoparticles as reagents in chemical reactions has been the preparation of hollow semiconductor colloids via the nanoscale Kirkendall effect. Alivisatos *et al.* reported the preparation of discrete hollow cobalt oxide, or cobalt sulfide NPs by the oxidation/sulfidation of dispersed superparamagnetic CoNP precursors.[76, 77] Hollow cobalt selenide ($CoSe_2$) nanowires have also been prepared by the combination of dipolar NP assembly[81] and the nanoscale Kirkendall effect using ferromagnetic CoNPs passivated with small molecule surfactants.[69, 78] Using these design principles we haved developed a facile synthetic

methodology to use ferromagnetic nanoparticles as dipolar precursors to prepare cobalt oxide nanowires.

Herein, we report the synthesis and characterization of hollow cobalt oxide nanowires via the *"Colloidal Polymerization"* of ferromagnetic polystyrene coated cobalt nanoparticles (PS-CoNPs). The *Colloidal Polymerization* process is described as a combination of dipolar nanoparticle assembly and a chemical reaction converting colloidal precursors into a fused 1-D material. In this report, cobalt oxide nanowires were formed by the magnetic pre-organization of metallic PS-CoNPs into 1-D mesostructures and subsequent oxidation of the assembled colloids. This process is reminiscent of the step-growth polymerization of A-B small molecule monomers to form macromolecules, as dipolar metallic PS-CoNPs were employed as "colloidal monomers" to form interconnected 1-D mesostructures and is a mesoscale variation of supramolecular polymerization.[79-82] This particular approach enabled the preparation of very fine cobalt oxide nanowires that were passivated with a polymeric steric layer that imparted colloidal stability when dispersed in organic media. Furthermore, calcination of the polymer coated cobalt oxide nanowires was achieved along with spectroscopic, electrical and electrochemical characterization of these nanomaterials, which confirmed for the first time the viability of this synthetic methodology (*i.e., Colloidal Polymerization via dipolar assembly & the Kirkendall effect)* to form electroactive materials.

5.2: Results and Discussion

5.2.1 Colloidal Polymerization of ferromagnetic metallic cobalt nanoparticles into 1-D cobalt oxide nanostructures.

The synthesis of PS-coated cobalt oxide nanowires was conducted by bubbling O_2 into 1,2-dichlorobenzene (DCB) dispersions of ferromagnetic PS-CoNPs at 175 °C for varying reaction times in the absence of an external magnetic field (i.e. zero field conditions) (Scheme 5.1). Well defined ferromagnetic PS-CoNPs were prepared using amine end- functional polystyrene surfactants in the thermolysis of dicobaltoctacarbonyl ($Co_2(CO)_8$) as reported previously. Amine terminated PS surfactants were synthesized using controlled polymerizations,[83-85] namely, atom transfer radical polymerization (ATRP)[86] which enabled precise control of polymer molar mass, composition and functional group placement. TEM images of ferromagnetic PS-CoNPs (Fig 5.1 (a,b)) confirmed the preparation of uniformly sized colloids (D = 20 ± 2.4 nm) that self assembled into 1-D mesostructures due to interparticle dipolar associations when deposited onto a supporting substrate in zero field. We previously reported that our synthetic methods for PS-CoNPs enabled the preparation of well defined colloidal building blocks in appreciable quantities (~ 800 mg per reaction) and were easily redispersible in various organic solvents (e.g., toluene, tetrahydrofuran, methylene chloride) due to the polymer coating passivating the magnetic colloid. These synthetic conditions for this report were further optimized to enable nearly doubling of the yield of ferromagnetic PS-CoNPs (yield = 1.53 g) that were also readily stored as powders and redispersed into organic solvents.

In the conversion of PS-CoNPs into PS-coated cobalt oxide nanowires, the oxidation reaction was carried out by bubbling oxygen into the PS-CoNP ferrofluid at elevated temperature (T = 175 °C). The use of ferromagnetic PS-CoNPs was essential to the formation of cobalt oxide nanowires under zero field conditions, as superparamagnetic CoNPs were unable to polymerize due to the absence of a permanent dipole above cryogenic temperatures.[69] A striking feature of 1-D mesostructures formed via this Colloidal Polymerization was the presence of hollow inclusions in every nanoparticle repeating unit within cobalt oxide nanowires. These hollow inclusions were formed in the oxidation reaction due to a *non-uniform* diffusion and reaction of O_2 with Co atoms throughout the metallic NP. Under these conditions, oxidation of the NP was confined to the outer shell, resulting in depletion of Co atoms from the colloidal core to satisfy the valency of O atoms in the growing cobalt oxide phase. This phenomenon has been described by the nanoscale Kirkendall effect and resulted in both the formation of hollow cores and a dimensional expansion of the cobalt oxide NP shell. PS-coated nanowires were formed due to coalescence of expanding cobalt oxide NP shells formed in the oxidation reaction of pre-organized PS-CoNP colloidal monomers. By varying the oxidation time of metallic PS-CoNPs in DCB, non-aggregated nanowires of either cobaltous oxide (PS-CoO), or cobalt cobaltite (PS-Co_3O_4) could be achieved as determined using x-ray diffraction (XRD) after a reaction time of three hours, or one week, respectively. The yields of these PS-coated cobalt oxide nanowires were also conducted on gram scales (yield = 1.04 g) that were enabled by improvements in the synthesis of ferromagnetic PS-CoNPs.

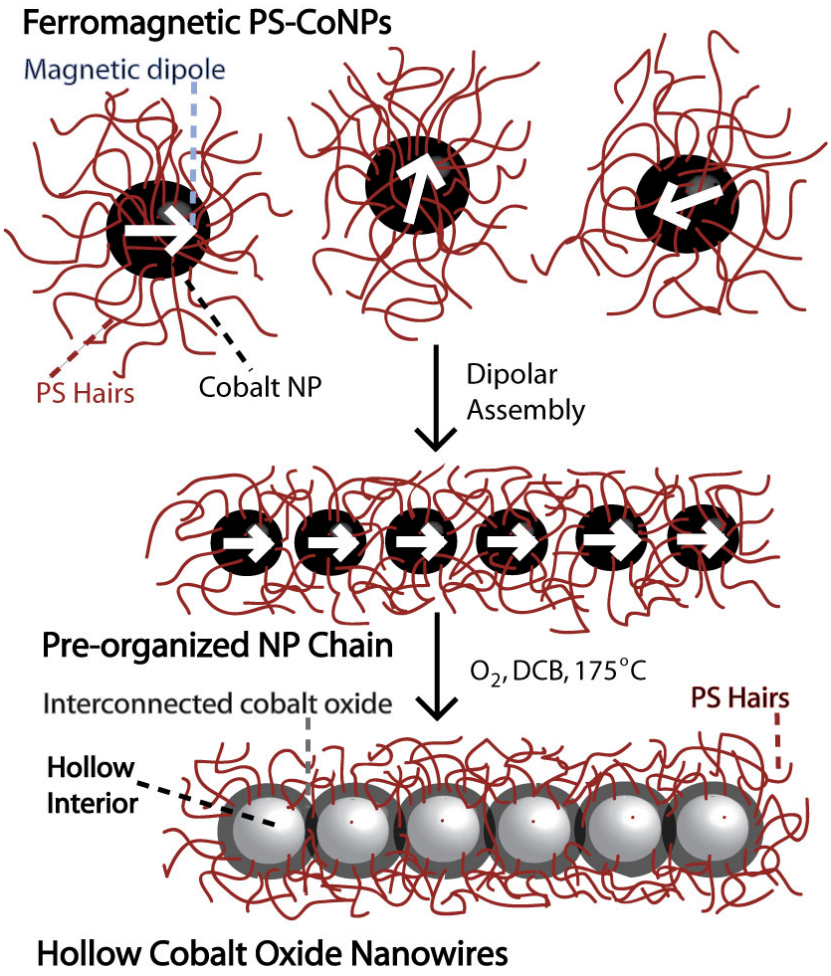

Scheme 5.1: Colloidal Polymerization of ferromagnetic PS-CoNPs into Cobalt Oxide Nanowires

5.2.2 TEM and FE-SEM imaging of PS-CoNPs and PS-cobalt oxide nanowires.

The formation of interconnected hollow nanowires was confirmed using transmission electron microscopy (TEM) of samples drop cast onto supporting surfaces (Fig. 5.1 (a,b)). The dipolar PS-CoNP precursors were imaged as discrete colloids (D = 20 nm $\pm$ 2.4 nm) assembled into NP-chains spanning microns in length. TEM showed that the native polymer coated cobalt nanoparticles appeared as a dark solid sphere due to

the high electron density of the cobalt core (Figure 5.1 (a,b)). After the oxidation reaction, a hollow inclusion in every cobalt oxide nanoparticle could be observed along the structurally intact 1-D nanostructure. The kinetics of the Colloidal Polymerization were followed by the removal of aliquots over varying reaction time for TEM imaging. After a reaction time of three hours (Figure 5.1 (c,d)), three distinct regions of nanoparticle could be observed in TEM: (1) a lower electron density of the cobalt oxide shell, (2) a dark inner sphere of the cobalt core and (3) a interior voids corresponding to the coalescence of vacancies at the interface. After 24 hrs, PS-coated cobalt oxide nanowires were observed to be completely hollow due to the complete conversion of metallic CoNPs into CoO phases, indicated by XRD (see later discussion). As the oxidation time of PS-CoNPs in the DCB ferrofluid was extended over a period of one week, a similar morphology was observed. These hollow nanoparticles were also connected in 1-D morphology (Figure 5.1 (e,f)) that spanned from several hundred nanometers to microns in length, as imaged via SEM (Figure 5.2).

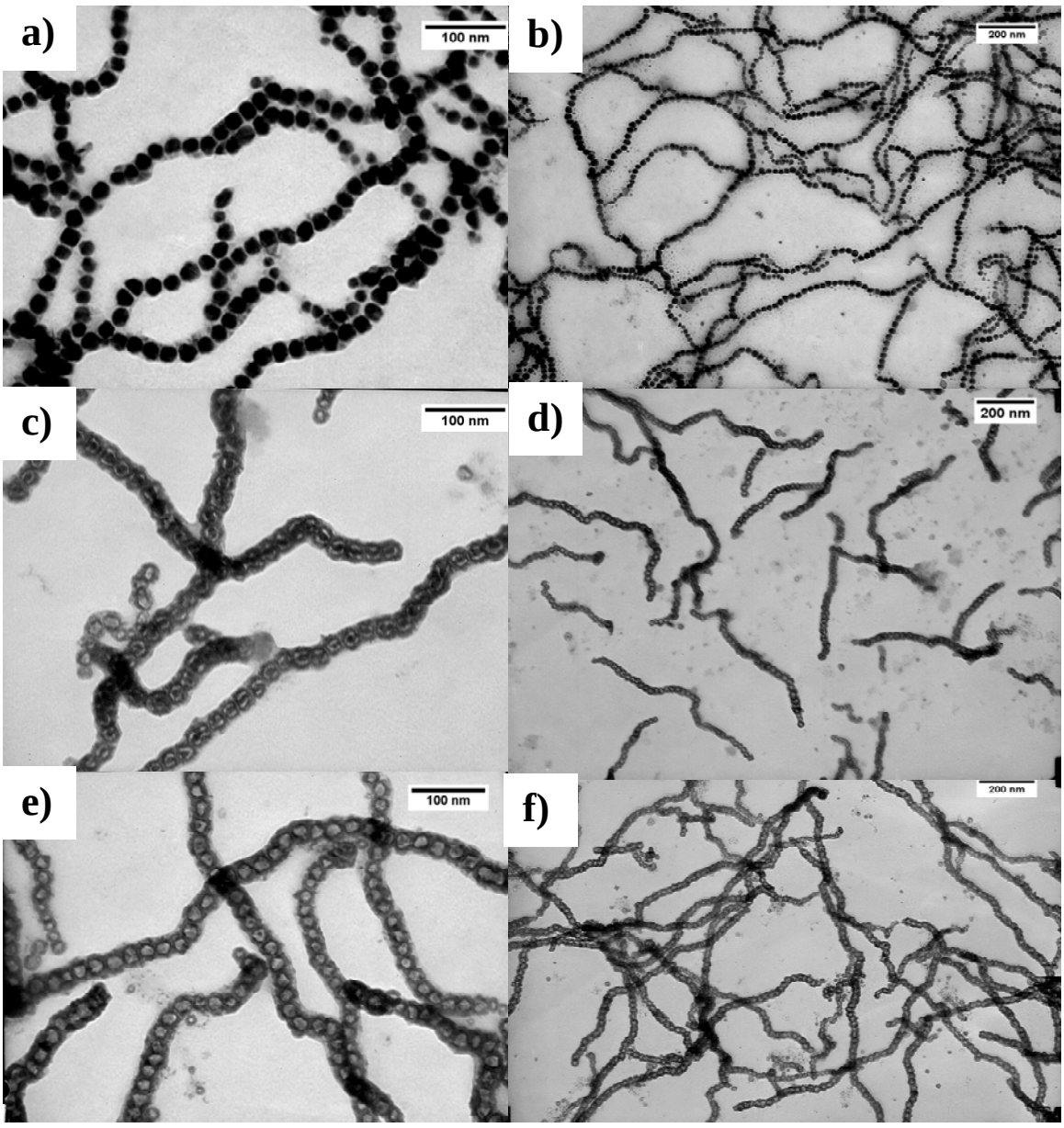

Figure 5.1*:* TEM images of the polystyrene coated cobalt nanoparticles with particle size, D = 20 ± 2.4 nm after oxidation for (a,b) 0 hours; (c,d) 3 hours, with particle diameter = 29 ± 2.7 nm, and (e,f) 1 week, with particle diameter = 32 ± 3.5 nm. All TEM samples were drop casted from 0.5 mg/mL toluene dispersion onto a carbon coated copper grid at zero field.

High resolution TEM (HR-TEM) provided further evidence of 1-D connectivity of these cobalt oxide NPs into nanowires. HR-TEM imaging (Figure 5.2) confirmed that

cobalt oxide NP shells was fused together to form 1-D chains after reaction times of 3 hrs (Figure 5.1), along with a dimensional expansion of nanowires from the conversion of PS-CoNPs into PS-CoO nanowires (D_{eff} = 29 nm). In contrast, PS-CoNPs precursors (D_{eff} = 20 nm) were imaged as discrete solid colloids that were separated by the outer PS shells (Figure 5.2 (a)). An additional dimensional expansion of the cobalt oxide nanowire diameters (D_{eff} = 32 nm) were observed from HR-TEM over extended oxidation times of one week and were attributed to the gradual conversion of PS-CoO nanowires into Co_3O_4 phases (Figure 5.2 (b)).

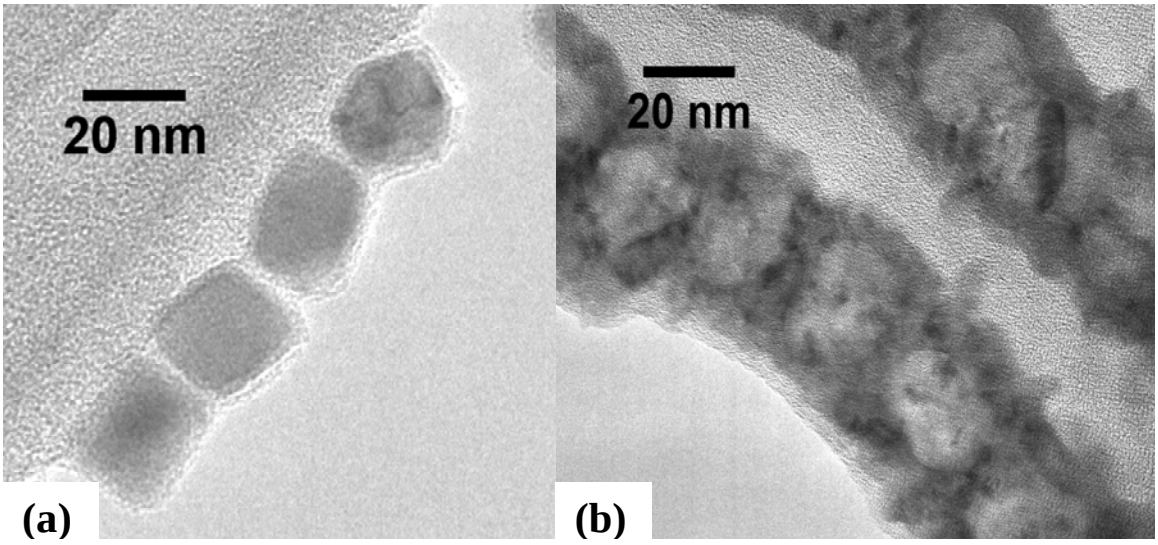

Figure 5.2: HRTEM of the (a) ferromagnetic PS-CoNP (b) PS-Co_3O_4 nanowires after 1-wk at 175°C

PS-CoNPs and PS-cobalt oxide nanowires were deposited onto ITO substrates via spin coating and imaged using field emission scanning electron microscopy (FE-SEM) to ascertain if discrete 1-D mesostructures were formed from the Colloidal Polymerization process. Thicker films of PS-cobalt oxide nanowires were cast onto ITO substrates and FE-SEM revealed the presence of non-aggregated 1-D chains that packed into a

mesoporous film (Figure 5.3 (a)). Discrete, non-agglomorated nanowires were also cast and imaged on ITO from dilute dispersions and were found to possess a distribution of chain lengths spanning hundreds of nanometers to several microns (Figure 5.3 (b)), which was attributed to the step-growth like nature of the Colloidal Polymerization of PS-CoNPs. FE-SEM qualitatively imaged morphology differences between the native PS-CoNPs and the conductive PS-cobalt oxide nanostructures. SEM images of the PS-CoNPs (Figure 5.3 (c)) showed 1-D chains of individual colloids that were associated via magnetostatic interactions, but separated by the polymer encapsulating shell. In contrast, PS-cobalt oxide nanowires were imaged via FE-SEM as beaded, but continuous 1-D mesostructures ranging from hundreds of nanometers to microns in length. (Figure 5.3 (d)).

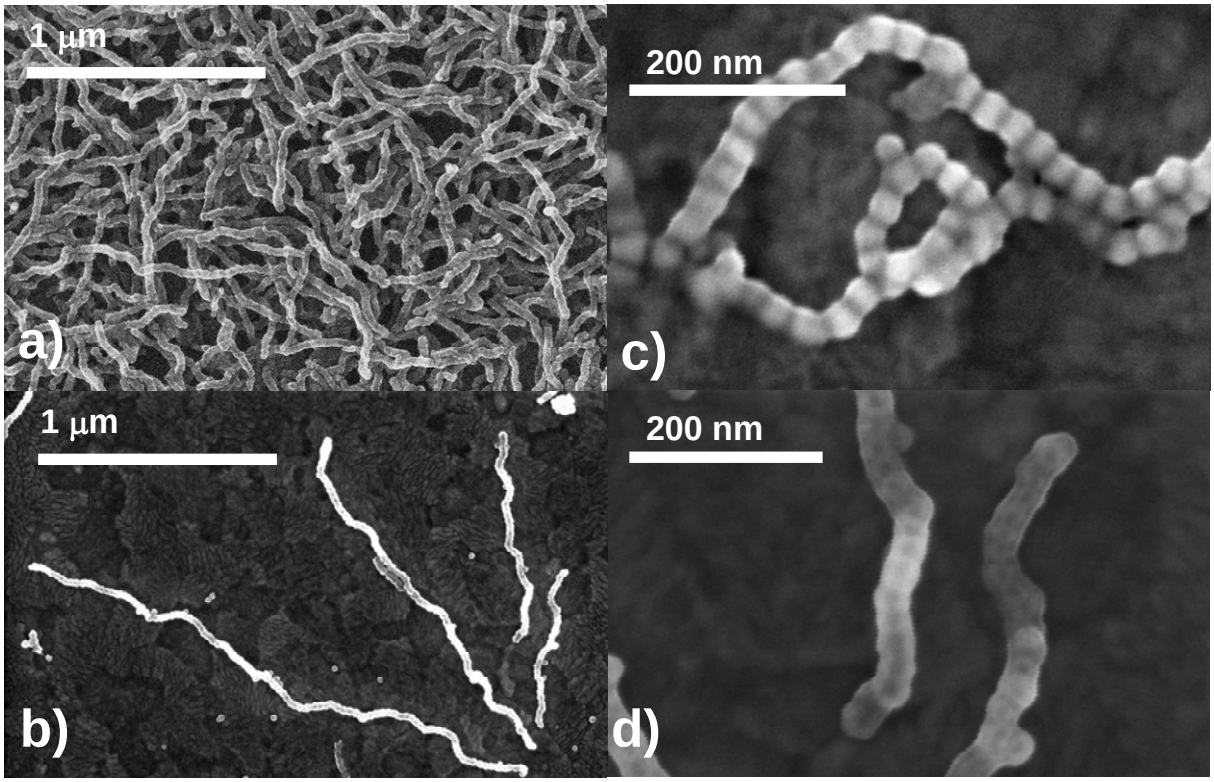

Figure 5.3*:* FE-SEM images of thick films (**a**) and isolated nanowires (**b**) of PS-Co_3O_4 materials spin coated onto ITO (**c**) high magnification FE-SEM of discrete chains of PS-CoNPs, (**d**) high magnification FE-SEM of PS-Co_3O_4 single nanowires

5.2.3 Solid state characterization of PS-coated cobalt oxide and calcined Co_3O_4 nanowires

To further improve the crystallinity of the cobalt oxide phase within the nanowire and to remove the PS organic shell, the as deposited film on ITO was calcined at 400 °C in air for 16 hours. Thermogravimetric analysis (TGA) of PS-coated nanowires confirmed that organics were fully degraded under these calcination conditions. FE-SEM of PS-Co_3O_4 films on ITO imaged the presence of 40 nm wide nanowires spanning microns in length. High resolution FE-SEM imaging visualized PS-coated nanowires possessing a relatively smooth surface morphology due to the glassy like nature of the polymer shell (Figure 5.4 (a, b)). FE-SEM after calcination revealed that the 1-D morphology of Co_3O_4 films were maintained, but the surface topography was considerably more roughened as evidenced by facets and small domains along oxidized nanowires (Figure 5.4 (c,d)). We have also confirmed via TEM that both the 1-D morphology and the porous inclusions of Co_3O_4 nanowires were preserved after the calcination process (Figure 5.5).

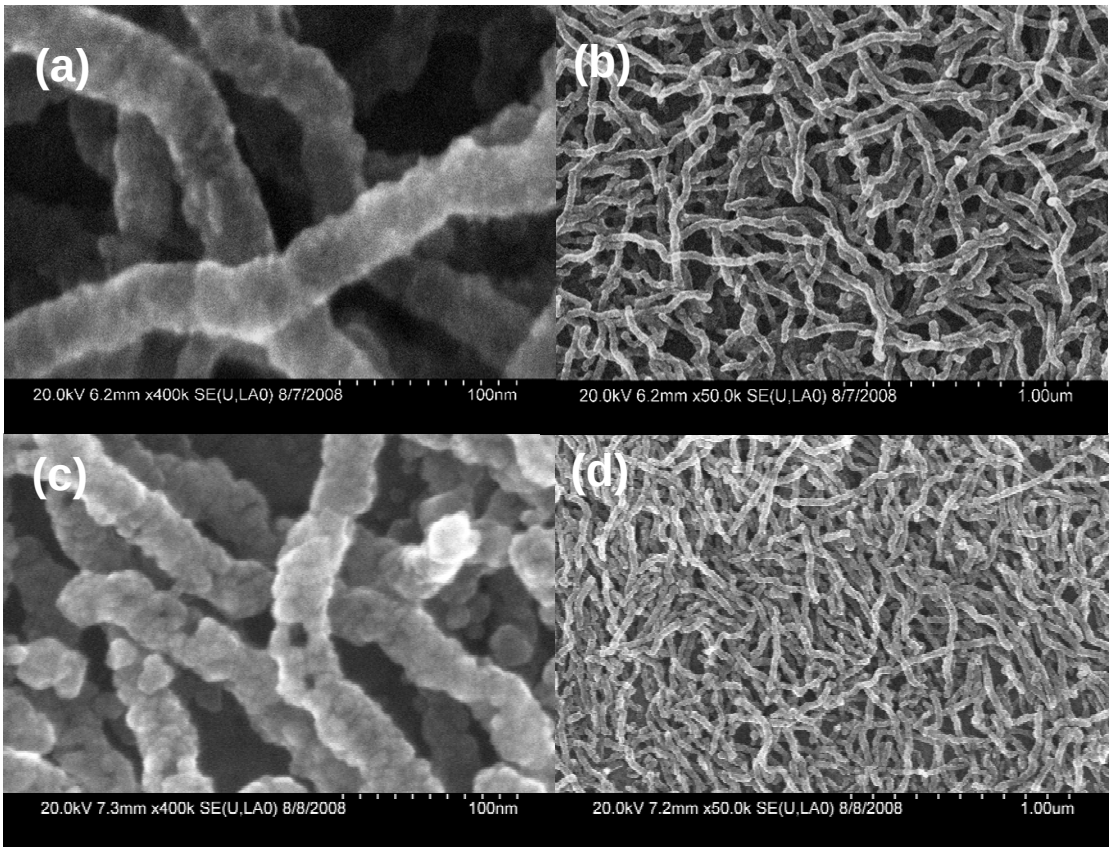

Figure 5.4*:* FE-SEM images of PS-Co_3O_4 nanowires cast on ITO at both high (a) and low (b) magnification and after calcinations in air at 400°C at high (c) and low (d) magnification.

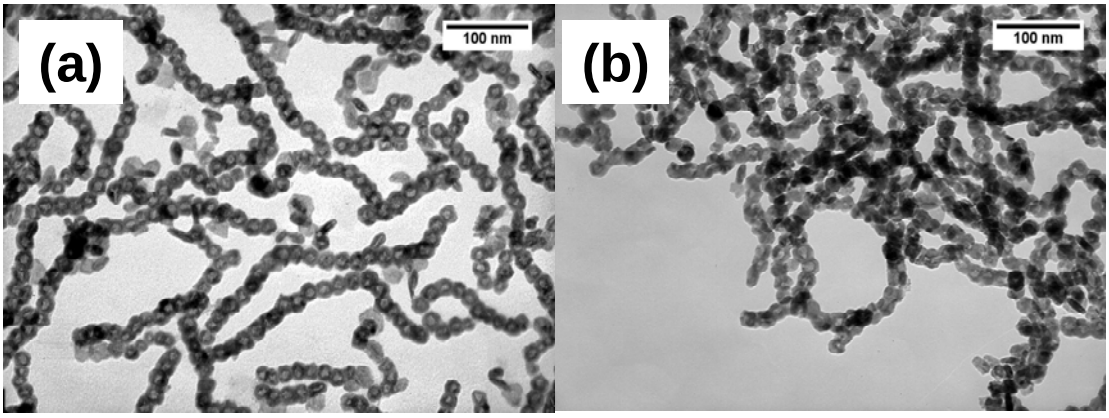

Figure 5.5: TEM of PS-Co_3O_4 nanowires on carbon coated Ni grid before (a) and after calcinations (b) with average particle and void dimension of 22 nm and 9 nm, respectively.

Powder x-ray diffraction was used to characterize the solid-state structure of PS-CoNP, PS-coated nanowires and calcined cobalt oxide materials. The XRD results confirmed the initial PS-CoNP precursors exhibited a metallic fcc-cobalt phase of low crystallinity (Figure 5.6 (a)) Subsequent oxidation of PS-CoNPs in DCB at 175 ° C over a 3 hr period converted these precursors to a mixture of rock salt-CoO and residual fcc-cobalt (Figure 5.6 (b)). Prolonged oxidations of PS-CoNPs over a period of one week predominantly yielded an amorphous phase of Co_3O_4 (Figure 5.6 (c)). Further calcination of PS-CoO NPs in air at 400 °C burned out the organic PS outer shells and yielded polycrystalline Co_3O_4 material, in which all diffraction peaks were indexed to spinel Co_3O_4 (Figure 5.6 (d)).

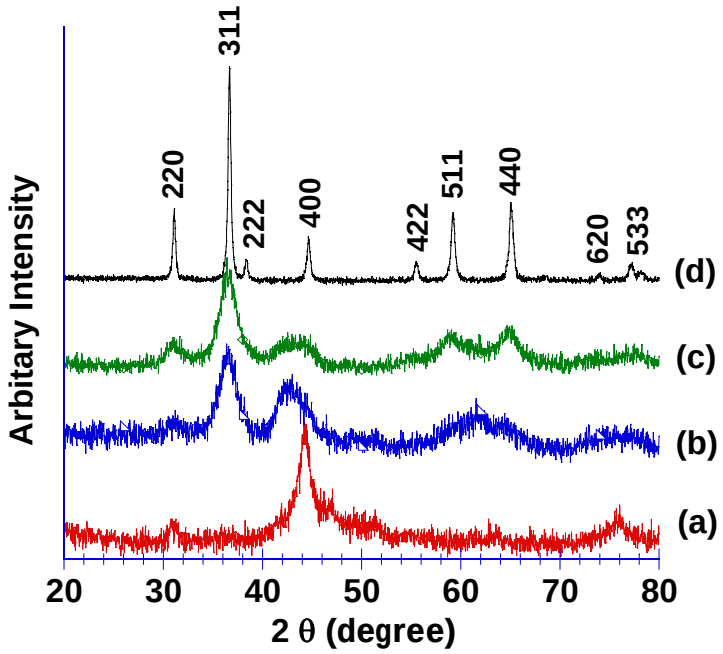

Figure 5.6: Overlay XRD patterns of the (a) polystyrene coated cobalt nanoparticles, (b) polystyrene coated cobalt oxide after 3 hours of oxidation, (c) after 1 week of oxidations and (d) after calcination at 400 °C in air. The diffraction peaks were indexed to the spinel-Co_3O_4 phase.

The magnetic properties of PS-coated and calcined cobalt oxide nanocomposites were measured using vibrating sample magnetometry (VSM) at room temperature and at 760 K (Figure 5.6). The general trend from the magnetometry indicated that both the saturation magnetization (M_s) and coercivity (H_c) significantly decreased after the Colloidal Polymerization process which was in agreement with the formation of antiferromagnetic CoO and Co_3O_4. The native PS-CoNPs (Figure 5.7 a-1), exhibited weakly ferromagnetic behavior at room temperature (M_s = 41.2 emu/g; H_c = 713 Oe). The magnetometry at room temperature revealed that PS-CoO materials (Figure 5.6 a-2) were weakly ferromagnetic after a 3 hours oxidation in DCB and exhibited a significant decrease in the saturation magnetization (M_s = 4.6 emu/g) and coercivity (H_c = 362 Oe) at room temperature. This ferromagnetic behavior was attributed to the presence of residual metallic cobalt, which was further supported by the XRD data in Figure 5.7. Similar magnetization behavior was also observed in wurtzite CoO, in which the presence of metallic Co impurities resulted in a hysteresis curve.[87] The magnetization (M = 2.07 emu/g at 10,000 Oe) and coercivity (H_c = 260 Oe) of PS-Co_3O_4 were further decreased by prolonged 1-wk. oxidation times. The magnetometry of PS-Co_3O_4 materials exhibited a linear relationship of magnetization (M) vs. applied field (H) behavior due to the presence rock-salt CoO and spinel Co_3O_4 phases as indicated by the linearity of magnetometry above and below 5000 Oe and -5000 Oe (Figure 5.7 (b)). The magnetometry of the PS-coated Co_3O_4 nanocomposite (Figure 5.7 (b)) also exhibited weakly ferromagnetic behavior as evidenced by a small hysteresis which was attributed

to trace Co metal. Calcined Co_3O_4 nanowires (Figure 5.7 (c)) exhibited a linear magnetization curve with a reduced M value. The linear curve was consistent with the paramagnetic behavior of Co_3O_4 nanoparticles at room as reported elsewhere.[88]

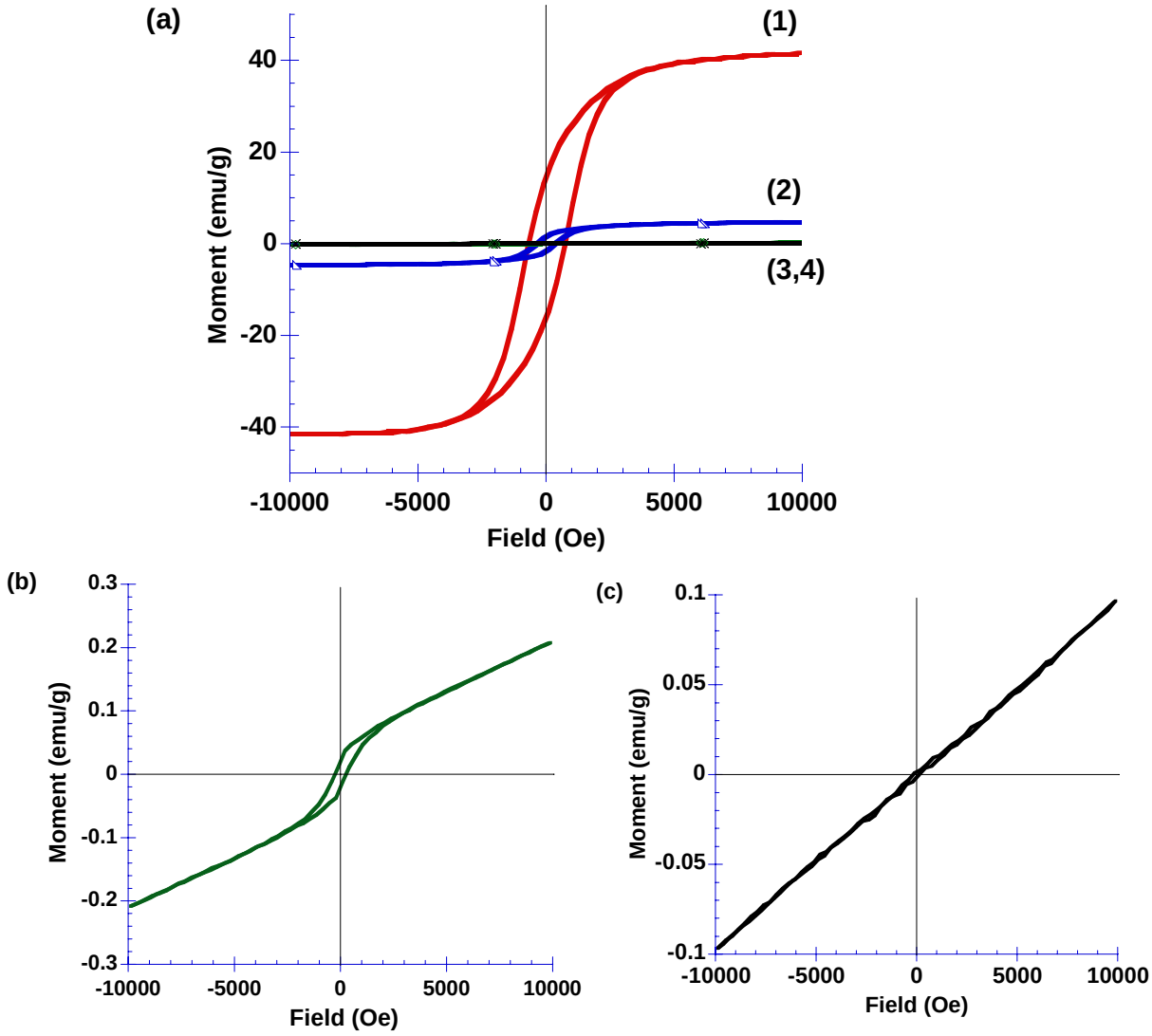

Figure 5.7: (a) Overlay hysteresis curves of applied magnetic field (H) vs. magnetization (M_s) of nanocomposites A-D at 27 °C: PS coated CoNPs (**1**), polystyrene coated cobalt oxide after 3 hours of oxidation (**2**), polystyrene coated cobalt oxide after 1 week of oxidation (**3**) and bare Co_3O_4 nanowires after calcination of **C** at 400 °C (**4**). (b) high resolution magnetometry of of PS-coated cobalt oxide materials after 1-wk oxidation time (**3**) and calcined Co_3O_4 nanowires after calcination in air at 400 °C.

5.2.4 Spectroscopic characterization of Co_3O_4 nanowires

Characterization of polymer coated and calcined cobalt oxide nanowires was conducted using Raman spectroscopy to confirm the formation of the Co_3O_4 phase (Figure 5.8). Raman spectroscopic characterization was complicated by the strong absorption of Co_3O_4 films in the visible wavelength regime, as evidenced by the black appearance of this material. Although Raman spectroscopic characterization of Co_3O_4 materials has primarily been conducted using microprobe Raman techniques, we were able to acquire quality Raman spectra of Co_3O_4 nanowire films using standard approaches through formation of thin films on reflective Ag substrates. PS-coated cobalt oxide nanowires were spin-coated onto clean Ag subtrates and measured both before and after calcination reactions in air at 400°C. The preparation of PS-Co_3O_4 nanowires after a solution oxidation time of 1-wk was confirmed in the Raman spectra by the presence of peaks at 483, 528 and 692 cm^{-1}, which correspond to E_g, F_{2g} and A_{1g} vibrational modes, respectively, for Co_3O_4.[18, 44, 89] After calcination of PS-coated nanowires, sharper and more intense peaks at 483, 528 and 692 cm^{-1} are observed. In addition, the A_{1g} peak shifted from 690 to 692 cm^{-1}, which has been correlated with an enhancement in electrical conductivity of Co_3O_4 thin films.[89] After calcination, an addition broad peak at 600 cm^{-1} was observed and assigned to a second F_{2g} mode that was expected based on previous Raman assignments of Co_3O_4 thin films. However, the relative intensity of this peak at 600 cm^{-1} was intuitively too high to arise solely from the formation of more crystalline Co_3O_4 nanowire thin films, and was identified to be trace graphitic carbon

(other broad carbon peaks around 1600 and 1350 cm^{-1} also observed) that was formed from pyrolysis of the organic PS coating.

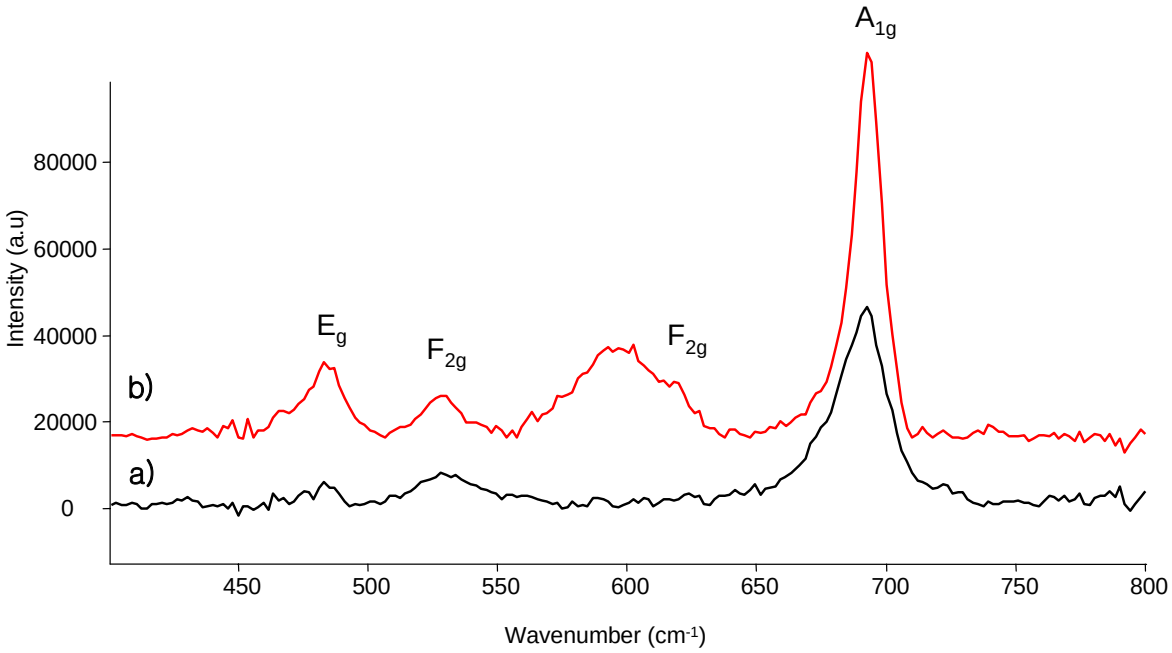

Figure 5.8: Raman spectroscopy of films on Ag substrates of (a): PS-Co_3O_4 nanowire films after solution oxidation times in DCB at 170°C for 1-week and (b) calcined Co_3O_4 nanowires after thermal treatment in air at 400 °C.

X-ray photoelectron spectroscopy (XPS) was also used to confirm the formation of Co_3O_4 nanowires after calcination in air at 400 °C. Al-Ka XPS was conducted of thin films deposited onto ITO substrates and measured in the regions of Co_{2p} and O_{1s} binding energy regions. XPS in the Co_{2p} region of binding energies exhibited two major peaks at 796.1 eV and 780.6 eV that corresponded to $2p_{1/2}$ and $2p_{3/2}$ spin-orbit components, respectively, with the $Co_{p1/2}$ peak at 796.1 eV being more intense (Figure 5.9). Weaker satellite peaks at 790.5 eV and 805.5 eV were also observed in the Al-Ka XPS. The formation of these peaks has been extensively observed in thin films of cobalt oxides

prepared from a variety of methods and were attributed to surface hydroxide species from exposure to air.[18, 44, 90-92]

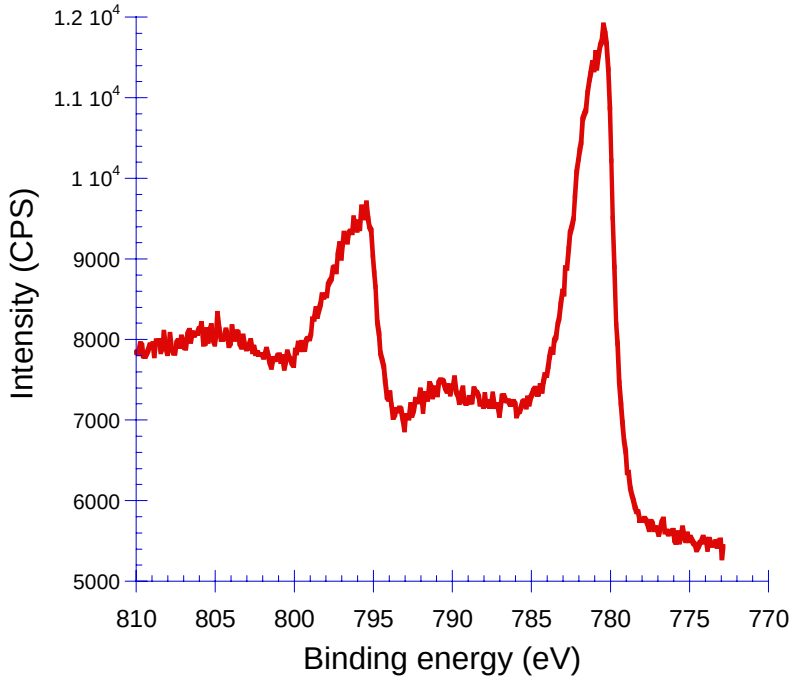

Figure 5.9: Co_{2p} XPS spectroscopy of calcined Co_3O_4 nanowires after thermal treatment in air at 400 °C

5.2.5 Spectroscopic determination of band edge energy levels of Co_3O_4 nanowires

Optical absorption spectroscopy and ultraviolent photoelectron spectroscopy (UPS) were conducted to determine the band edge energy levels of Co_3O_4 nanowires calcined at 400 °C. UV-visible absorption spectroscopy of Co_3O_4 nanowire films on ITO revealed two broad absorption bands centered around 450 nm and 750 nm, which was consistent with other literature reports on the optical properties for spinel type Co_3O_4 thin films. [44, 45, 91-93] The optical band gap energies were determined using the Tauc plot method and were in reasonable agreement with previous spectroscopic studies of cobalt oxide thin films indicative of two optical transitions at 1.45 eV and 2.26 eV. [44, 45, 91-95]

The optical transition from Co_3O_4 nanowires at 2.26 eV was attributed to a band gap transition from the valence band of the metal oxide, which was proposed to comprise of a mixture of both $Co^{2+,3+}$ 3*d* and *O* 2*p* states. The lower energy transition at 1.45 eV was assigned to transitions from mid-gap states[96] into the conduction band due to the presence of defect sites within these hollow Co_3O_4 nanowires. As previously discussed, Co_3O_4 nanowires prepared via Colloidal Polymerization resulted in the formation of hollow inclusions in nanoparticle repeating units that were fused along the 1-D mesostructure. As a result, these nanomaterials were anticipated to contain defect sites in the metal oxide phase, as a likely consequence of a greater number of surface Co ion sites accompanied by ion vacancies in the partially coordinated $Co^{2+,3+}$ ions within the spinel Co_3O_4 lattice.[90, 96] These assumptions were based on the presence of both hollow interior inclusions along the nanowire and the high degree of corrugation on the surface of calcined Co_3O_4 materials as observed via TEM (Figure 5.2 (b)) and FE-SEM (Figure 5.4 (c)), respectively. These band gap and mid-gap states assignments were also supported by modeling and valence band photoemission studies of non-stoichiometric Co_3O_4 films, in which the valence band was assigned to a mixture of both $Co^{2+,3+}$ 3*d* and the O 2*p* states.[90, 94] Extensive reports on the optical spectroscopy of Co_3O_4 materials have assigned these optical transitions to two direct band gaps from solely O 2*p* states in the valence band into Co^{2+} 3*d* conduction band states at 2.26 eV and into Co^{3+} conduction band 3*d* states at 1.45 eV.[44, 45, 91-93] However, given, the strong likelihood of defect sites being present in Co_3O_4 nanowires prepared via Colloidal Polymerization, it is anticipated

that optical transitions observed were not from two direct band gaps but arose from discrete band gap and mid-gap transitions.

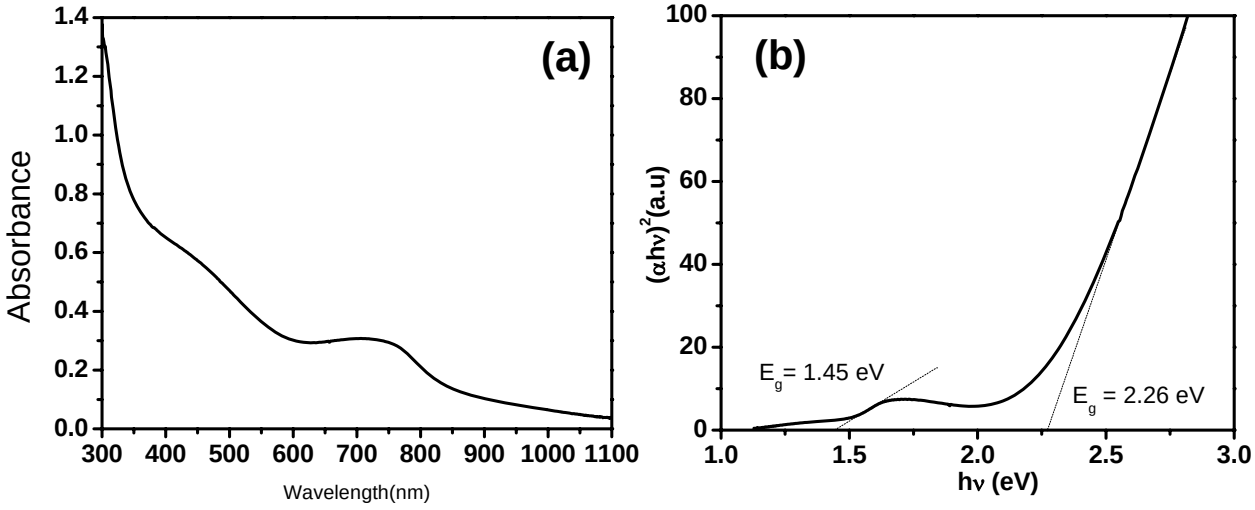

Figure 5.10: (a) UV-vis spectra of calcined Co_3O_4 nanowires on ITO. (b) Optical band gap energy Co_3O_4 nanowires obtained by extrapolation to $\alpha = 0$.

Due to the novel nanoscale structure of the cobalt oxide nanowires prepared via *Colloidal Polymerization*, UPS of calcined Co_3O_4 nanowire on Au substrates was conducted to determine the highest energy of the valence band (VB) in the metal oxide semiconductor. In the UPS experiment, the kinetic energy of the photoexcited electrons emitted from Co_3O_4 films were measured assuming electrical equilibration between the Au substrate, in which a common Fermi level ($E_f = 0$) was established (Figure 5.11). Because electrical contact and equilibrium between the Au substrate and the thin film was required, UPS measurements of PS coated nanowires were not conducted. While more detailed UPS studies have been conducted with full spectroscopic assignments of photoemitted electrons from Co_3O_4 thin films,[90] our interest for this investigation was focused on the determination of highest energy levels of the Co_3O_4 VB. The UPS

spectrum of Co_3O_4 on Au substrate shown in Figure 5.11 (a) has been normalized to the Fermi level of Au, in which $E_f = 0$. The edge of the highest energy population of the VB for Co_3O_4 was observed as a sharp increase at -0.5 eV relative to the mutual Fermi level of Au and the spectrometer ($E_f = 0$) in the UPS spectrum, while the lowest energy electrons were found at the -16.4 eV. The absolute difference in energies between the lowest and highest kinetic energy edges of the UPS spectrum was defined as the spectral width (SW), which afforded a SW = 15.9 eV. The threshold ionization potential (IP) of the Co_3O_4 nanowire material was obtained as the difference of the incident photon energy (for He(I) source = 21.2 eV) and the spectral width (15.9 eV) of the UPS spectrum (Figure 10 (a)),[97] which afforded an IP = 5.3 eV.

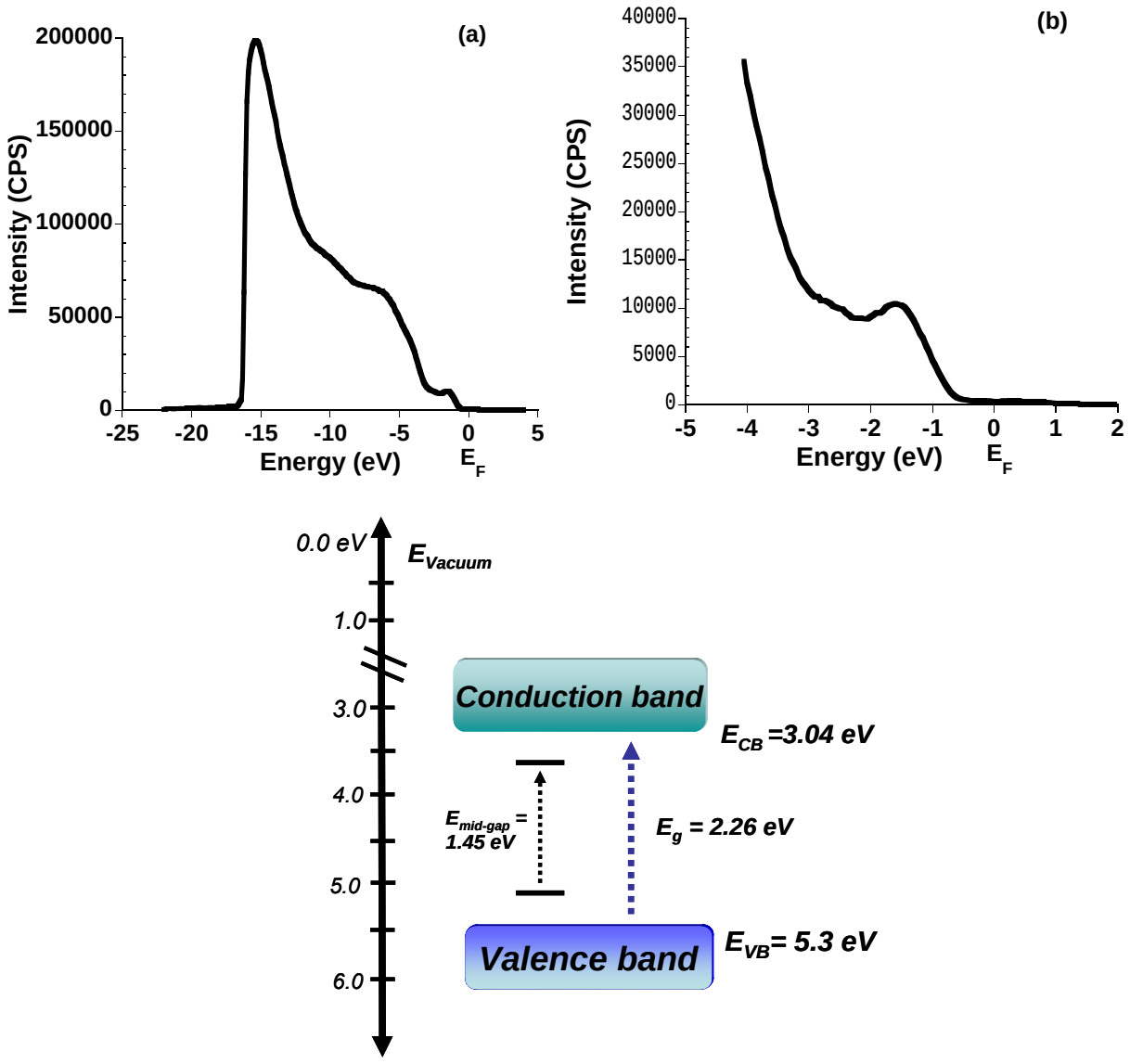

Figure 5.11: low (a) and high resolution (b) UPS spectra of calcined Co_3O_4 nanowires after thermal treatment in air at 400 °C on Au substrates and (c) energy level diagram for band edge energies for calcined Co_3O_4 nanowires.

From the UPS IP data, the energy of the Co_3O_4 VB with respect to vacuum was set to 5.3 eV, which in conjunction with the optical band gaps determined from the optical absorption spectroscopy (Figure 5.10), afforded a proposed band edge energy diagram for

calcined Co_3O_4 nanowires as shown in Figure 5.11 (c). Due to the polycrystalline nature of the Co_3O_4 nanowires prepared via Colloidal Polymerization, an assignment of the exact valence band and conduction band was difficult, because earlier calculations and modeling of band edge energies was primarily based on crystalline Co_3O_4.[90, 96] Based on the thorough photoemission studies on Co_3O_4 epitaxy film by Langell[90] and the optical band gap measurements (Figure 5.10), the highest energy level of valence band was assigned to a mixture of $Co^{2+,+3}$ ions *3d* and O *2p* orbitals with a band gap energy of 2.26 eV and a mid-gap transition of 1.45 eV. It is important to note that the values of the Co_3O_4 VB (5.3 eV) and conduction bands (3.04 eV) determined from UPS in vacuum and may deviate from values determined photoelectrochemically via Mott-Schottky measurements since solvent effects were not accounted for using the described methodology.

The current density (J)-voltage (V) characteristics of calcined Co_3O_4 nanowires was determined via conductive probe atomic force microscopy (C-AFM). Nanowires were spin coated onto Pt-coated Si subtrates and then analyzed with a Pt-tip for C-AFM J-V measurements in 20 μm^2 areas, with a bias of +1.0 to -1.0 V in air at room temperature. The worm-like morphology of the Co_3O_4 nanowires (Figure 5.12 (a)) was first resolved by tapping mode AFM using a silicon nitride cantilever. In height contrast imaging, bright features were assigned to the Co_3O_4 nanowires, while dark regions corresponded to voids formed from the interdigitation of 1-D components, which was consistent with the FE-SEM of the calcined film (Figure 5.3 (a)). The topography of the film was also imaged in tapping mode using a Pt cantilever for C-AFM prior to electrical

probing as shown in Figure 5.12 (b), however, resolution of nanowire features was compromised due to the use of non-optimal Pt-tips for visualization of individual nanoscale wires. Nevertheless, these Pt-tips were effective in current contrast C-AFM, which imaged very delicate nanoscale features, confirming that nanowires were uniformly conductive, as visualized as bright regions corresponding to Co_3O_4 semiconducting nanowires (Figure 5.12 (c)). Darker features in current mapped C-AFM images also corresponded to porosity generated from the void spaces in the nanowire thin film. The current density-voltage (*J-V)* characteristics of these Co_3O_4 NP films revealed a linear relationship (Figure 5.12 (e)) from -0.12 V to +0.12 V, indicative of Ohmic contact between the Pt tip and Co_3O_4 nanowires, while space-charge limiting current was observed above these potentials.[98] The symmetrical J-V plot further showed that these Co_3O_4 nanowires were in Ohmic contact with both the Pt tip junction as well as the Pt substrate on the bottom contact. This current-voltage behavior was consistent with the predicted behavior of Co_3O_4, which is a *p*-type semiconductor with electrical conductivity arising from hole carriers.[89] Quantitative determination of carrier mobilities via C-AFM was complicated by the 1-D nanoscale morphology of Co_3O_4 nanowires due to the additional geometrical terms in the space charge-limited current equation that is only valid for solid films. Quantitative measurements of electrical conductivity are currently in progress via microwave techniques.

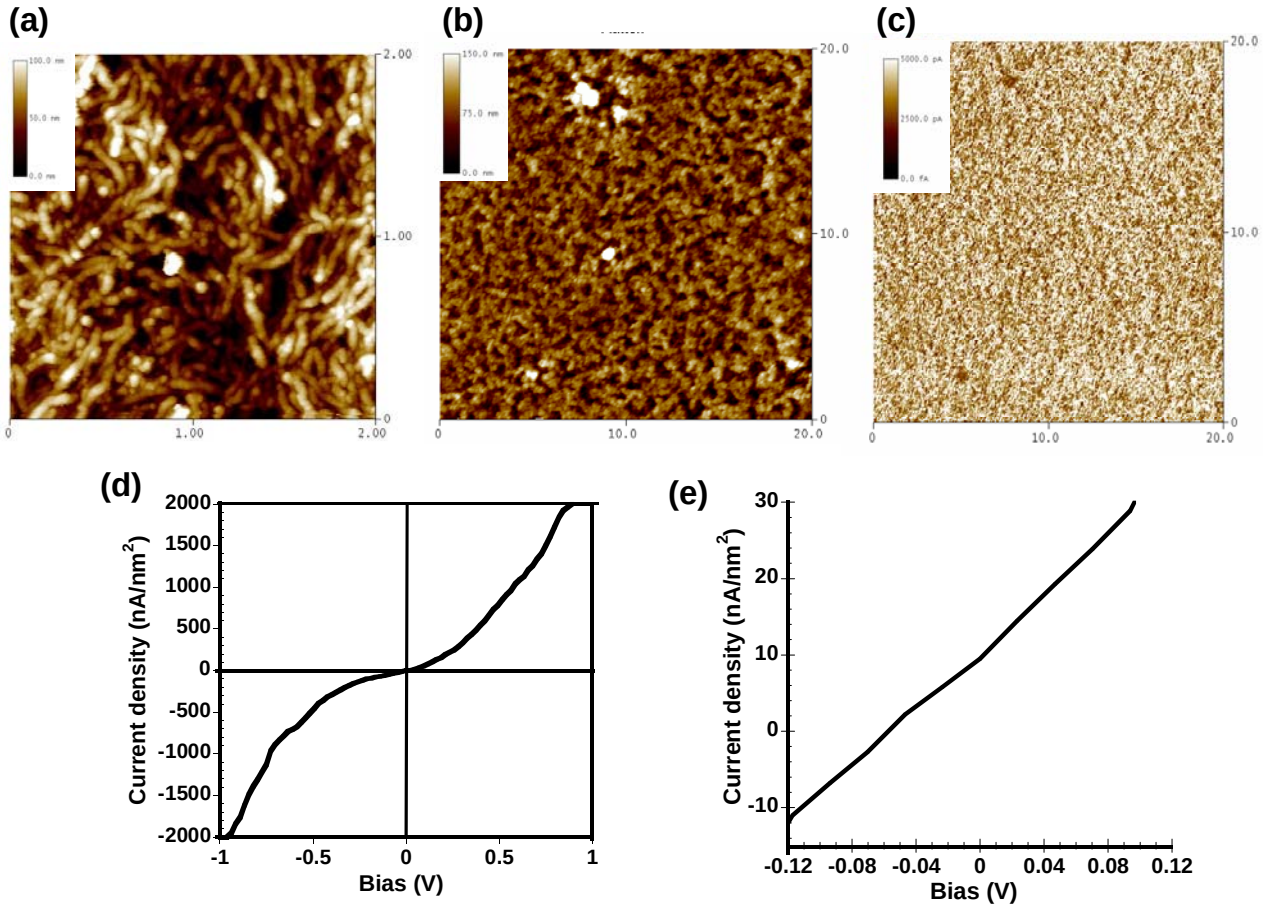

Figure 5.12: Tapping mode and conductive probe AFM images of calcined Co_3O_4 nanowires with (a) height contrast image (2 μm x 2 μm) in tapping mode using a silicon nitride cantilever, (b) height contrast image (20 μm x 20 μm) in tapping mode using a conductive Pt cantilever, (c) current contrast imaging (20 μm x 20 μm) using a Pt cantilever from +1.0 V to -1.0 V and (d) current density vs voltage plot of calcined Co_3O_4 nanowires (e) linear relationship in the current density vs voltage plot of calcined nanowires from -0.12 V to +0.12 V showing an Ohmic behavior at the Pt/Co_3O_4 junction.

5.2.6 Cyclic voltammetry (CV) of calcined Co_3O_4 nanowire films on ITO

Cyclic voltammetry was used characterize calcined Co_3O_4 nanowire films on ITO. To afford a polycrystalline Co_3O_4 materials, PS-Co_3O_4 films on ITO were first calcined in air at T = 400° C prior to electrochemical measurements and cleaned by exposure to UV-ozone to remove residual organics from the metal oxide surfaces. FE-SEM of calcined

films confirmed that the 1-D morphology of nanowires remained intact, as discussed previously (see Figure 5.5 for TEM, Figure 5.4 for SEM and Fig. 5.6 d for XRD). Cyclic voltammetry was performed on the films in 0.1 M NaOH electrolyte solution while cycling from 0.7 V to -0.9 V at 20 mV/s with respect to Ag/AgCl (3 M KCl) reference electrode (Figure 5.13). Multiple peaks within the voltammogram was consistent with the formation of a number of cobalt oxide phases at different oxidation states; specifically, anodic peaks at 0 V, 0.2 V, 0.6 V and corresponding cathodic peaks at 0.5 V, 0.2 V and -0.5 V. Assignments of these peaks were in agreement with previously reported phases of cobalt in water in the Pourbaix diagram and other recent reports and can be associated with the following reactions:[10, 21, 22, 99-101]

Anodic scan (toward positive potentials)

peak I-(0 V) Co_3O_4 formation:

$$3Co(OH)_2 + 2OH^- \rightleftharpoons Co_3O_4 + 4H_2O + e^- \quad (5.1)$$

peak II-(0.3 V) CoOOH formation:

$$Co_3O_4 + OH^- + H_2O \rightleftharpoons 3CoOOH + e^- \quad (5.2)$$

peak III-(0.6 V) CoO_2 formation:

$$CoOOH + OH^- \rightleftharpoons CoO_2 + H_2O + e^- \quad (5.3)$$

peak IV-Oxygen evolution reaction (OER):

$$4\ ^-OH \rightleftharpoons O_2 + 2H_2O + 4e^- \quad (5.4)$$

Cathodic scan (toward negative potentials)

peak V-(0.5 V) CoOOH formation:

$$CoO_2 + H_2O + e^- \rightleftharpoons CoOOH + OH^- \quad (5.5)$$

peak VI- (0.2 V) Co_3O_4 formation:

$$3CoOOH + e^- \rightleftharpoons Co_3O_4 + OH^- + H_2O \quad (5.6)$$

peak VII- (-0.5 V) $Co(OH)_2$ formation:

$$Co_3O_4 + H_2O + 2e^- \rightleftharpoons 3(Co(OH)_2 + 2OH^- \quad (5.7)$$

As previously determined by powder XRD (Figure 5.6 (d)), the initial state of the calcined cobalt oxide nanowires was found to be polycrystalline Co_3O_4 phase, which consisted of both the Co^{2+} and Co^{3+} oxidation states and can be seen in the cyclic voltammogram (peak I). In the anodic scan, from potential 0 V to 0.2 V, the Co_3O_4 phase was oxidized to the cobalt oxyhydroxide (CoOOH) phase with a Co^{+3} oxidation state and an uptake of hydroxide ions and water from the electrolyte media (peak II-eq. 5.2). Further anodic scanning to 0.6 V resulted in oxidation of the CoOOH to cobalt peroxide (CoO_2) with a Co^{+4} oxidation state and condensation reactions to release water (peak III-eq. 5.3). A large anodic peak in the voltammogram at 0.7 V was observed and attributed to electrocatalytic oxygen evolution (OER) by the Co_3O_4 nanowire thin film (peak IV-eq. 5.4) accompanied by the formation of bubbles in the electrochemical cell. In the cathodic scan to 0.5 V resulted in the reduction of CoO_2 to CoOOH, followed by the reduction to Co_3O_4 at 0.2 V. Further cathodic scan to -0.5 V resulted in the reduction of Co_3O_4 to $Co(OH)_2$ (peak VII-eq 5.6). As shown in Figure 5.13, these nanostructured cobalt oxide prepared via Colloidal Polymerization (i.e.,magnetic assembly and nanoscale Kirkendall reaction) undergo electrochemical charge transfer reactions Co(II)←→ Co(III)) ←→ Co(IV) in basic electrolyte, making these nanowires potential candidates for pseudocapacitive electrodes in hybrid electrochemical capacitors.[2]

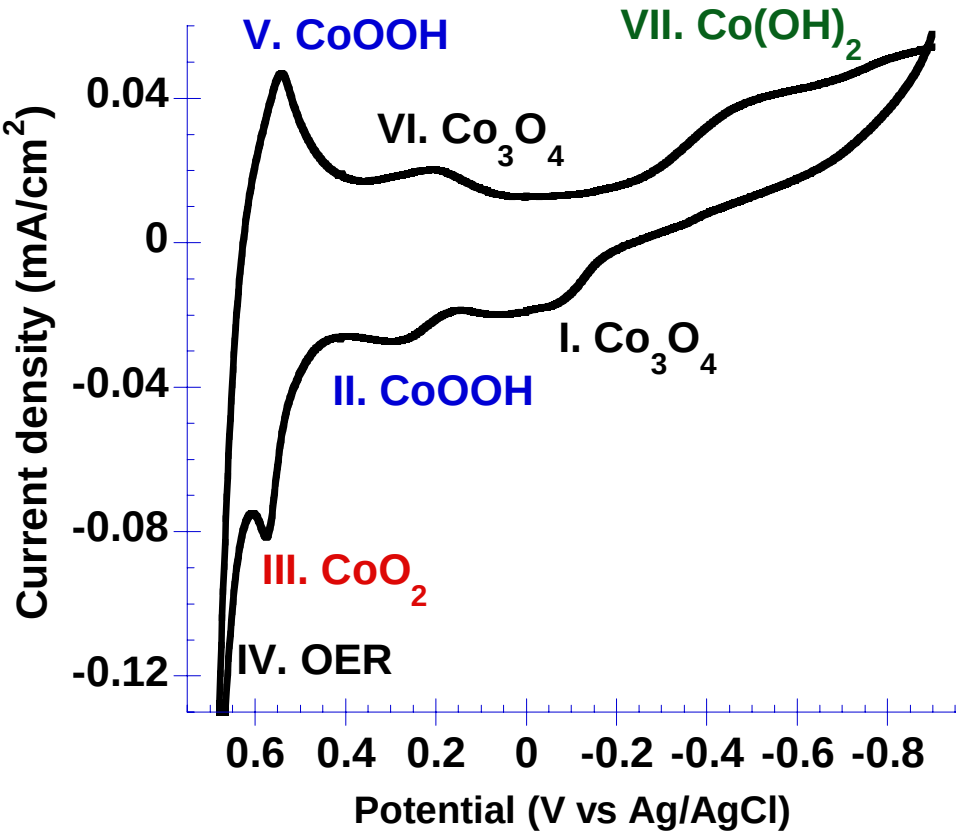

Figure 5.13: CV of calcined Co_3O_4 film on ITO at 20 mV/s scan rate in 0.1 M NaOH electrolyte solution.

5.3: Conclusion

In conclusion, Colloidal Polymerization of ferromagnetic PS-CoNPs into 1-D cobalt oxide nanowires is reported. We demonstrate the combination of dipolar assembly and oxidation of dipolar nanoparticles is a facile and robust method to prepare well-defined polymer coated cobalt oxide nanowires in gram scale quantities. We also demonstrate for the first time that these nanostructured cobalt oxide materials are electrically and electrochemically active and of interest for potential applications in energy storage. Future work will examine the effect of the nanoporosity of these cobalt

oxide wires as electrochemical supercapacitors and investigate Li ion insertion for Li-batteries.

5.4: Experimental

Materials

Anhydrous 1,2-dichlorobenzene (DCB), toluene (99.5%), lithium perchlorate ($LiClO_4$, 95%), and NaOH (99.99%) were purchased from Aldrich and used as received without further purification. Dicobalt octacarbonyl ($Co_2(CO)_8$) was purchased from Strem Chemicals and used as received. Compressed oxygen gas was purchased from Matheson Tri-gas. Thermolysis reactions were performed using an Omega temperature controller CSC32 with a K-type utility thermocouple and a Glas-Col fabric heating mantle. Calcination of the polymer coated cobalt oxide nanowires were performed in a Barnstead/Thermolyne small bench-top muffled furnace at 400 °C in air. Indium-doped tin oxides-coated glass (ITO) was obtained from Colorado Concept Coatings LLC. Electrochemical measurements were performed with a CH-instrument 600c potentiostat/galvanostat in a homebuilt Teflon compression cell (electrode area ~ 0.7 cm^2) sealed with perfluoroelastomer O-rings (Kalrez). A Pt coil and Ag/AgCl electrode (sat. KCl) were used as the counter and reference, respectively. The reference electrode was calibrated using a saturated calomel electrode (~44 mV vs SCE). UV-Vis spectra were obtained using Agilent UV-vis spectrometer (no. 8453A, Foster City, CA). TEM images were obtained on a JEM100CX II transmission electron microscope (JEOL) at an operating voltage of 60 kV, using in house prepared carbon coated copper grids (Cu, hexagon, 400 mesh) and carbon coated nickel grids (Ni, hexagon, 300 mesh). Image

analysis was performed using ImageJ software (Rasband, W.S., National Institute of Health, http://rsb.info.nih.gov/ij/, 1997-2007). Relative uncertainty of particle size determinations using ImageJ was found to be 1 % of diameter average (e.g., 20 nm $\pm$ 0.2 nm). SEM images were taken on a Hitachi 4800 FE-SEM (20 kV accelerating voltage) on the as prepared sample (i.e., no metallic over coating). AFM measurements were performed on a Digital Instrument Dimension 3100 Scanning Probe Microscope in tapping mode. Conducting-tip AFM (C-AFM) measurements were made with a Dimension 3100 Nanoscope IV system (Veeco Metrology Group, Santa Barbara, CA) with the TUNA application module. Conducting Pt coated CSC38/Pt tips were procured from Mikromasch with a nominal force constant of 0.08 N/m. C-AFM measurements were made in contact mode in air with minimal force engagement, followed by a well-calibrated and controlled force load (3 N/m) at the conductive probe. The samples of investigation were made on a platinum coated silicon wafer which was held through the vacuum chuck which provided sample bias with respect to the conductive probe that was kept at ground potential. Both height and TUNA current channels were displayed and recorded upon application of an appropriate amount of sample bias. Current sensitivity was chosen on the basis of the nature of the sample which was 10nA/V in the present case. VSM measurements were obtained using a Waker HF 9H electromagnet with a Lakeshore 7300 controller and a Lakeshore 668 power supply. Magnetic measurements were carried out at room temperature (27 °C or 300 K) and low temperature (-213 °C or 60 K), with a maximum S-2 applied field of 1190 kA/m, a ramp rate of 2630 $Am^{-1}s^{-1}$ and a time constant of 0.1. XRD measurements were performed using the X'pert x-ray

diffractometer (PW1827) (Phillips) at room temperature with a CuKα radiation source at 40 kV and 30 mA. UPS and XPS analyses were conducted in a combined UPS-XPS Kratos Axis Ultra 165 with an average base pressure of 10^{-9} Torr. XPS data were collected with monochromatic Al(Kα) radiation at a pass energy of 20 eV. UPS spectra were obtained with a 21.2 eV He (I) excitation (SPECS UVS 10-35) and pass energy of 5 eV. For all UPS analyses, a 9 V bias was applied to improve the transmission of low KE electrons and to improve the determination of the energy of the low-KE edge. Separate UPS spectra and XPS spectra were measured for an atomically clean gold sample frequently to calibrate the Fermi energy (E_F). XPS spectra were acquired before UPS data acquisition. All characterization experiments were performed at normal takeoff angle (0°) unless otherwise noted. Raman spectra were acquired with 5 mW of radiation at 514.5 nm from a Coherent Innova 350C Ar^+ laser. Plasma lines were removed using a bandpass filter (3.0 nm bandwidth) from Pomfret Research Optics. Scattered light was collected and collimated by a plano-convex lens and passed through a holographic SuperNotch Plus filter (Kaiser Optical Systems before being focused through a polarization scrambler and a second SuperNotch Plus filter onto the 50 μm entrance slit of a Spex 270M monochromator. This monochromator utilizes a 1200 gr/mm grating blazed at 630 nm resulting in a spectral bandpass of 1 cm^{-1}. A 1340 x 400 pixel, thinned, back-illuminated CCD (Roper Scientific model 400-EB) held at -95 ^oC was used for detection. Images from this detector were processed by WinSpec32 software (Roper Scientific) and then were imported into Grams 32 (Galactic Industries) for spectral calibration and manipulation. Spectra were calibrated using known Ar^+ emission lines

observed by removing the laser bandpass filter. Typical integration times varied from 120-180 min per acquisition, accomplished by co-addition of individual 6 sec integrated spectra.

Preparation of PS-CoNPs (5.1), using amine end-functional polystyrene surfactants, PS-NH_2. PS-NH_2 (0.400 g; 7.27 x 10^{-2} mmol) was dissolved in DCB (10 mL) and transferred into a three- neck round bottom flask containing DCB (30 mL) and heated to 175 °C. Separately, $Co_2(CO)_8$ (1.00 g; 2.92 x 10^{-3} mol) was dissolved in DCB (8 mL) at room temperature in air, and was rapidly injected into the hot polymer solution via syringe. Upon injection, the reaction temperature dropped to 160 ºC and the reaction mixture was maintained at 160 ºC for 60 min followed by cooling to room temperature under argon. PS-CoNPs were isolated by precipitation into hexanes (500 mL), yielding a black powder (yield = 0.784 g) that was soluble in a wide range of organic solvents (e.g., methylene chloride, THF, toluene). Sample for TEM analysis was prepared by dispersing the isolated powder (1 mg) in toluene (2 mL) via sonication for 15 minutes followed by drop casting onto a carbon coated Cu grid. The particle size of the PS-CoNPs was determined to be 20 nm $\pm$ 2.4 nm via TEM. Magnetic properties of PS-CoNPs were measured using VSM at room temperature: M_s = 41.2 emu/g; H_c = 713 Oe and at 60 K: M_s = 43.7 emu/g; H_c = 1440 Oe. TGA analysis showed 41% of organics by mass.

Preparation of PS-CoO nanostructures (5.2). To a three- neck round bottom flask equipped with a reflux condenser and a stir bar, was charged with 16 mL of the as prepared ferrofluid of PS-CoNPs. The ferrofluid was heated to 175 °C and stirred at 300 rpm, while bubbling with oxygen for 3 hours of oxidation and was then allowed to cool

to room temperature. The ferrofluid was isolated by precipitation into hexanes (500 mL), followed by centrifugation at 5000 rpm for 15 minutes to yield a black powder (yield = 0.302 g) that was soluble in a wide range of organic solvents (e.g., methylene chloride, THF, toluene). TEM sample was prepared as previously described. The diameter of the PS-cobalt oxide nanowire **(5.2)** was determined to be 29 nm $\pm$ 2.7 nm via TEM. Magnetic properties of PS-cobalt oxide **(5.2)** were measured using VSM at room temperature: M_s = 4.6 emu/g; H_c = 363 Oe and at 60 K: M_s = 4.8 emu/g; H_c = 734 Oe. TGA analysis showed 34% of organics by mass.

Preparation of PS-Co_3O_4 nanostructures (5.3). To a three- neck round bottom flask equipped with a reflux condenser and a stir bar, was charged with 48 mL of the as prepared ferrofluid (c = 16 mg/mL). The ferrofluid was heated to 175 °C and stirred at 300 rpm, while bubbling with oxygen for 1 week of oxidation and was then allowed to cool to room temperature. The ferrofluid was isolated by precipitation into hexanes (500 mL), followed by centrifugation at 5000 rpm for 15 minutes to yield a black powder (yield = 0.575 g) that was soluble in a wide range of organic solvents (e.g., methylene chloride, THF, toluene). TEM sample was prepared as previously described. The diameter of the PS-cobalt oxide nanowire **(5.3)** was determined to be 32 nm ± 3.5 nm via TEM. Magnetic properties of PS-cobalt oxide **(5.3)** were measured using VSM at room temperature: M = 0.2 emu/g; at 10,000 Oe and at 60 K: M = 0.38 emu/g; at 10,000 Oe. TGA analysis showed 11% of organics by mass.

Preparation of PS-CoNPs (5.1), using amine end-functional polystyrene surfactants, PS-NH_2 on gram scale. PS-NH_2 (1.30 g; 2.89 x 10^{-1} mmol) was dissolved in DCB (10

mL) and transferred into a three- neck round bottom flask containing DCB (30 mL) and heated to 175 °C. Separately, $Co_2(CO)_8$ (2.00 g; 5.85 x 10^{-3} mol) was dissolved in DCB (12 mL) at room temperature in air, and was rapidly injected into the hot polymer solution. Upon injection, the reaction temperature dropped to 160 ºC and the reaction mixture was maintained at 160 ºC for 60 min followed by cooling to room temperature under argon. PS-CoNPs were isolated by precipitation into hexanes (500 mL), yielding a black powder (yield = 1.53 g) that was soluble in a wide range of organic solvents (e.g., methylene chloride, THF, toluene). Sample for TEM analysis was prepared by dispersing the isolated powder (1 mg) in toluene (2 mL) via sonication for 15 minutes followed by drop casting onto a carbon coated Cu grid. The particle size of the PS-CoNPs was determined to be 20 nm $\pm$ 2.4 nm via TEM. Magnetic properties of PS-CoNPs were measured using VSM at room temperature: M_s = 41.2 emu/g; H_c = 713 Oe and at 60 K: M_s = 43.7 emu/g; H_c = 1440 Oe. TGA analysis showed 41% of organics by mass.

Gram scale Preparation of PS-Co_3O_4 nanostructures (5.3). Isolated powders of PS-CoNPs (1.36 g) was redispersed in DCB (50 mL) via sonication for 15 minutes. The black solution was charged into a three- neck round bottom flask equipped with a reflux condenser and a stir bar. The ferrofluid was heated to 175 °C and stirred at 300 rpm, while bubbling with oxygen for a specific period of time. After 1 week of oxidation, the reaction was cooled to room temperature. The ferrofluid was isolated by precipitation into hexanes (500 mL), followed by centrifugation at 5000 rpm for 15 minutes to yield a black powder (yield = 1.04 g) that was soluble in a wide range of organic solvents (e.g., methylene chloride, THF, toluene). TEM sample was prepared as previously described.

The diameter of the PS-cobalt oxide nanowire **(5.3)** was determined to be 32 nm ± 3.5 nm via TEM. Magnetic properties of PS-cobalt oxide **(5.3)** were measured using VSM at room temperature: M = 0.2 emu/g; at 10,000 Oe and at 60 K: M = 0.38 emu/g; at 10,000 Oe. TGA analysis showed 11% of organics by mass.

Calcined cobalt cobaltite, Co_3O_4 nanostructures (5.4). The as- synthesized PS-cobalt oxide nanowire powders (**5.3**) were calcined at 400 °C in the furnace for 16 hours in air to yield polycrystalline Co_3O_4 nanowires **(5.4)** as determined from XRD. The magnetic properties of the calcined powders were measured using VSM at room temperature: M = 0.09 emu/g; at 10,000 Oe and at 60 K: M = 0.25 emu/g; 10,000 Oe.

TEM analysis of the calcined Co_3O_4 nanowires. TEM observation was conducted to interrogate the effect of calcination on the interior morphology and porosity of Co_3O_4 nanowires. PS-cobalt oxide nanowires dispersion were dropped cast onto a carbon coated Ni grids and calcined in air at 400 °C, as Cu grids were observed to embrittle after the high temperature thermal treatment. Figure 5.5 confirmed that both the 1-D morphology and interior porous inclusions of Co_3O_4 nanowires were preserved after the calcination process.

Preparation of cobalt oxide films on ITO. ITO slides were cut, and then cleaned with 10% aqueous Triton X-100 solution, followed by rinsing and sonication in nanopure (18 MΩ cm) water for 10 minutes. The ITO was then sonicated in absolute ethanol for 10 minutes. Once removed from ethanol, the slides were dried under a stream of N_2 and immedately etched with HI (50% aqueous solution). The acid etched slide was immediately spin coated (1000 rpm) with the nanoparticle dispersion in toluene (c = 25

mg/mL) to obtain thin films of the polymer coated colloids on ITO. Film thickness ranged from 50-60 nm as determined from AFM. The films were then dried under vacuum heating at 70 °C for several hours. For the calcined cobalt oxide film on ITO, a dispersion of polystyrene coated cobalt oxide was deposited as described previously. Then, the film was heated at 400 °C in air for 16 hours.

UV-visible absorption spectroscopy. A dispersion of polystyrene coated cobalt oxide nanowires was deposited onto ITO and calcined at 400 °C in air as described previously. The UV-Vis absorption spectra of the Co_3O_4 film on ITO were recorded using the Agilent UV-Visible Spectrometer (no. 8453A) and the spectra obtained were analyzed by Chemistation software.

Spectroscopic determination of band edge energy levels of Co_3O_4 nanowires. Co_3O_4 is a p-type semiconductor, in which the optical band gap (E_g) can be obtained from the absorption spectra. The band gap energies can be calculated using the equation 1:

$$(\alpha h\nu)^n = B(h\nu - E_g) \quad \text{..... Eq 5.8}$$

where, α is the absorption coefficient, hv is the photon energy, B is a constant characteristic to the material, and n equals either 1/2 for an indirect transition, or 2 for a direct transition. The absorption coefficient (α) was obtained using the optical transmission data at different wavelengths based on equation (5.9).

$$I = I_0 \exp(-\alpha t) \quad \text{..... Eq 5.9}$$

The band gap was determined by plotting $(\alpha hv)^2$ versus photon energy (Tauc plot) as shown in Figure 5.14. The band gap energy was estimated by extrapolating the Tauc Plot

to $\alpha = 0$ with intercepts at 1.45 and 2.26 eV, respectively. The best fit of $(\alpha h\nu)^2$ versus photon energy was found to be n = 2, suggesting that the obtained Co_3O_4 nanowires are semiconducting with a direct band gap transition.[92, 102]

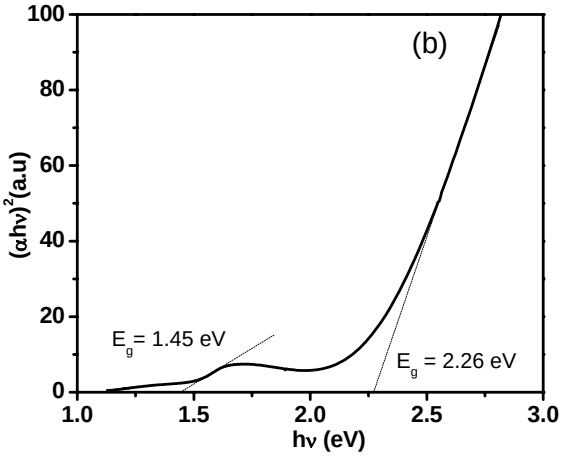

Figure 5.14: Optical band gap energy Co_3O_4 nanowires obtained by extrapolation to $\alpha = 0$.

Cyclic voltammetry measurements. A potential versus current profile for the polymer coated cobalt nanoparticles and cobalt oxide thin films on ITO were obtained at a sweep rate of 20 mV/s at room temperature in the potential range of 0.8 V and -0.9 V versus the Ag/AgCl (saturated KCl) in 0.1 M NaOH (aq). The electrolyte solution was purged with argon for 30 minutes and then transferred into the electrochemical cell via syringe prior to cyclic voltammetry experiments.

5.5: References

1. Alstrum-Acevedo, J. H.; Brennaman, M. K.; Meyer, T. J. *Inorg. Chem.* **2005,** *44*, 6802-6827.

2. Arico, A. S.; Bruce, P.; Scrosati, S.; Tarascon, J.-M.; Van Schalkwijk, W. *Nat. Mater.* **2005,** *4*, 366-377.

3. Kanan, M. W.; Nocera, D. G. *Science* **2008,** *321*, 1072-1075.

4. Osterloh, F. *Chem. Mater.* **2008,** *20*, 35-54.

5. Ryan, J. V.; Berry, A. D.; Anderson, M. L.; Long, J. W.; Stroud, R. M.; Cepak, V. M.; Browning, V. M.; Rolison, D. R.; Merzbacher, C. I. *Nature* **2000,** *406*, 169-172.

6. Long, J. W.; Dunn, B.; Rolison, D. R.; White, H. S. *Chem. Rev.* **2004,** *104*, 4463-4492.

7. Long, J. W.; Rolison, D. R. *Acc. Chem. Res.* **2007,** *40*, 854-862.

8. Alexander, B. D.; Kulesza, P. J.; Rutkowska, I.; Solarskac, R.; Augustynski, J. *J. Mater. Chem.* **2008,** *18*, 2298-2303.

9. Estrada, W.; Fantini, M. C. A.; de Castro, S. C.; Polo da Fonseca, C. N.; Gorenstein, A. *J. Appl. Phys.* **1993,** *74*, 5835-5841.

10. Svegl, F.; Orel, B.; Hutchins, M. G.; Kalcher, K. *J. Electrochem. Soc.* **1996,** *143*, (5), 1532-1539.

11. Poizot, P.; Laruelle, S.; Grugeon, S.; Dupont, L.; Tarascon, J.-M. *Nature* **2000,** *407*, 496-499.

12. Li, W.-Y.; Xu, L.-N.; Chen, J. *Adv. Func. Mater.* **2005,** *15*, 851-857.

13. Li, Y.; Tan, B.; Wu, Y. *J. Am. Chem. Soc.* **2006,** *128*, (44), 14258-14259.

14. Nam, K. T.; Kim, D.-W.; Yoo, P. J.; Chiang, C.-Y.; Meethong, N.; Hammond, P. T.; Chiang, Y.-M.; Belcher, A. M. *Science* **2006,** *312*, 885-888.

15. Li, Y.; Tan, B.; Wu, Y. *Nano Lett.* **2008,** *8*, (1), 265-270.

16. Shim, H.-S.; Shinde, V. R.; Kim, H.-J.; Sung, Y.-E.; Kim, W.-B. *Thin Solid Films* **2008,** *516*, 8573-8578.

17. Chen, Y. W. D.; Noufi, R. N. *J. Electrochem. Soc.* **1984,** *131*, (4), 731-5.

18. Schumacher, L. C.; Holzhueter, I. B.; Hill, I. R.; Dignam, M. J. *Electrochim. Acta* **1990,** *35*, (6), 975-984.

19. Monk, P. M. S.; Chester, S. L.; Higham, D. S.; Partridge, R. D. *Electrochim. Acta* **1994,** *39*, (15), 2277-84.

20. Castro, E. B.; Gervasi, C. A.; Vilche, J. R. *J. Appl. Electrochem.* **1998,** *28*, (8), 835-841.

21. Casella, I. G. *J. Electroanal. Chem.* **2002,** *520*, (1-2), 119-125.

22. Casella, I. G.; Gatta, M. *J. Electroanal. Chem.* **2002,** *534*, (1), 31-38.

23. Mendoza, L.; Albin, V.; Cassir, M.; Galtayries, A. *J. Electroanal. Chem.* **2003,** *548*, 95-107.

24. Spataru, N.; Terashima, C.; Tokuhiro, K.; Sutanto, I.; Tryk, D. A.; Park, S.-M.; Fujishima, A. *J. Electrochem. Soc.* **2003,** *150*, (7), E337-E341.

25. Lin, H.; Tang, W.; Kleiman-Shwarsctein, A.; McFarland, E. W. *J. Electrochem. Soc.* **2008,** *155*, (2), B200-B206.

26. He, T.; Chen, D.; Jiao, X.; Xu, Y.; Gu, Y. *Langmuir* **2004,** *20*, (19), 8404-8408.

27. Kim, J.-W.; Choi, S. H.; Lillehei, P. T.; Chu, S.-H.; King, G. C.; Watt, G. D. *Chem. Commun.* **2005**, (32), 4101-4103.

28. Hu, J.; Wen, Z.; Wang, Q.; Yao, X.; Zhang, Q.; Zhou, J.; Li, J. *J. Phys. Chem. B* **2006,** *110*, (48), 24305-24310.

29. Ohnishi, M.; Kozuka, Y.; Ye, Q.-L.; Yoshikawa, H.; Awaga, K.; Matsuno, R.; Kobayashi, M.; Takahara, A.; Yokoyama, T.; Bandow, S.; Iijima, S. *J. Mater. Chem.* **2006,** *16*, (31), 3215-3220.

30. Titirici, M.-M.; Antonietti, M.; Thomas, A. *Chem. Mater.* **2006,** *18*, (16), 3808-3812.

31. Chen, Y.; Zhang, Y.; Fu, S. *Mater. Lett.* **2007,** *61*, (3), 701-705.

32. Du, N.; Zhang, H.; Chen, B.; Wu, J.; Ma, X.; Liu, Z.; Zhang, Y.; Yang, D.; Huang, X.; Tu, J. *Adv. Mater.* **2007,** *19*, (24), 4505-4509.

33. Chen, C.-H.; Abbas, S. F.; Morey, A.; Sithambaram, S.; Xu, L.-P.; Garces, H. F.; Hines, W. A.; Suib, S. L. *Adv. Mater.* **2008,** *20*, (6), 1205-1209.

34. Chernavskii, P. A.; Pankina, G. V.; Zaikovskii, V. I.; Peskov, N. V.; Afanasiev, P. *J. Phys. Chem. C* **2008,** *112*, (26), 9573-9578.

35. Teng, F.; Xu, T.; Liang, S.; Buergen, G.; Yao, W.; Zhu, Y. *Catal. Commun.* **2008,** *9*, (6), 1119-1124.

36. Teng, F.; Yao, W.; Zheng, Y.; Ma, Y.; Xu, T.; Gao, G.; Liang, S.; Teng, Y.; Zhu, Y. *Talanta* **2008,** *76*, (5), 1058-1064.

37. Tian, L.; Yang, X.; Lu, P.; Williams, I. D.; Wang, C.; Ou, S.; Liang, C.; Wu, M. *Inorg. Chem.* **2008,** *47*, (13), 5522-5524.

38. Zhao, W.; Liu, Y.; Li, H.; Zhang, X. *Mater. Lett.* **2008,** *62*, (4-5), 772-774.

39. Chen, Y.; Hu, L.; Wang, M.; Min, Y.; Zhang, Y. *Colloids Surf., A* **2009,** *336*, (1-3), 64-68.

40. Park, J.; Shen, X.; Wang, G. *Sens. Actuators, B* **2009,** *B136*, (2), 494-498.

41. Salabas, E. L.; Rumplecker, A.; Kleitz, F.; Radu, F.; Schueth, F. *Nano Letters* **2006,** *6*, (12), 2977-2981.

42. Shaju, K. M.; Jiao, F.; Debart, A.; Bruce, P. G. *Physical Chemistry Chemical Physics* **2007,** *9*, (15), 1837-1842.

43. Benitez, M. J.; Petracic, O.; Salabas, E. L.; Radu, F.; Tueysuez, H.; Schueth, F.; Zabel, H. *Phys. Rev. Lett.* **2008,** *101*, (9), 097206/1-097206/4.

44. Dong, Z.; Fu, Y.; Han, Q.; Xu, Y.; Zhang, H. *J. Phys. Chem. C* **2007,** *111*, (50), 18475-18478.

45. Du, J.; Chai, L.; Wang, G.; Li, K.; Qian, Y. *Aust. J. Chem.* **2008,** *61*, (2), 153-158.

46. Zhang, H.; Wu, J.; Zhai, C.; Ma, X.; Du, N.; Tu, J.; Yang, D. *Nanotechnology* **2008,** *19*, (3), 035711/1-035711/5.

47. An, K.; Lee, N.; Park, J.; Kim, S.; Hwang, Y.; Park, J.; Kim, J.; Park, J.; Han, M. J.; Yu, J.; Hyeon, T. *J. Am. Chem. Soc.* **2004,** *128*, (9753-9760).

48. Guan, H.; Shao, C.; Wen, S.; Chen, B.; Gong, J.; Yang, X. *Mater. Chem. Phys.* **2003,** *82*, (3), 1002-1006.

49. Barakat, N. A. M.; Khil, M. S.; Sheikh, F. A.; Kim, H. Y. *J. Phys. Chem. C* **2008,** *112*, (32), 12225-12233.

50. Gu, Y.; Jian, F.; Wang, X. *Thin Solid Films* **2008,** *517*, (2), 652-655.

51. Redl, F. X.; Cho, K.-S.; Murray, C. B.; O'Brien, S. *Nature* **2003,** *423*, 968-971.

52. Manoharan, V. M.; Elsesser, M. T.; Pine, D. J. *Science* **2003,** *301*, 483-487.

53. Park, S.; Lim, J.-H.; Chung, S.-W.; Mirkin, C. A. *Science* **2004,** *16*, 348-351.

54. Benkoski, J. J.; Bowles, S. E.; Korth, B., D.; Jones, R. A.; Douglas, J. F.; Karim, A.; Pyun, J. *J. Am. Chem. Soc.* **2007,** *129*, 6291-6297.

55. Benkoski, J. J.; Bowles, S. E.; Korth, B. D.; Jones, R. L.; Douglas, J. F.; Karim, A.; Pyun, J. *J. Am. Chem. Soc.* **2007,** *129*, (28), 8694-8695.

56. DeVries, G. A.; Brunnbauer, M.; Hu, Y.; Jackson, A. M.; Long, B.; Neltner, B. T.; Uzun, O.; Wunsch, B. H.; Stellacci, F. *Science* **2007,** *315*, (5810), 358-361.

57. Carney, R. P.; De Vries, G. A.; Dubois, C.; Kim, H.; Kim, J. Y.; Singh, C.; Ghorai, P. K.; Tracy, J. B.; Stiles, R. L.; Murray, R. W.; Glotzer, S. C.; Stellacci, F. *J. Am. Chem. Soc.* **2008,** *130*, (3), 798-799.

58. De Vries, G. A.; Talley, F. R.; Carney, R. P.; Stellacci, F. *Adv. Mater.* **2008,** *20*, (22), 4243-4247.

59. Nakata, K.; Hu, Y.; Uzun, O.; Bakr, O.; Stellacci, F. *Adv. Mater.* **2008,** *20*, (22), 4294-4299.

60. Furst, E. M.; Suzuki, C.; Fermigier, M.; Gast, A. P. *Langmuir* **1998,** *14*, (26), 7334-7336.

61. Biswal, S. L.; Gast, A. P. *Phys. Rev. E: Stat., Nonlinear, Soft Matter Phys.* **2003,** *68*, (2-1), 021402/1-021402/9.

62. Goubault, C.; Jop, P.; Fermigier, M.; Baudry, J.; Bertrand, E.; Bibette, J. *Phys. Rev. Lett.* **2003,** *91*, (26, Pt. 1), 260802/1-260802/4.

63. Biswal, S. L.; Gast, A. P. *Anal. Chem.* **2004,** *76*, (21), 6448-6455.

64. Biswal, S. L.; Gast, A. P. *Phys. Rev. E: Stat., Nonlinear, Soft Matter Phys.* **2004,** *69*, (4-1), 041406/1-041406/9.

65. Cohen-Tannoudji, L.; Bertrand, E.; Bressy, L.; Goubault, C.; Baudry, J.; Klein, J.; Joanny, J.-F.; Bibette, J. *Phys. Rev. Lett.* **2005,** *94*, (3), 038301/1-038301/4.

66. Dreyfus, R.; Baudry, J.; Roper, M. L.; Fermigier, M.; Stone, H. A.; Bibette, J. *Nature* **2005,** *437*, (7060), 862-865.

67. Goubault, C.; Leal-Calderon, F.; Viovy, J.-L.; Bibette, J. *Langmuir* **2005,** *21*, (9), 3725-3729.

68. Singh, H.; Laibinis, P. E.; Hatton, T. A. *Nano Lett.* **2005,** *5*, 2149-2154.

69. Gao, J.; Zhang, B.; Zhang, X.; Xu, B. *Angew. Chem. Int. Ed.* **2006,** *45*, 1220-1223.

70. Pileni, M. P. *Acc. Chem. Res.* **2007,** *40*, 685-693.

71. Singh, H.; Hatton, T. A. *J. Magn. Magn. Mater.* **2007,** *315*, 53-64.

72. Cohen-Tannoudji, L.; Bertrand, E.; Baudry, J.; Robic, C.; Goubault, C.; Pellissier, M.; Johner, A.; Thalmann, F.; Lee, N. K.; Marques, C. M.; Bibette, J. *Phys. Rev. Lett.* **2008,** *100*, (10), 108301/1-108301/4.

73. Zerrouki, D.; Baudry, J.; Pine, D.; Chaikin, P.; Bibette, J. *Nature* **2008,** *455*, (7211), 380-382.

74. Erb, R. M.; Son, H. S.; Samanta, B.; Rotello, V. M.; Yellen, B. B. *Nature* **2009,** *457*, (7232), 999-1002.

75. Zhou, Z.; Liu, G.; Han, D. *ACS Nano* **2009,** *3*, (1), 165-172.

76. Yin, Y.; Rioux, R. M.; Erdonmez, C. K.; Hughes, S.; Somorjai, G. A.; Alivisatos, A. P. *Science* **2004,** *304*, (5671), 711-714.

77. Yin, Y.; Erdonmez, C. K.; Cabot, A.; Hughes, S.; Alivisatos, A. P. *Adv. Funct. Mater.* **2006,** *16*, (11), 1389-1399.

78. Butter, K.; Bomans, P. H. H.; Frederick, P. M.; Vroege, J.; Philipse, A. P. *Nature Mater.* **2003,** *2*, 88.

79. Ishida, Y.; Aida, T. *J. Am. Chem. Soc.* **2002,** *124*, (47), 14017-14019.

80. Zhao, D.; Moore, J. S. *Org. Biomol. Chem.* **2003,** *1*, (20), 3471-3491.

81. Scherman, O. A.; Ligthart, G. B. W. L.; Sijbesma, R. P.; Meijer, E. W. *Angew. Chem., Int. Ed.* **2006,** *45*, (13), 2072-2076.

82. Kumar, A. M. S.; Sivakova, S.; Marchant, R. E.; Rowan, S. J. *Small* **2007,** *3*, (5), 783-787.

83. Hawker, C. J.; Bosman, A. W.; Harth, E. *Chem. Rev.* **2001,** *101*, (12), 3661-3688.

84. Lacroix-Desmazes, P.; Lutz, J. F.; Chauvin, F.; Severac, R.; Boutevin, B. *Macromolecules* **2001,** *34*, 8866-8871.

85. Hawker, C. J.; Wooley, K. L. *Science* **2005,** *309*, (5738), 1200-1205.

86. Matyjaszewski, K.; Xia, J. *Chem. Rev.* **2001,** *101*, 2921-2990.

87. Risbud, A. S.; Snedeker, L. P.; Elcombe, M. M.; Cheetham, A. L.; Seshadri, R. *Chem. Mater* **2005,** *17*, 834-838.

88. Makhlouf, S. A. *J. Magn. Magn. Mater.* **2002,** *246*, (184-190).

89. Windisch, C. F.; Ferris, K.; Exarhos, G. J.; Sharma, S. K. *Thin Solid Films* **2002,** *420-421*, 89-99.

90. Langell, M. A.; Anderson, M. D.; Carson, G. A.; Peng, L.; Smith, S. *Phys. Rev. B: Condens. Matter Mater. Phys.* **1999,** *59*, (7), 4791-4798.

91. Gulino, A.; Fragala, I. *Inorg. Chim. Acta* **2005,** *358*, (15), 4466-4472.

92. Barreca, D.; Massign, C.; Daolio, S.; Fabrizio, M.; Piccirillo, C.; Armelao, L.; Tondello, E. *Chem. Mater.* **2001,** *13*, 588-593.

93. Gulino, A.; Fiorito, G.; Fragala, I. *J. Mater. Chem.* **2003,** *13*, (4), 861-865.

94. Belova, I. D.; Roginskaya, Y. E.; Shifrina, R. R.; Gagarin, S. G.; Plekhanov, Y. V.; Venevtsev, Y. N. *Solid State Commun.* **1983,** *47*, (8), 577-584.

95. Miedzinksa, K. M. E.; Hollebone, B. R.; Cook, J. G. *J. Phys. Chem. Solids* **1987,** *48*, (7), 649.

96. Cox, P. A., *Transition metal oxides: An introduction to their electronic structure and properties*. Clarendon Press Oxford: 1992; p 276.

97. Schlettwein, D.; Hesse, K.; Gruhn, N.; Lee, P. A.; Nebesny, K. W.; Armstrong, N. R. *J. Phys. Chem. B* **2001,** *105*, 4791-4800.

98. Rose, A. *Phys. Rev.* **1955,** *97*, (6), 1538.

99. Pourbaix, M., *Atlas of electrochemical equilibria in aqueous solutions*. Pergamon: London, 1966; p 322-329.

100. Barbero, C.; Planes, G. A.; Miras, M. C. *Electrochem. Commun.* **2001,** *3*, (3), 113-116.

101. Lichusina, S.; Chodosovskaja, A.; Selskis, A.; Leinartas, K.; Miecinskas, P.; Juzeliunas, E. *Chemija* **2008,** *19*, (3-4), 7-15.

102. Wang, G.; Shen, X.; Horvat, J.; Wang, B.; Liu, H.; Wexler, D.; Yao, J. *J. Phys Chem. C* **2009,** *113*, (11), 4357-4361.

CHAPTER 6

CONCLUSIONS AND FUTURE DIRECTIONS

The synthesis, assembly, and colloidal polymerization of polymer-coated ferromagnetic cobalt nanoparticles (PS-CoNPs) to form magnetic filaments and cobalt oxide nanowires were the central focus of this dissertation. In this study, a modular synthetic methodology, referred to as colloidal polymerization was developed using functional polymers and ferromagnetic nanoparticles as 'colloidal molecules' to form one-dimensional (1-D) mesostructures via dipolar assembly and a chemical reaction. Specifically, well-defined cobalt oxide nanowires were prepared by exploiting the ferromagnetic properties of these polymer-coated cobalt nanoparticles. To achieve 1-D mesostructures via colloidal polymerization, a facile synthetic methodology was developed to synthesize polymer-coated ferromagnetic cobalt nanoparticles. The following sections present the key findings and improvements in the synthesis, assembly and colloidal polymerization of ferromagnetic nanoparticles into cobalt oxide nanowires. These materials are anticipated to serve as novel electrode and catalysts materials for electrochemical energy storage and photoelectrochemical energy conversion.

6.1: Synthesis of polymer-coated ferromagnetic cobalt nanoparticles (PS-CoNPs)

A modular synthetic approach was developed to prepare uniformly-sized ferromagnetic cobalt nanoparticles as colloidal building blocks towards 1-D mesostructures by exploiting the inherent dipolar directionality embedded within the inorganic core. Although the synthesis of ferromagnetic cobalt nanoparticles was

reported by Thomas and Hess in the 1960s, this is the first demonstration using well-defined end-terminal polystyrene ligands to prepare uniform-sized ferromagnetic cobalt nanoparticles. Controlled radical polymerizations were utilized to prepare end-terminal polymeric ligands of precise molar mass, functionality and composition. Systematic evaluation of conditions indicated that a mixture of amine and phosphine oxide end-terminal polystyrene surfactants with M_n = 5000 g/mole in 4:1 weight ratios was found to be optimal in the synthesis of polymer-coated ferromagnetic cobalt nanoparticles. Additionally, the synthesis of uniform sized PS-CoNPs was found to be dependent on the feed weight ratios of the polymeric ligands to the metal carbonyl precursors. However, unlike small molecule systems, the particle size of CoNPs was not affected by varying the ratio of surfactants to the metal precursor. Ferromagnetic NPs synthesized using polymeric ligands were found to be face-centered cubic (f.c.c.) cobalt phases of uniform diameter (D = 15 ± 1.5 nm; M_s = 38 emu/g, H_c = 100 Oe at 20 ºC) that self-assembled into extended nanoparticle chains spanning several micrometers in length when solution cast onto supporting substrates These nanoparticle chains could be easily aligned into 1-D mesostructures by depositing the colloidal dispersion in the presence of a weak magnetic field (100 mT). The distinctive features of this modular synthetic methodology were the functionality and the long-term colloidal stability imparted by the well-defined polymeric surfactants.

6.1.1 Preparation of PS-CoNPs via a simplified synthetic methodology

A simplified methodology was developed, based on the synthetic method described in chapter 2, to prepare nearly 1.3 grams of well-defined PS-CoNPs per-

reaction batch. In this method, multi-gram quantities of end-terminal polystyrene surfactants were accomplished via atom transfer radical polymerization (ATRP). The dual-stage temperature thermolysis of dicobalt octacarbonyl in the presence of amine and phosphine oxide end-terminal polystryrene surfactants enabled uniform growth of the ferromagnetic cobalt nanoparticles. Further mechanistic investigations into the synthesis of PS-CoNPs were performed using various combinations of polymeric surfactants bearing either amine, phosphine oxide or carboxylic acid ligands. In this study, a single polymeric ligand system (amine end-functional polystyrene) was found to yield PS-CoNPs with comparable size, size distributions, and magnetic properties relative to CoNPs prepared from combinations of polymeric ligands as described in chapter 2. The versatility of these polymer-coated ferromagnetic cobalt nanoparticles to form well-defined colloidal mesostructures was further demonstrated via the self-assembly of dipolar colloids into various morphologies exhibited flux-closure nano-ring and lamellae features by modulating the length of the polymer hairs of the dipolar colloids. The self-assembly of these dipolar nanoparticle building blocks were also found to be consistent with recent theoretical modeling.

6.1.2 Future directions

In the present study, the preparation of ferromagnetic cobalt nanoparticles coated with glassy polystyrene shells improved the colloidal stability and processability in organic media. Future directions will target the application of either styrenic or methacrylate functional copolymers in the thermolysis of metal carbonyl precursors to expand the functionality of these dipolar colloids. The stability of methacrylate based

copolymers in the hot injection method has been confirmed by Han et al.[1] Additionally, functional copolymers with various feed ratios of ligating groups such as R-PO_3H_2, R-COOH, and R_3-PO could be systematically investigated to promote chemical and oxidative stabilities.

6.2: Dipolar assembly of ferromagnetic nanoparticles into dense arrays of actuating microscopic filament

The preparation of "artificial cilia" was successfully demonstrated via field induced bottom-up assembly using magnetic nanoparticles as "colloidal molecules". This study was also the first example of both organizing dipolar colloids (D = 23.5 nm) organizing into 1-D mesoscopic chains and *in-situ* optical imaging of filaments while dispersed in dimethylformamide (DMF). In this study, dipolar colloids were first functionalized with crosslinkable copolymers via a ligand exchange reaction with an aldehyde functional polystyrenic ligand with the expectation that a chemical crosslinking would be necessary to form static 1-D chains. However, under these experimental conditions, it was found that the formation of stable magnetic filaments was independent of the nanoparticle chemistry due to the strong dipolar interactions between ferromagnetic nanoparticles. This attractive feature allowed reversible formation of magnetic filaments with tunable stiffness by controlling the external magnetic fields.

In the designed experimental setup as described in chapter 4, non-aggregated bundles of magnetic filaments were prepared in a dimethylformamide (DMF) flow cell equipped with static and oscillating magnetic fields. In the present study, the application of orthogonal magnetic fields resulted in the formation of vertically-aligned magnetic

filaments spanning micrometers in length. The aligned brushes were actuated with an alternating magnetic field, mimicking the motion of cilium found in biological systems. This methodology could also serves as a platform for the formation of other functional 1-D mesostructures utilizing magnetic colloids as structural directing agents.

6.2.1: Future directions

Based on the platform described in chapter 4, *in situ* organization and optical visualization of sub-50 nm magnetic nanoparticles could be extended toward the preparation of other functional 1-D mesostructures such as TiO_2 nanowires, which have potential applications in energy conversion such as dye-sensitized solar cell (DSSC)[2], and hydrogen fuel generation.[3, 4] As demonstrated by Hatton et al., sol-gel chemistry could be utilized to permanently link the pre-assembled sub-micron sized magnetic beads.[5] First, the magnetic building blocks could be either functionalized with polar copolymers or directly synthesized with polyvinylpyrrolidone surfactants[6, 7], to impart water solubility and enable localized hydrolysis of the titania sol precursors along the 1-D chains.[5] Subsequently, the titania-cobalt nanowires could be converted to hollow metal oxide semiconductor nanowires via a calcination treatment in air. This hybrid p-type cobalt oxides and n-type TiO_2 was anticipated to exhibit interesting photoelectrochemical properties, in which oxidation and reduction processes could be compartmentalized within the nanostructured p-n domains.[8] Furthermore, these hybrid materials also have the potential as photoelectrodes that exhibit wavelength-dependent switching of photocurrent direction, which could be utilized in information processing devices controlled by light with varying energies.[9]

6.3: Colloidal polymerization of ferromagnetic cobalt nanoparticles

6.3.1: Preparation of hollow cobalt oxide nanowires

A novel methodology referred to as colloidal polymerization was developed to prepare well-defined polymer-coated cobalt oxide nanowires via a facile and template-free process. The colloidal polymerization process is described as a combination of dipolar nanoparticle assembly and a chemical reaction converting the colloidal precursors into a fused 1-D nanomaterial. This study enabled the preparation of large quantities of semiconductor cobalt oxide nanowires with sub-50 nm in diameter and is anticipated to exhibit enhanced activity over their bulk counterparts in various applications such as (photo)electrocatalysts for water-splitting, CO sensors, and electrochromic devices. It was found that discrete (non-aggregating) cobalt oxide nanowires spanning several hundreds of nanometers to micrometers in length were formed due to the dominant head-to-tail magnetostatic interactions. Kinetic investigation indicated that fused 1-D nanomaterials were formed after 3 hours of oxidation, while prolonged oxidation resulted in the formation of hollow inclusions in every repeating unit along the nanowires. Further calcination treatment of the amorphous polymer-coated cobalt oxide nanowires yielded polycrystalline Co_3O_4 phase while preserving the morphology of the hollow nanowires.

6.3.2: Electrochemical characterizations

The electronic and electrochemical properties of these semiconductor oxide nanowires were further explored using a wide range of spectroscopic and electrochemical characterizations for potential applications as photocatalysts for solar fuels. Although

the synthesis of discrete hollow cobalt oxide nanoparticles and cobalt selenide nanowires have been reported, this study confirmed, for the first time, the electrochemical properties of these p-type semiconductor oxide nanowires prepared via the nanoscale Kirkendall reaction. A standardized protocol in the films preparation, treatment, and electrochemical characterization were established in chapter 5. These 1-D nanostructured cobalt oxides prepared via colloidal polymerization (i.e., the combination of magnetic assembly and nanoscale Kirkendall reaction) undergo electrochemical charge transfer reactions of Co^{II} $\leftrightarrow Co^{III} \leftrightarrow Co^{IV}$ in basic media, making these nanowires attractive as potential nanostructured electrodes in energy storage and conversion devices.

6.3.3: Future directions

The concept of colloidal polymerization could be further expanded from the 'colloidal homopolymers' of cobalt oxide nanowires to 'colloidal block-copolymers' by polymerizing two different 'colloidal monomers'. This process is reminiscent of step copolymerization to yield 1-D colloidal mesostructures with controlled morphology. The ability to control structure, composition, and sequence of 1-D colloidal mesostructures, allow for systematic investigation of structure-property correlations targeted for a specific application. In particular, the main motivation of designing an asymmetric semiconductor oxide nanowire was to enhance photoelectrochemical properties of the photoelectrode by promoting the separation of photo-generated charges in solar fuel cell applications. The asymmetric nanowires are expected to create a large gradient for directed charge separation and collection.

In the proposed method, platinum-coated superparamagnetic cobalt nanoparticles or $CoPt_3$ alloy, serving as the second 'colloidal monomers', could be synthesized via transmetallation reactions.[10, 11] In the transmetallation reaction, the cobalt core (Co^0) was spontaneously reduced by Au^{3+} or Pt^{4+} complexes to form hollow AuNPs or PtNPs, respectively. Hou and Zhang et al. have elegantly demonstrated the formation of hollow metallic nanowires with Au or Pt shells via the galvanic exchange reaction utilizing the pre-assembled superparamagnetic cobalt nanoparticles as the 1-D template (in the presence of an external magnetic field). Hence, superparamagnetic cobalt nanoparticles were chosen as the precursor material over ferromagnetic nanoparticles to obtain discrete, platinum-shell, cobalt-core colloidal monomers. Alternative, an oscillating magnetic field could be applied to scramble the magnetic dipoles of ferromagnetic nanoparticles to prevent the polymerization of nanoparticles into nanowires during the transmetallation reaction, which has been illustrated by Xu et al.[12]

Through the Design of Experiments (DOE) approach discussed in chapter 4, discrete magnetic filaments could be organized into evenly spaced arrays without the need for surface-patterning processes. By introducing two "colloidal monomers" (i.e.: CoNPs and Pt-CoNPs) into the flow cell in the presence of an orthogonal magnetic field, colloidal random-copolymers could be realized. Alternatively, sequential addition of the "colloidal monomers" could result in a di-block structure with cobalt and platinum-coated cobalt colloidal meso-block copolymers. Subsequent oxidation and calcination treatment would permanently locked the vertically aligned 1-D asymmetric hollow semiconductor-metal nanowires (Schottky junction).[13] It was anticipated that photo-

generated electrons from the semiconductor Co_3O_4 are transferred to the platinum domains to generate hydrogen from water upon illumination. Concurrently, photo-generated holes along the Co_3O_4 nanowires could undergo the oxygen evolution reaction (OER). The concept of synthesizing various types of heterostructures using dipolar colloids as 'colloidal monomers', could serve as an enabling platform for structure-properties investigation in the search for efficient photoelectrocatalysts.

Although a standardized protocol for the electrochemical characterization of cobalt oxide nanowires were established, further investigation in the calcination treatment, the interfacial contact of the nanowires to the working electrode (i.e.: ITO), the surface treatment and activation of the cobalt oxide nanowires film could potentially improved the electrochemical activities of these cobalt oxide nanowires for high performance energy storage and conversion devices. The calcination procedure is a necessary step to obtain polycrystalline Co_3O_4 nanowires, which simultaneous removed the passivating polystyrene shells. However, the conductivity of ITO decreases after the calcination procedure, which could explained for the modest electrochemical activities. A systematic study on the effect of calcination temperatures on the electrochemical activities of the nanowires could be investigated to enhance the electrochemical activities of these Co_3O_4 nanowires. Similarly, a systematic investigation on the surface treatment such as acid etching[14] and UV-plasma treatment[15] on the film morphology and (photo)electrochemical activities of these cobalt oxide nanowires could lead to an efficient nanostructured (photo)electrode in energy storage and solar fuel cells application.

6.4: References

1. Zhou, Z.-H.; Liu, G.-J.; Han, D.-H. *ACS Nano* **2009,** *3*, 165-172.

2. Graetzel, M. *Nature* **2001,** *414*, 338-334.

3. Fujishima, A.; Honda, K. *Nature* **1972,** *238*, 36-37.

4. Bard, A. J.; Fox, M. A. *Acc. Chem. Res.* **1995,** *28*, (3), 141-5.

5. Bandara, J.; Weerasinghe, H. *Sol. Energy Mater. Sol. Cells* **2005,** *85*, (3), 385-390.

6. Yan, N.; Zhang, J.-G.; Tong, Y.; Yao, S.; Xiao, C.; Li, Z.; Kou, Y. *Chem. Commum.* **2009**, 4423-4425.

7. Vasquez, Y.; Sra, A. K.; Schaak, R. E. *J Am Chem Soc* **2005,** *127*, 12504-12505.

8. Long, M.; Cai, W.; Kisch, H. *J. Phys. Chem. C* **2008,** *112*, (2), 548-554.

9. Beranek, R.; Kisch, H. *Angew. Chem., Int. Ed.* **2008,** *47*, (7), 1320-1322, S1320/1-S1320/5.

10. Park, J.-I.; J., C. *J. Am. Chem. Soc.* **2001,** *123*, 5743-5746.

11. Liang, H.-P.; Zhang, H.-M.; Hu, J.-S.; Guo, Y.-G.; Wan, L.-J.; Bai, C.-L. *Angew. Chem., Int. Ed.* **2004,** *43*, 1540-1543.

12. Gao, J.; Zhang, B.; Zhang, X.; Xu, B. *Angew. Chem. Int. Ed.* **2006,** *45*, 1220-1223.

13. Nozik, A. J. *Appl. Phys. Lett.* **1977,** *30*, 567-569.

14. Nagasubramanian, G.; Gioda, A. S.; Bard, A. J. *J. Electrochem. Soc.* **1981,** *128*, 2158-2164.

15. Kim, Y.; Yoo, B. J.; Vittal, R.; Lee, Y.; Park, N.-G.; Kim, K.-J. *J. Power Sources* **2007,** *175*, 914-919.

REFERENCES

Chapter 1

1. Lalatonne, Y.; Motte, L.; Russier, V.; Ngo, A. T.; Bonville, P.; Pileni, M. P. *J. Phys. Chem. B* **2004,** *108*, (6), 1848-1854.

2. Maier, S.; Kik, P. G.; Atwater, H. A.; Meltzer, S.; Harel, E.; Koel, B. E.; Requicha, A. *Nature Mater.* **2003,** *2*, 229.

3. Braun, E.; Eichen, Y.; Sivan, U.; Ben-Yoseph, G. *Nature* **1998,** *391*, 775.

4. Fort, E.; Ricolleau, C.; Sau-Peuyo, J. *Nano Lett* **2003,** *3*, 65-67.

5. Nam, K. T.; Kim, D.-W.; Yoo, P. J.; Chiang, C.-Y.; Meethong, N.; Hammond, P. T.; Chiang, Y.-M.; Belcher, A. M. *Science* **2006,** *312*, (5775), 885-888.

6. Law, M.; Greene, L. E.; Johnson, J. C.; Saykally, R.; Yang, P. *Nat. Mater.* **2005,** *4*, (6), 455-459.

7. Sun, Y. G.; Mayers, B. T.; Xia, Y. *Adv. Mater.* **2003,** *15*, 641-646.

8. Kinge, S.; Crego-Calama, M.; Reinhoudt, D. N. *Chem. Phys. Chem.* **2008,** *9*, 20-42.

9. Minko, S.; A., K.; Gorodyska, G.; Stamm, M. *J. Am. Chem. Soc.* **2002,** *129*, 10912-10917.

10. Kiriy, A.; Minko, S.; Gorodyska, G.; Stamm, M. *Nano Lett* **2002,** *2*, 881-885.

11. Srivastava, S.; Kotov, N. A. *Soft Matter* **2009,** *5*, 1146-1156.

12. Warner, M. G.; Hutchison, J. E. *Nat. Mater.* **2003,** *2*, (4), 272-277.

13. Lee, J.; Govorov, A. O.; Kotov, N. A. *Angew. Chem. Int. Ed.* **2005,** *44*, (45), 7439-7442.

14. Dujardin, E.; Peet, C.; Stubbs, G.; Culver, J. N.; Mann, S. *Nano. Lett.* **2003,** *3*, 413-417.

15. Tang, Z.; Wang, Y.; Sun, K.; Kotov, N. A. *Adv. Mater.* **2005,** *17*, (3), 358-363.

16. Bockstaller, M. R.; Lapetnikov, Y.; Margel, S.; Thomas, E. L. *J. Am. Chem. Soc.* **2003,** *125*, 5276.

17. Bockstaller, M. R.; Mickiewics, R. A.; Thomas, E. L. *Adv. Mater.* **2005,** *17*, 1331-1349.

18. Wang, X.-S.; Guerin, G.; Wang, H.; Wang, Y.-S.; Manners, I.; Winnik, M. A. *Science* **2007,** *317*, 644-647.

19. Cui, H. G.; Chen, Z. Y.; Zhong, S.; Wooley, K. L.; Pochan, D. J. *Science* **2007,** *317*, 647-650.

20. Yin, Y.; Lu, Y.; Gates, B.; Xia, Y. N. **2001,** *123*, 8718-8729.

21. Yin, Y.; Xia, Y. *J. Am. Chem. Soc.* **2003,** *125*, (8), 2048-2049.

22. Safran, S. A. *Nature Mater.* **2003,** *2*, (2), 71-72.

23. DeVries, G. A.; Brunnbauer, M.; Hu, Y.; Jackson, A. M.; Long, B.; Neltner, B. T.; Uzun, O.; Wunsch, B. H.; Stellacci, F. *Science* **2007,** *315*, (5810), 358-361.

24. Jackson, A. M.; Myerson, J. W.; Stellacci, F. *Nat. Mater.* **2004,** *3*, (5), 330-336.

25. DeVries, G. A.; Brunnbauer, M.; Hu, Y.; Jackson, A. M.; Long, B.; Neltner, B. T.; Uzun, O.; Wunsch, B. H.; Stellacci, F. *Science* **2007,** *315*, (5810), 358-361.

26. Jackson, A. M.; Hu, Y.; Silva, P. J.; Stellacci, F. *J. Am. Chem. Soc.* **2006,** *128*, (34), 11135-11149.

27. DeVries, G. A.; Talley, C. E.; Carney, R. P.; Stellacci, F. *Adv. Mater.* **2008,** *20*, 4243-4247.

28. DeVries, G. A.; Centrone, A.; Stellacci, F. *Proc. SPIE* **2007,** *6788*, 676880Y.

29. Nie, Z.; Fava, D.; Kumacheva, E.; Zou, S.; Walker, G. C.; Rubinstein, M. *Nat. Mater.* **2007,** *6*, (8), 609-614.

30. Fava, D.; Nie, Z.-H.; Winnik, M. A.; Kumacheva, E. *Adv. Mater.* **2008,** *20*, 4318-4322.

31. Nie, Z.; Fava, D.; Rubinstein, M.; Kumacheva, E. *J. Am. Chem. Soc.* **2008,** *130*, (11), 3683-3689.

32. Pileni, M. P. *Acc. Chem. Res.* **2007,** *40*, (8), 685-693.

33. Murray, C. B.; Sun, S.; Gaschler, W.; Doyle, H.; Betley, T. A.; Kagan, C. R. *IBM J. Res. Dev.* **2001,** *45*, (1), 47-56.

34. Sobal, N. S.; Ebels, U.; Mhwald, H.; Giersig, M. *J. Phys. Chem. B* **2003,** *107*, 7351-7354.

35. Hyeon, T. *Chem. Commun.* **2003**, 927-934.

36. Murray, C. B.; Sun, S.; Doyle, H.; Betley, T. *MRS Bull.* **2001,** *26*, (12), 985-991.

37. Hilgendorff, M.; Tesche, B.; Giersig, M. *Aust. J. Chem.* **2001,** *54*, 497–501.

38. Lalatonne, Y.; Richardi, J.; Pileni, M. P. *Nat. Mater.* **2004,** *3*, (2), 121-125.

39. Germain, V.; Pileni, M. P. *Adv. Mater.* **2005,** *17*, 1424-1429.

40. Sun, S. *Adv. Mater.* **2006,** *18*, 393-403.

41. Latham, A. H.; Williams, M. E. *Acc. Chem. Res.* **2007,** *41*, 411-420.

42. Lu, A. H.; Salabas, E. L.; Schueth, F. *Angew. Chem. Int. Ed.* **2007,** *46*, (8), 1222-1244.

43. Jeong, U.; Teng, X.; Wang, Y.; Yang, H.; Xia, Y. *Adv. Mater.* **2007,** *19*, (1), 33-60.

44. Pyun, J. *Polym. Rev.* **2007,** *47*, 231-263.

45. Lin, X. M.; Jaeger, H. M.; Sorensen, C. M.; Klabunde, K. J. *J. Phys.Chem. B* **2001,** *105*, (17), 3353-3357.

46. Huber, D. L. *Small* **2005,** *1*, 482-501.

47. Rosensweig, R. E. *Sci. Am.* **1982,** *247-257*, 136.

48. Odenbach, S. *Proc. Appl. Math. Mech.* **2002,** *1*, 28-32.

49. Popplewell, J.; Rosensweig, R. E. *J. Appl. Phys. D* **1996,** *29*, (9), 2297-2203.

50. Elmore, W. C. *Phys. Rev.* **1938,** *54*, 309-310.

51. Liu, J.; Lawrence, E. M.; Wu, A.; Ivey, M. L.; Flores, G. A.; Javier, K.; Bibette, J.; Richard, J. *Phys. Rev. Lett.* **1995,** *74*, 2828-2831.

52. Massart, R. *IEEE Trans. Magn.* **1981,** *17*, 1247-1248.

53. Skjeltorp, A. T.; Ugelstad, J.; Ellingsen, T. *J. Colloid Interface Sci.* **1986,** *113*, (2), 577-82.

54. Skjeltorp, A. T.; Akselvoll, J.; de Lange Kristiansen, K.; Helgesen, G.; Toussaint, R.; Flekkoy, E. G.; Cernak, J., Self-assembly and dynamics of magnetic holes. In *Forces, growth and form in soft condensed matter: At the interface between physics and biology*, Belushkin, A. V., Ed. Kluwer Academic: Netherlands, 2004; pp 165-179.

55. Skjeltorp, A. T. *Phys. Rev. Lett.* **1983,** *51*, (25), 2306-9.

56. Skjeltorp, A. T. *J. Appl. Phys.* **1985,** *57*, (8, Pt. 2A), 3285-90.

57. Hayter, J. B.; Pynn, R.; Charles, S. W.; Skjeltorp, A. T.; Trewhella, J.; Stubbs, G.; Timmins, P. *Phys. Rev. Lett.* **1989,** *62*, 1667-1670.

58. Krebs, M. D.; Erb, R. M.; Yellen, B. B.; Samanta, B.; Bajaj, A.; Rotello, V. M.; Alsberg, E. *Nano Lett.* **2009,** *9*, 1812-1817.

59. Charles, S. W. *J. Magn. Magn. Mater.* **1990,** *85*, (1-3), 277-84.

60. Ginder, J. M. *MRS Bulletin* **1998,** *23*, (8), 26-29.
61. Winslow, W. M. *J. Appl. Phys.* **1949,** *20*, 1137-1141.

62. Bossis, G.; Lacis, S.; Meunier, A.; Volkova, O. *J. Magn. Magn. Mater.* **2002,** *252*, 224-228.

63. Jolly, M. *Mater. Res. Soc. Symp. Proc.* **2000,** *604*, 167-176.

64. Zubarev, A. Y.; Iskakova, L. Y. *Phys. Rev. E* **2000,** *61*, (5-B), 5415-5421.

65. Chantrell, R. W.; Bradbury, A.; Popplewell, J.; Charles, S. W. *J. Appl. Phys.* **1982,** *53*, 2742.

66. Promislow, J. H. E.; Gast, A. P. *Langmuir* **1996,** *12*, 4095-4102.

67. Lattuada, M.; Hatton, T. A. *J. Am. Chem. Soc.* **2007,** *129*, 12878-12889.

68. Isojima, T.; Suh, S. K.; Vander Sande, J. B.; Hatton, T. A. *Langmuir* **2009,** *25*, (14), 8292-8298.

69. Zhao, N.; Gao, M. *Adv. Mater.* **2009,** *21*, 184-187.

70. Dyab, A. K. F.; Ozmen, M.; Ersoz, M.; Paunov, V. N. *J. Mater. Chem.* **2009,** *19*, (21), 3475-3481.

71. Yuet, K. P.; Hwang, D. K.; Haghgooie, R.; Doyle, P. S. *Langmuir* **2010,** *26*, 4281-4287.

72. Zerrouki, D.; Baudry, J.; Pine, D.; Chaikin, P.; Bibette, J. *Nature* **2008,** *455*, (7211), 380-382.

73. Ge, J.-P.; Hu, Y.; Zhang, T.; Huynh, T.; Yin, Y. *Langmuir* **2008,** *24*, 3671-3680.

74. Xu, X.; Friedman, G.; Humfeld, K. D.; Majetich, S. A.; Asher, S. A. *Chem. Mater.* **2002,** *14*, 1249-1256.

75. Camargo, P. H. C.; Li, Z.-Y.; Xia, Y. *Soft Matter* **2007,** *3*, 1215-1222.

76. Xu, X.; Majetich, S. A.; Asher, S. A. *J. Am. Chem. Soc.* **2002,** *124*, (46), 13864-13868.

77. Jiles, D. C. *Acta Mater.* **2003,** *51*, (19), 5907-5939.

78. Ross, C. *Ann. Rev. Mater. Res.* **2001,** *31*, 203-235.

79. Majetich, S. A.; Jin, Y. *Science* **1999,** *284*, (5413), 470-473.

80. Frenkel, J.; Dorfman, J. *Nature* **1930,** *126*, (3173), 274.

81. Kittel, C. *Phys. Rev.* **1946,** *70*, 965-71.

82. Darling, S. B.; Bader, S. D. *J. Mater. Chem.* **2005,** *15*, (39), 4189-4195.

83. Tlusty, T.; Safran, S. A. *Science* **2000,** *290*, 1328-1331.

84. Jacobs, I. S.; Bean, C. P. *Phys Rev.* **1955,** *100*, 1060-1067.

85. de Gennes, P. G.; Pincus, P. A. *Phys.Kondens.Materie* **1970,** *11*, (3), 189-198.

86. Chantrell, R. W.; Bradbury, A.; Popplewell, J.; Charles, S. W. *J. Phys. D: Appl. Phys.* **1980,** *13*, (7), L119-L122.

87. Chantrell, R. W.; Bradbury, A.; Popplewell, J.; Charles, S. W. *J. Appl. Phys.* **1982,** *53*, (3, Pt. 2), 2742-4.

88. Weis, J. J.; Levesque, D. *Phys. Rev. Lett.* **1993,** *71*, (17), 2729-32.

89. Levesque, D.; Weis, J. J. *Phys. Rev. E.* **1994,** *49*, 5131-5140.

90. Klokkenburg, M.; Vonk, C.; Claesson, E. M.; Meeldijk, J. D.; Erne, B. H.; Philipse, A. P. *J. Am. Chem. Soc.* **2004,** *126*, (51), 16706-16707.

91. Morozov, K. I.; Shliomis, M. I. *Lecture Notes in Physics* **2002,** *594*, (Ferrofluids), 162-184.

92. Workum, K. V.; Douglas, J. F. *Phys. Rev. E.* **2005,** *71*, 031502.

93. Siracusano, S.; Stassi, A.; Baglio, V.; Arico, A. S.; Capitanio, F.; Tavares, A. C. *Electrochim. Acta* **2009,** *54*, 4844-4850.

94. Stambaugh, J.; Van Workum, K.; Douglas, J. F.; Losert, W. *Phys. Rev. E* **2005,** *72*, (3-1), 031301/1-031301/4.

95. Clarke, A. S.; Patey, G. N. *J. Chem. Phys.* **1994,** *100*, 2213-2219.

96. Lavender, H. B.; Iyer, A. K.; Singer, S. J. *J. Chem. Phys.* **1994,** *101*, (9), 7856-7867.

97. Weis, J. J. *J. Phys.: Condens. Matter* **2003,** *15*, S1471–S1495.
98. Wei, D.; Patey, G. N. *Phys. Rev. Lett.* **1992,** *68*, 2043-2045.

99. Stevens, M. J.; Grest, G. S. *Phys. Rev. Lett.* **1994,** *72*, (23), 3686-3689.

100. Stevens, M. J.; Grest, G. S. *Phys. Rev. E* **1995,** *51*, (6-A), 5976-5983.

101. Benkoski, J. J.; Jones, R. L.; Douglas, J. F.; Karim, A. *Langmuir* **2007,** *23*, 3530-3537.

102. Bazylinski, D. A.; Frankel, R. B. *Nat. Rev. Microbio.* **2004,** *2*, (3), 217-230.
103. Bazylinski, D. A.; Garratt-Reed, A. J.; Frankel, R. B. *Microsc. Res. Tech.* **1994,** *27*, (5), 389-401.

104. Penniga, I.; deWaard, H.; Moskowitz, B. M.; Bazylinski, D. A.; Frankel, R. B. *J. Magn. Magn. Mater.* **1995,** *149*, 279-286.

105. Proksh, R. B.; Schaffer, T. E.; Moskowitz, B. M.; Dahlberg, E. D.; Bazylinski, D. A.; Frankel, R. B. *Appl. Phys. Lett.* **1995,** *66*, 2582-2584.

106. Tripp, S. L.; Dunin-Borkowski, R. E.; Wei, A. *Angew. Chem. Int. Ed.* **2003,** *42*, (45), 5591-5593.

107. Klem, M. T.; Young, M.; Douglas, T. *Mater. Today* **2005,** *8*, (9), 28-37.

108. Midgley, P. A.; Dunin-Borkowski, R. *Nat. Mater.* **2009,** *8*, 271-280.

109. Kasama, T.; Posfai, M.; Chong, R. K. K.; Finlayson, A. P.; Buseck, P. R.; Frankel, R. B.; Dunin-Borkowski, R. *Am. Mineral.* **2006,** *91*, 1216-1229.

110. Philipse, A. P.; Maas, D. *Langmuir* **2002,** *18*, (9977-9984).

111. Thomas, J. R. *J. Appl. Phys.* **1966,** *37*, 2914-2915.

112. Harle, O. L.; Thomas, J. R. Dispersions of ferromagnetic cobalt particles. 3228882, 19620330., 1966.

113. Thomas, J. R. Dispersions of discrete particles of ferromagnetic metals. 3228881, 19630104., 1966.

114. Hess, P. H.; Parker, P. H., Jr. *J. Appl. Polym. Sci.* **1966,** *10*, (12), 1915-27.

115. Smith, T. W.; Wychick, D. *J. Phys. Chem.* **1980,** *84*, 1621-1629.

116. Griffiths, C. H.; O'Horo, M. P.; Smith, T. W. *J. Appl. Phys.* **1979,** *50*, 7108-7115.

117. Burke, N. A. D.; Stoever, H. D. H.; Dawson, F. P. *Chem. Mater.* **2002,** *14*, (11), 4752-4761.

118. Butter, K.; Philipse, A. P.; Vroege, G. J. *J. Magn. Magn. Mater.* **2002,** *252*, (1-3), 1-3.

119. Butter, K.; Bomans, P. H. H.; Frederick, P. M.; Vroege, J.; Philipse, A. P. *Nature Mater.* **2003,** *2*, 88.

120. Platonova, O. A.; Bronstein, L. M.; Solodovnikov, S. P.; Yanovskaya, I. M.; Obolonkova, E. S.; Valetsky, P. M.; Wenz, E.; Antonietti, M. *Colloid. Polym. Sci.* **1997,** *275*, (5), 426-431.

121. Diana, F. S.; Lee, S. H.; Petroff, P. M.; J., K. E. *Nano Letters* **2003,** *3*, 891-895.

122. Abes, J. I.; Cohen, R. E.; Ross, C. A. *Chem. Mater.* **2003,** *15*, 1125-1131.

123. Murray, C. B.; Norris, D. J.; Bawendi, M. G. *J. Am. Chem. Soc.* **1993,** *115*, 8706-8715.

124. Puntes, V. F.; Krishnan, K. M.; Alivisatos, A. P. *Science* **2001,** *291*, (5511), 2115-2117.

125. Puntes, V. F.; Gorostiza, P.; Aruguete, D. M.; Bastus, N. G.; Alivisatos, A. P. *Nature Mater.* **2004,** *3*, 263-268.

126. Puntes, V. F.; Zanchet, D.; Erdonmez, C. K.; Alivisatos, A. P. *J. Am. Chem. Soc.* **2002,** *124*, (43), 12874-12880.

127. Peng, X.-G.; Wickham, J.; Alivisatos, A. P. *J. Am. Chem. Soc.* **1998,** *120*, 5343-5344.

128. Puntes, V. F.; Bastus, N. G.; Pagonabarraga, I.; Iglesias, O.; Labarta, A.; Batlle, X. *Int. J. Nanotechnology* **2005,** *2*, 62-70.

129. Bao, Y.; Beerman, M.; Krishnan, K. M. *J. Magn. Magn. Mater.* **2003,** *266*, (3), L245-L249.

130. Chung, S. H.; McMichale, R. D.; Pierce, D. T.; Unguris, J. *Phys. Rev. B* **2010,** *81*, 024410-024417.

131. Ross, C. A.; Hwang, M.; Shima, M.; Cheng, J. Y.; Farhoud, M.; Savas, T. A.; Smith, H. I.; Schwarzacher, W. *Phys. Rev. B* **2002,** *65*, 144417-8.

132. Korth, B. D.; Keng, P.; Shim, I.; Bowles, S. E.; Tang, C.; Kowalewski, T.; Nebesny, K. W.; Pyun, J. *J. Am. Chem. Soc.* **2006,** *128*, (20), 6562-6563.

133. Keng, P. Y.; Kim, B. Y.; Shim, I.-B.; Sahoo, R.; Veneman, P. E.; Armstrong, N. R.; Yoo, H.; Pemberton, J. E.; Bull, M. M.; Griebel, J. J.; Ratcliff, E. L.; Nebesny, K. G.; Pyun, J. *ACS Nano* **2009,** *3*, 3143-3157.

134. Tripp, S. L.; Dunin-Borkowski, R. E.; Wei, A. *Angew. Chem. Int. Ed.* **2003,** *42*, 5591-5593.

135. Tripp, S. L.; Pusztay, S. V.; Ribbe, A. E.; Wei, A. *J. Am. Chem. Soc.* **2002,** *124*, (27), 7914-7915.

136. Chen, J.; Wiley, B.; McLellan, J.; Xiong, Y.; Li, Z.-Y.; Xia, Y. *Nano Lett.* **2005,** *5*, 2058-2062.

137. Hu, M.-J.; Lu, Y.; Zhang, S.; Guo, S.-R.; Lin, B.; Zhang, M.; Yu, S.-H. *J. Am. Chem. Soc.* **2008,** *130*, (11606-11607).

138. Cebula, D. J.; Charles, S. W.; Popplewell, J. *Colloid. Polym. Sci.* **1981,** *259*, 395.

139. Cebula, D. J.; Charles, S. W.; Popplewell, J. *J. Magn. Magn. Mater.* **1983,** *39*, 67.

140. Klokkenburg, M.; Erne, B. H.; Wiedenmann, A.; Petukhov, V.; Philipse, A. P. *Phys. Rev. E* **2007,** *75*, 051408.

141. Benkoski, J. J.; Bowles, S. E.; Jones, R. L.; Douglas, J. F.; Pyun, J.; Karim, A. *J. Polym. Sci., Part B: Polym. Phys.* **2008,** *46*, (20), 2267-2277.

142. Benkoski, J. J.; Bowles, S. E.; Korth, B., D.; Jones, R. A.; Douglas, J. F.; Karim, A.; Pyun, J. *J. Am. Chem. Soc.* **2007,** *129*, 6291-6297.

143. Benkoski, J. J.; Bowles, S. E.; Jones, R. A.; Douglas, J. F.; Pyun, J.; Karim, A. *J. Polym. Sci., Part B: Polym. Phys.* **2008,** *46*, 2267-2277.

144. Bowles, S. E.; Wu, W.; Kowalewski, T.; Schalnat, M.; Davis, R. J.; Pemberton, J. E.; Shim, I.; D., K. B.; Pyun, J. *J. Am. Chem. Soc.* **2007,** *129*, 8694-8695.

145. Sorensen, C. M., Magnetism. In *Nanoscale materials in chemistry*, Klabunde, K. J., Ed. John Wiley and Sons, Inc: 2001; pp 169-221.

146. Neuberger, T.; Schopf, B.; Hofmann, H.; Hofmann, M.; Von Rechenberg, B. *J. Magn. Magn. Mater.* **2005,** *293*, (1), 483-496.

147. Elmore, W. *Phys. Rev.* **1938,** *54*, 309.

148. Dave, M. J.; Mehta, R. V.; Shah, H. S.; Desai, J. N.; Naik, Y. G. *Indian J. Pure App. Phys.* **1968,** *6*, 364-366.

149. Hayes, C. F.; Hwang, S. R. *J. Coll. Inter. Sci.* **1977,** *60*, (3), 443-7.

150. Sahoo, Y.; Cheon, M.; Wang, S. X.; Luo, H.; Furlani, E. P.; Prasad, P. N. *J. Phys. Chem. B* **2004,** *108*, 3380-3383.

151. Klokkenburg, M.; Erne, B. H.; Meeldijk, J. D.; Wiedenmannm, A.; Petukhov, A. V.; Dullens, R. P. A.; Philipse, A. P. *Phys. Rev. Lett.* **2006,** *97*, 185702.

152. Pileni, M. P. *J. Phys. D: Appl. Phys.* **2008,** *41*, (134002), 1-9.

153. Jimenez, J.; Sheparovych, R.; Pita, M.; Garcia, A. N.; Dominguez, E.; Minko, S.; Katz, E. *J. Phys. Chem. C* **2008,** *112*, 7337-7344.

154. Hone, J.; Whitney, M.; Piskoti, C.; Zettl, A. *Phys. Rev. B* **1999,** *59*, R2514-R2516.

155. Du, F.; Fischer, J. E.; Winey, K. I. *Phys. Rev. B* **2005,** *72*, 121404-121404-4.

156. Correa-Duarte, M. A.; Grzelczak, M.; Salgueirino-Maceira, V.; Giersig, M.; Liz-Marzan, L. M.; Farle, M.; Sierazdki, K.; Diaz, R. *J. Phys. Chem. B.* **2005,** *109*, 19060-19063.

157. Yuan, J.; Gao, H.; Schacher, F.; Xu, Y.; Richter, R.; Tremel, W.; Muller, A. H. E. *ACS Nano* **2009,** *3*, 1441-1450.

158. Williams, M. E.; Hutchins, B. M.; Platt, M.; Hancock, W. O. *ECS Trans.* **2007,** *3*, 1-7.

159. Wilson, R. J.; Hu, W.; Wong, C. P. F.; Koh, A. L.; Gaster, R. S.; Earhart, C. M.; Fu, A.-H.; Heilshorn, S. C.; Sinclair, R.; Wang, S. X. *J. Magn. Magn. Mater.* **2009,** *321*, 1452-1458.

160. Cheng, G.; Romero, D.; Fraser, G. T.; Hight Walker, A. R. *Langmuir* **2005,** *21*, 12055-12059.

161. Wang, H.; Chen, Q.-W.; Sun, L.-X.; Qi, H.-P.; Yang, X.; Zhou, S.; Xiong, J. *Langmuir* **2009,** *25*, 7135-7139.

162. Legrand, J.; Ngo, A. T.; Petit, C.; Pileni, M. P. *Adv. Mater.* **2001,** *13*, (1), 58-62.

163. Germain, V.; Richard, J.; Ingert, D.; Pileni, M. P. *J. Phys. Chem. B.* **2005,** *109*, 5541-5547.

164. Germain, V.; Pileni, M. P. *J. Phys. Chem. B* **2005,** *109*, 5548-5553.

165. Chitu, L.; Chushkin, Y.; Luby, S.; Majkova, E.; Satka, A.; Ivan, J.; Smrcok, L.; Buchal, A.; Giersig, M.; Hilgendorff, M. *Mater. Sci. Eng. C* **2007,** *27*, 23-28.

166. Kim, Y.; Yoo, B. J.; Vittal, R.; Lee, Y.; Park, N.-G.; Kim, K.-J. *J. Power Sources* **2007,** *175*, 914-919.

167. Pileni, M. P. *Acc. Chem. Res.* **2007,** *40*, (8), 685-693.

168. Maye, M. M.; Nykypanchuk, D.; Cuisinier, M.; Lelie, D. v. d.; Gang, O. *Nature Mater.* **2009,** *8*, 388-391.

169. Shenhar, R.; Rotello, V. M. *Acc. Chem. Res.* **2003,** *36*, (7), 549-561.

170. Perepichka, D. F.; Rosei, F. *Angew. Chem. Int. Ed.* **2007,** *46*, 6006-6008.

171. Prabhu, V. M.; Hudson, S. D. *Nature Mater.* **2009,** *8*, 365-366.

172. Philip, J.; Mondain-Monval, O.; Calderon, F. L.; Bibette, J. *J. Phys. D: Appl. Phys.* **1997,** *30*, 2798-2803.

173. Goubault, C.; Jop, P.; Fermigier, M.; Baudry, J.; Bertrand, E.; Bibette, J. *Phys. Rev. Lett.* **2003,** *91*, (26, Pt. 1), 260802/1-260802/4.

174. Cohen-Tannoudji, L.; Bertrand, E.; Bressy, L.; Goubault, C.; Baudry, J.; Klein, J.; Joanny, J.-F.; Bibette, J. *Phys. Rev. Lett.* **2005,** *94*, (3), 038301/1-038301/4.

175. Goubault, C.; Leal-Calderon, F.; Viovy, J.-L.; Bibette, J. *Langmuir* **2005,** *21*, (9), 3725-3729.

176. Wang, N.; Cao, X.; Kong, D.; W., C.; Guo, L.; C., C. *J. Phys. Chem. C* **2008,** *112*, 6613-6619.

177. Sheparovych, R.; Sahoo, Y.; Motornov, M.; Wang, S. X.; Luo, H.; Prasad, P. N.; Sokolov, I.; Minko, S. *Chem. Mater.* **2006,** *18*, 591-593.

178. Xiong, Y.; Chen, Q.; Tao, N.; Ye, J.; Tang, Y.; Feng, J.; Gu, X. *Nanotechnology* **2007,** *18*, (34), 345301/1-345301/5.

179. Corr, S. A.; Byrne, S. J.; Tekoriute, R.; Meledandri, C. J.; Brougham, D. F.; Lynch, M.; Kerskens, C.; O'Dwyer, L.; Gun'ko, Y. K. *J. Am. Chem. Soc.* **2008,** *130*, (13), 4214-4215.

180. Byrne, S. J.; Corr, S. A.; Gun'ko, Y. K.; Kelly, J. M.; Brougham, D. F.; Ghosh, S. *Chem. Commun.* **2004**, (22), 2560-2561.

181. Furst, E. M.; Suzuki, C.; Fermigier, M.; Gast, A. P. *Langmuir* **1998,** *14*, (26), 7334-7336.

182. Furst, E. M.; P., G. A. *Phys. Rev. Lett.* **1999,** *82*, 4130-4133.

183. Furst, E. M.; Gast, A. P. *Phys. Rev. E: Stat. Phys., Plasmas, Fluids, Relat. Interdiscip. Top.* **2000,** *62*, (5-B), 6916-6925.

184. Biswal, S. L.; Gast, A. P. *Phys. Rev. E: Stat., Nonlinear, Soft Matter Phys.* **2003,** *68*, (2-1), 021402/1-021402/9.

185. Dreyfus, R.; Baudry, J.; Roper, M. L.; Fermigier, M.; Stone, H. A.; Bibette, J. *Nature* **2005,** *437*, 862.

186. Li, D.; Rogers, J.; Biswal, S. L. *Langmuir* **2009,** *25*, 8944-8950.

187. Lyles, B. F.; Terrot, M. S.; Hammond, P. T.; Gast, A. P. *Langmuir* **2004,** *20*, (8), 3028-3031.

188. Singh, H.; Laibinis, P. E.; Hatton, T. A. *Nano Lett.* **2005,** *5*, 2149-2154.

189. Benkoski, J. J.; Deacon, R. M.; Land, H. B.; Baird, L. M.; Breidenich, J. L.; Srivivasan, R.; Clatterbaugh, G. V.; Keng, P. Y.; Pyun, J. *Soft Matter* **2010,** 6, 602-609.

190. Centrone, A.; Hu, Y.; Jackson, A. M.; Zerbi, G.; Stellacci, F. *Small* **2007,** *3*, (5), 814-817.

191. Nakata, K.; Hu, Y.; Uzun, O.; Barkr, O.; Stellacci, F. *Adv. Mater.* **2008,** *20*, 4294-4299.

192. Redl, F. X.; Cho, K.-S.; Murray, C. B.; O'Brien, S. *Nature* **2003,** *423*, 968-971.

193. Manoharan, V. M.; Elsesser, M. T.; Pine, D. J. *Science* **2003,** *301*, 483-487.

194. Park, J.-I.; Kim, M. G.; Jun, Y.-W.; Lee, J. S.; Lee, W.-R.; Cheon, J. *J. Am. Chem. Soc.* **2004,** *126*, 9072-9078.

195. Frankamp, B. L.; Boal, A. K.; Tuominen, M.; Rotello, V. *J. Am. Chem. Soc.* **2005,** *127*, 9731-9735.

196. Philipse, A. P.; van Bruggen, M. P. B.; Pathmamanoharan, C. *Langmuir* **1994,** *10*, 92-99.

197. Ohmori, M.; Matijevic, E. *J. Coll. Inter. Sci.* **1992,** *150*, 594.

198. Ohmari, M.; Matijevic, E. *J. Coll. Inter. Sci.* **1993,** *160*, 288-292.

199. Kobayashi, K.; Horie, M.; Konno, M.; Rodriguez-Gonzalez, B.; Liz-Marzan, L. M. *J. Phys. Chem. B.* **2003,** *107*, 7420-7425.

200. Salgueirino-Maceira, V.; Correa-Duarte, M. A.; Hucht, A.; Farle, M. *J. Magn. Magn. Mater.* **2006,** *303*, (1), 163-166.

201. Salgueirino-Maceira, V.; Correa-Duarte, M. A. *J. Mater. Chem.* **2006,** *16*, 3593-3597.

202. Zhang, F.; Wang, C.-C. *J. Phys. Chem. C* **2008,** *112*, (39), 15151-15156.

203. Singh, H.; Laibinis, P. E.; Hatton, T. A. *Langmuir* **2005,** *21*, (24), 11500-11509.

204. Liu, S.; Wood, L. F.; Ohman, D. E.; Collinson, M. M. *Chem. Mater.* **2007,** *19*, 2752-2756.

205. Zhuang, J.; Wu, H.-M.; Yang, Y.-G.; Cao, C. *J. Am. Chem. Soc.* **2007,** *129*, 14166-14167.

206. Kowalewski, T.; Tsarevsky, N. V.; Matyjaszewski, K. *J. Am. Chem. Soc.* **2002,** *124*, 10632-10633.

207. Kulkarni, P.; McCullough, L. A.; Kowalewski, T.; Porter, L. M. *Synthetic Metals* **2009,** *159*, (3-4), 177-181.

208. Kulbaba, K.; Resendes, R.; Cheng, A.; Bartole, A.; Safa-Sefat, A.; Coombs, N.; Stover, H. D. H.; Greedan, J. E.; Ozin, G. A.; Manners, I. *Adv. Mater.* **2001,** *13*, 732-736.

209. Liu, Y.; Chen, Q. *Nanotechnology* **2008,** *19*, (47), 475603/1-475603/6.

210. Marinakos, S. M.; Novak, J. P.; Brousseau III, L. C.; House, B.; Edeki, E. M.; Feldhaus, J. C.; Feldheim, D. L. *J. Am. Chem. Soc.* **1999,** *121*, 8518-8522.

211. Skrabalak, S. E.; Chen, J.; Sun, Y.; Lu, X.; Au, L.; Cobley, C. M.; Xia, Y. *Acc. Chem. Res.* **2008,** *41*, (12), 1587-1595.

212. Kim, S.-W.; M., K.; Lee, W. Y.; Hyeon, T. *J. Am. Chem. Soc.* **2002,** *124*, 7642-7643.

213. Oldenburg, S. J.; Averitt, R. D.; Westcott, S. L.; Halas, N. J. *Chem. Phys. Lett.* **1998,** *288*, 243-247.

214. Chen, J.; Wiley, B. J.; J., M.; Xiong, Y.; Li, Z.-Y.; Xia, Y. N. *Nano. Lett.* **2005,** *5*, 2058-2062.

215. Chen, J.; Saeki, F.; Wiley, B. J.; Cang, H.; Cobb, M. J.; Li, Z.-Y.; Au, L.; Zhang, H.; Kimmey, M. B.; Li, X.; Xia, Y. N. *Nano Lett* **2005,** *5*, 473-477.

216. Bard, A. J.; Faulkner, L. R., *Electrochemical methods: Fundamentals and applications*. 2 ed.; John Wiley & Sons, Inc: 2001.

217. Liang, H.-P.; Zhang, H.-M.; Hu, J.-S.; Guo, Y.-G.; Wan, L.-J.; Bai, C.-L. *Angew. Chem., Int. Ed.* **2004,** *43*, 1540-1543.

218. Vasquez, Y.; Sra, A. K.; Schaak, R. E. *J. Am. Chem. Soc.* **2005,** *127*, 12504-12505.

219. Guo, S.; Fang, Y.; Dong, S.; Wang, E. *J. Phys. Chem. C.* **2007,** *111*, 17104-17109.

220. Guo, S.; Dong, S.; Wang, E. *J. Phys. Chem. C.* **2009,** *113*, 5485-5492.

221. Zeng, J.; Huang, J.; Lu, W.; Wang, X.; Wang, B.; Zhang, S.; Hou, J. *Adv. Mater.* **2007,** *19*, 2172-2176.

222. Zhai, J.; Huang, M.; Zhai, Y.; Dong, S. *J. Mater. Chem.* **2007,** *18*, 923-928.

223. Schwartzberg, A. M.; Olson, T. Y.; Talley, C. E.; Zhang, J. Z. *J. Phys. Chem. C* **2007,** *111*, (44), 16080-16082.

224. Liang, H.-P.; Wan, L.-J.; Bai, C.-L.; Jiang, L. *J. Phys. Chem. B* **2005,** *109*, 7795-7800.

225. Smigelskas, A. D.; Kirkendall, E. O. *Trans. AIME* **1947,** *171*, 130.

226. Fan, H. J.; Goseles, U.; Zacharias, M. *Small* **2007,** *3*, (10), 1660-1671.

227. Yin, Y.; Rioux, R. M.; Erdonmez, C. K.; Hughes, S.; Somorjai, G. A.; Alivisatos, A. P. *Science* **2004,** *304*, (5671), 711-714.

228. Yin, Y.; Erdonmez, C. K.; Cabot, A.; Hughes, S.; Alivisatos, A. P. *Adv. Funct. Mater.* **2006,** *16*, (11), 1389-1399.

229. Cabot, A.; Puntes, V. F.; Shevchenko, E.; Yin, Y.; Balcells, L.; Marcus, M. A.; Hughes, S.; Alivisatos, A. P. *J. Am. Chem. Soc.* **2007,** *129*, 10358-10360.

230. Gao, J.; Zhang, B.; Zhang, X.; Xu, B. *Angew. Chem. Int. Ed.* **2006,** *45*, 1220-1223.

231. Keng, P. Y.; Kim, B. Y.; Shim, I.; Sahoo, R.; Veneman, P. E.; Armstrong, N. R.; Yoo, H.-M.; Pemberton, J. E.; Bull, M. M.; Griebel, J. J.; Ratcliff, E. L.; W., N. K.; Pyun, J. *ACS Nano* **2009,** *3*, (10), 3143-3157.

Chapter 2

1. Klokkenburg, M.; Vonk, C.; Claesson, E. M.; Meeldijk, J. D.; Erne, B. H.; Philipse, A. P. *J. Am. Chem. Soc.* **2004,** *126*, (51), 16706-16707.

2. Goubault, C.; Leal-Calderon, F.; Viovy, J.-L.; Bibette, J. *Langmuir* **2005,** *21*, (9), 3725-3729.

3. Grzybowski, B. A.; Stone, H. A.; Whitesides, G. M. *Nature* **2000,** *405*, 1033-1036.

4. Germain, V.; Pileni, M.-P. *Adv. Mater.* **2005,** *17*, (11), 1424-1429.

5. Cheng, G.; Romero, D.; Fraser, G. T.; Walker, A. R. H. *Langmuir* **2005,** *21*, (26), 12055-12059.

6. Thomas, J. R. *J. Appl. Phys.* **1966,** *37*, (7), 2914-15.

7. Safran, S. A. *Nature Mater.* **2003,** *2*, (2), 71-72.

8. Bao, Y.; Beerman, M.; Krishnan, K. M. *J. Magn. Magn. Mater.* **2003,** *266*, (3), L245-L249.

9. Vestal, C. R.; Zhang, Z. J. *J. Am. Chem. Soc.* **2002,** *124*, (48), 14312-14313.

10. Marutani, E.; Yamamoto, S.; Ninjbadgar, T.; Tsujii, Y.; Fukuda, T.; Takano, M. *Polymer* **2004,** *45*, (7), 2231-2235.

11. Platonova, O. A.; Bronstein, L. M.; Solodovnikov, S. P.; Yanovskaya, I. M.; Obolonkova, E. S.; Valetsky, P. M.; Wenz, E.; Antonietti, M. *Colloid. Polym. Sci.* **1997,** *275*, (5), 426-431.

12. Rutnakornpituk, M.; Thompson, M. S.; Harris, L. A.; Farmer, K. E.; Esker, A. R.; Riffle, J. S.; Connolly, J.; St. Pierre, T. G. *Polymer* **2002,** *43*, (8), 2337-2348.

13. Sohn, B. H.; Cohen, R. E. *Chem. Mater.* **1997,** *9*, (1), 264-269.

14. Tadd, E. H.; Bradley, J.; Tannenbaum, R. *Langmuir* **2002,** *18*, (6), 2378-2384.

15. Wang, X.-S.; Arsenault, A.; Ozin, G. A.; Winnik, M. A.; Manners, I. *J. Am. Chem. Soc.* **2003,** *125*, (42), 12686-12687.

16. Garcia, C. B. W.; Zhang, Y.; Mahajan, S.; DiSalvo, F.; Wiesner, U. *J. Am. Chem. Soc.* **2003,** *125*, (44), 13310-13311.

17. Sun, S.; Murray, C. B. *J. Appl. Phys.* **1999,** *85*, (8, Part 2A), 4324-4330.

18. Griffiths, C. H.; O'Horo, M. P.; Smith, T. W. *J. Appl. Phys.* **1979,** *50*, 7108-7115.

19. Burke, N. A. D.; Stoever, H. D. H.; Dawson, F. P. *Chem. Mater.* **2002,** *14*, (11), 4752-4761.

20. Matyjaszewski, K.; Xia, J. *Chem. Rev.* **2001,** *101*, (9), 2921-2990.

21. Hawker, C. J.; Bosman, A. W.; Harth, E. *Chem. Rev.* **2001,** *101*, (12), 3661-3688.

22. Benoit, D.; Chaplinski, V.; Braslau, R.; Hawker, C. J. *J. Am. Chem. Soc.* **1999,** *121*, (16), 3904-3920.

23. Skaff, H.; Ilker, M. F.; Coughlin, E. B.; Emrick, T. *J. Am. Chem. Soc.* **2002,** *124*, (20), 5729-5733.

24. Puntes, V. F.; Krishnan, K. M.; Alivisatos, A. P. *Science* **2001,** *291*, (5511), 2115-2117.

25. Puntes, V. F.; Zanchet, D.; Erdonmez, C. K.; Alivisatos, A. P. *J. Am. Chem. Soc.* **2002,** *124*, (43), 12874-12880.

26. Redl, F. X.; Cho, K.-S.; Murray, C. B.; O'Brien, S. *Nature* **2003,** *423*, 968-971.

27. Shevchenko, E. V.; Talapin, D. V.; Rogach, A. L.; Weller, H. *Nanopart. Assem. Superstruct.* **2006**, 341-368.

28. Urban, J. J.; Talapin, D. V.; Shevchenko, E.; Kagan, C. R.; Murray, C. B. *Nature Mater.* **2007,** *6*, 115-121.

29. Zeng, H.; Li, J.; Liu, J. P.; Wang, Z. L.; Sun, S. *Nature* **2002,** *420*, 395.

30. Stober, W.; Fink, A. *J. Coll. Inter. Sci.* **1968,** *26*, 62-69.

31. Philipse, A. P.; Vrij, A. *J. Colloid Interface Sci.* **1989,** *128*, (1), 121-36.

32. Van Helden, A. K.; Jansen, J. W.; Vrij, A. *J. Coll. Inter. Sci.* **1981,** *2*, 354-368.

33. Latham, A. H.; Williams, M. E. *Acc. Chem. Res.* **2007,** *41*, 411-420.

34. Puntes, V. F.; Gorostiza, P.; Aruguete, D. M.; Bastus, N. G.; Alivisatos, A. P. *Nature Mater.* **2004,** *3*, (4), 263-268.

35. Harrowven, D. C.; Guy, I. L. *Chem. Comm.* **2004,** *17*, 1968-1969.

Chapter 3

1. Furst, E. M.; Suzuki, C.; Fermigier, M.; Gast, A. P. *Langmuir* **1998,** *14*, (26), 7334-7336.

2. Furst, E. M.; Gast, A. P. *Phys. Rev. Lett.* **1999,** *82*, (20), 4130-4133.

3. Sun, S.; Murray, C. B.; Weller, D.; Folks, L.; Moser, A. *Science* **2000,** *287*, (5460), 1989-1992.

4. Cohen-Tannoudji, L.; Bertrand, E.; Bressy, L.; Goubault, C.; Baudry, J.; Klein, J.; Joanny, J.-F.; Bibette, J. *Phys. Rev. Lett.* **2005,** *94*, (3), 038301/1-038301/4.

5. Goubault, C.; Leal-Calderon, F.; Viovy, J.-L.; Bibette, J. *Langmuir* **2005,** *21*, (9), 3725-3729.

6. Singh, H.; Laibinis, P. E.; Hatton, T. A. *Nano Lett.* **2005,** *5*, 2149-2154.

7. Singh, H.; Laibinis, P. E.; Hatton, T. A. *Langmuir* **2005,** *21*, 11500-11509.

8. ingh, H.; Hatton, T. A. *J. Magn. Magn. Mater.* **2007,** *315*, 53-64.

9. Hess, P. H.; Parker, P. H., Jr. *J. Appl. Polym. Sci.* **1966,** *10*, (12), 1915-27.

10. Thomas, J. R. *J. Appl. Phys.* **1966,** *37*, 2914-2915.

11. de Gennes, P. G.; Pincus, P. A. *Phys.Kondens.Materie* **1970,** *11*, (3), 189-198.

12. Griffiths, C. H.; O'Horo, M. P.; Smith, T. W. *J. Appl. Phys.* **1979,** *50*, 7108-7115.

13. Chantrell, R. W.; Bradbury, A.; Popplewell, J.; Charles, S. W. *J. Phys. D: Appl. Phys.* **1980,** *13*, (7), L119-L122.

14. Chantrell, R. W.; Bradbury, A.; Popplewell, J.; Charles, S. W. *J. Appl. Phys.* **1982,** *53*, (3, Pt. 2), 2742-4.

15. Cheng, G.; Romero, D.; Fraser, G. T.; Hight Walker, A. R. *Langmuir* **2005,** *21*, 12055-12059.

16. Gao, J.; Zhang, B.; Zhang, X.; Xu, B. *Angew. Chem. Int. Ed.* **2006,** *45*, 1220-1223.

17. Tripp, S. L.; Puzstay, S. V.; Ribbe, A. E.; Wei, A. *J. Am. Chem. Soc.* **2002,** *124*, 7914-7915.

18. Tripp, S. L.; Dunin-Borkowski, R. E.; Wei, A. *Angew. Chem. Int. Ed.* **2003,** *42*, 5591-5593.

19. Xiong, Y.; Ye, J.; Gu, X.; Chen, Q. *J. Phys. Chem. B* **2007,** *111*, 6998-7003.

20. Chen, M.; Liu, J. P.; Sun, S. *J. Am. Chem. Soc.* **2004,** *126*, (27), 8394-8395.

21. Farrell, D.; Cheng, Y.; Ding, Y.; Yamamuro, S.; Sanchez-Hanke, C.; Kao, C.; Majetich, S. A. *J. Magn. Magn. Mater.* **2004,** *282*, 1-5.

22. Farrell, D.; Cheng, Y.; McCallum, R. W.; Sachan, M.; Majetich, S. A. *J. Phys. Chem. B* **2005,** *109*, 13409-13419.

23. Farrell, D.; Ding, Y.; Majetich, S. A.; Sanchez-Hanke, C.; Kao, C. *J. Appl. Phys.* **2004,** *95*, 6636-6638.

24. Goa, Y. H. B., Y.P.; Beerman, M.; Yasuhara, A.; Shindo, D.; Krishnan, K. *Appl. Phys. Lett.* **2004,** *84*, (17), 3361.

25. Puntes, V. F.; Gorostiza, P.; Aruguete, D. M.; Bastus, N. G.; Alivisatos, A. P. *Nature Mater.* **2004,** *3*, 263-268.

26. Sun, S.; Murray, C. B. *J. Appl. Phys.* **1999,** *85*, (8, Pt. 2A), 4325-4330.

27. Hilgendorff, M.; Tesche, B.; Giersig, M. *Aust. J. Chem.* **2001,** *54*, 497–501.

28. Pileni, M.-P. *Adv. Func. Mater.* **2001,** *11*, (5), 323-336.

29. Pileni, M. P. *J. Phys. Chem. B* **2001,** *105*, (17), 3358-3371.

30. Lalatonne, Y.; Motte, L.; Russier, V.; Ngo, A. T.; Bonville, P.; Pileni, M. P. *J. Phys. Chem. B* **2004,** *108*, (6), 1848-1854.

31. Lalatonne, Y.; Richardi, J.; Pileni, M. P. *Nature Mater.* **2004,** *3*, (2), 121-125.

32. Giersig, M.; Hilgendorff, M. *Eur. J. Inorg. Chem* **2005**, 3571-3583.

33. Pileni, M. P. *Acc. Chem. Res.* **2007,** *40*, (8), 685-693.

34. Shen, L.; Stachowiak, A.; Fateen, S.-E. K.; Hatton, T. A. *Langmuir* **2001,** *17*, 288-299.

35. Butter, K.; Philipse, A. P.; Vroege, G. J. *J. Magn. Magn. Mater.* **2002,** *252*, (1-3), 1-3.

36. Butter, K.; Bomans, P. H. H.; Frederik, P. M.; Vroege, G. J.; Philipse, A. P. *Nature Mater.* **2003,** *2*, (2), 88-91.

37. Klokkenburg, M.; Vonk, C.; Claesson, E.; Meeldijk.J.; Erne, B.; Philipse, A. *J. Am. Chem. Soc.* **2004,** *126*, 16706-16707.

38. Benkoski, J. J.; Bowles, S. E.; Korth, B. D.; Jones, R. L.; Douglas, J. F.; Karim, A.; Pyun, J. *J. Am. Chem. Soc.* **2007,** *129*, 6291-6297.

39. Benkoski, J. J.; Jones, R. L.; Douglas, J. F.; Karim, A. *Langmuir* **2007,** *23*, 3530-3537.

40. Hyeon, T. *Chem. Commun.* **2003**, 927-934.

41. Lu, A.-H.; Salabas, E. L.; Schuth, F. *Angew. Chem. Int. Ed.* **2007,** *46*, 1222-1224.

42. Leslie-Pelecky, D. L.; Rieke, R. D. *Chem. Mater.* **1996,** *8*, (8), 1770-1783.

43. Pyun, J. *Polym. Rev.* **2007,** *47*, 231-263.

44. Burke, N. A. D.; Stover, H. D. H.; Dawson, F. R. *Chem. Mater.* **2002,** *14*, 4752-4761.

45. Grubbs, R. B. *J. Polym. Sci., Part A: Polym. Chem.* **2005,** *43*, 4323-4336.

46. Balazs, A. C.; Emrick, T.; Russell, T. P. *Science* **2006,** *314*, 1107-1110.

47. Glogowski, E.; Tangirala, R.; Russell, T. P.; Emrick, T. *J. Polym. Sci., Part A: Polym. Chem.* **2006,** *44*, 5076-5086.

48. Grubbs, R. B. *Polym. Rev.* **2007,** *47*, 197-215.

49. Boal, A. K.; Frankamp, B. L.; Uzun, O.; Tuominen, M. T.; Rotello, V. M. *Chem. Mater.* **2004,** *16*, (17), 3252-3256.

50. Hong, R.; Fisher, N. O.; Emrick, T.; Rotello, V. M. *Chem. Mater* **2005,** *17*, 4617-4621.

51. Frankamp, B. L.; Fischer, N. O.; Hong, R.; Srivastava, S.; Rotello, V. M. *Chem Mater.* **2006,** *18*, (4), 956-959.

52. Lutz, J.-F.; Stiller, S.; Hoth, A.; Kaufner, L.; Pison, U.; Cartier, R. *Biomacromol.* **2006,** *7*, 3132-3138.

53. Xie, J.; Xu, C.; Xu, Z.; Hou, Y.; Young, K. L.; Wang, S. X.; Pourmond, N.; Sun, S. *Chem. Mater.* **2006,** *18*, (23), 5401-5403.

54. Frankamp, B. L.; Boal, A. K.; Tuominen, M. T.; Rotello, V. M. *J. Am. Chem. Soc.* **2005,** *127*, (27), 9731-9735.

55. Kim, B.-S.; Qiu, J.-M.; Wang, J.-P.; Taton, T. A. *Nano Lett.* **2005,** *5*, (10), 1987-1991

56. Kim, M. S.; Y.F., C.; Liu, Y. C.; Peng, X. G. *Adv. Mater.* **2005,** *17*, 1429-1432.

57. Vestal, C. R.; Zhang, Z. J. *J. Am. Chem. Soc.* **2002,** *124*, (48).

58. Matsuno, R.; Yamamoto, K.; Otsuka, H.; Takahara, A. *Chem. Mater.* **2003,** *15*, (1), 3-5.

59. Wang, Y.; Teng, X.; Wang, J.-S.; Yang, H. *Nano Letters* **2003,** *3*, 789-793.

60. Marutani, E.; Yamamoto, S.; Ninjbadgar, T.; Tsujii, Y.; Fukuda, T.; Takano, M. *Polymer* **2004,** *45*, (7), 2231-2235.

61. Matsuno, R.; Yamamoto, K.; Otsuka, H.; Takahara, A. *Macromol.* **2004,** *37*, (6), 2203-2209.

62. Ninjbadgar, T.; Yamamoto, S.; Fukuda, T. *Solid State Sci* **2004,** *6*, 879-885.

63. Gravano, S. M.; Dumas, R.; Liu, K.; Patten, T. E. *J. Polym. Sci., Part A: Polym. Sci.* **2005,** *43*, 3675-3688.

64. Gelbrich, T. F., M.; Schmidt, A. M. *Macromol.* **2006,** *39*, (9), 3469-3472.

65. Sun, Y.; Ding, X.; Zheng, Z.; Cheng, X.; Hu, X. P., Y. *Chem. Commun.* **2006,** *26*,

2765-2767.

66. Wakamatsu, H.; Yamamota, K.; Nakao, A.; Aoyagi, T. *J. Magn. Magn. Mater* **2006,** *302*, (2), 327-333.

67. Lattuada, M.; Hatton, T. A. *Langmuir* **2007,** *23*, 2158-2168.

68. Hess, P. H.; Parker, P. H. *J. Appl. Polym. Sci.* **1966,** *10*, 1915.

69. Platonova, O. A.; Bronstein, L. M.; Solodovnikov, S. P.; Yanovskaya, I. M.; Obolonkova, E. S.; Valetsky, P. M.; Wenz, E.; Antonietti, M. *Colloid Polym. Sci.* **1997,** *275*, 426-431.

70. Rutnakornpituk, M. T., M.S.; Harris, L.A.; Farmer K.E.; Esker, A.R.; Riffle, J.S.; Connolly, J.; Pierre, T.G. *Polymer* **2002,** *43*, 2337-2348.

71. Tadd, E.; Bradley, J.; Tannenbaum, R. *Langmuir* **2002,** *18*, 2378-2384.

72. Diana, F. S.; Lee, S.-H.; Petroff, P. M.; Kramer, E. J. *Nano Lett.* **2003,** *3*, (7), 891-895.

73. Liu, G. J.; Yan, X. H.; Curda, C.; Lal, J. *Chem. Mater.* **2005,** *17*, 4985-4991.

74. Puntes, V. F.; Krishnan, K. M.; Alivisatos, A. P. *Science* **2001,** *291*, (5511), 2115-2117.

75. Puntes, V. F.; Zanchet, D.; Erdonmez, C. K.; Alivisatos, A. P. *J. Am. Chem. Soc.* **2002,** *124*, (43), 12874-12880.

76. Korth, B. D.; Keng, P.; Shim, I.; Bowles, S. E.; Tang, C.; Kowalewski, T.; Nebesny, K. W.; Pyun, J. *J. Am. Chem. Soc.* **2006**, (128), 6562-6563.

77. Hawker, C. J.; Bosman, A. W.; Harth, E. *Chem. Rev.* **2001,** *101*, (12), 3661-3688.

78. Lacroix-Desmazes, P.; Lutz, J. F.; Chauvin, F.; Severac, R.; Boutevin, B. *Macromol.* **2001,** *34*, 8866-8871.

79. Matyjaszewski, K.; Xia, J. *Chem. Rev.* **2001,** *101*, 2921-2990.

80. Ing, H. R.; Manske, R. H. F. *J. Am. Chem. Soc.* **1926,** *48*, 2348-2351.

81. Williams, R. H.; Hamilton, L. A. *J. Am. Chem. Soc.* **1952,** *74*, 5418-5419.

82. Skaff, H.; Ilker, M. F.; Coughlin, E. B.; Emrick, T. *J. Am. Chem. Soc.* **2002,** *124*, (20), 5729-5733.

83. Witt, D.; Rachon, J. *Phosphorus, sulfur and silicon* **1994,** *91*, 153-164.

84. Pascual, S.; Coutin, B.; Tardi, M.; A., P.; J.-P, V. *Macromol.* **1999**, (32), 1432-1437.

85. Samia, A.; Hyzer, K.; Schlueter, J.; Qin, C.-J.; Jiang, S.; Bader, S.; Lin, X.-M. *J. Am. Chem. Soc.* **2005,** *127*, G126-4126.

86. Weis, J. J. *J. Phys.: Condens. Matter* **2003,** *15*, S1471–S1495.

87. Diehl, M. R.; Yu, J.-Y.; Heath, J. R.; Held, G. A.; Doyle, H.; Sun, S.; Murray, C. B. *J. Phys. Chem. B* **2001,** *105*, (33), 7913-7919.

88. Bao, Y.; Beerman, M.; Krishnan, K. M. *J. Magn. Magn. Mater.* **2003,** *266*, L245-L249.

89. Dinega, D. P.; Bawendi, M. G. *Angew. Chem. Int. Ed.* **1999,** *38*, (12), 1788-1791.

90. Sun, S.; Murray, C. B. *J. Appl. Phys.* **1999,** *85*, (8), 4325-4330.

91. Wei, D.; Patey, G. N. *Phys. Rev. Lett.* **1992,** *68*, 2043-2045.

92. Stevens, M. J.; Grest, G. S. *Phys. Rev. Lett.* **1994,** *72*, (23), 3686-3689.

93. Stevens, M. J.; Grest, G. S. *Phys. Rev. E* **1995,** *51*, (6-A), 5976-5983.

94. Stevens, M. J.; Grest, G. S. *Phys. Rev. E* **1995,** *51*, (6-A), 5962-75.

95. Tlusty, T.; Safran, S. A. *Science* **2000,** *290*, 1328-1331.

96. Stambaugh, J.; Van Workum, K.; Douglas, J. F.; Losert, W. *Phys. Rev. E* **2005,** *72*, (3-1), 031301/1-031301/4.

97. Van Workum, K.; Douglas, J. F. *Phys. Rev. E* **2005,** *71*, (3-1), 031502/1-031502/15.

98. Van Workum, K.; Douglas, J. F. *Phys. Rev. E* **2006,** *73*, (3-1), 031502/1-031502/17.

99. Lavender, H. B.; Iyer, A. K.; Singer, S. J. *J. Chem. Phys.* **1994,** *101*, (9), 7856-7867.

100. Miller, M. A.; Wales, D. J. *J. Phys. Chem. B* **2005,** *109*, 23109-23112.

101. Arshady, R.; Kenner, G. W.; Ledwith, A. *Makromol. Chem* **1976**, (177), 2911-2918.

102. Ryu, S. W.; Hirao, A. *Macromol.* **2000,** *33*, 4765-4771.

Chapter 4

1 Fearing, R. S. "Challenges for Effective Millirobots," *Int. Symp. on Micro-NanoMechatronics and Human Science*, Nagoya Japan: Nov. 5-8, **2006**.

2 Phee, L.; Accoto, D.; Menciassi, A.; Stefanini, C.; Carrozza, M. C.; Dario, P. *IEEE Trans. on Biomedical Engin.* **2002**, *49*, 613.

3 Hill, C.; Amodeo, A.; Joseph, J. V.; Patel, H. R. H. *Expert Rev. Anticancer Ther.* **2008**, *8*, 1891.

4 Wood, R. J.; Avadhanula, S.; Fearing, R. S. *IEEE Int. Conf. on Intelligent Robots and Systems*, Las Vegas, NV: Oct 28-30, **2003**.

5 Sahai, R.; Avadhanula, S.; Groff, R.; Steltz, E.; Wood, R.; Fearing, R. S. *Proc. 2006 IEEE Intl. Conf. on Robotics and Automation*, Orlando, FL: May, **2006**.

6 Abbott, J. J.; Nagy, Z.; Beyeler, F.; Nelson, B. J. *IEEE Robotics & Automation Magazine* **2007**, *14*, 92.

7 Dong, L.; Nelson, B. J. *IEEE Robotics & Automation Magazine* **2007**, *14*, 111.

8 Wood, R. J.; Steltz, E.; Fearing, R. S., *IEEE Int. Conf. on Robotics and Automation*,Barcelona: April, **2005**.

9 E. M. Purcell, "Life at low Reynolds number," *Am. J. Phys*. **1977**, *45*, 3.

10 Furst, E. M.; Suzuki, C.; Fermigier, M.; Gast, A. P. Langmuir **1998**, *14*, 7334.

11 Furst, E. M.; Gast, A. P. Phys. Rev. Lett. **1999**, *82*, 4130.

12 Dreyfus, R.; Baudry, J.; Roper, M. L.; Fermigier, M.; Stone, H. A.; Bibette, J. *Nature* **2005**, *437*, 862.

13 Singh, H.; Laibinis, P. E.; Hatton, T. A. *Nano Lett*. **2005**, *5*, 2149-2154.

14 Singh, H.; Laibinis, P. E.; Hatton, T. A. *Langmuir* **2005**, *21*, 11500-11509.

15 Evans, B. A.; Shields, A. R.; Lloyd, C. R.; Washburn, S.; Falvo, M. R.; Superfine, R. *Nano Lett*. **2007**, 7, 1428.

16 Zhou, Z. H.; Liu, G. J.; Han, D. H. *ACS Nano* **2009**, *3*, 165.

17 Keng, P. Y.; Shim, I.; Korth, B. D.; Douglas, J. F.; Pyun, J. *ACS Nano* **2007**, *1*, 279.

18 Korth, B. D.; Keng, P.; Shim, I.; Bowles, S.; Nebesny, K.; Tang, C.; Kowalewski, T.; Pyun, J. *J. Am. Chem. Soc*. **2006**, *128*, 6562.

19 Bowles, S. E.; Wu, W.; Kowalewski, T.; Schalnat, M. C.; Davis, R. J.; Pemberton, J. E.; Shim, I.; Korth, B. D.; Pyun, J. *J. Am. Chem. Soc.* **2007**, *129*, 8694.

20 Benkoski, J. J.; Bowles S. E.; Jones, R. L.; Douglas, J. F.; Pyun, J.; Karim, A. *J. Polym. Sci. Part B-Polym. Phys.* **2008**, *46*, 2267.

21 Benkoski, J. J.; Bowles S. E.; Korth, B. D.; Jones, R. L.; Douglas, J. F.; Karim, A.; Pyun, J. *J. Am. Chem. Soc*. **2007**, *129*, 6291-6297

22 Benkoski, J. J.; Jones, R. L.; Douglas, J. F.; Karim, A. *Langmuir* **2007**, *23*, 3530.

23 Benkoski, J. J.; Hu, H.; Karim, A. *Macromol. Rapid Commun.* **2006**, *27*, 1212.

24 den Toonder, J. M. J.; Bos, F. M.; Broer, D. J.; Filippini, L.; Gillies, M.; de Goede, J.; Mol, G. N.; Reime, M.; Talen, W.; Wilderbeek, J. T. A.; Khatavkar, V.; Anderson, P. D. *Lab Chip* **2008**, **8**, 533.

25 Tabata, O.; Kojima, H.; Kasatani, T.; Isono, Y.; Yoshida, R., Micro Electro Mechanical Systems, **2003**. MEMS-03 Kyoto. IEEE The Sixteenth Annual International Conference 2003, 12.

26 van Oosten, C. L.; Bastiaansen, C. W. M.; Broer, D. J. *Nature Materials* **2009**, *8*, 677.

27 Zubarev, A. Y.; Iskakova L. Y. *Physica A* **2006**, *367*, 55.

28 Buyevich, Y. A.; Ivanov, A. O. *Physica A* **1992**, *190*, 276.

29 Zubarev, A. Y.; Iskakova, L. Y. *Physica A* **2004**, *335*, 325.

30 Klokkenburg, M.; Erné, B. H.; Meeldijk, J. D.; Wiedenmann, A.; Petukhov, A. V.; Dullens, R. P. A.; Philipse, A. P. *Phys. Rev. Lett.* **2006**, *97*, 185702.

31 Klokkenburg, M.; Dullens, R. P. A.; Kegel, W. K.; Erné, B. H.; Philipse, A. P. *Phys. Rev. Lett.* **2006**, *96*, 037203.

32 Klokkenburg, M.; Erné, B. H. *J. Magnetism and Magnetic Matls.* **2006**, *306*, 85.

33 One can calculate the strength of the magnetic dipolar interaction energy (E_{mag}) for two PS-CoNPs in contact: $E_{mag} = -\mu^2 \left(2\pi\mu_r\mu_0 r^3\right)^{-1}$ where μ is the magnetic dipole moment, μ_0 is the permeability of free space, μ_r is the relative permeability of water, and r is the center-to-center distance between the two particles in contact. For 23.5 nm PS-CoNPs in a poor solvent such as water, this value is 10x greater than thermal energy at room temperature (1 k_BT). However, if the polystyrene shell swells by a factor of 2 in a good solvent such as DMF, the magnetic attraction drops to -7 k_BT.

34 van Workum, K.; Douglas, J. F. *Macromol. Symp.* **2005**, *227*, 1.

35 van Workum, K.; Douglas, J. F. *Phys. Rev. E* **2005**, *71*, 031502.

36 Stambaugh, J.; van Workum, K.; Douglas, J. F.; Losert, W. *Phys. Rev. E* **2005**, *72*, 031301.

37 Tavares, J. M.; Weis, J. J.; Telo da Gama, M. M. *Phys. Rev. E* **2002**, *65*, 061201.

38 Klug, A *Angew. Chem. Int. Ed.* **1983** *22*, 565.

39 Pollard, T. D.; Cooper, J. A. *Ann. Rev. Biochem.* **1986**, *55*, 987.

40 Disanza, A.; Steffen, A.; Hertzog, M. *Cell Mol. Life Sci.* **2005**, *62*, 955.

41 Cebers, A. *Curr. Opin. Coll. Int. Sc*., **2005**, *10*, 167.

42 Cebers, A. *Magnitnaya Gidrodinamika*, **2005**, *41*, 63.

43 Belovs, M.; Cebers, A. *Phys.Rev.E*, **2009**, *79*, 051503 (Erratum, **2009**, *79*, 069906 (E)).

44 Silverstein, R. M.; Webster, F. X. Spectrometric Identification of Organic Compounds. John Wiley & Sons, Inc: **1998**.

45 Untreated glass slides were cleaned prior to use using a Harrick plasma cleaner. For the 5 min exposure, the chamber was pumped down to 500 millitorr with 10 W supplied to the RF coil. Epoxy-functionalized cover slips were prepared by immersing them in a 1 vol % solution of (3-glycidoxypropyl)trimethoxy silane in toluene. The cover slips were immersed overnight before rinsing with toluene and drying with nitrogen gas. Fluorinated cover slips were prepared by exposing them to a saturated vapor of (heptadecafluoro-1,1,2,2-tetrahydrodecyl)dimethylchlorosilane for three hours. Excess silane was removed by first rinsing with acetone followed by a gentle wash with soap and water.

Chapter 5

1. Alstrum-Acevedo, J. H.; Brennaman, M. K.; Meyer, T. J. *Inorg. Chem.* **2005,** *44*, 6802-6827.

2. Arico, A. S.; Bruce, P.; Scrosati, S.; Tarascon, J.-M.; Van Schalkwijk, W. *Nat. Mater.* **2005,** *4*, 366-377.

3. Kanan, M. W.; Nocera, D. G. *Science* **2008,** *321*, 1072-1075.

4. Osterloh, F. *Chem. Mater.* **2008,** *20*, 35-54.

5. Ryan, J. V.; Berry, A. D.; Anderson, M. L.; Long, J. W.; Stroud, R. M.; Cepak, V. M.; Browning, V. M.; Rolison, D. R.; Merzbacher, C. I. *Nature* **2000,** *406*, 169-172.

6. Long, J. W.; Dunn, B.; Rolison, D. R.; White, H. S. *Chem. Rev.* **2004,** *104*, 4463-4492.

7. Long, J. W.; Rolison, D. R. *Acc. Chem. Res.* **2007,** *40*, 854-862.

8. Alexander, B. D.; Kulesza, P. J.; Rutkowska, I.; Solarskac, R.; Augustynski, J. *J. Mater. Chem.* **2008,** *18*, 2298-2303.

9. Estrada, W.; Fantini, M. C. A.; de Castro, S. C.; Polo da Fonseca, C. N.; Gorenstein, A. *J. Appl. Phys.* **1993,** *74*, 5835-5841.

10. Svegl, F.; Orel, B.; Hutchins, M. G.; Kalcher, K. *J. Electrochem. Soc.* **1996,** *143*, (5), 1532-1539.

11. Poizot, P.; Laruelle, S.; Grugeon, S.; Dupont, L.; Tarascon, J.-M. *Nature* **2000,** *407*, 496-499.

12. Li, W.-Y.; Xu, L.-N.; Chen, J. *Adv. Func. Mater.* **2005,** *15*, 851-857.

13. Li, Y.; Tan, B.; Wu, Y. *J. Am. Chem. Soc.* **2006,** *128*, (44), 14258-14259.

14. Nam, K. T.; Kim, D.-W.; Yoo, P. J.; Chiang, C.-Y.; Meethong, N.; Hammond, P. T.; Chiang, Y.-M.; Belcher, A. M. *Science* **2006,** *312*, 885-888.

15. Li, Y.; Tan, B.; Wu, Y. *Nano Lett.* **2008,** *8*, (1), 265-270.

16. Shim, H.-S.; Shinde, V. R.; Kim, H.-J.; Sung, Y.-E.; Kim, W.-B. *Thin Solid Films* **2008,** *516*, 8573-8578.

17. Chen, Y. W. D.; Noufi, R. N. *J. Electrochem. Soc.* **1984,** *131*, (4), 731-5.

18. Schumacher, L. C.; Holzhueter, I. B.; Hill, I. R.; Dignam, M. J. *Electrochim. Acta* **1990,** *35*, (6), 975-984.

19. Monk, P. M. S.; Chester, S. L.; Higham, D. S.; Partridge, R. D. *Electrochim. Acta* **1994,** *39*, (15), 2277-84.

20. Castro, E. B.; Gervasi, C. A.; Vilche, J. R. *J. Appl. Electrochem.* **1998,** *28*, (8), 835-841.

21. Casella, I. G. *J. Electroanal. Chem.* **2002,** *520*, (1-2), 119-125.

22. Casella, I. G.; Gatta, M. *J. Electroanal. Chem.* **2002,** *534*, (1), 31-38.

23. Mendoza, L.; Albin, V.; Cassir, M.; Galtayries, A. *J. Electroanal. Chem.* **2003,** *548*, 95-107.

24. Spataru, N.; Terashima, C.; Tokuhiro, K.; Sutanto, I.; Tryk, D. A.; Park, S.-M.; Fujishima, A. *J. Electrochem. Soc.* **2003,** *150*, (7), E337-E341.

25. Lin, H.; Tang, W.; Kleiman-Shwarsctein, A.; McFarland, E. W. *J. Electrochem. Soc.* **2008,** *155*, (2), B200-B206.

26. He, T.; Chen, D.; Jiao, X.; Xu, Y.; Gu, Y. *Langmuir* **2004,** *20*, (19), 8404-8408.

27. Kim, J.-W.; Choi, S. H.; Lillehei, P. T.; Chu, S.-H.; King, G. C.; Watt, G. D. *Chem. Commun.* **2005**, (32), 4101-4103.

28. Hu, J.; Wen, Z.; Wang, Q.; Yao, X.; Zhang, Q.; Zhou, J.; Li, J. *J. Phys. Chem. B* **2006,** *110*, (48), 24305-24310.

29. Ohnishi, M.; Kozuka, Y.; Ye, Q.-L.; Yoshikawa, H.; Awaga, K.; Matsuno, R.; Kobayashi, M.; Takahara, A.; Yokoyama, T.; Bandow, S.; Iijima, S. *J. Mater. Chem.* **2006,** *16*, (31), 3215-3220.

30. Titirici, M.-M.; Antonietti, M.; Thomas, A. *Chem. Mater.* **2006,** *18*, (16), 3808-3812.

31. Chen, Y.; Zhang, Y.; Fu, S. *Mater. Lett.* **2007,** *61*, (3), 701-705.

32. Du, N.; Zhang, H.; Chen, B.; Wu, J.; Ma, X.; Liu, Z.; Zhang, Y.; Yang, D.; Huang, X.; Tu, J. *Adv. Mater.* **2007,** *19*, (24), 4505-4509.

33. Chen, C.-H.; Abbas, S. F.; Morey, A.; Sithambaram, S.; Xu, L.-P.; Garces, H. F.; Hines, W. A.; Suib, S. L. *Adv. Mater.* **2008,** *20*, (6), 1205-1209.

34. Chernavskii, P. A.; Pankina, G. V.; Zaikovskii, V. I.; Peskov, N. V.; Afanasiev, P. *J. Phys. Chem. C* **2008,** *112*, (26), 9573-9578.

35. Teng, F.; Xu, T.; Liang, S.; Buergen, G.; Yao, W.; Zhu, Y. *Catal. Commun.* **2008,** *9*, (6), 1119-1124.

36. Teng, F.; Yao, W.; Zheng, Y.; Ma, Y.; Xu, T.; Gao, G.; Liang, S.; Teng, Y.; Zhu, Y. *Talanta* **2008,** *76*, (5), 1058-1064.

37. Tian, L.; Yang, X.; Lu, P.; Williams, I. D.; Wang, C.; Ou, S.; Liang, C.; Wu, M. *Inorg. Chem.* **2008,** *47*, (13), 5522-5524.

38. Zhao, W.; Liu, Y.; Li, H.; Zhang, X. *Mater. Lett.* **2008,** *62*, (4-5), 772-774.

39. Chen, Y.; Hu, L.; Wang, M.; Min, Y.; Zhang, Y. *Colloids Surf., A* **2009,** *336*, (1-3), 64-68.

40. Park, J.; Shen, X.; Wang, G. *Sens. Actuators, B* **2009,** *B136*, (2), 494-498.

41. Salabas, E. L.; Rumplecker, A.; Kleitz, F.; Radu, F.; Schueth, F. *Nano Letters* **2006,** *6*, (12), 2977-2981.

42. Shaju, K. M.; Jiao, F.; Debart, A.; Bruce, P. G. *Physical Chemistry Chemical Physics* **2007,** *9*, (15), 1837-1842.

43. Benitez, M. J.; Petracic, O.; Salabas, E. L.; Radu, F.; Tueysuez, H.; Schueth, F.; Zabel, H. *Phys. Rev. Lett.* **2008,** *101*, (9), 097206/1-097206/4.

44. Dong, Z.; Fu, Y.; Han, Q.; Xu, Y.; Zhang, H. *J. Phys. Chem. C* **2007,** *111*, (50), 18475-18478.

45. Du, J.; Chai, L.; Wang, G.; Li, K.; Qian, Y. *Aust. J. Chem.* **2008,** *61*, (2), 153-158.

46. Zhang, H.; Wu, J.; Zhai, C.; Ma, X.; Du, N.; Tu, J.; Yang, D. *Nanotechnology* **2008,** *19*, (3), 035711/1-035711/5.

47. An, K.; Lee, N.; Park, J.; Kim, S.; Hwang, Y.; Park, J.; Kim, J.; Park, J.; Han, M. J.; Yu, J.; Hyeon, T. *J. Am. Chem. Soc.* **2004,** *128*, (9753-9760).

48. Guan, H.; Shao, C.; Wen, S.; Chen, B.; Gong, J.; Yang, X. *Mater. Chem. Phys.* **2003,** *82*, (3), 1002-1006.

49. Barakat, N. A. M.; Khil, M. S.; Sheikh, F. A.; Kim, H. Y. *J. Phys. Chem. C* **2008,** *112*, (32), 12225-12233.

50. Gu, Y.; Jian, F.; Wang, X. *Thin Solid Films* **2008,** *517*, (2), 652-655.

51. Redl, F. X.; Cho, K.-S.; Murray, C. B.; O'Brien, S. *Nature* **2003,** *423*, 968-971.

52. Manoharan, V. M.; Elsesser, M. T.; Pine, D. J. *Science* **2003,** *301*, 483-487.

53. Park, S.; Lim, J.-H.; Chung, S.-W.; Mirkin, C. A. *Science* **2004,** *16*, 348-351.

54. Benkoski, J. J.; Bowles, S. E.; Korth, B., D.; Jones, R. A.; Douglas, J. F.; Karim, A.; Pyun, J. *J. Am. Chem. Soc.* **2007,** *129*, 6291-6297.

55. Benkoski, J. J.; Bowles, S. E.; Korth, B. D.; Jones, R. L.; Douglas, J. F.; Karim, A.; Pyun, J. *J. Am. Chem. Soc.* **2007,** *129*, (28), 8694-8695.

56. DeVries, G. A.; Brunnbauer, M.; Hu, Y.; Jackson, A. M.; Long, B.; Neltner, B. T.; Uzun, O.; Wunsch, B. H.; Stellacci, F. *Science* **2007,** *315*, (5810), 358-361.

57. Carney, R. P.; De Vries, G. A.; Dubois, C.; Kim, H.; Kim, J. Y.; Singh, C.; Ghorai, P. K.; Tracy, J. B.; Stiles, R. L.; Murray, R. W.; Glotzer, S. C.; Stellacci, F. *J. Am. Chem. Soc.* **2008,** *130*, (3), 798-799.

58. De Vries, G. A.; Talley, F. R.; Carney, R. P.; Stellacci, F. *Adv. Mater.* **2008,** *20*, (22), 4243-4247.

59. Nakata, K.; Hu, Y.; Uzun, O.; Bakr, O.; Stellacci, F. *Adv. Mater.* **2008,** *20*, (22), 4294-4299.

60. Furst, E. M.; Suzuki, C.; Fermigier, M.; Gast, A. P. *Langmuir* **1998,** *14*, (26), 7334-7336.

61. Biswal, S. L.; Gast, A. P. *Phys. Rev. E: Stat., Nonlinear, Soft Matter Phys.* **2003,** *68*, (2-1), 021402/1-021402/9.

62. Goubault, C.; Jop, P.; Fermigier, M.; Baudry, J.; Bertrand, E.; Bibette, J. *Phys. Rev. Lett.* **2003,** *91*, (26, Pt. 1), 260802/1-260802/4.

63. Biswal, S. L.; Gast, A. P. *Anal. Chem.* **2004,** *76*, (21), 6448-6455.

64. Biswal, S. L.; Gast, A. P. *Phys. Rev. E: Stat., Nonlinear, Soft Matter Phys.* **2004,** *69*, (4-1), 041406/1-041406/9.

65. Cohen-Tannoudji, L.; Bertrand, E.; Bressy, L.; Goubault, C.; Baudry, J.; Klein, J.; Joanny, J.-F.; Bibette, J. *Phys. Rev. Lett.* **2005,** *94*, (3), 038301/1-038301/4.

66. Dreyfus, R.; Baudry, J.; Roper, M. L.; Fermigier, M.; Stone, H. A.; Bibette, J. *Nature* **2005,** *437*, (7060), 862-865.

67. Goubault, C.; Leal-Calderon, F.; Viovy, J.-L.; Bibette, J. *Langmuir* **2005,** *21*, (9), 3725-3729.

68. Singh, H.; Laibinis, P. E.; Hatton, T. A. *Nano Lett.* **2005,** *5*, 2149-2154.

69. Gao, J.; Zhang, B.; Zhang, X.; Xu, B. *Angew. Chem. Int. Ed.* **2006,** *45*, 1220-1223.

70. Pileni, M. P. *Acc. Chem. Res.* **2007,** *40*, 685-693.

71. Singh, H.; Hatton, T. A. *J. Magn. Magn. Mater.* **2007,** *315*, 53-64.

72. Cohen-Tannoudji, L.; Bertrand, E.; Baudry, J.; Robic, C.; Goubault, C.; Pellissier, M.; Johner, A.; Thalmann, F.; Lee, N. K.; Marques, C. M.; Bibette, J. *Phys. Rev. Lett.* **2008,** *100*, (10), 108301/1-108301/4.

73. Zerrouki, D.; Baudry, J.; Pine, D.; Chaikin, P.; Bibette, J. *Nature* **2008,** *455*, (7211), 380-382.

74. Erb, R. M.; Son, H. S.; Samanta, B.; Rotello, V. M.; Yellen, B. B. *Nature* **2009,** *457*, (7232), 999-1002.

75. Zhou, Z.; Liu, G.; Han, D. *ACS Nano* **2009,** *3*, (1), 165-172.

76. Yin, Y.; Rioux, R. M.; Erdonmez, C. K.; Hughes, S.; Somorjai, G. A.; Alivisatos, A. P. *Science* **2004,** *304*, (5671), 711-714.

77. Yin, Y.; Erdonmez, C. K.; Cabot, A.; Hughes, S.; Alivisatos, A. P. *Adv. Funct. Mater.* **2006,** *16*, (11), 1389-1399.

78. Butter, K.; Bomans, P. H. H.; Frederick, P. M.; Vroege, J.; Philipse, A. P. *Nature Mater.* **2003,** *2*, 88.

79. Ishida, Y.; Aida, T. *J. Am. Chem. Soc.* **2002,** *124*, (47), 14017-14019.

80. Zhao, D.; Moore, J. S. *Org. Biomol. Chem.* **2003,** *1*, (20), 3471-3491.

81. Scherman, O. A.; Ligthart, G. B. W. L.; Sijbesma, R. P.; Meijer, E. W. *Angew. Chem., Int. Ed.* **2006,** *45*, (13), 2072-2076.

82. Kumar, A. M. S.; Sivakova, S.; Marchant, R. E.; Rowan, S. J. *Small* **2007,** *3*, (5), 783-787.

83. Hawker, C. J.; Bosman, A. W.; Harth, E. *Chem. Rev.* **2001,** *101*, (12), 3661-3688.

84. Lacroix-Desmazes, P.; Lutz, J. F.; Chauvin, F.; Severac, R.; Boutevin, B. *Macromolecules* **2001,** *34*, 8866-8871.

85. Hawker, C. J.; Wooley, K. L. *Science* **2005,** *309*, (5738), 1200-1205.

86. Matyjaszewski, K.; Xia, J. *Chem. Rev.* **2001,** *101*, 2921-2990.

87. Risbud, A. S.; Snedeker, L. P.; Elcombe, M. M.; Cheetham, A. L.; Seshadri, R. *Chem. Mater* **2005,** *17*, 834-838.

88. Makhlouf, S. A. *J. Magn. Magn. Mater.* **2002,** *246*, (184-190).

89. Windisch, C. F.; Ferris, K.; Exarhos, G. J.; Sharma, S. K. *Thin Solid Films* **2002,** *420-421*, 89-99.

90. Langell, M. A.; Anderson, M. D.; Carson, G. A.; Peng, L.; Smith, S. *Phys. Rev. B: Condens. Matter Mater. Phys.* **1999,** *59*, (7), 4791-4798.

91. Gulino, A.; Fragala, I. *Inorg. Chim. Acta* **2005,** *358*, (15), 4466-4472.

92. Barreca, D.; Massign, C.; Daolio, S.; Fabrizio, M.; Piccirillo, C.; Armelao, L.; Tondello, E. *Chem. Mater.* **2001,** *13*, 588-593.

93. Gulino, A.; Fiorito, G.; Fragala, I. *J. Mater. Chem.* **2003,** *13*, (4), 861-865.

94. Belova, I. D.; Roginskaya, Y. E.; Shifrina, R. R.; Gagarin, S. G.; Plekhanov, Y. V.; Venevtsev, Y. N. *Solid State Commun.* **1983,** *47*, (8), 577-584.

95. Miedzinksa, K. M. E.; Hollebone, B. R.; Cook, J. G. *J. Phys. Chem. Solids* **1987,** *48*, (7), 649.

96. Cox, P. A., *Transition metal oxides: An introduction to their electronic structure and properties*. Clarendon Press Oxford: 1992; p 276.

97. Schlettwein, D.; Hesse, K.; Gruhn, N.; Lee, P. A.; Nebesny, K. W.; Armstrong, N. R. *J. Phys. Chem. B* **2001,** *105*, 4791-4800.

98. Rose, A. *Phys. Rev.* **1955,** *97*, (6), 1538.

99. Pourbaix, M., *Atlas of electrochemical equilibria in aqueous solutions.* Pergamon: London, 1966; p 322-329.

100. Barbero, C.; Planes, G. A.; Miras, M. C. *Electrochem. Commun.* **2001,** *3*, (3), 113-116.

101. Lichusina, S.; Chodosovskaja, A.; Selskis, A.; Leinartas, K.; Miecinskas, P.; Juzeliunas, E. *Chemija* **2008,** *19*, (3-4), 7-15.

102. Wang, G.; Shen, X.; Horvat, J.; Wang, B.; Liu, H.; Wexler, D.; Yao, J. *J. Phys Chem. C* **2009,** *113*, (11), 4357-4361.

Chapter 6

1. Zhou, Z.-H.; Liu, G.-J.; Han, D.-H. *ACS Nano* **2009,** *3*, 165-172.

2. Graetzel, M. *Nature* **2001,** *414*, 338-334.

3. Fujishima, A.; Honda, K. *Nature* **1972,** *238*, 36-37.

4. Bard, A. J.; Fox, M. A. *Acc. Chem. Res.* **1995,** *28*, (3), 141-5.

5. Bandara, J.; Weerasinghe, H. *Sol. Energy Mater. Sol. Cells* **2005,** *85*, (3), 385-390.

6. Yan, N.; Zhang, J.-G.; Tong, Y.; Yao, S.; Xiao, C.; Li, Z.; Kou, Y. *Chem. Commum.* **2009**, 4423-4425.

7. Vasquez, Y.; Sra, A. K.; Schaak, R. E. *J Am Chem Soc* **2005,** *127*, 12504-12505.

8. Long, M.; Cai, W.; Kisch, H. *J. Phys. Chem. C* **2008,** *112*, (2), 548-554.

9. Beranek, R.; Kisch, H. *Angew. Chem., Int. Ed.* **2008,** *47*, (7), 1320-1322, S1320/1-S1320/5.

10. Park, J.-I.; J., C. *J. Am. Chem. Soc.* **2001,** *123*, 5743-5746.

11. Liang, H.-P.; Zhang, H.-M.; Hu, J.-S.; Guo, Y.-G.; Wan, L.-J.; Bai, C.-L. *Angew. Chem., Int. Ed.* **2004,** *43*, 1540-1543.

12. Gao, J.; Zhang, B.; Zhang, X.; Xu, B. *Angew. Chem. Int. Ed.* **2006,** *45*, 1220-1223.

13. Nozik, A. J. *Appl. Phys. Lett.* **1977,** *30*, 567-569.

14. Nagasubramanian, G.; Gioda, A. S.; Bard, A. J. *J. Electrochem. Soc.* **1981,** *128*, 2158-2164.

15. Kim, Y.; Yoo, B. J.; Vittal, R.; Lee, Y.; Park, N.-G.; Kim, K.-J. *J. Power Sources* **2007,** *175*, 914-919.